

**A GEOLOGICAL AND GEOPHYSICAL STUDY OF THE
1929 GRAND BANKS SLIDE**

By
Curtis William McCall

A Thesis Submitted to
Saint Mary's University, Halifax, Nova Scotia
in Partial Fulfillment of the Requirements for
the Degree of Master of Science in Applied Science

October 20th, 2006, Halifax, Nova Scotia

© Copyright by Curtis William McCall, 2006

Approved: *Supervisor*
Dr. David J.W. Piper
Research Scientist

Approved: *External Examiner*
Dr. David Mosher
Research Scientist

Approved: *Committee Member*
Dr. Georgia Pe-Piper
Professor of Geology

Approved: *Committee Member*
Dr. Andrew MacRae
Professor of Geology



Library and
Archives Canada

Bibliothèque et
Archives Canada

Published Heritage
Branch

Direction du
Patrimoine de l'édition

395 Wellington Street
Ottawa ON K1A 0N4
Canada

395, rue Wellington
Ottawa ON K1A 0N4
Canada

Your file Votre référence

ISBN: 978-0-494-23855-4

Our file Notre référence

ISBN: 978-0-494-23855-4

NOTICE:

The author has granted a non-exclusive license allowing Library and Archives Canada to reproduce, publish, archive, preserve, conserve, communicate to the public by telecommunication or on the Internet, loan, distribute and sell theses worldwide, for commercial or non-commercial purposes, in microform, paper, electronic and/or any other formats.

The author retains copyright ownership and moral rights in this thesis. Neither the thesis nor substantial extracts from it may be printed or otherwise reproduced without the author's permission.

AVIS:

L'auteur a accordé une licence non exclusive permettant à la Bibliothèque et Archives Canada de reproduire, publier, archiver, sauvegarder, conserver, transmettre au public par télécommunication ou par l'Internet, prêter, distribuer et vendre des thèses partout dans le monde, à des fins commerciales ou autres, sur support microforme, papier, électronique et/ou autres formats.

L'auteur conserve la propriété du droit d'auteur et des droits moraux qui protègent cette thèse. Ni la thèse ni des extraits substantiels de celle-ci ne doivent être imprimés ou autrement reproduits sans son autorisation.

In compliance with the Canadian Privacy Act some supporting forms may have been removed from this thesis.

Conformément à la loi canadienne sur la protection de la vie privée, quelques formulaires secondaires ont été enlevés de cette thèse.

While these forms may be included in the document page count, their removal does not represent any loss of content from the thesis.

Bien que ces formulaires aient inclus dans la pagination, il n'y aura aucun contenu manquant.


Canada

ABSTRACT

A GEOLOGICAL AND GEOPHYSICAL STUDY OF THE 1929 GRAND BANKS SLIDE

by Curtis William McCall

The St. Pierre Slope off the Grand Banks of Newfoundland is the site of a large submarine failure complex that was the result of the 1929 Grand Banks earthquake. A 2000 km² area has been investigated in detail using seismic reflection, sidescan sonar and core data. Failure development and evolution is strongly influenced by local changes in gradient on the slope. Documented modes of failure are mass flows, slumps, and isolated occurrences of glides and creep. The total volume of sediment involved in initial failure is estimated at 93 km³: 47 km³ as MTDs on the slope and 46 km³ that evacuated, likely contributing to the 1929 turbidity current. The total volume of the turbidite is conservatively estimated at 175 km³, suggesting that at least 222 km³ (47 km³ + 175km³) of sediment was eroded and displaced during the 1929 event.

October 20th, 2006

TABLE OF CONTENTS

Table of Contents	iii
List of Tables	vi
List of Figures	vii
List of Abbreviations	xi
Acknowledgements	xii
Chapter 1	Introduction 1
1.1	Objectives..... 3
1.2	Data coverage..... 5
1.3	Regional setting..... 6
1.4	Local geologic setting 7
1.5	Previous Work on MTDs from St. Pierre Slope 10
1.6	Previous stratigraphic studies..... 12
1.6.1	Late Cenozoic stratigraphy 12
1.6.2	Quaternary stratigraphy..... 14
1.6.2.1	Acoustic- and shallow core-based stratigraphy of the St. Pierre Slope 14
1.6.2.2	Shallow core-based stratigraphy of Laurentian Fan..... 15
1.6.3	The Laurentian Channel outlet..... 18
Chapter 2	Methods 20
2.1	Acoustic instruments and data 20
2.1.1	Huntec DTS..... 22
2.1.2	Sidescan sonar..... 22
2.2	Piston and associated trigger weight cores 23
2.2.1	Laboratory techniques 24
2.2.2	Accelerator Mass Spectroscopy Radiocarbon Dating..... 25
2.3	Bathymetry..... 26
2.4	Classification of disturbed seabed..... 26
2.4.1	Acoustic facies 26
2.4.2	Core-based disturbed facies 27
2.5	Determining stratigraphic thicknesses from Huntec DTS data... 27
2.5.1	Definition of terms 28
2.6	Distinction between valleys and channels 30
2.7	Errors and limitations..... 30
Chapter 3	Acoustic data 32
3.1	Introduction..... 32
3.2	Geological and bathymetric features that may influence failure 33
3.2.1	Till distribution 33
3.2.2	Pockmarks..... 34
3.2.3	Shallow faults..... 36

	3.2.4 Gentle and steep slopes.....	36
3.3	Seismic stratigraphy.....	37
	3.3.1 Introduction.....	37
	3.3.2 Type section and correlation.....	39
	3.3.3 Depth variation of reflections.....	43
3.4	Disturbed seabed.....	43
	3.4.1 Introduction.....	43
	3.4.2 Acoustic facies of surface sediment failures.....	46
3.5	Geographic distribution of surface failure.....	60
3.6	Volumes of sediment involved in surface failure.....	65
	3.6.1 Volume of sediment existing as failed bodies at the surface.....	65
	3.6.2 Total volume of sediment that failed.....	66
	3.6.3 Total volume of sediment evacuated.....	67
	3.6.4 Volume estimates applied to the entire region of surface failure.....	67
3.7	Subsurface disturbed bodies.....	69
Chapter 4	Core data.....	71
4.1	Introduction.....	71
4.2	Radiocarbon dates obtained from sediment cores.....	73
4.3	Sedimentary facies.....	75
4.4	Stratigraphic distribution of sedimentary facies in undisturbed cores.....	79
	4.4.1 Downcore facies distribution on the slope and rise.....	79
	4.4.2 Other downcore variations in undisturbed cores.....	85
	4.4.2.1 Undrained shear strength.....	85
	4.4.2.2 Color shifts in a and b.....	89
	4.4.2.3 Cracks associated with gas expansion.....	90
	4.4.2.4 Magnetic susceptibility.....	91
4.5	Disturbed cores.....	91
	4.5.1 Introduction.....	91
	4.5.2 Descriptions of cores containing disturbed sediments.....	93
Chapter 5	Discussion.....	106
5.1	Introduction.....	106
5.2	Integration of seismic and core data.....	106
	5.2.1 Age model for key reflections.....	106
	5.2.2 Core stratigraphy related to key reflections.....	109
5.3	Undisturbed sediment facies related to facies from other studies.....	111
5.4	Source area and transportation for sediment facies from undisturbed cores.....	113
5.5	Sedimentation rates.....	118
5.6	Mass Transport Deposits: core-seismic integration.....	121
5.7	Observed failure types in seismic reflection data.....	130

5.7.1	Gradients and distribution.....	130
5.7.2	MTD Lithology.....	134
5.8	Evolution and progression of failure types	134
5.9	Sediment budget from failure volumes.....	139
5.10	Implications for tsunami modelling	140
5.11	Comparisons with other similar failure complexes.....	141
5.11.1	Eastern Canadian Margin with emphasis on the Scotian Slope	141
5.11.2	European and Mediterranean Margins.....	142
Chapter 6	Conclusions.....	147
	References.....	152
	Appendix 1.....	160
	Appendix 2.....	196

LIST OF TABLES

Table 3.1	Mean depths below seafloor for the six key reflections in undisturbed and disturbed areas, and mean thicknesses of surface MTDs on the St. Pierre Slope and rise.	Page 42
Table 3.2	Classification of disturbed seabed based on acoustic character from Huntex DTS seismic reflection data.	47
Table 4.1	AMS radiocarbon dates for benthic mollusc samples recovered from St. Pierre Slope shallow sediment cores. Ages quoted as radiocarbon years before present (BP).	74
Table 4.2	The seven facies from undisturbed cores from the St. Pierre Slope and rise. IRD refers to ice-rafted detritus.	76
Table 4.3	Classification of sediments from cores that sampled areas affected by sediment failure.	92
Table 4.4	Analyses for SO_4^{++} , NH_4^+ and pE from 91020 TWC- and PC-40.	100
Table 5.1	Comparison of core-sampled sediments from this study to core-sampled sediments from previous studies from this region.	112
Table 5.2	Comparison of MTD facies sampled by cores to MTDs imaged by seismic data.	122
Table 5.3	Comparison of MTDs documented on the eastern Canadian margin.	143

LIST OF FIGURES

	Page
Figure 1.1 Regional map of the southeastern Canadian margin.	2
Figure 1.2 Bathymetry map of study area and vicinity.	8
Figure 1.3 Sidescan sonar images of the upper St. Pierre Slope and head of Eastern Valley	10
Figure 2.1 Locations of seismic reflection, core, and sidescan sonar data used for this thesis.	21
Figure 2.2 Illustration of MTD showing five main components (A-D) used in estimating depths, areas, and volumes of failed and evacuated sediments.	28
Figure 3.1 Locations of seismic reflection and sidescan sonar figures of Chapter 3.	33
Figure 3.2 Sleevegun dip profile of upper St. Pierre Slope showing downslope extent of till tongues I-VI on the upper slope.	35
Figure 3.3 Hunttec DTS dip profile of the upper St. Pierre Slope showing the upslope limit of continuous reflections.	35
Figure 3.4 Surface render showing the variable gradients encountered on St. Pierre Slope.	37
Figure 3.5 Hunttec DTS seismic reflection strike profile of type section 1 showing five key reflections (Q100-brown to Q93- blue) from upper St. Pierre Slope at ~700 mbsl.	38
Figure 3.6 Hunttec DTS seismic reflection dip profile of type section 2 showing six key reflections (Q100-brown to Q91-yellow) from middle St. Pierre Slope at ~925 mbsl.	41
Figure 3.7 Bathymetry map showing distribution of acoustic Classes I-V	44
Figure 3.8 Hunttec DTS seismic reflection dip profile of a body of Class I.	48
Figure 3.9 Hunttec DTS seismic reflection strike profile perpendicular to Figure 3.8.	49

Figure 3.10	Huntec DTS seismic reflection profile and sidescan sonar images of the middle St. Pierre Slope showing bodies of Classes I and II.	50
Figure 3.11	Huntec DTS seismic reflection strike profile of a body of subclass A of Class II.	52
Figure 3.12	Huntec DTS seismic reflection strike profile near the head of a tributary valley of upper Eastern St. Pierre Valley showing a body of subclass B of Class III.	53
Figure 3.13	Huntec DTS seismic reflection dip (A) and strike (B) profiles across a tributary valley of upper Eastern St. Pierre Valley showing stacked bodies of subclass A of Class II. On the rise, stacking of subclass A occurs in valleys and on flat, undissected seabed (C).	54
Figure 3.14	SAR sidescan sonar images of the middle St. Pierre Slope showing a plan view perspective of Class I and subclass A of Class II.	55
Figure 3.15	Huntec DTS seismic reflection dip profile of the middle St. Pierre Slope showing a body of Class III.	57
Figure 3.16	Huntec DTS seismic reflection strike profile of a body of Class IV.	58
Figure 3.17	Huntec DTS seismic reflection dip profile of Class V.	59
Figure 3.18	Surface render of St. Pierre Slope generated from regional bathymetric maps showing zones of the seabed based on seabed morphology.	61
Figure 3.19	Huntec DTS seismic reflection profile showing bodies of subclasses A and B of Class II within a valley.	62
Figure 3.20	Bathymetry map of the upper to middle St. Pierre Slope showing the locations of Figures 3.12, 3.13b and 3.19 within a tributary valley of upper Eastern St. Pierre Valley.	63
Figure 3.21	An enlarged section of Figure 3.11. Profile shows stacked, internally incoherent bodies with hyperbolic to undulating surface reflections characteristic of bodies of Class II.	69

Figure 4.1	Map of St. Pierre Slope and vicinity showing locations of the eighteen cores used for this study.	72
Figure 4.2	Piston core stratigraphy of the upper St. Pierre Slope. Gray and brown muds of facies C have been distinguished.	80
Figure 4.3	Piston core stratigraphy of the middle St. Pierre Slope. Gray and brown muds of facies C have been distinguished.	81
Figure 4.4	Piston core stratigraphy of the lower St. Pierre slope and rise. Gray and brown muds of facies D have been distinguished.	82
Figure 4.5	Bathymetry map showing locations and downcore color plots of piston cores that sampled undisturbed sediments.	84
Figure 4.6A	Five cores representing the undisturbed stratigraphy of St. Pierre Slope and core 90015-07 taken from a ~56-m-deep failure plane.	86
Figure 4.6B	Shear strength (kPa) vs depth below seafloor (m) for the five undisturbed cores with best-fit lines.	87
Figure 4.6C	Su best-fit lines of the five undisturbed cores related to Su values from 90015-07.	88
Figure 4.7	Downcore photos of sediment cores showing facies I, II, and III.	96
Figure 4.8	Downcore photos of sediment cores that facies III and V.	99
Figure 4.9	Projected position of piston core 84003-05 within Hunttec DTS seismic reflection dip profile and SeaMARC I and SAR sidescan sonar images.	102
Figure 4.10	Downcore plots for piston core 90015-07.	105
Figure 5.1	Hunttec DTS seismic reflection profile of the upper and mid St. Pierre Slope showing radiocarbon dates for the key reflections and locations of till tongues I-III.	108
Figure 5.2	Seismic reflection and core data integration showing the sediment equivalent for reflections Q97, Q99 and Q100.	110
Figure 5.3	Regional map of eastern Canadian margin showing likely source areas for sediment sampled by cores.	115

Figure 5.4	Extrapolation of sedimentation rates using seismic reflection and core data.	120
Figure 5.5	Integration of core 2001043-42 and Hunttec DTS seismic reflection data .	123
Figure 5.6	Integration of core 2001043-41 and Hunttec DTS seismic reflection data .	125
Figure 5.7	Integration of core 91020-40 and Hunttec DTS seismic reflection data .	127
Figure 5.8	Cartoon of a rotational slump deposit (acoustic Class I) showing likely (a) and unlikely (b) sampling point for core 84003-05.	129
Figure 5.9	Cartoon of mass transport deposits documented on the St. Pierre Slope from Hunttec DTS data.	131
Figure 5.10	Cartoon of mass transport deposits documented on or near valley walls.	132
Figure 5.11	Hunttec DTS seismic reflection profile, sidescan sonar image (B) and cartoon (C) of multiple failures.	138

LIST OF ABBREVIATIONS

AMS	accelerator mass spectroscopy
[#] C	carbon isotopes
DTS	depth to seafloor from echosounder (when in Appendix 1)
DTS	deep-tow seismic
GMT	Greenwich Mean Time
GPS	Global positioning system
GSCA	Geologic Survey of Canada (Atlantic)
Hz	hertz
ka	thousands of years ago
kHz	kilohertz
kPa	kilopascal
LGM	Last Glacial Maximum
m kyr ⁻¹	metres/ thousand years
Ma	millions of years ago
mbsf	metres below seafloor
mbsl	metres below sea-level
MCGL	mud clast conglomerate
Mg m ⁻³	megagram/ cubic meter
ms	milliseconds
Ms	surface-wave magnitude (Rayleigh wave)
MST	multi sensor track
MTDs	mass transport deposits
SAR	Système Acoustique Remorqué
SI	Systeme Internationale
TC	turbidity current
TWTT	two way travel time
σ	standard deviation

ACKNOWLEDGEMENTS

Many thanks to my supervisor, Dr. David JW Piper, for access to his knowledge and ideas of a far-reaching grasp, and who waited patiently for the completion of this thesis. If it wasn't for his unrelenting 'nudges', I doubt I would have garnered the motivation to complete this project. Thank you.

I thank Dr. Georgia Pe-Piper for her all-around support and for originally getting me interested in the MSc program at St. Mary's University. And yes, Georgia, it's finally finished!

Thanks also to Dr. David Mosher, Dr. Andrew MacRae, Dr. Pierre Jutras, Calvin Campbell, Kate Jarett, Kimberley Jenner, Thian Hundert, Jon MacKie and many others that over the four years provided useful insight and guidance.

For financial support, I thank David and Georgia once again, not only were both of you my backbone for knowledge, you were also my financial lifeline. Also, this work was partly supported by an NSERC grant through the CanCOSTA project and partly by Geological Survey of Canada A-base and PERD funding for continental slope studies.

Lastly, the support and encouragement (and of course the occasional thesis joke) from friends was paramount. From 'study buddies' to 'party friends', it was all kept at a reasonable level, at least according to us.

CHAPTER 1

Introduction

On November 18th, 1929, the St. Pierre Slope was the site of a massive underwater earthquake, known worldwide as the 1929 Grand Banks earthquake. The M_s 7.2 earthquake occurred beneath the ridge between St. Pierre Valley and Eastern Valley with an epicentral position of 44°41' N, 56°00' W and focal depth of 16.8 km (Dewey and Gordon, 1984) (Figure 1.1). The initial shock at approximately 20:30 GMT was followed by two aftershocks at around 23:00 and 02:00 (November 19th) GMT that produced earthquake-induced ground accelerations that triggered widespread surficial failure of Holocene and Pleistocene sediments. Failure is thought to have been instantaneous within 100 km of the epicentre as documented by deep-sea cable breaks (Doxsee, 1948; Heezen and Ewing, 1952; Piper et al., 1988). Subsequent cable breaks downslope on the Laurentian Fan were sequential from 1 to 13 hours after the earthquake (Piper et al., 1988). These breaks are attributed to a turbidity current that developed from failed sediments and swept down from the upper slope to the Sohm Abyssal Plain, reaching a maximum flow velocity of 19 m/s (68 km/h) as deduced from cable break times (Piper et al., 1988). Such a massive current was first thought to have been generated by a single cataclysmic slumping event (Heezen and Drake, 1964). However, interpretation of GLORIA and SeaMARC I sidescan sonar data, and high-resolution seismic reflection data (mostly 3.5 kHz) from the upper Laurentian Fan and St. Pierre Slope show that this likely was not the case (Masson et al, 1985, Piper et al., 1985).

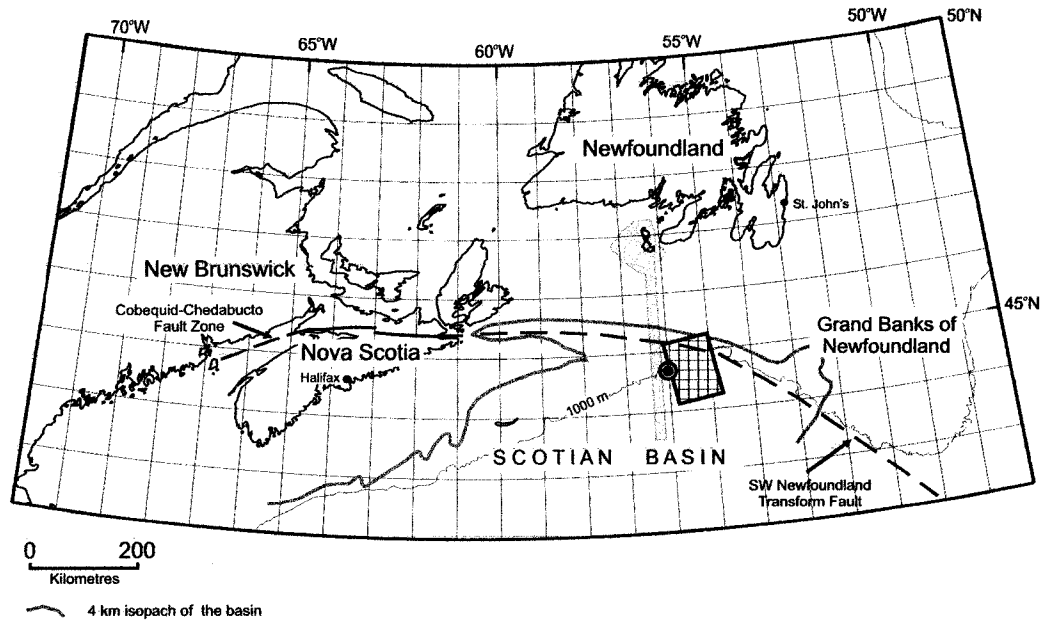


Figure 1.1- Regional map of the southeastern Canadian margin showing extent of the deepest parts (>4 km) of the Scotian Basin, study area (hatched box) and the 1929 Grand Banks earthquake epicentre (●) (modified from Pe-Piper, 2002). The full extent of France's exclusive economic zone (EEZ) is shown (turquoise).

Instead, it is apparent that sediment failures (or mass transport deposits (MTDs)) are numerous and widespread in the form of slides and debris flows (Piper et al., 1999a).

Failure seemingly occurred both synchronously (instantaneous during earthquakes shocks) and asynchronously (occurring after initial shocks), but timing of the subsequent failures is uncertain, and may possibly be related to the two aftershocks that occurred 2.5 and 5.5 hours after the initial shock. Additional sidescan sonar imaging of the failures by SAR (Système Acoustique Remorqué) in 1990 shows the observed failures to be 'fresh', lacking any substantial surficial veneer (Piper et al., 1999a), thus demonstrating the likely relationship of observed sediment failures with the recent earthquake of 1929.

‘Mass transport deposits’, for the purpose of this study, are defined as most deepwater features or stratigraphic intervals that have been resedimented (i.e. moved through a gravity-driven process) since their time of original deposition. This includes deposits such as *glides*, *slumps*, *mass flows* and *creep*.

A *glide* is a mass of sediment that moves downslope on a planar glide plane (e.g. failure plane) or shear surface and shows little or no internal deformation; whereas a *slump* is a mass of sediments that moves downslope on a concave-up glide plane or shear surface and undergoes rotational movements typically causing moderate to extensive internal deformation (Embley and Jacobi, 1977). Glides represent translational movements, whereas slumps represent rotational movements. Movement downslope of a glide or slump block may result in disintegration into numerous, smaller blocks of various sizes that through further downslope movement and subsequent incorporation of water, transform these deposits into *mass flows* that accumulate and deposit as mud clast conglomerates. This process is inferred from seismic reflection data where mass flows are seen immediately downslope and in contact with glide or slump deposits. There is no obvious structure within these mass flows; the deposits typically consist of a matrix with ‘floating’ mud clasts. *Creep* is the gradual downslope displacement of a sediment mass along a failure (or shear) plane. Structure within the translated mass is retained and only slightly distorted, as represented by undulating reflections above the flat failure plane.

1.1 Objectives

Shallow MTDs are fairly well documented on the eastern Canadian margin, particularly on the Scotian Margin where many Late Pleistocene, complex, shallow

MTDs have been documented that closely resemble the disturbed seabed facies documented in this study (Piper et al., 1985; Hughes Clarke et al., 1992; Mosher et al., 1994; Mulder and Moran, 1995; Gauley, 2001; Piper and McCall, 2003; Mosher et al., 2004). The complex relationship between MTDs and the surrounding environment, e.g. highly variable gradients and failure evolution, makes the St. Pierre Slope a unique location for study. Although MTDs at the surface have been studied extensively through sidescan sonar data, no comprehensive seismic reflection- or core-based study has been completed to date. Acoustic data from the St. Pierre Slope show widespread, acoustically incoherent deposits at the seafloor, from just below 500 mbsl to 3300 mbsl, with documentation restricted only by the extent of seismic reflection coverage. Interpretation and systematic classification of observed MTDs, and their interrelations with one another and the surrounding environment has been undertaken in this thesis through integration of these data sets.

This study uses the observed disturbed and undisturbed sediments of St. Pierre Slope to understand the dynamics of sediment mass failures on the slope, particularly those related to the 1929 Grand Banks earthquake, by: I) *Sedimentology*: (a) construct a composite stratigraphy of sediment types from cores containing undisturbed sediments and an acoustic-based stratigraphy to about 75 mbsf, (b) determine rates of sedimentation on the slope and rise and relate these to past climates and current flows; II) *Geomorphology*: (a) establish MTD and evacuation geometries, (b) relate gradients to MTD and evacuation volumes; and III) *MTD classification*: (a) categorize MTDs sampled by piston cores (mesoscale) and imaged in high-resolution seismic data

(macroscale), (b) relate MTDs to other documented MTDs on the eastern Canadian margin and European margin.

Integrating core data, seismic reflection profiles, appropriate sidescan sonar data and submersible observations, and using published and unpublished accounts, will lend insight into the dynamics of failures on the St. Pierre Slope and rise.

The practical applications of this study include: (a) future telecommunication risk evaluation, (b) public safety (e.g. tsunami risk evaluation), and (c) risk associated with drilling into subsurface sediments (petroleum exploration).

Throughout this thesis reference will be made to deposits at the surface as either ‘failed sediments’, ‘disturbed sediments’ or ‘MTDs’ all of which are synonymous.

1.2 Data coverage

With this study largely being based on high-resolution seismic reflection profiles, it was imperative to define a study region that had relatively dense seismic data coverage so as to represent the volume and style of failure as accurately as possible. Data coverage is densest in the middle slope from about 800-1400 mbsl, with an adequate amount of data coverage on the upper and lower slopes at 500-800 mbsl and 1400-2100 mbsl. Downslope of 2100 mbsl to ~3300 mbsl, seismic coverage is sporadic, providing only a general picture of the volume and style of deposition of MTDs. Piston cores are numerous both throughout the defined study area and its outer limits, particularly on the upper and middle slopes. Sidescan sonar data provided a plan view of the seafloor that enabled the visualization of the location of piston cores within morphologically distinct areas and the association of seismic reflection profiles with seabed features of particular

interest. A color relief map, generated from isobaths that were selected from 12 kHz data, demonstrates highly variable gradients on the slope, permitting relationships between slope morphology and MTDs to be studied in plan view, in addition to being studied from 2D seismic reflection profiles.

1.3 Regional setting

The St. Pierre Slope is located in a sedimentary basin complex broadly known as the Scotian Basin (Figure 1.1), which is located under the continental shelf and slope offshore Nova Scotia and southwestern Newfoundland. The basin, covering an area in excess of 50,000 square miles, extends from the Yarmouth Arch to the central Grand Banks and from the edge of the ‘coastal plain’ on the inner shelf to the continental rise (Wade and MacLean, 1990; MacLean and Wade, 1992). The basin comprises shallow basement platforms and ridges that flank deep marginal sedimentary basins leading to the Atlantic Ocean basin to the south.

Development of the basin began in the Mesozoic (~230 Ma) as a series of grabens and half-grabens that resulted from regional extension of the crust. The grabens are floored with redbeds and filled variably with redbeds and salt of Triassic and Early Jurassic age (Jansa and Wade, 1975). The following is a simplified Mesozoic-Cenozoic stratigraphy of the Scotian Basin. The continental redbeds of Eurydice and evaporites of Argo formations are the oldest of the Mesozoic sediments. Continental clastic rocks of the Mohican and evaporitic dolostones of the Iroquois formations formed during the Early-Mid Jurassic. During the Middle and Late Jurassic, the Mohawk, Mic Mac, Abenaki and Verrill Canyon formations, composed of clastic and carbonate facies, formed along the basin margin. Thick fluvial-deltaic deposits of the Lower Cretaceous

comprise the Mississauga and Logan Canyon formations, whereas the overlying Dawson Canyon and Wyandot formations consist of Upper Cretaceous transgressive marine shales and minor limestones, and chalk and marl, respectively. The topmost succession consists of mudstones, conglomerates and sandstones of the Banquereau Formation deposited during the uppermost Cretaceous and during the Paleogene transgression and subsequent Neogene regression. Overlying these formations are Quaternary sediments of the Laurentian formation.

Salt diapirs and pillows are common beneath the basin and these diapirs frequently uplift, deform and sometimes rupture overlying sediment layers (MacLean and Wade, 1992). Slope oversteepening and shallow faulting can be a consequence of salt tectonics and present an initiation point for failure of sediment. Additionally, because diapirism causes deformation and occasional rupture of overlying and adjacent sediments, it has a tendency to facilitate upward migration of gas and fluids along these disturbed areas, which also can contribute to slope instability.

1.4 Local geologic setting

St. Pierre Slope extends from the shelf break at 200 mbsl to 2100 mbsl where the continental slope gives way to the continental rise. The slope is bounded to the west by the Eastern Valley and to the east by the Grand Banks Valley (Figure 1.2). Slope valleys dissect the area, with the largest being the St. Pierre Valley (thalweg depth of

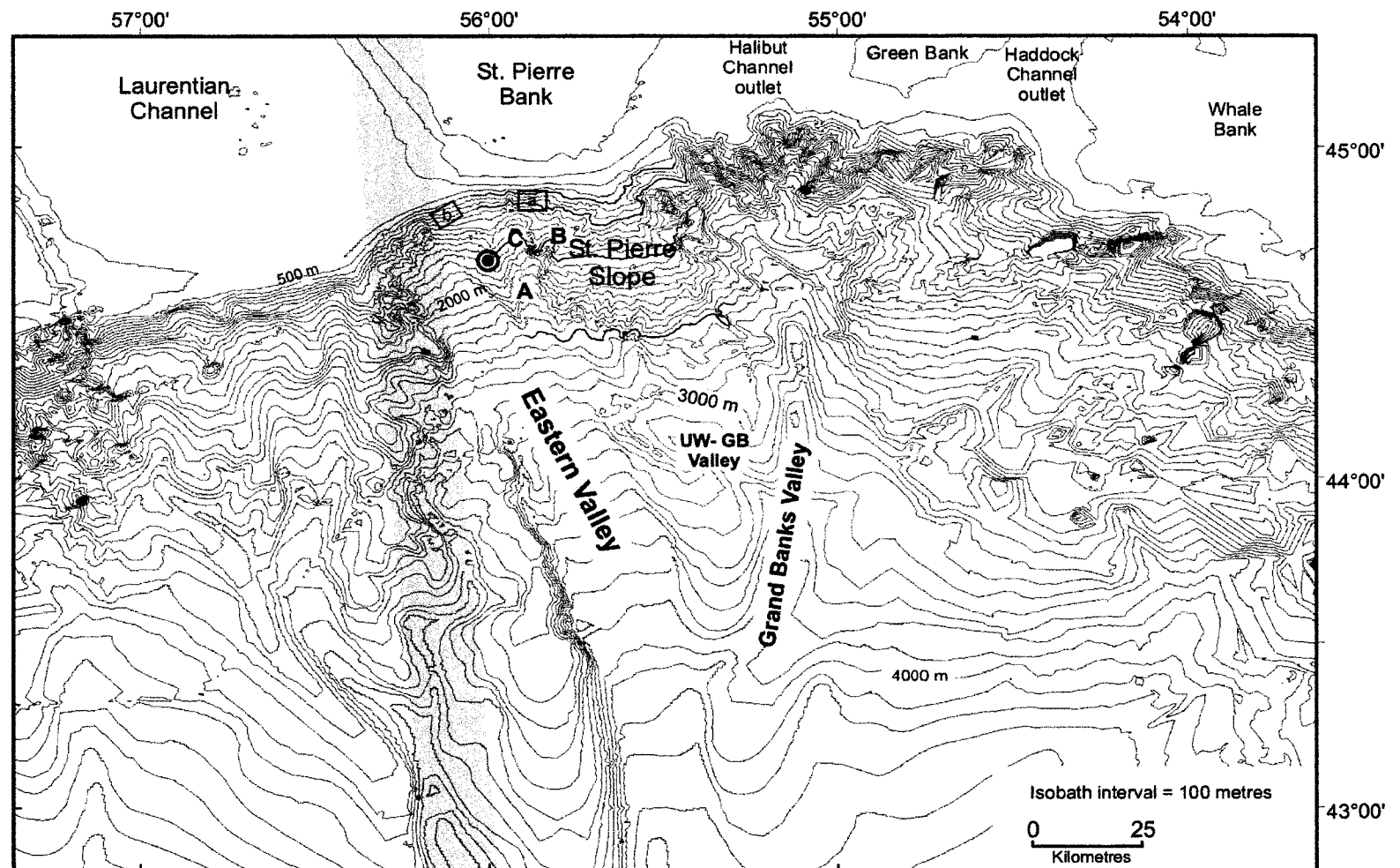


Figure 1.2- Bathymetry map of study area (yellow) and vicinity. Epicentre (●) of 1929 Grand Banks earthquake, major valleys and associated tributary valleys, and upper boundaries of upper, mid and lower slope, and rise (red lines) are shown. Boxes represent locations of Figures 1.3 a and b. UW-GB Valley= upper Western Grand Banks Valley; A= St. Pierre Valley; B= upper Eastern St. Pierre Valley; C= upper Western St. Pierre Valley. A section of France's exclusive economic zone (EEZ) is shown (turquoise). Bathymetry courtesy of GSCA.

300 m), which likely originated from proglacial erosional processes. Farther downslope to about 3500 mbsl, the seafloor is broadly incised by Grand Banks Valley and associated tributary valleys, and at about 4000 mbsl, the Grand Banks Valley merges with Eastern Valley. Gradients of the upper, middle and lower slope generally do not exceed 5° , except on and near valley heads and sidewalls, and at scarps. The rise (which begins at ~2500 mbsl) is much gentler with gradients usually not exceeding 1° .

On the upper slope, stretching from the head of Eastern Valley to the western edge of the canyons off Halibut Channel, arcuate headscarps are visible in water depths exceeding 500 m. At the head of Eastern Valley these headscarps are numerous with widths generally not exceeding 750 m, with the larger headscarps present off St. Pierre Bank just below the 500 m isobath (Figure 1.3). Failure has not occurred above the 500 m isobath as sediments are more consolidated due to till deposition and iceberg scouring (Bonifay and Piper, 1988; Piper et al., 1999a).

Numerous MTDs exist throughout the study area, transforming a seabed that presumably was once smooth and undisturbed to one of high surface irregularity (Figure 1.3). MTDs on the rise are generally thicker and stacked (Piper et al., 2005). Pockmarks are widespread on the upper and middle slope down to 1000 mbsl and in some areas lie within a few metres from headscarps and sidewalls in undisturbed sediments, and clearly cut rotational slumps (Figure 1.3) (Piper et al., 1999a).

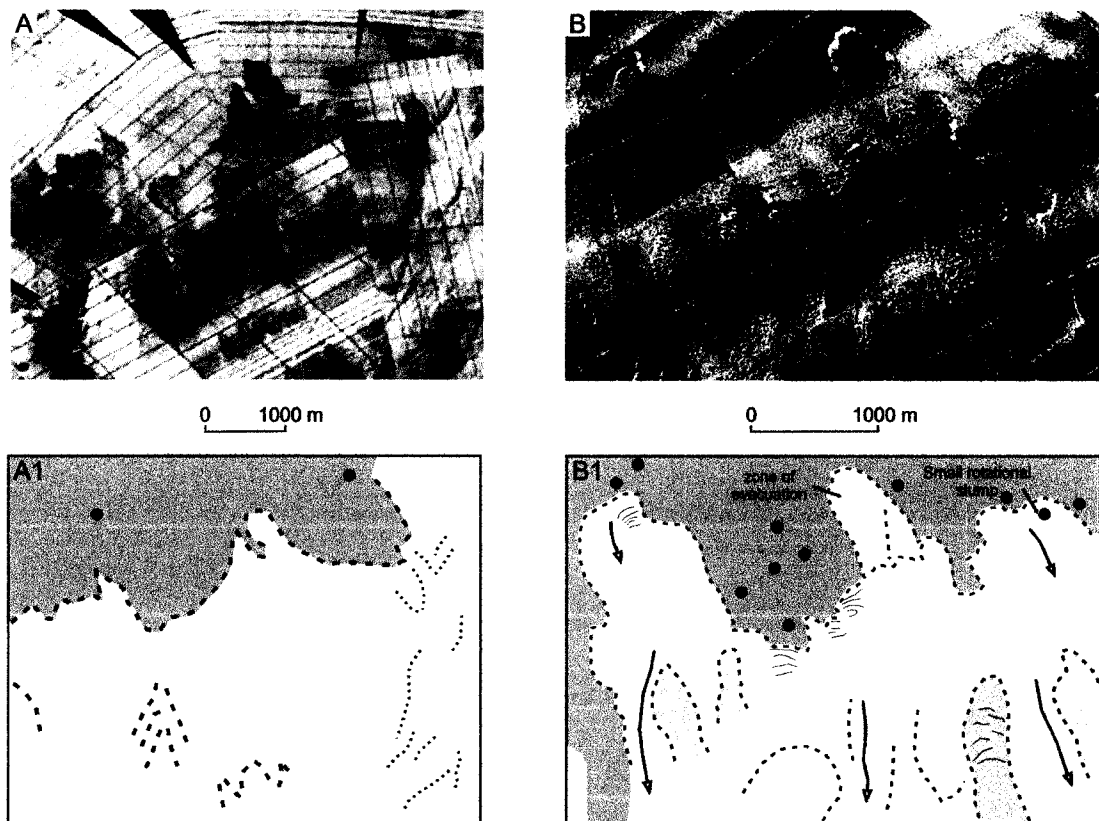


Figure 1.3- A) SeaMARC I sidescan sonar images and associated interpretation (A1) of upper St. Pierre Slope. In A1, headscarps (dashed lines), downslope-trending lineations (dotted lines) and pockmarks (●) are illustrated. B) SAR sidescan sonar images and associated interpretation (B1) from head of Eastern Valley. In B1, numerous headscarps (dashed lines), mass transport deposits (peach- blocky debris flows, orange- rotational slide), flow channels (arrows), sub-parallel ridges (lines) and pockmarks (●) are illustrated. Undisturbed seabed is in gray. Interpretation from Piper et al. (1999a). Locations of figures are in Figure 1.2.

1.5 Previous work on MTDs from St. Pierre Slope

Studies pertaining to mass transport deposits encountered on the St. Pierre Slope have chiefly utilized sidescan sonar data with some accompanying high resolution seismic reflection data (mainly 3.5 kHz data) to ascertain failure properties and characteristics (Piper et al., 1985; Piper et al., 1988; Hughes Clarke et al., 1990; Piper et al., 1999a). Piper et al. (1999a) interpreted SAR data and older SeaMARC I data to arrive at the most complete published study on MTDs from this region to date. The authors

defined the slope quantitatively and showed that St. Pierre Slope is composed of several distinct seabed zones (these zones are not related to the seabed zones described in Chapter 3). The *disturbed seabed zone* consists of flat seabed or dissected seabed, both of which have rotational slumps and debris flow deposits of varying size. Slumps in the area involve both small (thin- a few metres) and large amounts of sediment (thick- tens of metres). Debris flow deposits typically exist immediately downslope of rotational slumps and near steep slopes of St. Pierre Valley. Seabed zones mildly affected by the 1929 event include: *valley floors, gullied ridges and spurs* (mostly Laurentian Fan), and *flat, undisturbed seabed* to 1400 mbsl. The *valleys* commonly have complex sediment facies deposited on the floor, and valley walls that are up to hundreds of metres in height. The *flat, undisturbed seabed zone* is primarily restricted to the upper continental slope, to depths of about 550 m. Seabed facies distribution on the St. Pierre Slope is as follows. The middle slope (700- 1400 mbsl) is characterized by widespread failure, predominantly slumping with some debris flow deposits. In water depths between 700-900 mbsl and farther downslope, initiation of failure (predominantly slumping) appears to have been caused by a local increase in gradient: up to 10° and 6°, respectively. The lower slope (1400-1900 mbsl) is dominated by large rotational slumps that are partially covered by smaller rotational slumps. The transition of slumps into debris flows is visible in sidescan sonar sonograms. Farther downslope, debris flow deposits are the main features and occur on gradients of 1-5°, but pass downslope onto the St. Pierre Valley walls where mean gradients are 3-5° but locally can exceed 20°.

1.6 Previous stratigraphic studies

Comprehensive studies on the shallow (>75 m thickness) stratigraphic succession of St. Pierre Slope are lacking. Piper and Skene (1998) and Skene and Piper (2003) conducted studies on Laurentian Fan beginning at 3000 mbsl and Bonifay and Piper (1988) on the upper St. Pierre Slope down to about 600 mbsl using both seismic reflection and core data. Piper and Normark (1989), MacDonald (2001), and Piper et al. (2005) interpreted deep multichannel seismic reflection data to arrive at a late Cenozoic stratigraphy of the St. Pierre Slope, each subsequent paper building on the former. However, no core stratigraphy has been described for the main part of St. Pierre Slope, nor has a high-resolution seismic stratigraphy been attempted. This study will aim to bridge the gap between the previously established seismic and core stratigraphies, forming the first complete late Quaternary stratigraphic record from the upper St. Pierre Slope down to the rise, including the Laurentian Fan.

1.6.1 Late Cenozoic stratigraphy

Piper and Normark (1989) developed a Late Cenozoic stratigraphic sequence using high-resolution multichannel seismic reflection profiles for the upper 0.8 seconds of sediment for the upper to middle St. Pierre Slope. The base of the sequence is a local erosion surface (reflection E) with broad, shallow channels. These channels are draped by packets of reflections that have locally eroded the channel walls and are capped by pronounced reflection 'D'. Locally, the surface of reflection D is disrupted by low relief channels and shows levee growth. Elsewhere, this reflection is overlain by parallel reflections interpreted as a prograded mud sequence. By 100 ms above D, gullies are

developed and become widespread about 200 ms above D to reflection C. Levee development above reflection C seems localized particularly on the west flank of Halibut Channel and along small valleys existing at the east edge of Laurentian Channel. Reflection B marks a period of substantial local erosion and the apparent termination of levee-like aggradation. Upslope, reflection B marks the base of acoustically incoherent sediments that pass downslope into well-stratified sediments. Reflection A marks the top of well-stratified sediments. There is some levee growth and gully cutting above reflection A.

Inferred events associated with the above-defined reflections of the St. Pierre Slope are as follows (Piper and Normark, 1989): E- lowstand of sea-level and cutting of slope valleys; D- highstand of sea-level and deposition of mud drape; C- Lowstand and widespread development of slope gullies; and A and B- slope crossing glaciation and some slope gully cutting.

Building on the Late Cenozoic seismic stratigraphy, MacDonald (2001) and Piper et al. (2005) used new multichannel seismic reflection profiles together with Miocene-Pliocene biostratigraphic picks from the Hermine E-94 well on the Grand Banks. The framework completed by Piper et al. (2005) follows that of MacLean and Wade (1992) but with a slightly different age interpretation resulting from the data obtained from the Hermine E-94 well. They defined reflections Q10, Q30, Q40, Q50, Q70, Q80 and Q90 (oldest to youngest). Reflection Q10 is fairly continuous from the upper slope to the rise and has been correlated to reflection C of Piper and Normark (1989) with an age of basal Quaternary. Reflections Q30, Q40, Q50 and Q70 are traced over wide areas from the upper to lower slope but are interrupted in places by MTDs and buried failure scarps,

especially in the middle slope. Correlation of these reflections from the slope to rise was done by event correlation of MTDs and failure scarps. Reflections Q80 and Q90 were difficult to correlate due to shallow erosion and mostly were recognised in less-dissected areas on the upper slope.

On the upper slope, acoustically incoherent units (a total of six- I, II, III, IV, V and VI) are interpreted as ‘till tongues’ emplaced by glacial activity. The deepest well-developed till tongue immediately overlies reflection Q50. Acoustically incoherent bodies exist down to reflection Q30 but it is unclear whether these are till tongues or MTDs. A 30 ka radiocarbon age obtained from a 56-m-deep failure plane is at or near Q91, which is just below the horizon of the youngest of six defined till tongues. The till tongues, compared with dated sections of the J-Anomaly Ridge and Bermuda Rise, provide a consistent age model corresponding to marine isotopic stages (MIS) 2, 4, 6, 8, 10 and 12 (Piper et al., 2005). Reflections Q50 and Q10 have been correlated to reflections Q and B of Laurentian Fan (Skene, 1998) using industry seismic profiles (courtesy of TGS Nopec- survey conducted in 1998) (Piper et al., 2005).

1.6.2 Quaternary stratigraphy

1.6.2.1 Acoustic- and shallow core-based stratigraphy of the St. Pierre Slope

The upper slope stratigraphy of the St. Pierre Slope has been described by Bonifay and Piper (1988) using seismic reflection profiles and piston cores obtained from St. Pierre Slope. Five separate acoustic facies were distinguished (designated a to e): a lowermost sedimentary facies (e) characterized by incoherent reflections overlain by four distinct stratified sedimentary facies with variable thicknesses of 5-20 metres (facies a to

d). The lowermost sedimentary unit consists of slumped morainal diamict and proglacial sediments and has been dated at 11.5- 12.0 ka by radiocarbon dating. Penetration by cores into this unit was poor (none exceeded 1.5 m penetration) implying that the sediments are either pebbly or highly consolidated. Sediments of the remaining four units contain turbidite and rare ice-rafted debris. The sediments are bioturbated and yield ages ranging between 3.3- 11.8 ka. Sedimentation rates close to the ice margin were estimated at 20 m kyr⁻¹.

Distribution of sediment on the continental slope and rise has been summarized by Piper (1991). The shelf-edge consists of Late Quaternary sands with variable gravel patches grading seawards into silty muds. These Quaternary sedimentary sequences comprise alternating till and glaciomarine beds, the result of repeated advance and retreat of the ice margin. The slope is composed predominantly of dissected or discontinuous stratified mud sequences with occasional slumps and debris flow deposits. Thick stratified mud sequences with minor silt interbeds begin around 3000 mbsl and continue to the basin. Floorings local channels are Upper Pleistocene to Holocene sand or gravel deposits (thicknesses upwards of 100 m) that may be accompanied by a drape of pelagic or hemipelagic sediments. These shallow subsurface and surficial sediments of the St. Pierre Slope developed in response to Late Quaternary glacial events, specifically the last major glacial advance of the Wisconsinan glaciation and subsequent Holocene processes.

1.6.2.2 Shallow core-based stratigraphy of Laurentian Fan

Piper and Skene (1998), using information from four piston cores (two of which are used in this study = 87003-09 and -10) from >3000 mbsl, ascertained the

sedimentation history within the last 15 ka on Laurentian Fan. Four events of rapid iceberg discharge, identified in cores as brick red mud beds a, b, c and d (BRM), deposited brick red gravely, sandy mud seaward of the Gulf of St. Lawrence. The oldest bed (BRM-d) underlies a detrital carbonate (DC) bed on the Laurentian Fan that corresponds to DC-1 in the Labrador Sea (Andrews and Tedesco, 1992) and Heinrich layer 1 in the North Atlantic (Dowdeswell et al., 1995). Both of these layers, DC-1 and H-1, are thought to represent catastrophic collapses of the Laurentide Ice Sheet, that produced large and rapid discharge of icebergs, which subsequently increased the concentration of IRD and detrital carbonates in thin sediment layers. Radiocarbon ages for the brick red mud beds are: d- ~14ka, c- >12.9 ka, b- between 12.55 and 13 ka, and a- <10.5 ka. An age of <10.5 ka for BRM-a places it within the Younger Dryas, a period of extreme climate fluctuation. Grain sizes from the four beds suggest an ice rafted component that diminishes distally and a fine mud component that increases distally, the latter suggests suspension fallout from a surface plume as represented by resultant nepheloid layers.

Skene and Piper (2003) built upon the stratigraphic record of Laurentian Fan since the time of the Last Glacial Maximum (LGM) using information obtained from 10 piston cores. They identified five lithofacies from the cores: a) bioturbated, olive-gray silty mud with varying amounts of biogenic carbonate; b) olive-gray and reddish-brown silt laminated mud with rare fine to very fine sand beds; c) poorly sorted, light gray and brick-red gravely, sandy mud; d) colour-banded silty mud with colours alternating between olive-gray and reddish-brown on a cm scale; and e) commonly massive brown silty mud, that occasionally contains silt laminae. The dominant depositional processes

for these lithofacies include hemipelagic sedimentation, turbidity currents and ice rafting. Sediments were delivered from the following areas: reddish sediment from the Gulf of St. Lawrence and Laurentian Channel and greenish sediment from St. Pierre Bank through Grand Banks Valley. Ice rafted beds exist on a volumetrically small scale but are significant chronologically and include Heinrich layers H0-H2. Ages obtained from the cores using radiocarbon dating and stable oxygen isotopes suggest a sedimentation rate exceeding 10 m kyr^{-1} for the reddish-brown turbidites deposited between LGM ($\sim 18\text{ ka}$) and 14 ka . Less is known of the olive-gray turbidites except that they had a lower sedimentation rate and include sediments derived from Newfoundland and the Grand Banks. Accumulation rates of hemipelagic units are on the magnitude of approximately 0.1 m kyr^{-1} .

Four major phases of deposition since H2 (21 ka) were established: I) around the LGM (18 ka)- the Laurentian Fan was the site of primarily hemipelagic deposition with small amounts of turbidites; II) after LGM to 14 ka - hemipelagic deposition in deep water and rare events depositing reddish-brown turbidites on Laurentian Fan; III) post 14 ka - coeval deposition of reddish colour-banded and brown mud turbidites on central portions of Laurentian Fan, olive-gray hemipelagic muds deposited on the western side of Laurentian Fan and olive-gray turbidites deposition on eastern side of Laurentian Fan; and IV) widespread hemipelagic deposition off Laurentian Channel beginning at 12 ka .

In Chapter 5 (Table 5.1), the above core-based facies from previous authors (i.e. Bonifay and Piper, 1988; Piper and Skene, 1998; Skene and Piper, 2003) have been related to each other and to the defined sediment facies of this study (seen in Chapter 4).

1.6.3 The Laurentian Channel ice outlet

Building on previous work (e.g. Bonifay and Piper, 1988 for St. Pierre Slope; Moran and Fader, 1997 for Halibut Channel), Piper and MacDonald (2002) used seismic reflection and piston core data to approximate the position and timing of Late Wisconsinan ice-margins on the upper Laurentian Slope seaward of Laurentian Channel. A prominent morainal ridge identified in seismic data at 500 mbsl represents the Last Glacial Maximum ice grounding line at about 18 ka. A change in thermal regime or a subglacial meltwater outburst between ~16.5 and ~16.4 ka resulted in release of sediment-laden meltwater that caused widespread erosion and gully formation on the continental slope. This erosion surface is overlain by diamict that extends to 700 mbsl and may represent till deposition from a glacial surge. By 16.3 ka the ice margin had retreated upslope likely to the prominent moraine at 380 mbsl located at the mouth of Laurentian Channel. This ice position likely persisted until 14.2 ka, supplying sediment to the Laurentian Fan as represented by mud turbidite deposition. Deposition of these turbidites ceased abruptly, typically existing ~0.5m above the topmost turbidite is a distinctive bed of ice-rafted sandy gravely mud derived from the Gulf of St. Lawrence that is dated at 14ka (Piper and Skene, 1998). Ice then retreated rapidly northwards up Laurentian Channel synchronous with Heinrich event 1 at about 14 ka. Following this retreat, ice occupied Halibut Channel (Moran and Fader, 1997) and crossed St. Pierre Bank (Bonifay and Piper, 1988) at about 12 ka. At about this time, slumping of proglacial sediments on the upper slope likely resulted from loading by a late-ice advance across St. Pierre Bank. DeVernal et al. (1996) show reduced meltwater runoff, low temperatures and extensive sea-ice cover during the Younger Dryas event, dated at 10.8 and 10.3 ka

through examination of cores 90031-047 and 044, respectively taken in and at the outlet of Laurentian Channel. Meltwater pulses did occur both before (11.7 ka) and after (10.1 ka) the Younger Dryas event.

CHAPTER 2

Methods

2.1 Acoustic instruments and data

Seismic reflection data from Geological Survey of Canada (Atlantic) cruises 91020, 99036, 2001043, 2002046 and 2003033 aboard the CCGS *Hudson*, and sidescan sonar data from IFREMER SAR (cruise 90015) and SeaMARC I (cruise 83017) instruments were used for this thesis (Figure 2.1) (cruise reports are housed at the GSCA). The main source of seismic reflection data was the Hunttec DTS system, with conventional seismic reflection (airgun), 3.5 kHz and 12 kHz being used in places.

During cruises 99036, 2001043, 2002046 and 2003033, the differential global positioning system (DGPS) was used for navigation and is accurate to within a few metres. Cruise 91020 utilized the BIONAV integrated navigation system with the Trimble GPS and Loran-C receiver as the main source of input. Good GPS fixes were available on a 24-hour basis. During acquisition of SeaMARC I data, Loran-C system was used in combination with transit satellite fixes with no overland phase lag correction performed on Loran-C data. During acquisition of SAR data, GPS was used for 15 hours per day for navigation and Loran-C for the remainder, therefore significant transition gaps exist between the systems. SeaMARC I towfish position was estimated by length of cable out and SAR towfish position was estimated by slant range and pressure depth, heading of towfish was recorded as well. Geographic positions of sidescan sonar data (TIFF images) and associated interpretations from SAR and particularly the SeaMARC I are only approximate due to the imprecise navigation methods described above.

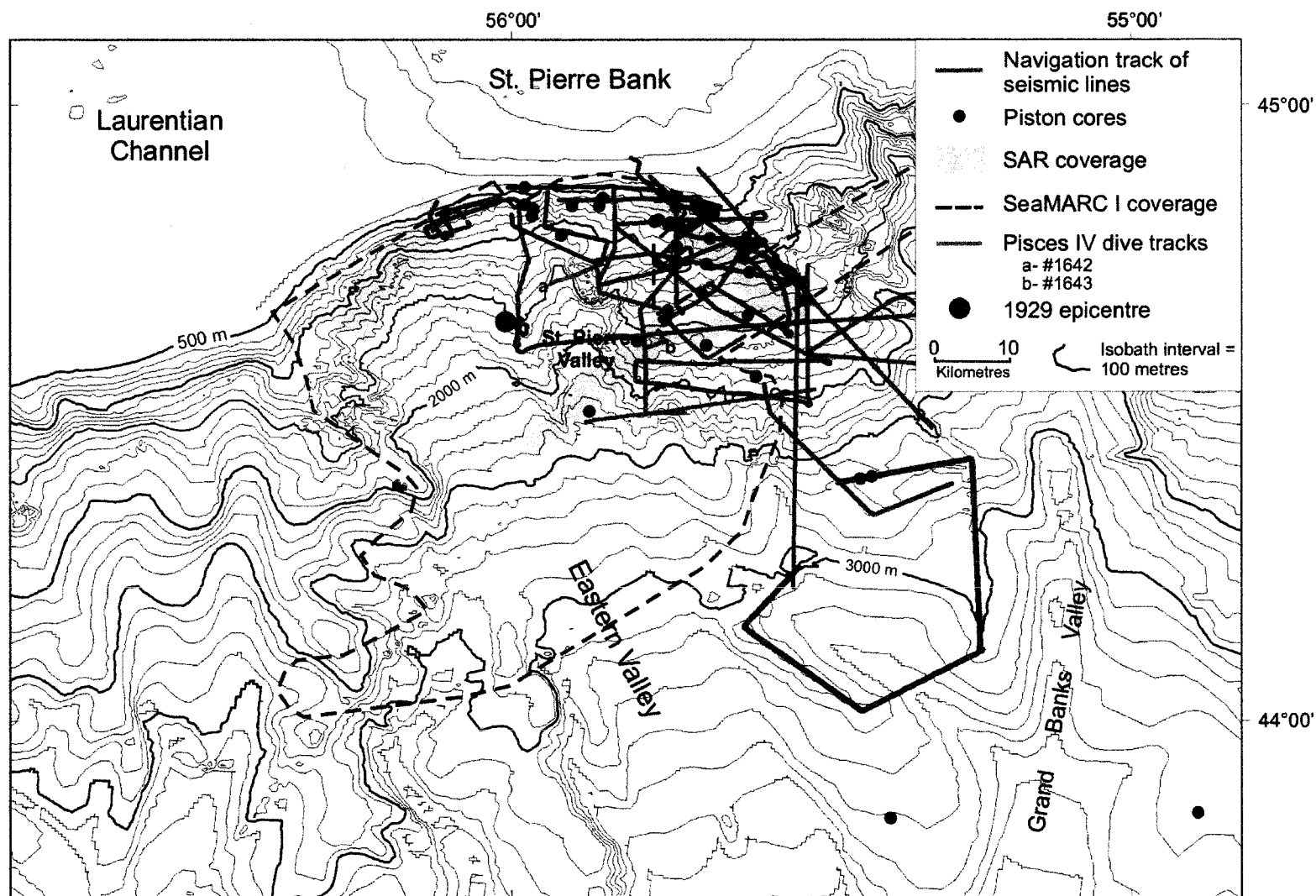


Figure 2.1- Locations of seismic reflection lines and cores used for this study. SAR coverage is shown in green and SeaMARC I coverage is outlined (dashed line). Selected Pisces IV submersible dive tracks are shown.

2.1.1 Hunttec DTS

Approximately 1,000 line-km of Hunttec Deep-Towed Seismic (DTS) sparker and boomer data were collected during cruises 91020*, 99036, 2001043*, 2002046 and 2003033. All seismic records considered useful for this study were copied at 50% the original size and used as working copies.

The Hunttec DTS system (commonly referred to as a ‘fish’) is towed about 100 m below the sea surface and is heave and depth compensated. Seismic signals are normally received on a 5 m-long, 10-element oil filled streamer towed behind the fish. Signals are filtered at 500 Hz-10 kHz with spreading loss gain recovery. Early cruises utilized a boomer sound source; a sparker was used during cruises of 2001, 2002 and 2003. The source can be operated at 100-1000 Joules input. The signal contains a broad frequency bandwidth (up to 6 kHz), which yields an optimal vertical resolution of about 0.25-0.5 m. Signal levels are generally sufficient to yield acoustic imaging up to 100 ms below the seafloor. Further information on Hunttec DTS sparker and boomer systems and details regarding the conventional seismic reflection (airgun) and 3.5 kHz systems are summarised in Mosher and Simpkin (1999).

Gradients labelled in Hunttec DTS figures are true maximum gradients and not along profile apparent-gradients.

2.1.2 Sidescan sonar

The SeaMARC I is a deeply towed instrument consisting of a 4.5 kHz subbottom profiler and 27 kHz and 30 kHz sidescan sonar transducers producing records with slant

* Primary sources for most of the seismic data available and used for this study.

range corrections and a swath width of up to 5 km (Kosalos and Chayes, 1983).

Interpretations of SeaMARC I data are found in Piper et al. (1985). The IFREMER SAR (Système Acoustique Remorqué) is a deeply towed package consisting of two sidescan sonar transducers operating at 170 kHz and 190 kHz and a 3.5 kHz subbottom profiler. The swath produced is 1.5 km wide and the system is capable of 0.25-metre resolution. Interpretations of SAR data are in Piper et al. (1999a).

2.2 Piston and associated trigger weight cores

A total of eighteen piston cores and most associated trigger weight cores were obtained during cruises 84003, 86034, 87003, 90015, 91020, 99036, 2001043, and 2002046. Cores were chosen from the slope and rise, in water depths ranging between 500 and 3300 mbsl, to provide a complete composite stratigraphy of the study area. All cores are located at the GSC Atlantic core facility. Cores collected before 1985 are stored at ambient temperature ($\sim 21^{\circ}\text{C}$) and later cores in cold storage at $\sim 4^{\circ}\text{C}$. All piston cores after 1985 were collected using the AGC Long Corer. This device obtains a core sample with an inner diameter of 99.2 mm and an open diameter of 106 mm, with barrel lengths from 10 to 16 m. The core head is 3 m long, 0.6 m diameter and weighs approximately 900 kg. The core pipe is in 3.3 m lengths, 4.25" inner diameter, with 3/8" wall thickness, and exterior couplings secured by setscrews. The liner used is a CAB plastic extruded into 3.3 m lengths. A catcher is used at all coring sites. The core uses a 3/4" wire cable on the Pengo winch. The corer is operated using a handling system including a rotating core-head cradle, outboard support brackets, a monorail transport system, a lifting winch and a processing half-height sea going container. The piston corer uses the following

dimensions for a 13 m core: head 2.5 m, scope 3.5 m', barrels and cutter 7'; trip arm dip 1 m, wire 16 m, trigger weight core 4 m. The scope is appropriate for 2 m penetration of the trigger weight core. Most of the piston cores used for this thesis have trigger weight cores. The trigger weight core is acquired through gravity processes as the apparatus is lowered through the water column and not through the free fall process associated with the piston core. The procedure of acquiring piston cores sometimes disturbs the upper few metres of sediment, thus disrupting the stratigraphy and making stratigraphic placement of the core difficult (Buckley et al., 1994; Skinner and McCave, 2003). The trigger weight core essentially captures some of this upper few metres of sediment with minimal disturbance to the stratigraphic record. Procedure for storage of piston and trigger weight cores once ashore is described in Gauley (2001) and further details on the coring apparatus can be viewed in Hundert (2003).

2.2.1 Laboratory techniques

All piston cores have downcore plots that show core lithology and sediment color, and an interpretation of MTDs for cores containing disturbed sediments (Appendix 2). Cores collected in 1999 to 2002 have the most complete analyses. This includes Geotek multi-sensor track (MST) and spectrophotometer data. The MST device measures Gamma Ray alternative; a proxy for bulk density, P-wave velocity and magnetic susceptibility at a resolution of 1 cm. Discrete P-wave velocity and shear strength measurements are taken in 10 cm intervals where possible on split cores. Color is measured using a Minolta Spectrophotometer at 5 cm intervals on a split core face. Measurements are expressed in terms of the L*, a*, and b* color values. Shear strength

measurements accompany most cores. Cores collected in 1984 to 1991 lack magnetic susceptibility and spectrophotometer measurements.

A few of these older cores were reanalysed to acquire spectrophotometer data.

Geotechnical and spectral data aided in the discrimination of both the undisturbed and disturbed facies. All sediment colors were first distinguished during visual description of the cores. Some colors, e.g. tan mud and brick red mud, were confirmed by high values in spectral 'a*' and for tan mud, usually a strong increase in magnetic susceptibility further confirmed identification. Bulk density and shear strength measurements of cores taken from zones affected by failure of sediment (e.g. downslope of scarps) were used to estimate the in situ thickness of sediment cover prior to failure.

2.2.2 Accelerator Mass Spectroscopy (AMS) Radiocarbon Dating

Accelerator mass spectroscopy (AMS) radiocarbon dating was conducted on selected carbonate material, such as foraminifera and mollusc shells, using the ratio of ^{14}C to ^{12}C as a measure of age. Carbon is extracted from the carbonate and then the carbon sample is ionized. The AMS charges the carbon ions that are then accelerated toward a detector (Bowman, 1990). Due to their different masses, the ions reach the detector at different times, allowing the measurement of the two carbon isotopes. AMS can date material in the ca. 200-40,000 year age range. Since the samples were from a marine environment, they require a reservoir correction of -410 years applied to them in order to account for the time-lag between isotopic changes in the atmosphere and changes in the ocean (Stuiver et al., 1998). AMS radiocarbon dating was utilized in this study, as opposed to conventional methods, due to the smaller sample size required (50-100 mg).

2.3 Bathymetry

The regional bathymetric grid provided in this report was generated from depth soundings compiled by the Geological Survey of Canada (Atlantic). The compilation consists of single beam echo soundings corrected to a common seawater velocity of 1463 m/s for depth conversion. Approximately 210 000 points were used after cleaning of outliers. Other more detailed regional bathymetric maps exist but are under copyright terms that prohibit distribution outside the GSCA. A detailed bathymetry of the St. Pierre Slope was completed by Martin Morrison using 12 kHz data digitized at 1-minute intervals at a seawater velocity of 1463 m/s and is published in Piper et al. (1999a).

All bathymetry maps and shaded relief maps have been produced using the Geographic Reference System. The system consists of latitude and longitude, and treats the globe as if it were a sphere. The sphere is divided into 360 equal parts called degrees. Each degree can be further subdivided into 60 minutes, each composed of 60 seconds. The standard origin is where the Greenwich Prime Meridian meets the Equator. All points north of the Equator and east of the Prime Meridian are positive.

2.4 Classification of disturbed seabed

2.4.1 Acoustic facies

Failures were identified and classified based on displayed acoustic character from high-resolution seismic reflection data following a similar approach to Nardin et al. (1979) and Lee et al. (2002). In most cases, features showing properties of disturbed seabed, such as rotated blocks, were of sufficient size to be captured and subsequently identified in the high-resolution seismic data. However, in some instances the footprint of the Hunttec DTS system in deep water was too large, masking features critical for

categorizing the deposit into one of the defined MTD facies. In such cases, sidescan sonar data aided in the identification and discrimination of one acoustic facies from another as its resolution is of a finer scale.

If an MTD is located on a steep gradient or its components are dipping (slumped beds), the imaging capabilities of the seismic source are further reduced. If a body and its components are tilted by an angle $>15^\circ$, coherent reflections will not be returned (Mosher and Simpkin, 1999). This situation is important for the internal components of a body, such as bedding plane contacts, which can become masked.

2.4.2 Core-based disturbed facies

MTDs were identified and classified in piston and trigger weight cores based on observed sediment character and physical properties. These features include but are not limited to dipping or disturbed beds and laminations, dipping facies contacts, mud clasts and mixing of contiguous lithologies, and variations in bulk density, shear strength and sediment color. The seven cores that sampled MTDs were projected onto the nearest seismic reflection line to get an idea of the surface and subsurface acoustic environment from which the core was taken. Cores were also projected onto sidescan sonar images wherever data permitted, giving a plan view of the area where each core was obtained.

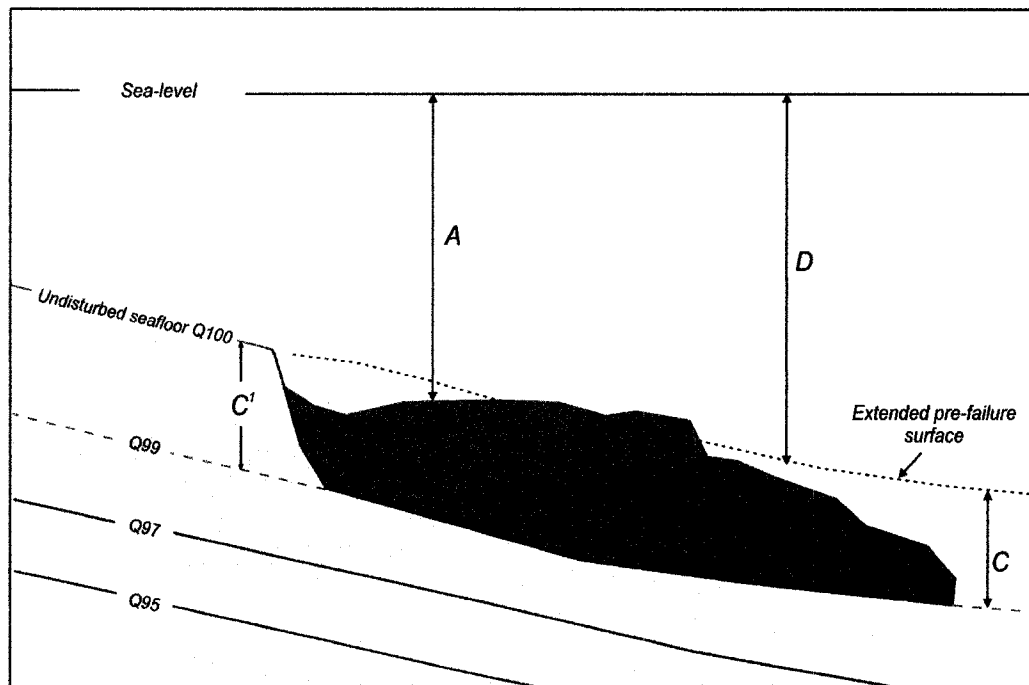
2.5 Determining stratigraphic thicknesses from Hunttec DTS data

The following paragraphs and illustrations deal with the procedure of measuring and calculating depths, total areas and volumes of MTDs, total amount of in-situ sediment that was disturbed, and total amount of sediment ‘missing’ (transported from in-

situ to elsewhere). Values are listed in Appendix 1. Figure 2.2 illustrates a typical situation encountered in the Hunttec DTS data.

2.5.1 Definition of terms

Depth to present seafloor from sea-level ('A' in Figure 2.2) = time from sea-level to seafloor measured from 12 kHz data and correlated to Hunttec DTS data



- A = Depth to present seafloor from sea-level (ms)
- B = Thickness of MTD (ms)
- C = Total thickness of original stratigraphy disturbed during failure (ms)
- C¹ = Depth used for extending undisturbed seafloor into disturbed area (ms) and for obtaining the value of C
- D = Depth to pre-failure seafloor from sea-level (ms)

Figure 2.2 - Illustration of a MTD showing five main components (A-D) used in estimating depths and volumes of failed and evacuated sediments.

to ensure correct location. Time is in milliseconds. Conversions from ms to metres are based on an assumption of a 1463 m/s velocity through seawater. This assumption of 1463 m/s is cited throughout the literature and has been published in numerous works.

Thickness of MTDs ('B' in Figure 2.2) = time from the seafloor to the base (failure plane) of the MTD. Time is in milliseconds. Conversions from ms to metres are based on a sediment velocity assumption of 1500 m/s (this is the same for all millisecond-to-meter depth conversions in sediments). If the time is 25 ms, depth conversion gives 18.75 m. This is as follows:

1500 m/s is TTWT (two way travel time)

- only need one-way travel time, so
 - $1500/2 = 750$ metres/second
- convert second to milliseconds, so
 - $750/1000 = 0.75$ metres/millisecond
- $0.75 \text{ m/ms} * 25 \text{ ms} = 18.75 \text{ m.}$

Total thickness of original stratigraphy disturbed during failure ('C' in Figure 2.2) = the time of the nearest undisturbed stratigraphy (C^1) was extended into areas affected by failure to give an estimate of the total thickness of sediment that was disrupted during failure. Thicknesses were taken from this extended surface down to base of the MTD. Time is in milliseconds and is converted to depth using the procedure above (for B).

Depth to pre-failure seafloor from sea-level ('D' in Figure 2.2) = this is calculated as follows: $(A+B) - C = D$. Time is in milliseconds. Conversions from ms to metres are based on an assumption of a 1463 m/s velocity through seawater. Below is an example of the process of calculating the 'D' value:

e.g. $A = 1000$ milliseconds (ms), $B = 15$ ms, $C = 40$ ms

Therefore: $D = (1000\text{ms} + 15\text{ ms}) - 40\text{ ms} = 975\text{ ms}$ time to pre-failure seafloor from sea-level

The cross sectional area of an MTD was calculated by multiplying the lateral extent of the MTD by its mean thickness. Lateral extent was estimated from the seismic record using 1 minute equivalent to 150-160 m of ship motion at a steaming velocity of 4-6 knots. Volume estimates are described in detail in Chapter 3.

2.6 Distinction between valleys and channels

Valleys and channels are mentioned throughout this thesis. The distinction here is that valleys are greater in both vertical and horizontal extent with heights being many tens of metres and widths many kilometres (e.g. St. Pierre Valley). In contrast, channels are defined as subtle topographic depressions that are a few metres in height and tens of metres wide (see Figure 3.10).

2.7 Errors and limitations

There are several errors and or limitations that are associated with measurements from field and lab instruments, as well as human measurements and interpretation, that are unavoidable and thus are reflected in this thesis.

The Hunttec DTS has an optimal vertical resolution of 0.25-0.5 m. However, the tool is limited in its horizontal resolution, which is measured in hundreds of metres (known as ‘footprint’) compared with a horizontal resolution of 10 m (per pixel) of the sidescan sonar tool.

Due to the limitations of the seismic and sonar tools discussed above, the core-seismic correlation does have some uncertainty, specifically in pinpointing where the

core penetrates the seismic profile (or where to place the core within the profile, e.g. above or below the 'surface' reflection). Synthetic seismograms could have aided this problem, but due to the presence of gas expansion throughout the cores, measured velocity data is erroneous. If further study is needed, a velocity assumption of 1500 m/s could be used.

Radiocarbon ages for reflections Q99 (orange reflection) and Q91 (yellow reflection) have been estimated at 15.3 ka and 30.2 ka respectively (Ch. 4, 5). These ages have associated errors due to, for example, a reservoir correction of -410 years and analytical error that assigns the age a +/- value up to 300 years. Therefore, the ages stated can vary by as much as 750 years. Reliable radiocarbon ages for reflections Q93, Q95 and Q97 bounded below by Q91 and above by Q99 are unknown but were extrapolated. The assumption is that sedimentation rates from about 30 ka to 15 ka remained relatively constant, this is known not to occur as sedimentation rates can cease or are accelerated depending on the sedimentary process involved (e.g. turbidity currents).

Volume estimates are just that, estimates. All values are expressed as whole numbers and have been rounded to the nearest ten million, i.e. numbers are expressed as 30,000,000 (e.g. 3.0×10^7) or 660,000,000 instead of 30,223,298 or 663,871,043. Also, all volume estimates are based on subjectively outlining or dividing the slope into specific areas (e.g. upper slope, gentle to steep gradients- see Ch.3, pg 65). There may be areas that have thinner sediment disturbance or conversely, areas that have thicker sediment disturbance, all of which would change the volume estimates (perhaps by as much as +/- 15%). However, after careful consideration and calculations, I believe these volume estimates are as accurate as the current data allows.

CHAPTER 3

Acoustic data

3.1 Introduction

This chapter describes the submarine environment of St. Pierre Slope on the basis of acoustic geophysical data, which Hunttec DTS two-dimensional seismic reflection data and sidescan sonar data (most reported by Piper et al. 1999a). In addition, coincident airgun seismic reflection data (reported by MacDonald, 2001 and Piper et al., 2005) have been used to image further into the subsurface.

Given the complexity of events resulting from the 1929 earthquake, it was imperative to establish a systematic classification of the acoustic types observed within the seismic data. This chapter presents a classification of acoustic types that exhibit properties of disturbed sediments and relates these acoustic types to defined subsurface reflection horizons and their immediate environment settings (i.e. local changes in gradient, morphological features like valleys, channels, etc.).

Locations of acoustic data illustrated in this chapter are shown in Figure 3.1. For convenience, the term ‘depth’ is used throughout the text for reflection time (which is two way travel time) measured from seismic reflection profiles. For the depths penetrated by the Hunttec DTS system, 1 ms is equivalent to ~0.75-0.80 m of sediment.

All work with Hunttec DTS data throughout this chapter (and most of this thesis) is new and is integrated with previous interpretations based almost entirely on sidescan sonar data.

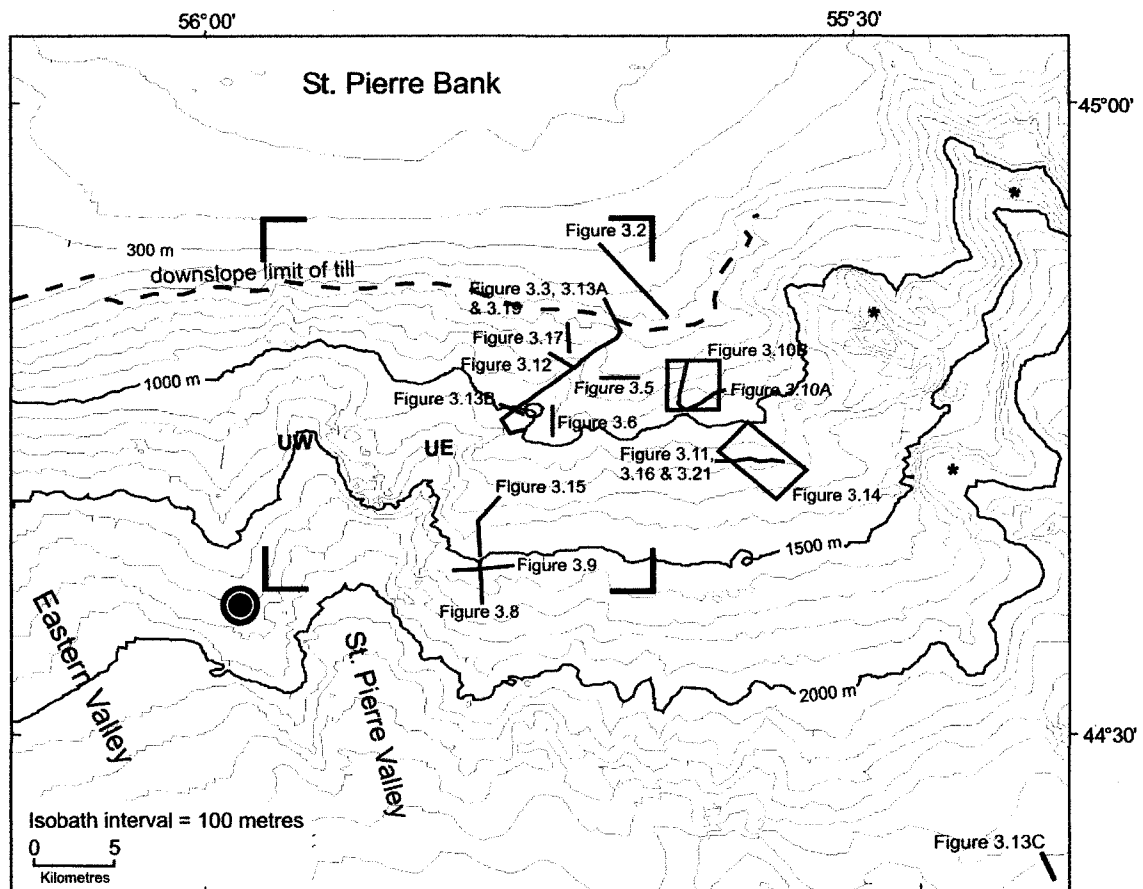


Figure 3.1- Bathymetry map of study area showing locations of seismic reflection (black) and sidescan sonar figures (blue boxes), and the approximate downslope limit of till (dashed red). Tributary valleys of Grand Banks Valley (*), outline of Figure 3.4 (corner outline) and earthquake epicentre (circle) are shown. UW= upper Western St. Pierre Valley; UE= upper Eastern St. Pierre Valley.

3.2 Geological and bathymetric features that may influence failure

3.2.1 Till distribution

The seismic architecture of the study area closely resembles that of other glaciated continental margins (Mosher et al., 2004). The outer shelf and upper slope off St. Pierre Bank are predominantly composed of overconsolidated tills that have proved difficult to sample due to compaction (Bonifay and Piper, 1988; Piper and MacDonald, 2002). The occurrence of acoustically incoherent units on the outer shelf and upper St. Pierre Slope have been documented using conventional single channel seismic reflection data

complemented by piston core analyses (Bonifay and Piper, 1988; Piper and MacDonald, 2002; Piper et al., 2005). These units in water depths less than 350 m acoustically resemble a facies identified by King and Fader (1986) as till. From 350 to 550 mbsl, a marked transition in sediment composition is apparent from seismic reflection data, where acoustically incoherent units interfinger downslope with stratified sediments, with these incoherent units locally extending downslope to 550 mbsl (Figure 3.2). Such features, termed till tongues, have been interpreted by Piper and MacDonald (2002) and Piper et al. (2005) as representing glacial advances and intervening retreats. Piper et al. (2005) recognized a total of six ‘till tongues’ (I–VI). Till tongues III and VI pinch out farther downslope compared to I, II, IV, and V (Figure 3.2). These wedge-shaped till tongues that terminate near the 450-m isobath seem to be extensions of the stacked incoherent sediment bodies that occur beneath the outer shelf. Locally, other incoherent units have been seen downslope of these till tongues, but they exhibit a more transparent acoustic nature and have been identified as mass transport deposits (Piper et al., 2005). Sidescan sonar data reveal numerous scarps, none shallower than about the 550-m isobath, that are headscarps from retrogressive failures that stopped at the till limit (Piper et al., 1999a). Huntect DTS high-resolution seismic reflection data show a similar situation of acoustically incoherent units in the upper slope with scarps downslope (Figure 3.3).

3.2.2 Pockmarks

Pockmarks are known to occur in the area (Piper et al., 1985, 1999a, 2005; McCall et al., 2005), but no thorough investigation as to their occurrence and significance

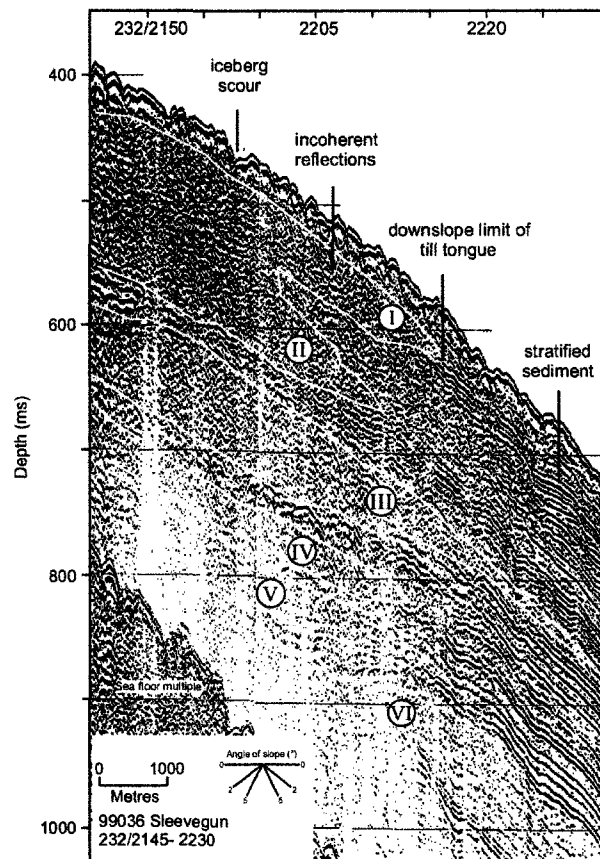


Figure 3.2- Sleevegun seismic reflection dip profile of upper St. Pierre Slope showing downslope extent of till tongues I-IV on the upper slope. Figure modified from MacDonald (2001). For figure location, see Figure 3.1.

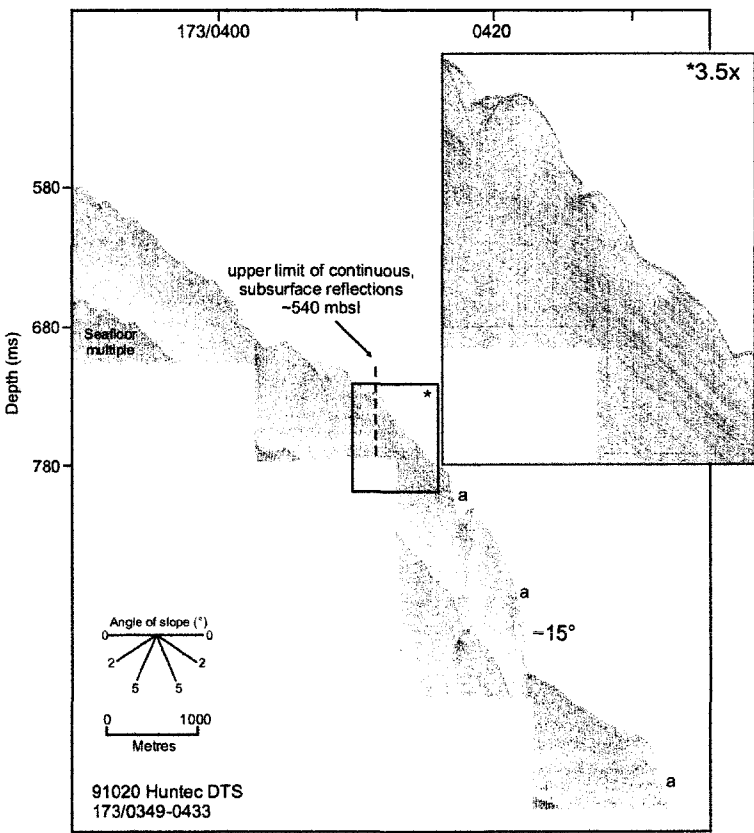


Figure 3.3 - Hunttec DTS seismic reflection dip profile of the upper St. Pierre Slope showing acoustically incoherent units upslope of continuous reflections (inset). Some continuous reflections are upslope of the marked limit (dashed line). Scarps (a) begin below the 550-m isobath. For figure location, see Figure 3.1.

has been completed to date. In seismic reflection data, pockmarks return as surface hyperbolae and are near scarps in undisturbed seabed (see Figures 3.5 and 3.10). Sidescan sonar imagery shows multiple pockmarks in undisturbed seabed from 400 to 1700 mbsl that locally cut rotational failures in places (McCall et al., 2005).

3.2.3 Shallow faults

Distribution of deep-seated faults has been established using multichannel seismic profiles (MacLean and Wade, 1992). The modern shelf break approximately corresponds to the shelf break at the base of the Tertiary and a series of basin-dipping normal faults underlie the outer shelf and upper slope. Faulting in the shallow subsurface has been studied previously only from a small area of the upper slope (Piper and MacDonald, 2002).

3.2.4 Gentle and steep slopes

Huntec DTS data are vertically exaggerated and a gradient scale has been provided in each figure. Bathymetric data coverage for the slope is not sufficiently dense to allow construction of a comprehensive gradient map. However, in some areas the bathymetry data did allow for the construction of crude bathymetric renders (color relief maps) (Figure 3.4). Where bathymetry data permitted, gradients were calculated and have been labelled to demonstrate the steepness of this terrain.

Seafloor gradients on the St. Pierre Slope are highly variable as a result of erosional valleys and scarps caused by shallow sediment failure. Where the slope has minimal dissection, mainly between the tributaries of Grand Banks and St. Pierre Valleys, gradients typically do not exceed 5°. Headwalls and sidewalls of valleys show

localized gradients as high as 20° but typically these walls do not surpass 10°. Scarps show steep gradients that in places surpass 40° (Figure 3.4). Immediately downslope of these scarps and valley walls, acoustic packages interpreted as failed sediments are common.

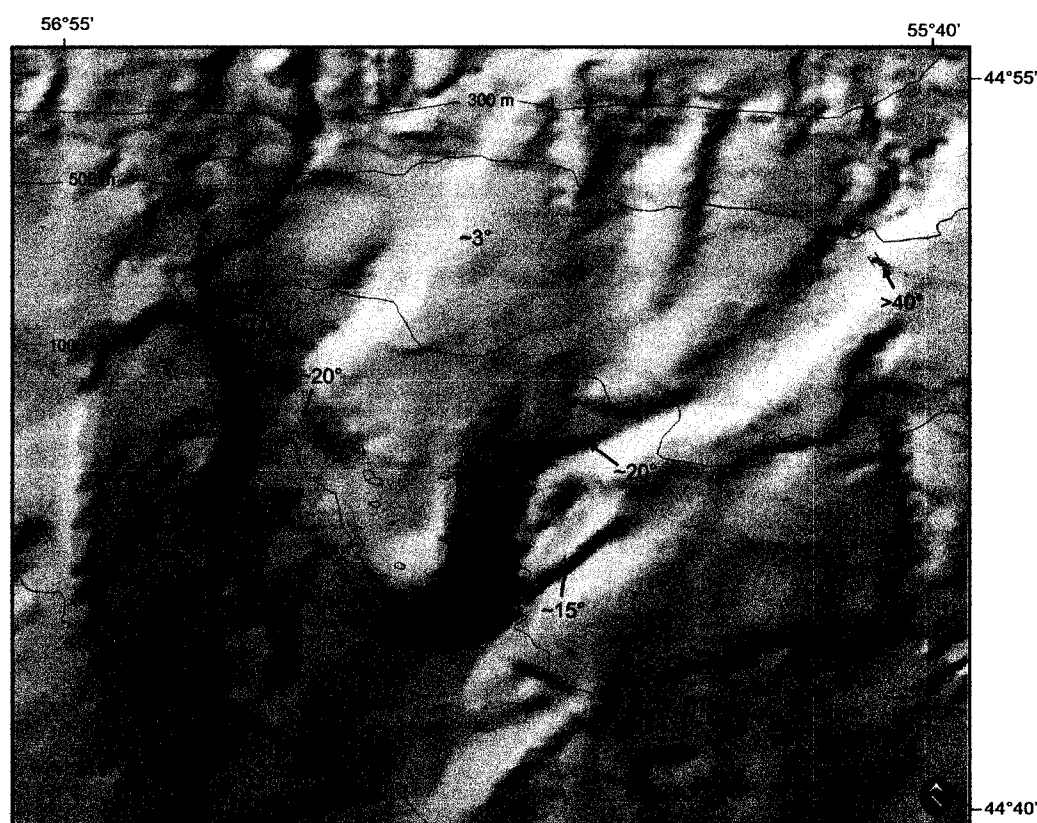


Figure 3.4 - Surface render showing the variable gradients encountered on St. Pierre Slope. Gradient values were extracted from the bathymetry map that was used to render this surface. Gradient values exceeding 20° appear to be localized. Upper Western (UW) and upper Eastern (UE) St. Pierre Valleys display sidewall gradients as high as 10-20°. For figure location, see Figure 3.1.

3.3 Seismic stratigraphy

3.3.1 Introduction

Six key reflections were chosen and then traced throughout the study area to establish a seismic stratigraphy for the upper ~100 milliseconds (two-way travel time-TWTT) of sediment. The primary goals for tracing the six reflections throughout the

study area were to determine the nature and occurrence of MTDs, their relationship to topography (e.g. gradients) and each other, and to arrive at a regional seismic stratigraphy of the St. Pierre Slope.

Starting from a type section from the upper and middle slope (Figures 3.5 and 3.6), six individual reflections were traced along Hunttec DTS sparker and boomer seismic reflection profiles. Density of Hunttec DTS coverage was pivotal in establishing where a reflection could be mapped in any given area (see Figure 2.1). In the lower St. Pierre Slope, sparse data coverage and absence of tie-lines made correlation difficult. Conversely, the middle St. Pierre Slope (800-1400 mbsl) has dense Hunttec DTS coverage

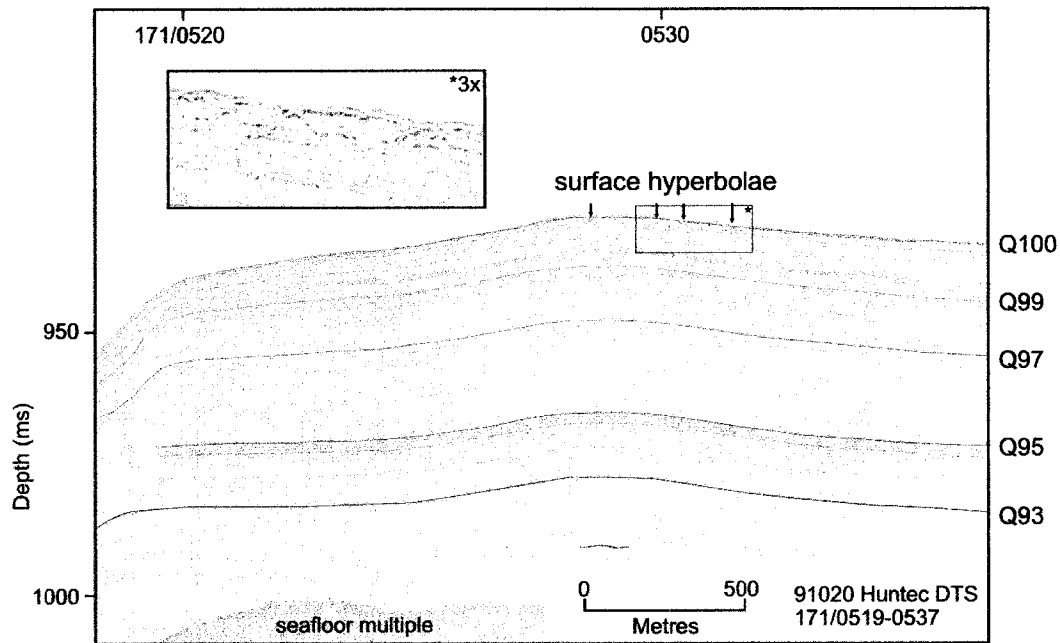


Figure 3.5- Hunttec DTS seismic reflection strike profile of type section 1 showing five key reflections (Q100-brown to Q93- blue) from upper St. Pierre Slope at ~700 mbsl. Note the absence of the yellow reflection (Q91) due to equipment penetration limits. Note surface hyperbolae (marked and inset). For figure location, see Figure 3.1.

and thus all six reflections are well correlated in this area. Areas deeply dissected by valleys, e.g. the upper slope, posed a problem as reflections could not always be correlated from one side of the valley to the other.

3.3.2 Type section and correlation

The six key reflections defined in the study area have been labelled as follows: Q100 (seabed), Q99, Q97, Q95, Q93, and Q91, with a respective color scheme of brown, orange, green, red, blue, and yellow. All but yellow (Q91) are defined in the type section from the upper slope shown in Figure 3.5 and all are shown in the type section from the middle slope shown in Figure 3.6. Each of the six key reflections essentially displays a distinct acoustic character and is illustrated in Table 3.1. Reflections were initially chosen based on relation to MTDs, and prominence and position within a seismic section, i.e. med-high amplitude, positive, coherent reflections with an average spacing of 10-15 ms between neighbouring key reflections. However, some reflections that were at first easily traced in one region were in another region untraceable as they had deteriorated in amplitude and appearance, making detection and recognition a challenge.

Reflections were transferred from one seismic line to another using crossovers at tie lines. Where reflection continuity was broken by erosional valleys or sediment failure, reflection placement and correlation relied solely on acoustic characteristics. The two reflection packages being compared typically were <1 km apart. If there were no close seismic reflection lines, supplemental 3.5 kHz echosounder lines proved useful in aiding the correlation.

Of the six reflections, the yellow reflection (Q91) is the deepest and was not as easily detected as the others due to equipment limitations (Figure 3.5). The Hunttec DTS boomer system that was used during cruise 91020 had less penetration as compared to the Hunttec DTS sparker system utilized during cruises 99036, 2001043 and 2003033, which generally penetrated to yellow. The yellow reflection occurs on average at 64 ms sub-

bottom and is the third reflection down in a package of four that are relatively widely spaced, medium amplitude, coherent reflections.

The blue reflection (Q93) is the topmost reflection of a high amplitude doublet that has high lateral continuity throughout the upper slope, and a mean depth of 47 ms sub-bottom.

The red reflection (Q95) and the associated underlying reflection package are the most distinct subsurface reflections in this study and, along with the blue reflection, are the reflections correlated most widely in this region. It is the topmost reflection in a package of six high amplitude, prominent reflections. It is the most laterally continuous and recorded reflection in the upper slope region, and has a mean depth of 34 ms sub-bottom.

The green reflection (Q97) has a mean depth of 20 ms and is the bottom reflection in a package of three fairly high amplitude reflections.

The orange reflection (Q99) has a mean depth of 11 ms and is the bottom reflection of a doublet. Orange is separated from green by ~10 ms of predominantly coherent reflections. It is a medium to high amplitude reflection, as depicted by amplitude variation throughout the slope. It is very similar to blue in acoustic character.

Overlying the orange reflection is a mix of coherent, high to low amplitude reflections and thin incoherent zones. The tops of these zones terminate at the brown reflection (Q100), which is defined as the present seafloor in areas not disturbed by surficial failure. In zones of disturbed seabed, as would be expected, it has largely been removed.

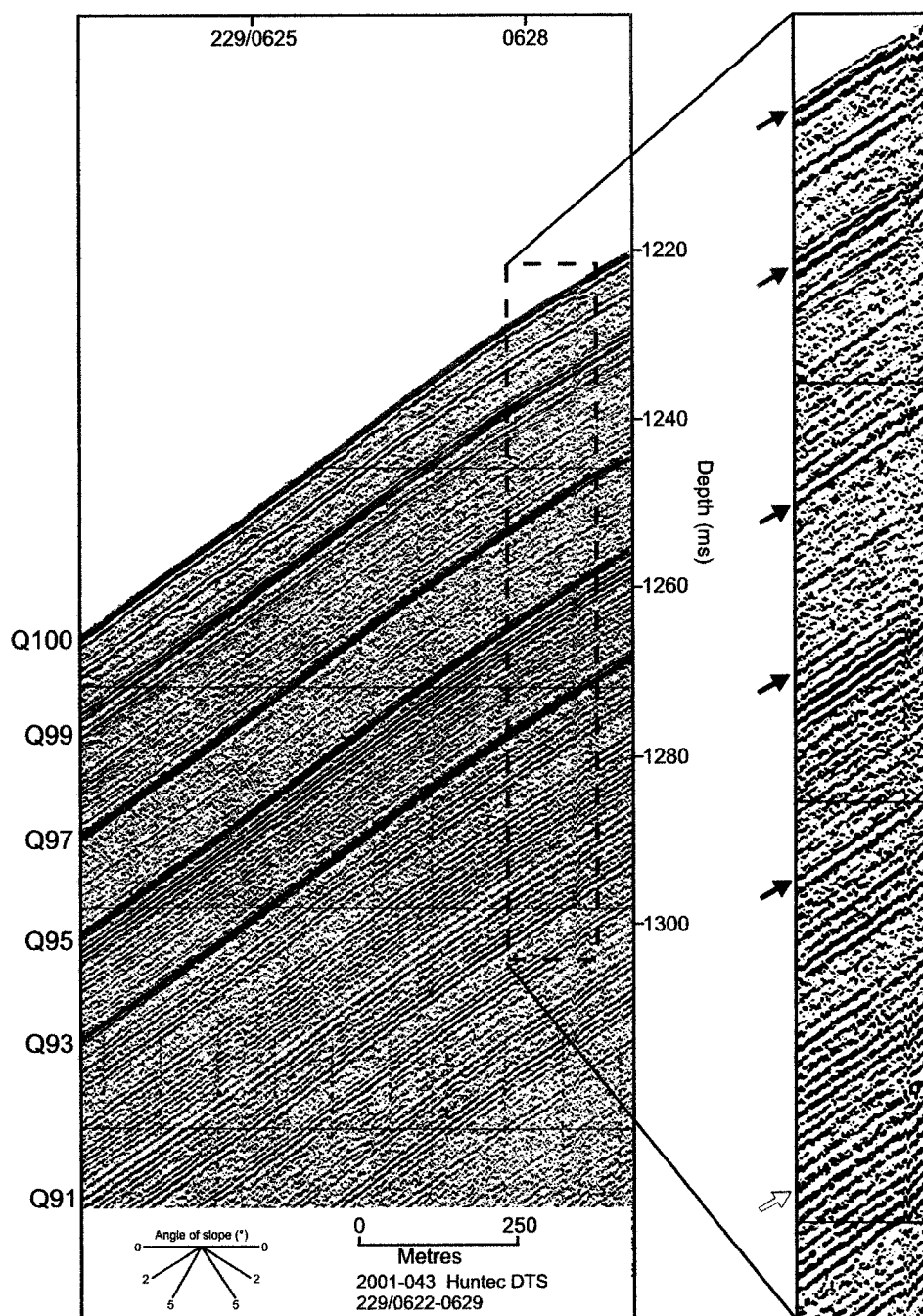


Figure 3.6 - Hunttec DTS seismic reflection dip profile of type section 2 showing six key reflections (Q100-brown to Q91-yellow) from middle St. Pierre Slope at ~925 mbsl. For figure location, see Figure 3.1.

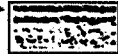
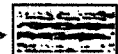
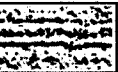
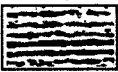
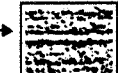
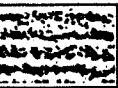
Reflection	Mean reflection depths (in ms, TWT) below seafloor in undisturbed (a) and disturbed (b) stratigraphy				Reflection characteristics and typical appearance in Huntex DTS seismic reflection data
	Upper slope		Middle slope	Lower slope	
	525-650m (700-860 ms)	650-800 m (860-1075 ms)	800-1400 m (1075-1875 ms)	1400-2100 m (1875-2800 ms)	
Q100 (Brown)	(a) surface (b) largely evacuated	(a) surface (b) largely evacuated	(a) surface (b) largely evacuated	(a) surface (b) largely evacuated	High amplitude reflection representing the surface of the seafloor. Largely evacuated from disturbance. 
Q99 (Orange)	(a) 14.6 \pm 3.2 (b) 6.9 \pm 4.2	(a) 10.4 \pm 2.7 (b) 7.2 \pm 3.8	(a) 9.3 \pm 2.8 (b) 6.6 \pm 3.5	(a) 11.5 \pm 1.5 (b) 6.6 \pm 4.1	The bottommost reflection of a doublet. Reflection strength is variable in the slope. Near the basal plane of the majority of MTDs. 
Q97 (Green)	(a) 24.7 \pm 5.3 (b) 14.6 \pm 4.6	(a) 20.1 \pm 4.2 (b) 15.2 \pm 5.5	(a) 19.8 \pm 3.2 (b) 17.3 \pm 4.5	(a) 24.5 \pm 1.8 (b) 19.3 \pm 4.7	The bottommost reflection in a package of three fairly high amplitude reflections. 
Q95 (Red)	(a) 39.2 \pm 6.7 (b) 28.9 \pm 8.1	(a) 34.1 \pm 5.4 (b) 28.4 \pm 7.8	(a) 33.2 \pm 4.03 (b) 28.1 \pm 8.55	(a) 34.4 \pm 1.9 (b) 33.7 \pm 7.7	Topmost reflection in a package of six high amplitude reflections. The most laterally continuous reflection of the six key reflections. 
Q93 (Blue)	(a) 49.6 \pm 7.7 (b) 39.8 \pm 9.4	(a) 43.6 \pm 5.7 (b) 40.6 \pm 7.4	(a) 46.1 \pm 5.1 (b) 40.5 \pm 7.8	(a) 61.8 \pm 8.6 (b) 52.9 \pm 9.5	Topmost reflection of a high amplitude doublet. Lateral continuity is very good. Surrounding reflections have poor lateral continuity. Similar to acoustic character of Q99. 
Q91 (Yellow)	(a) not detected (b) not detected	(a) not detected (b) not detected	(a) 62.3 \pm 8.9 (b) 58 \pm 9.2	(a) 74.6 \pm 6.1 (b) 70.8 \pm 21.1	Third reflection down in a package of four high amplitude reflections. Lateral continuity is good in the middle and lower slope but poor in the upper slope. 
Mean thickness of surface MTDs	6.9		8.5	9.0	Below 2100 mbsl, thickness of surface MTDs increases to an average of 10.5 ms.

Table 3.1- Mean depths below seafloor for the six key reflections in undisturbed and disturbed areas, and mean thicknesses of surface MTDs on the St. Pierre Slope and rise. Standard deviation is shown (\pm).

3.3.3 Depth variation of reflections

Mean depths for each of the six reflections throughout the study area were calculated using the data from Appendix 1 and are listed in Table 3.1. These values are ‘depths’ (or TWTT) from the seafloor to the appropriate reflection. In most cases, depths were measured every 2 to 3 minutes (according to Huntect DTS horizontal time). Mean reflection depths were calculated for the upper, middle, and lower St. Pierre Slope, as was average thickness of disturbed bodies at the surface. On the upper slope, in places shallower than the 650-m isobath, four of the key reflections, Q99, Q97, Q95 and Q93, have mean depths of about 15, 25, 40 and 50 ms, respectively. These four reflections shallow downslope of the 650-m isobath, with depths very similar to those of the middle slope (Table 3.1). Mean reflection depths on the lower slope are similar to mean depths recorded from the middle slope except for the two deepest reflections, yellow (91) and blue (Q93), where there is a marked increase. The mean depth of the blue reflection increases by 15 ms and the yellow reflection by 12 ms, possibly due to increased deposition from turbidites.

3.4 Disturbed Seabed

3.4.1 Introduction

Disturbed sediments at the surface are recognized in Huntect DTS profiles as bodies with incoherent, distorted or discontinuous reflections, that overlie well-stratified sediments (Figure 3.7). In places, sidescan sonar data (Piper et al., 1999a) have been used to confirm the character of disturbed sediments. Continuity of reflections Q100-Q97 was heavily disrupted due to the prevalence of shallow surficial disturbance of the seabed. Deeper reflections Q95-Q91 were not as frequently disrupted and consequently were

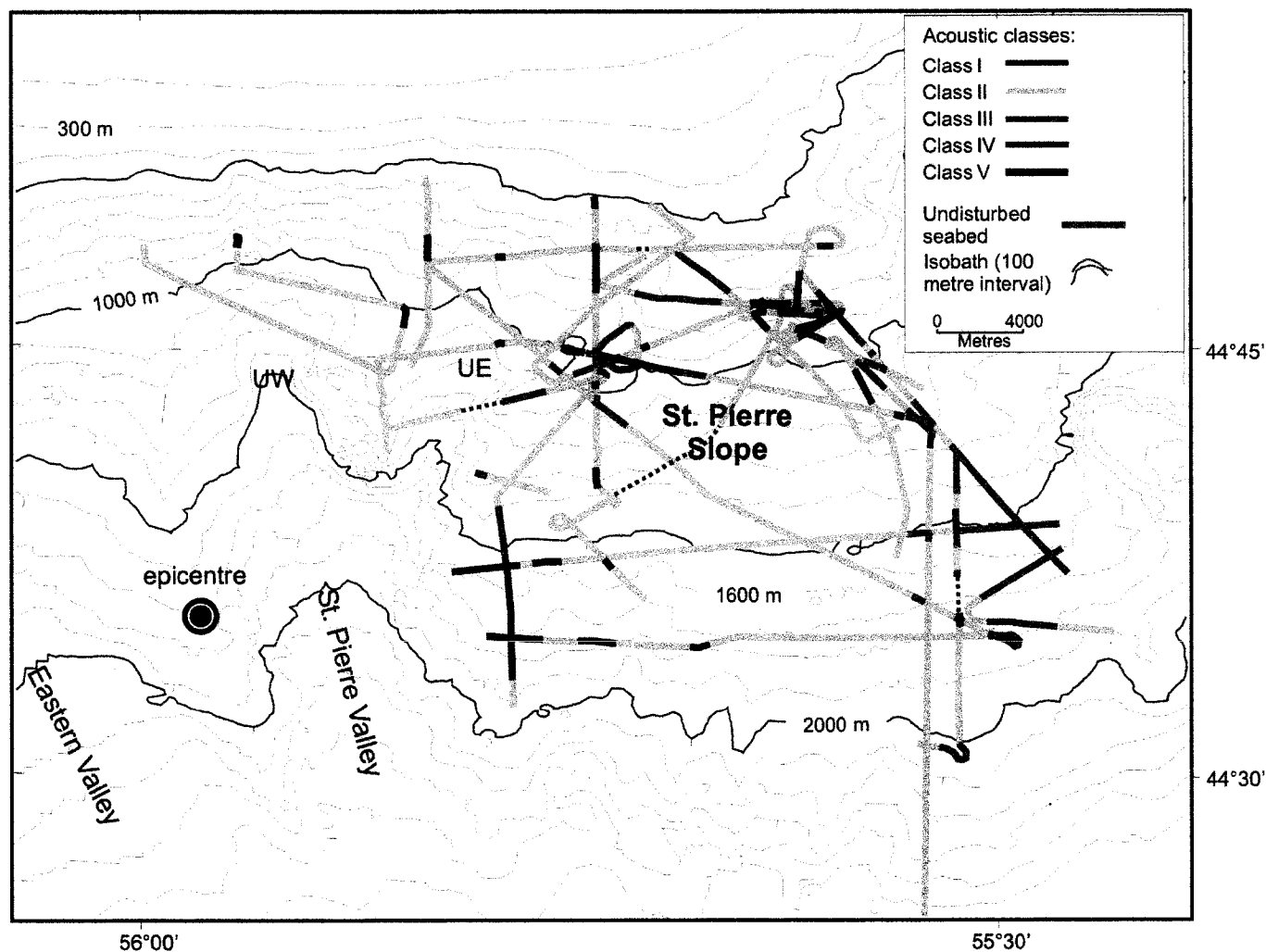


Figure 3.7- Bathymetry map of St. Pierre Slope showing distribution of acoustic Classes I-V along navigation tracks of Hunttec DTS seismic lines. Dashed lines mark areas of either bad data or where no identification of class could be established. Figure covers slightly smaller geographic area as Figure 3.1. UW= upper Western St. Pierre Valley; UE= upper Eastern St. Pierre Valley.

correlated over a larger area. Disturbance of the seabed on the flat to gentle slopes ($<5^\circ$) typically extends down to the orange reflection (Q99) or a reflection within ± 2 ms of orange. In some places, however, the seabed has been disrupted to just below the blue reflection (Q93). On steeper slopes ($>5^\circ$), disturbance of the seabed down to the red reflection (Q95) is common.

A body of disturbed sediment is typically bounded upslope by an abrupt termination of stratified sediment. This abrupt termination represents a headwall or sidewall scarp that is also seen in sidescan sonar (Piper et al., 1999a). In some areas, disturbed bodies are separated from their associated head- and sidewall scarps by depressions that show slightly hyperbolic to smooth, continuous surface reflections. This variable surface return may represent roughness due to erosion of the surface during transport and evacuation of overlying material, as noted in other studies (e.g. Lee and Chough, 2001). In these evacuation zones, tiny incoherent packages with hyperbolic surface returns are common and extend down a few milliseconds from a planar surface.

The surface of the observed disturbed bodies is highly variable, ranging from hyperbolic diffractions of varying intensity to continuous reflections that are smooth to undulating in nature. Hyperbolic diffractions, depending on the nature of the surface roughness, are either large (up to 260 metres wide and tens of ms high) or numerous, small and overlapping (tens of metres wide and a few ms high). The internal reflection character of disturbed bodies is highly variable and its description is limited by the resolution of the seismic system, particularly in deeper water.

3.4.2 *Acoustic classes of surface sediment failures*

Five classes of disturbed seabed were identified and classified based on acoustic character from seismic reflection data throughout the study area (Table 3.2). Of these five classes, four are represented by actual bodies of acoustically incoherent to partially coherent reflections that compare with the acoustic character of MTDs described in the literature (e.g. Lee et al. 2002). The fifth class represents a surface, where there seems to have been little or no deposition of sediment, and proof of removal of sediment (i.e. scars) and erosion are the dominant processes. Following are the five defined classes of disturbed seabed based on seabed morphology and coherency, continuity, and geometry of the surface and subsurface reflections seen in the seismic reflection data.

Class I – *Rotational slumps*

Class I bodies display hyperbolic to hummocky surface expressions. Near the headwall in dip profile, incoherent bodies with hyperbolic surface and subsurface reflections intermix with isolated continuous reflections (Figure 3.8). Surface hyperbolae extend up to 260 metres laterally, with relatively low amplitudes of up to ten ms. Adjacent hyperbolic crests are tens to hundreds of metres apart. Conversely, near the headwall in strike profile, hyperbolic diffractions at the surface are a few metres laterally, with amplitudes of a few ms (Figure 3.9). Adjacent hyperbolic crests are a few to tens of metres apart. Internally, bodies are predominantly acoustically incoherent, especially away from the headwall, but in places near the headwall and the base, short, continuous reflections are mixed with hyperbolic diffractions. Scars from the presumed evacuation of material are noticeably absent between the headwall and bodies. Instead, the body and

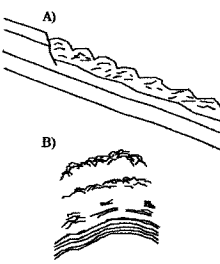
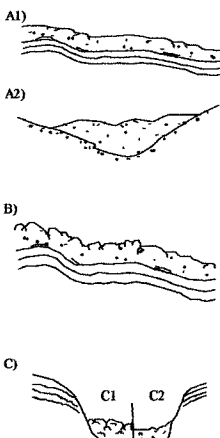
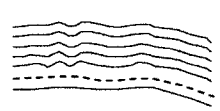

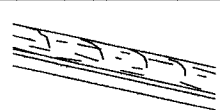
Class	Line drawing	Description	Occurrence	Interpretation
I		Hyperbolic or hummocky surface expression that is step-like in places. Hyperbolae are large in dip (A) and smaller in strike (B) profiles. Internally, bodies are mostly incoherent but in places near the headwall and the base are a mix of hyperbolic and flat, dipping reflections. Plane separating body from underlying continuous reflections is undulating and usually segmented, and near the headwall, is concave-up and in places is step-like.	On gentle and steep valley walls, and undissected seabed. Typical gradients of 1-7°. Associated with Classes II and III.	Rotational slump
II		Internally, bodies are acoustically incoherent. Smooth (A1, A2 = subclass A) or rough (B = subclass B) surface returns. Bodies display fairly continuous surface reflections (A1, A2) or hyperbolic surface reflections (B). Bodies bounded upslope by scars or by bodies of Class I deposit either on flat to gentle seabed as sheet like feature (A1, B) or in depressions with a lens-shaped geometry (A2). In places, bodies disrupt underlying continuous reflections, a probable sign of erosion. Near valley heads (C1), the surface of the bodies show hyperbolic diffractions and further downslope from the valley head, the surface is smoother (C2).	On gentle slopes, typically <4°. Along axes of valleys and channels, at the base of valley heads and on undissected seabed. Associated with Classes I, III and IV.	Mass flow deposits
III		Internally coherent seabed with laterally continuous reflections. Reflections from the surface down to the failure plane (dashed line) are wavy to undulating.	On gentle slopes (<2°). Associated with Classes I and II.	Possible creep deformation
IV		Type example (blue). Semi-continuous, internal reflections that in places have a slight dip. Bounded to one side by a scarp and to the other by a body of Class II.	One deposit documented on a 2° slope at ~1150 mbsl. Associated with Class II.	Glide block
V		Internally coherent seabed with continuous reflections disrupted in places by surface hyperbolae that extend down a few milliseconds into the sub-bottom.	Highly variable gradients. Typically on valley walls and at sites of sediment evacuation.	Erosional or evacuation surface

Table 3.2- Classification of disturbed seabed based on acoustic character from Hunttec DTS seismic reflection data.

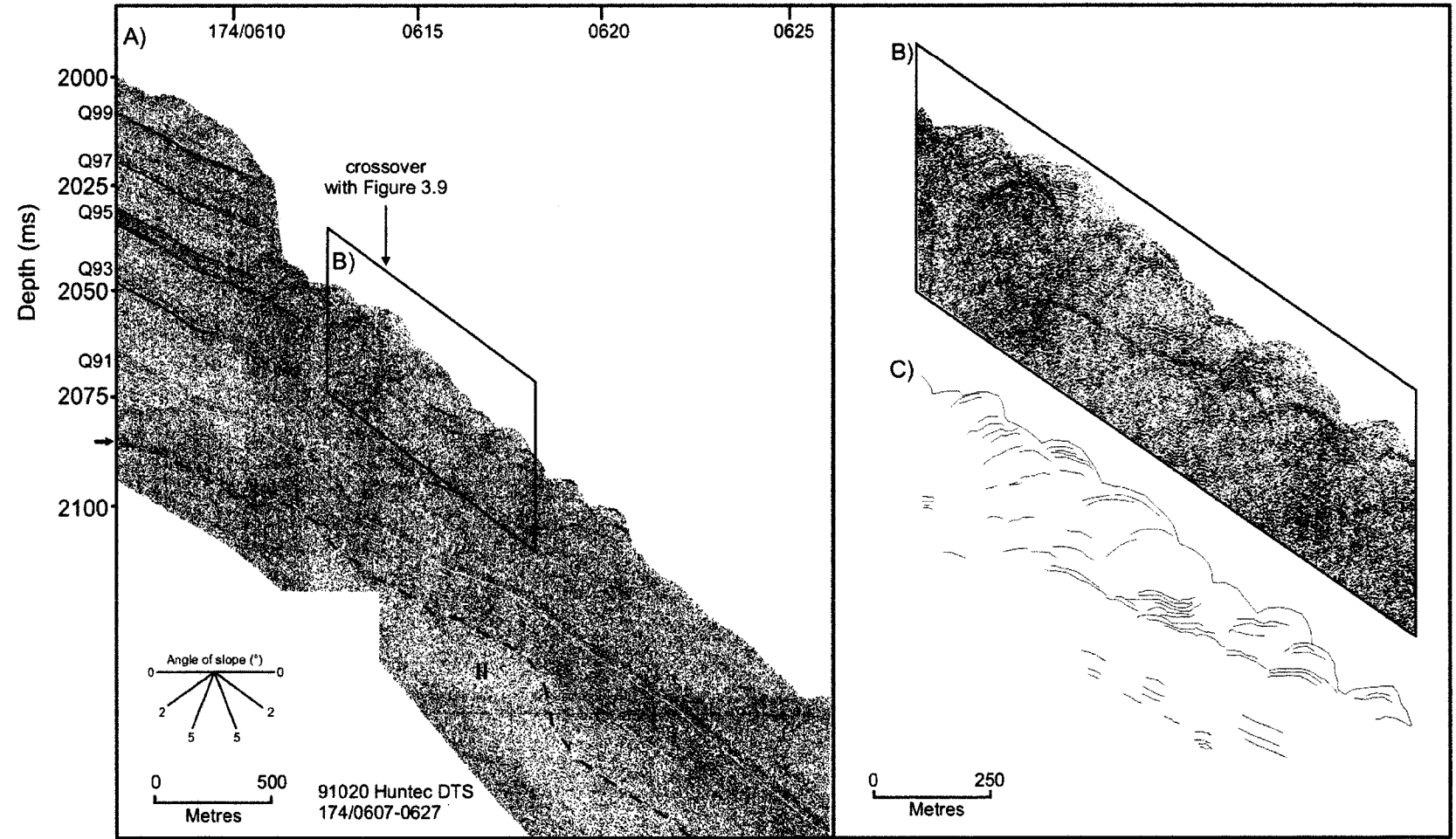


Figure 3.8- Hunttec DTS seismic reflection dip profile of a body that is mostly acoustically incoherent with a hyperbolic surface expression characteristic of Class I (A, B). Some reflections in the subsurface are continuous (C). There seems to have been multiple episodes of disturbance as deposits appear stacked (C). Note buried body that displays properties of Class II (surface marked by dashed purple line and arrow). For figure location, see Figure 3.1.

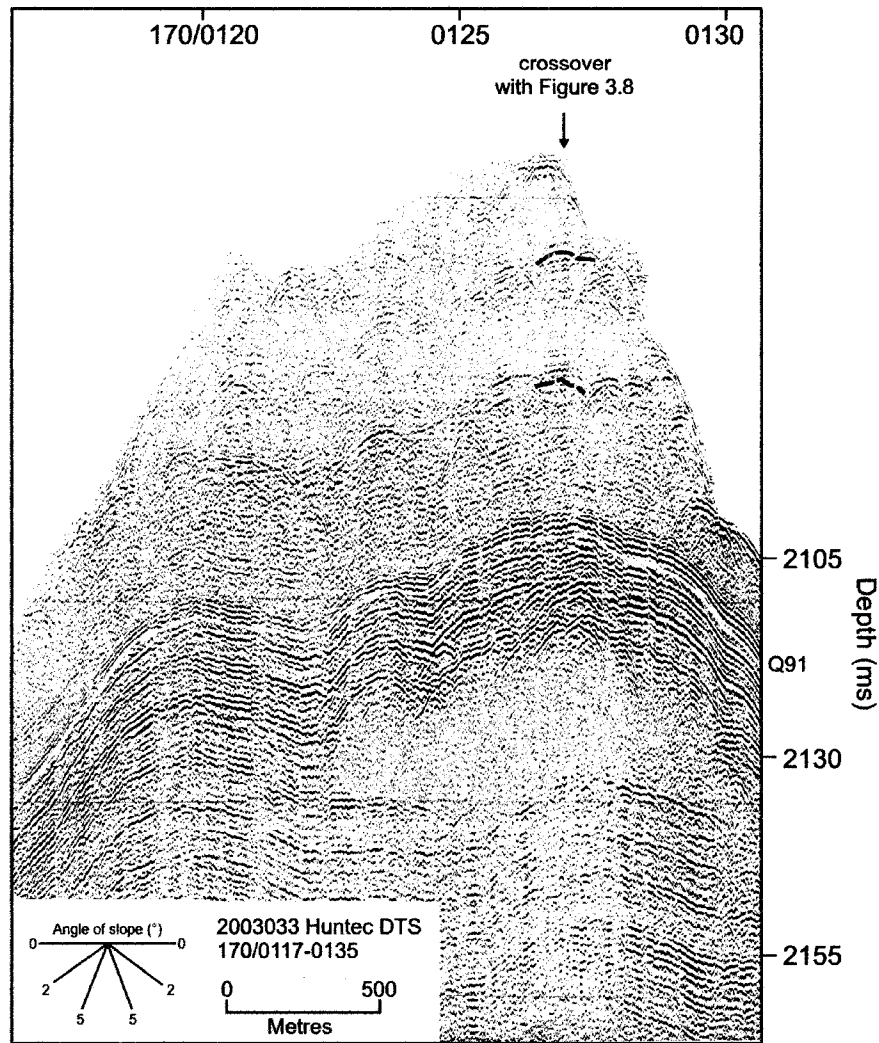


Figure 3.9- Hunttec DTS seismic reflection strike profile perpendicular to Figure 3.8. Surface shows smaller hyperbolic diffractions. Plane separating body from underlying continuous reflections is just a few ms above Q91. The body is mostly internally incoherent near the surface but near to ~15 ms above Q91, reflections are short and continuous. Note buried body that displays properties of Class II (peach and captured in dip profile in Figure 3.8). Approximate positions of Q93 (blue) and Q95 (red) are shown. For figure location, see Figure 3.1.

headwall are adjacent, with the surface of the body forming a slight negative deviation from the original seabed position (Figures 3.8 and 3.10A). Headwall height, measured from the top of the headwall down to the surface of the body, ranges from a few to tens of ms. The bases of these bodies typically are underlain by continuous reflections and near the headwall, normally are concave-up and in places shows a step-like morphology.

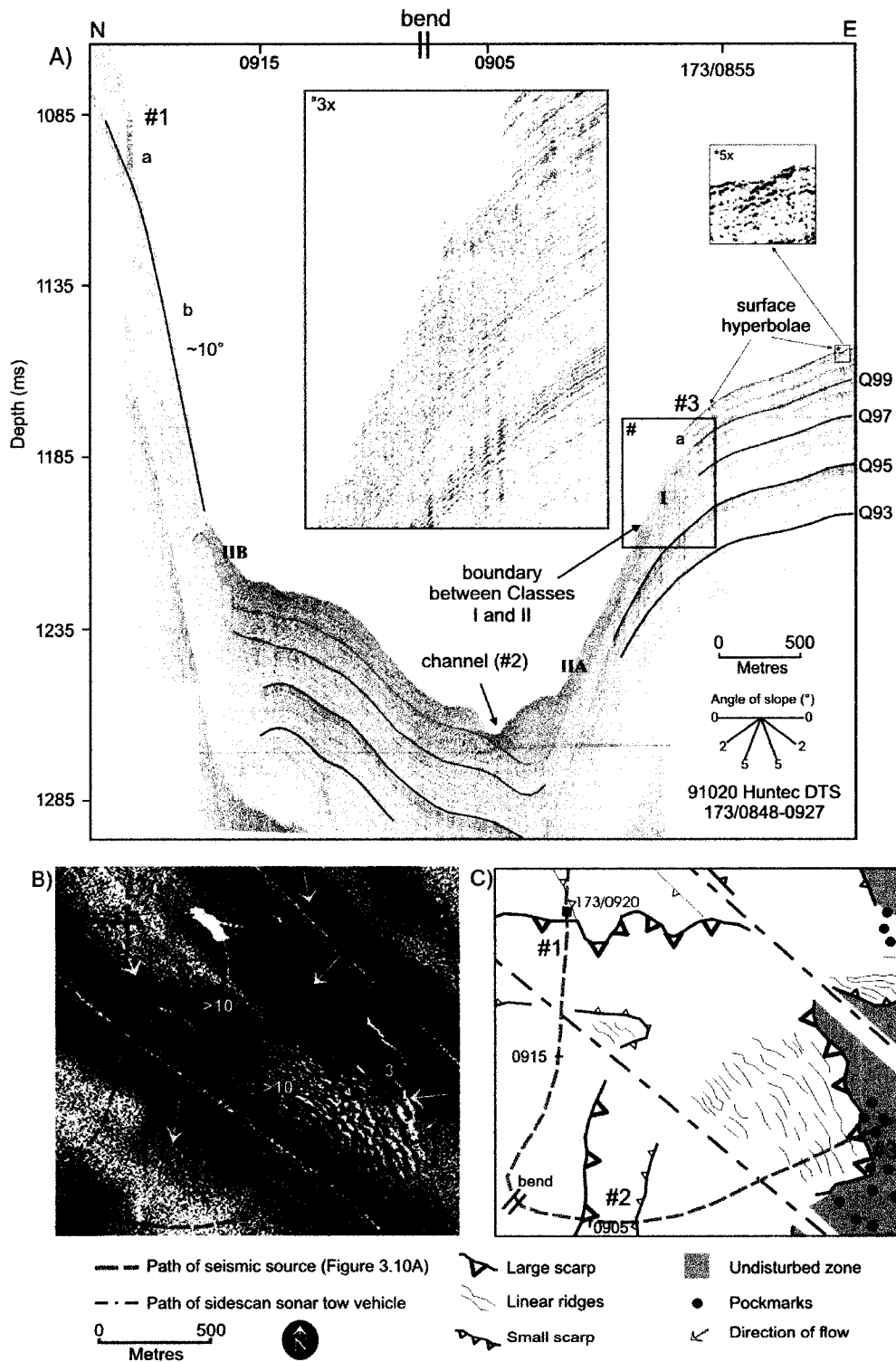


Figure 3.10- A) Hunttec DTS seismic reflection profile of the middle St. Pierre Slope showing bodies of Classes I (pink shading and inset) and II (orange shading). Scarps (a) and scars (b) of Class V are visible. Numbers 1-3 denote features imaged (B) and interpreted (C) in sidescan sonar data. A few gradients have been labelled in B. For figure location, see Figure 3.1.

Sidescan sonar images corresponding to Figure 3.10A show a seabed with numerous scarps (#1 and #3 in Figure 3.10C), pockmarks, juxtaposed linear ridges (near #3) and a channel (#2), that when respectively viewed in Huntect DTS data are steeply dipping walls, small surface hyperbolae, overlapping hyperbolic diffractions and a slight depression within a Class II deposit (Figure 3.10A).

The observed hyperbolic surface and subsurface diffractions, concave-up and step-like base, proximity of the body to the headwall and location on gradients $>5^\circ$ are features that have been recognized as slumps composed of rotated blocks on the Scotian margin (Hughes Clarke et al., 1992; Mosher et al., 1994, 2004), elsewhere on the Grand Banks margin (Savoye et al., 1990) and on international margins (e.g. Lee and Chough, 2001). Some of these types of failures observed in sidescan sonar have been interpreted as being retrogressive (Piper et al., 1999a).

Class II – *Mass flow deposits*

Class II bodies are internally incoherent, and in places are internally transparent. Surface reflections range from weak to strong, undulating, continuous reflections to strong overlapping hyperbolic reflections. The class, therefore, has been subdivided into two subclasses: A) bodies with undulating to slightly concave-down surface reflections and B) bodies with strong, overlapping hyperbolic reflections. These surface reflections from both subclasses typically extend down a few milliseconds into the subsurface. Bodies of subclass IIA typically are bounded on either side by walls a few to tens of milliseconds in height or by bodies of subclass IIB. They generally occur downslope of, and thus are bounded upslope by, bodies assigned to Class I (Figure 3.10). Geometry is sheet-like in appearance and thickness is generally uniform, not exceeding 15 ms. The

plane (or slip plane) separating the body from underlying continuous reflections is discontinuous and in places ‘steps-up or -down’ to a different stratigraphic level (Figures 3.11 and 3.13).

Bodies of subclass IIB are common at the base of steep slopes (usually $>10^\circ$), where they form as wedge-shaped bodies with concave-up bases (Figure 3.10- orange at base of ‘b’ and Figure 3.12). The steep slope is represented by a valley headwall, valley sidewall, scar or scarp. Bodies at the base of these steep slopes are 10- 50 ms thick but

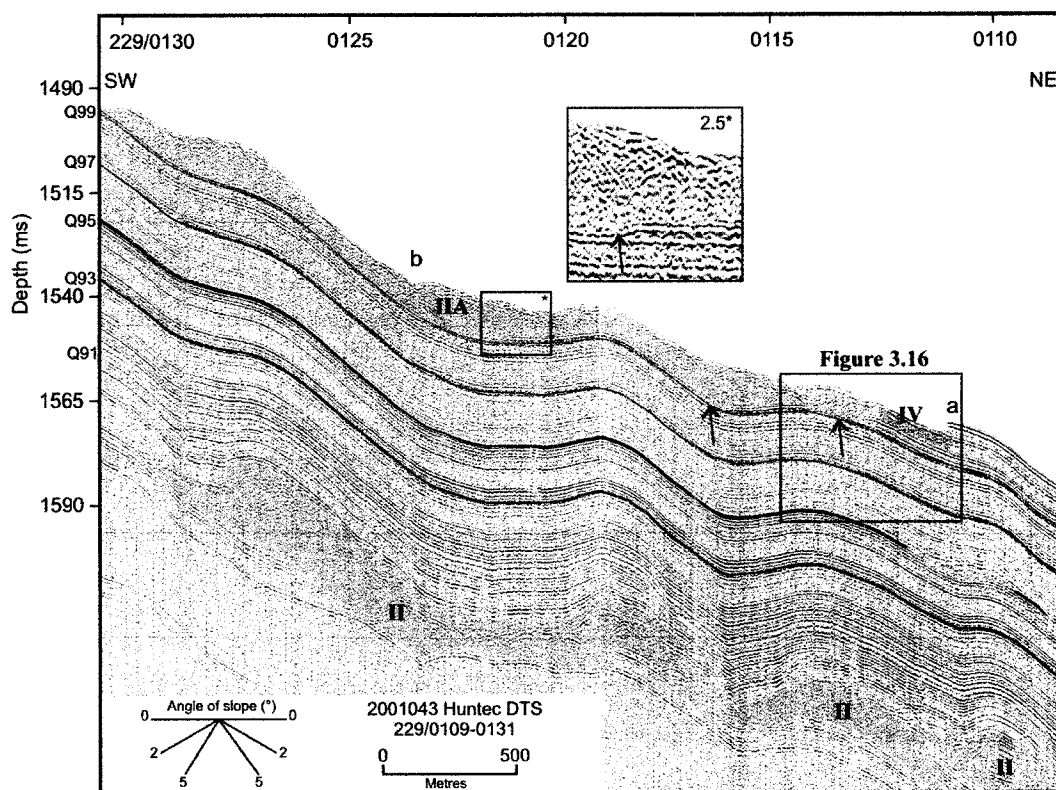


Figure 3.11- Hunttec DTS seismic reflection strike profile of a body of subclass A of Class II (orange). The plane separating the body from the underlying continuous reflections is broken in places (arrows and inset). ‘a’ denotes a scarp that is pictured in Figure 3.14. A body of Class IV is shown (blue, see Figure 3.16). For figure location, see Figure 3.1.

generally do not exceed 30 ms in thickness. The plane (or reflection) that separates a body from underlying continuous reflections is usually broken but this typically is not severe (little to no deformation) (Figure 3.12).

Stacking of bodies from subclass IIA is common in valleys on the slope (Figure 3.13A,B), and further downslope on the rise, in both valleys and undissected seabed (Figure 3.13C). Stacking of bodies is apparent from laterally extensive subsurface reflections that separate packages of incoherent reflections (Figure 3.13), and may represent penecontemporaneous events or events separated by long periods of time.

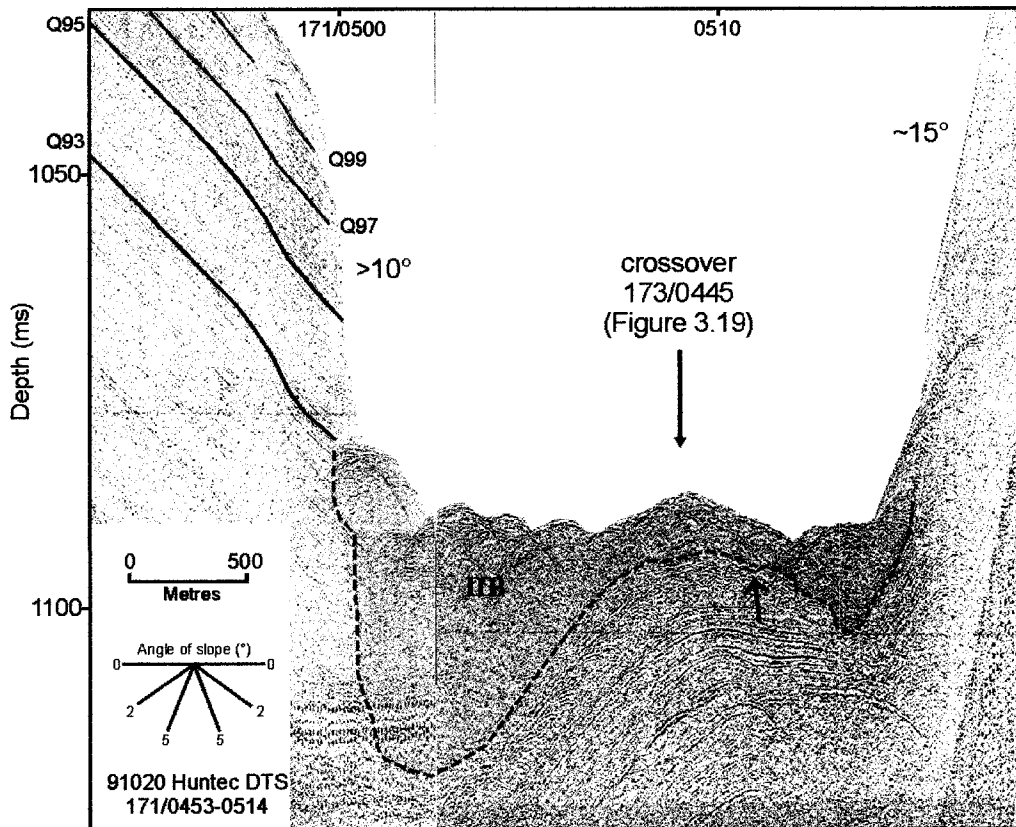


Figure 3.12- Hunttec DTS seismic reflection strike profile near the head of a tributary valley of upper Eastern St. Pierre Valley showing a body of subclass IIB with overlapping hyperbolic surface reflections. Continuous reflections underlying the body are disrupted in places (arrow). For figure location, see Figure 3.1.

Sidescan sonar images corresponding to the seismic reflection profile of Figure 3.11 show a seabed surface of varying topographic relief: linear ridges and large scarps on the west and a more uniform appearance with relatively minimal disturbance near and

to the east of the dashed yellow line of Figure 3.14. This area with uniform appearance corresponds to the body of subclass IIA depicted in Figure 3.11.

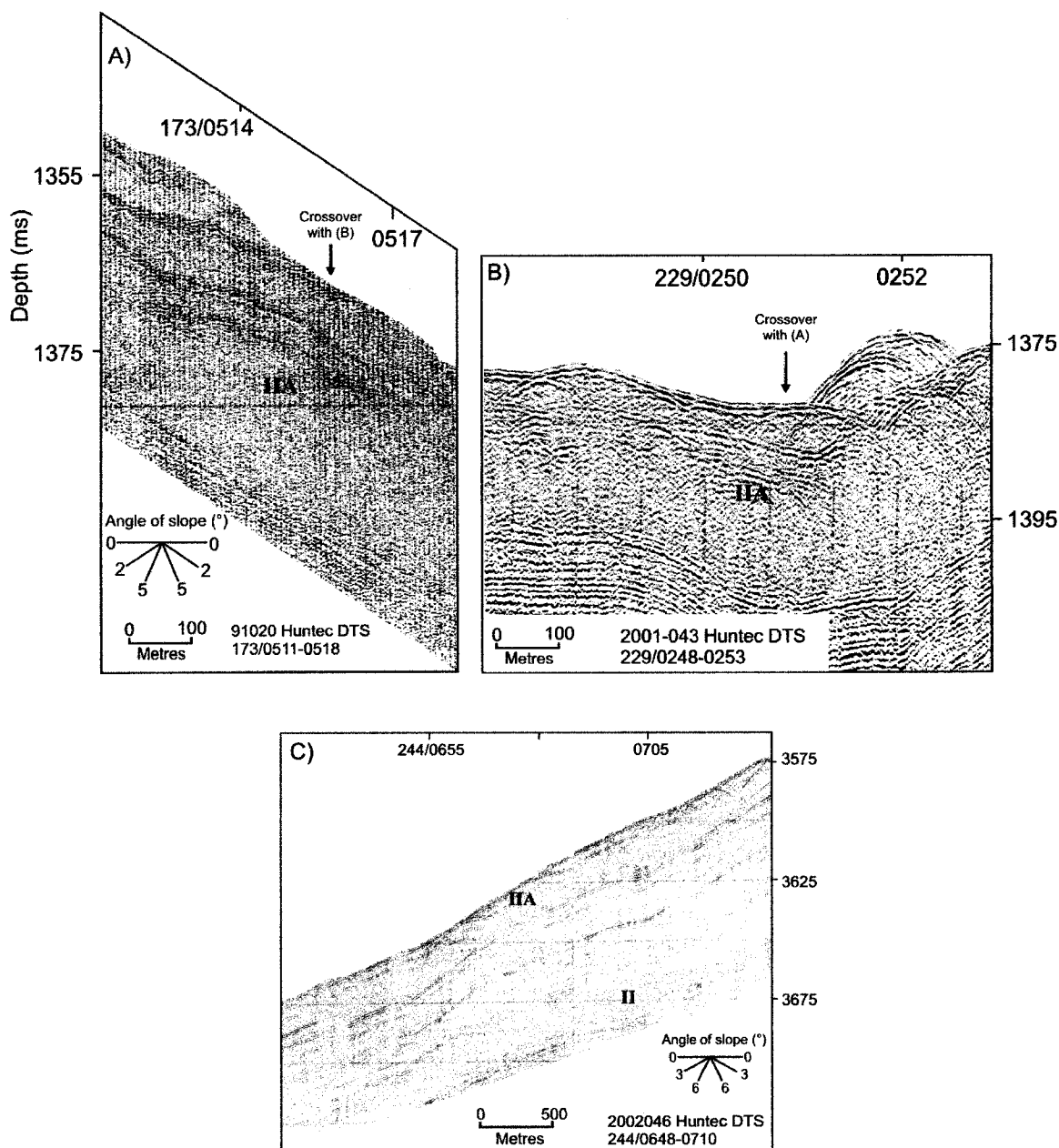


Figure 3.13- Hunttec DTS seismic reflection dip (A) and strike (B) profiles across a tributary valley of upper Eastern St. Pierre Valley showing stacked bodies of subclass IIA. C) On the rise, stacking of subclass IIA occurs in valleys and on flat, undissected seabed, and in places interrupts underlying continuous reflections. For figure location, see Figure 3.1.

The various surface returns reflect variation in the surface roughness of these bodies (Masson et al., 1998, Lee et al., 2002), i.e. strong hyperbolic surface returns (Class IIB) likely represent large blocks at the surface of a mass flow deposit and smooth continuous returns (Class IIB) signify a smooth mass flow deposit. Internal acoustic transparency of bodies has been recognized and interpreted by others (Embley, 1976, Piper et al., 1985) to represent possible internal homogenization of failed bodies, but a lack of acoustic impedance contrast is the only definite conclusion. Nardin et al. (1979)

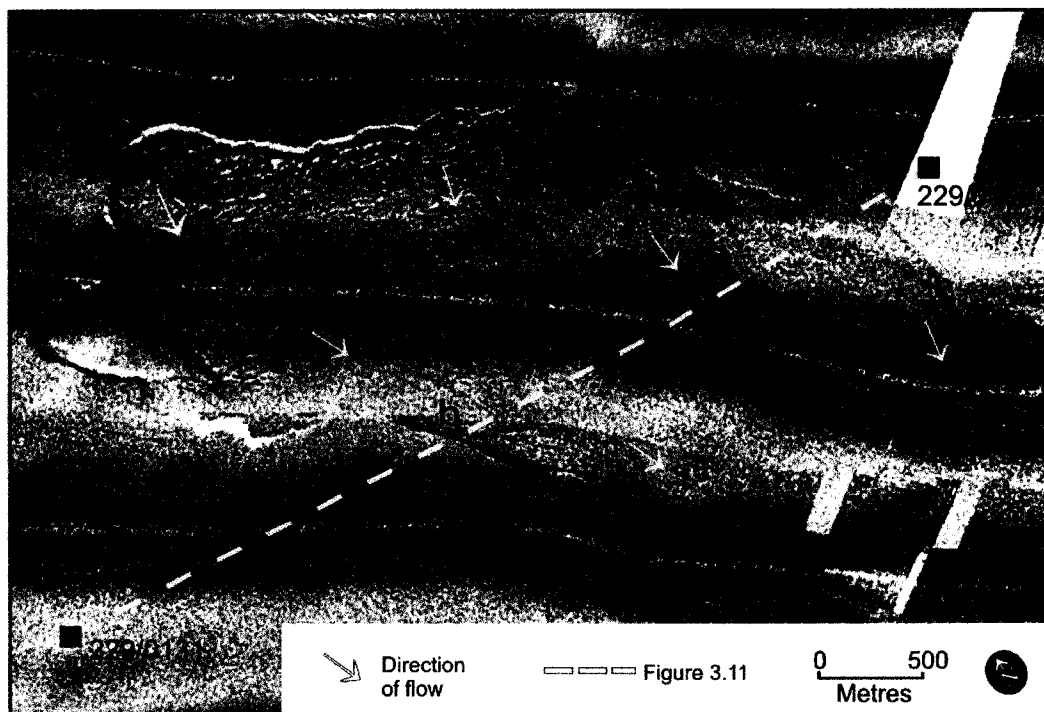


Figure 3.14- SAR sidescan sonar images of the middle St. Pierre Slope showing a plan view perspective of subclass IIA. 'a' and 'b' denote the scarps pictured in Figures 3.11 and 3.16. In the upper left corner, note the presence of linear ridges similar to the ridges pictured in Figure 3.10B that have been interpreted as Class I. Note the scarp that bounds the MTD complex on one side ('a' in Figures 3.11 and 3.14).

postulated that disintegration of failed bodies by shear deformation and mixing with water could produce this internal homogenization of bodies, thus giving internal transparency (Lee et al., 2002). The features discussed above are seen elsewhere on the

eastern Canadian margin. In particular, Mosher et al. (2004) recognized stacked debris flow deposits bounded upslope by a rotational slump that shows features consistent with retrogression-like failure. A similar deposit was found near the wreck of the Titanic, where a series of imbricate blocks exist upslope of a debris flow deposit (Savoye et al., 1990).

Class III – Possible creep deformation

This class was documented in one area. At the surface and internally, the body exhibits continuous to semi-continuous, wavy reflections. Wavelengths are variable, ranging from 200- 400 m, with subtle wave heights of a few to 10 ms. The transition from normal continuous reflections to wavy continuous reflections begins about 10 ms above the blue reflection (Q93) (Figure 3.15, inset). The body is present on gradients not exceeding 4°. At the seafloor, deposits of subclass IIA with thicknesses of no more than 15 ms and that lack internal coherency, follow the wavy surface morphology of this possible creep deposit.

Two scarps upslope of this creep-like body are shallow and extend down to the orange reflection (Q99), and a scarp downslope of this body extends down to the green reflection (Q97). Downslope of Class III is a deposit of Class I (depicted in Figure 3.8), that connects to Figure 3.15 at about 174/0607, demonstrating a possible connection between the two classes of deposit. In shallower water, upslope of this body, a depression (or gap) is bounded on either side by topographic highs about 15 ms in height (Figure 3.15). Laterally this 'gap' is ~ 300 m wide and it may be evidence of lateral spreading.

Lee and Chough (2001) recognized a similar situation in the South Korea Plateau and interpreted it as follows from shallow to deeper water: creep-like deformation, headscarp, scar and finally slumps and glides. This wavy continuous reflection pattern suggests development through deformation (Syvitski et al., 1987, Lee et al., 2002). These statements, together with the association of Class II, are suggestive of movements produced from creep-like deformation (Lee et al., 2002). However, the possibility that

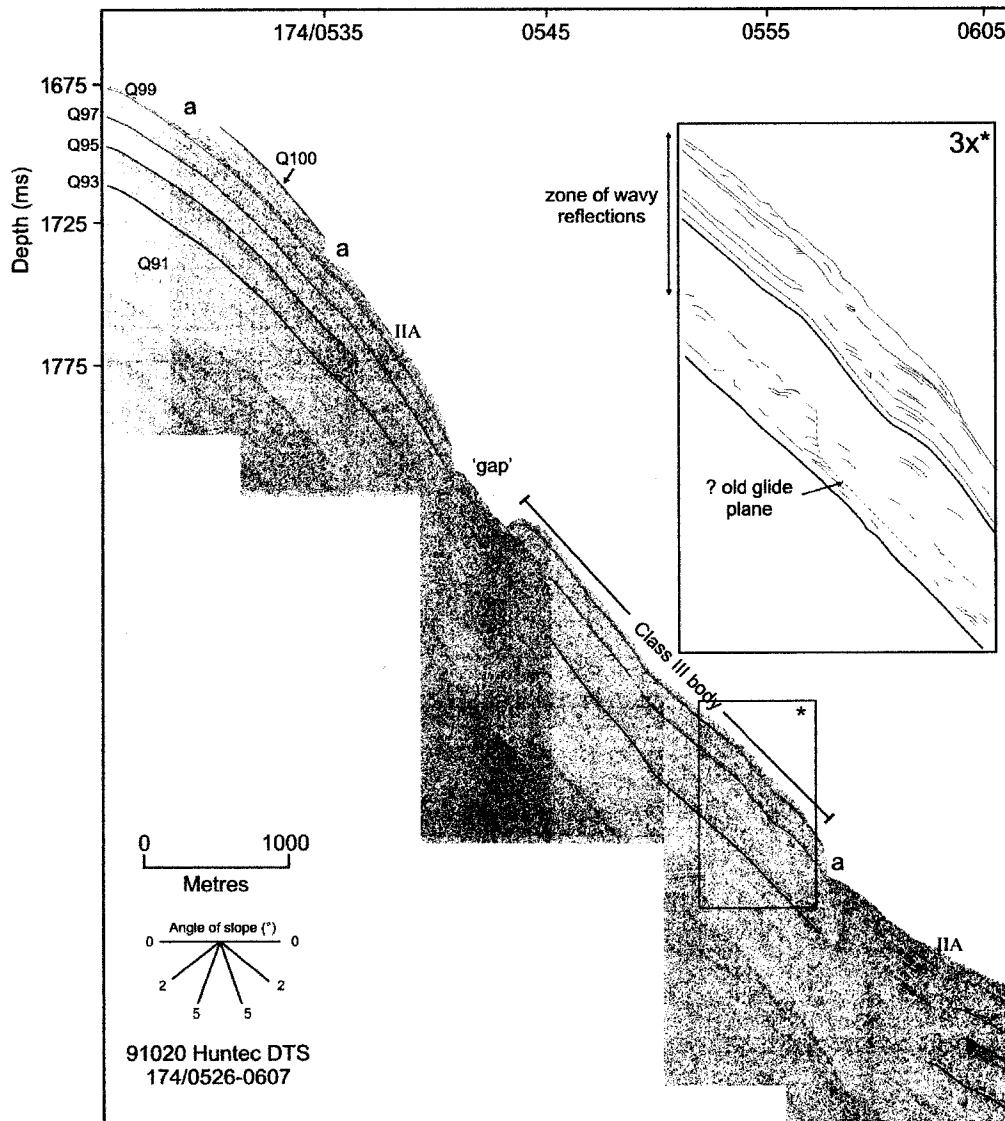


Figure 3.15- Hunttec DTS seismic reflection dip profile of the middle St. Pierre Slope showing a body of Class III (inset). Note the scarps (a), 'gap' and possible old glide plane. For figure location, see Figure 3.1.

this feature results from a drape of sediment conforming to an older irregular failure body cannot be excluded.

Class IV - *Glide block*

This class was documented in one area from the middle slope. The surface of the body shows a continuous, flat surface reflection. Internally, reflections become less coherent and continuous with depth, until the body terminates at a basal continuous reflection (Figure 3.16). Thickness of the body is uniform at 4.5 ms and extends about 250 m laterally. The body is juxtaposed to one side by a body of Class IIA and to the other side, appears to extend beneath continuous reflections that terminate at a scarp (Figure 3.16).

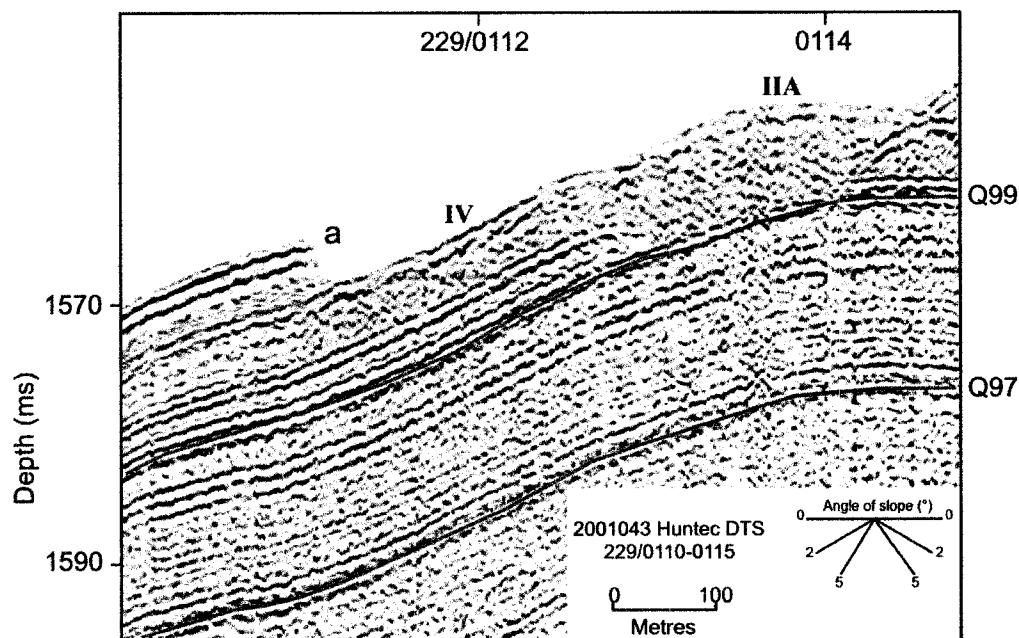


Figure 3.16- Hunttec DTS seismic reflection strike profile of a body of Class IV (blue) bounded to one side by a body of Class IIA (orange) and to the other side, appears to extend beneath a series of continuous reflections that terminate at a scarp (a). Context of this section is also visible in Figure 3.11 and Figure 3.14 (match the 'a'). For figure location, see Figure 3.1. Note- section is flipped horizontal when compared to 3.11.

The observed scarp, slightly distorted subsurface reflections, and inferred planar glide plane are typical of glide complexes that have been documented elsewhere in similar environments (Mulder and Cochonat, 1996; Lee and Chough, 2001; Lee et al., 2002). However, an alternative interpretation is that the body marks a transition between undisturbed stratigraphy and a body of Class II. This situation shows some similarities to a marginal slide block that marks the transition between a slump zone and undisturbed seabed as documented in Mosher et al. (1994).

Class V – Erosional surfaces

Class V consists of continuous reflections that in places are disrupted at the

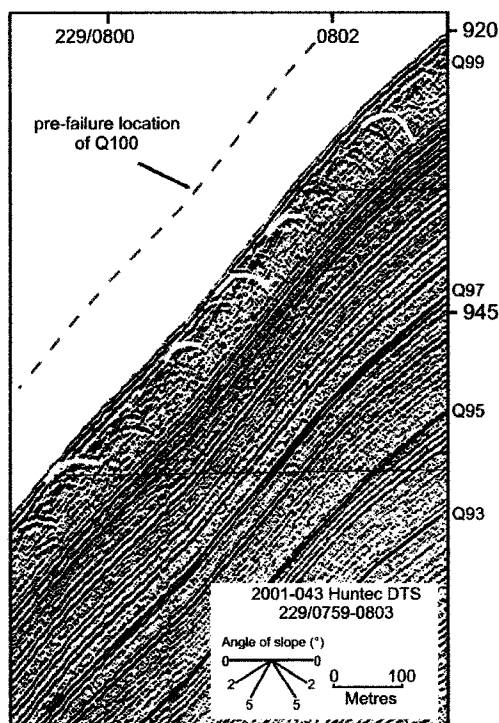


Figure 3.17- Hunttec DTS seismic reflection profile showing Class V. Some hyperbolic diffractions are labelled (yellow). Approximate position of brown (Q100) if failure had not taken place is shown. For figure location, see Figure 3.1.

surface by hyperbolae (Figure 3.17).

Representative sections display a nearly planar seabed of parallel, laterally continuous reflections. Cutting these parallel reflections are intermittent hyperbolae that extend down from the surface to a few milliseconds sub-bottom. Generally, lateral spacing of hyperbolae does not exceed more than a few tens of metres. This class is well represented within the study area on steep valley walls and areas where material has presumably been evacuated (e.g. Figure 3.10- 'b').

The presence of small hyperbolic diffractions at the surface and subsurface suggests an erosional surface of pits and scours. Similar features interpreted as surface erosion have been documented on the eastern levee of Eastern Valley in water depths exceeding 5500 ms and have been attributed to a large turbidity current (Piper et al., 1999a).

3.5 Geographic distribution of surface failure

Interpretations from seismic reflection data combined with bathymetric maps reveal a general relationship between gradients and the identified acoustic facies (Classes I-V). The seabed has been divided into zones based on gradients and identifiable features (e.g. valleys, channels, scarps, etc.) allowing for a distribution of failure classes to be established in relation to these divisions (Figure 3.18).

Zone 1- flat to gentle sloping seabed with very minimal dissection

Zones of flat to gentle sloping seabed are essentially undissected with gradients typically not exceeding 5°. To the west of the study area, this zone from the upper slope down to 1600 mbsl is bounded by upper Eastern St. Pierre Valley and St. Pierre Valley (Figure 3.18). To the east, this zone is bounded by tributary valleys of Grand Banks Valley. At about 1600 mbsl, the seabed becomes irregular due to small tributary valleys and this marks the downslope boundary for this zone. Some of these small tributary valleys merge with Grand Banks Valley and others with St. Pierre Valley.

Class II is the dominant acoustic class within this zone, forming as thin sheets < 15 ms thick. One body of Class I and the only example of Class IV are documented on the sidewall of a small valley at the eastern edge of this zone at 1100-1200 mbsl (Figures

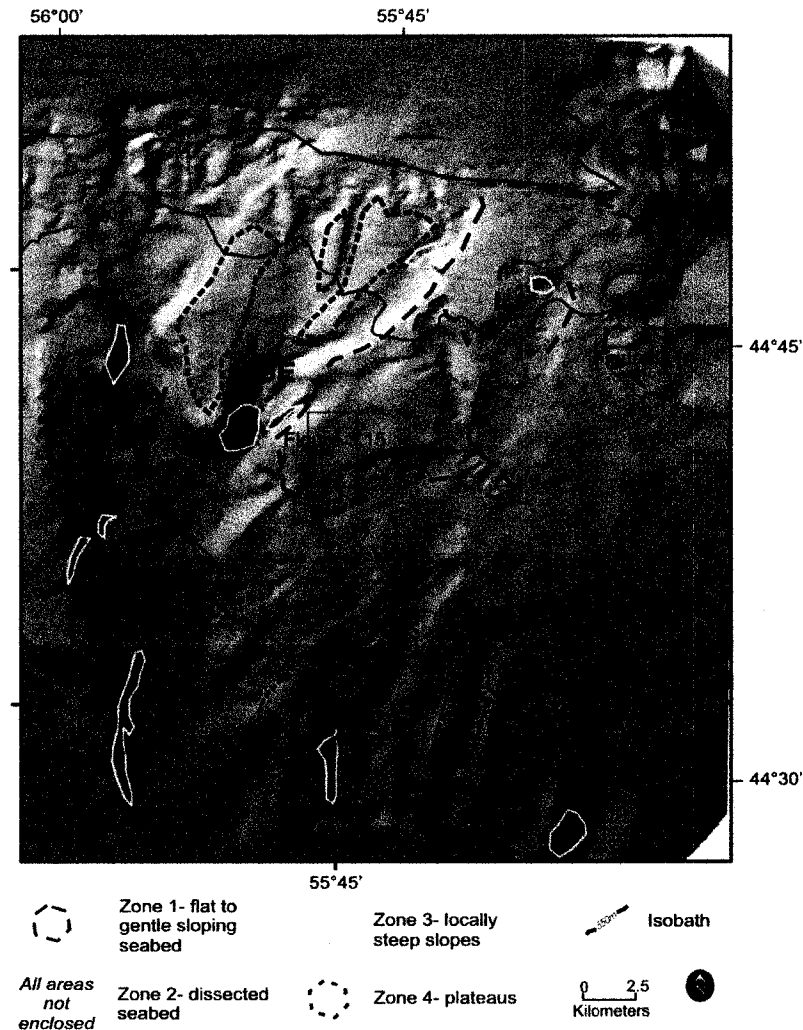


Figure 3.18- Surface render of St. Pierre Slope generated from regional bathymetric maps showing seabed morphology zones. The 550-m isobath corresponds to the approximate downslope limit of till. Each polygon of Zone 3 outlines an area where there are localized steep slopes. Not all areas of steep slopes have been outlined. Locations of Figures 3.14 and 3.15 are shown as they are isolated cases. Note- St. Pierre Valley is useful for orientation when comparing to other figures.

3.14 and 3.16). The one deposit of Class III is documented near the lower limit of this zone at about 1450 mbsl (Figure 3.15). Undisturbed seabed is found throughout this zone.

Zone 2- dissected seabed

Large valleys are mainly restricted to the central and western parts of the study area, beginning at about 500 mbsl (Figure 3.18). Prominent valleys within the study area are St. Pierre Valley and its two upper slope tributaries, Upper Western and Upper Eastern St. Pierre Valleys, and tributaries of Grand Banks Valley to the east. Other smaller valleys cut the upper, middle and lower slope. Valley sidewall gradients range from a few degrees up to 20°, and locally exceed 60°, as discussed below in Zone 3.

Classes I and II are well represented in this zone (Figure 3.19). Small feeder

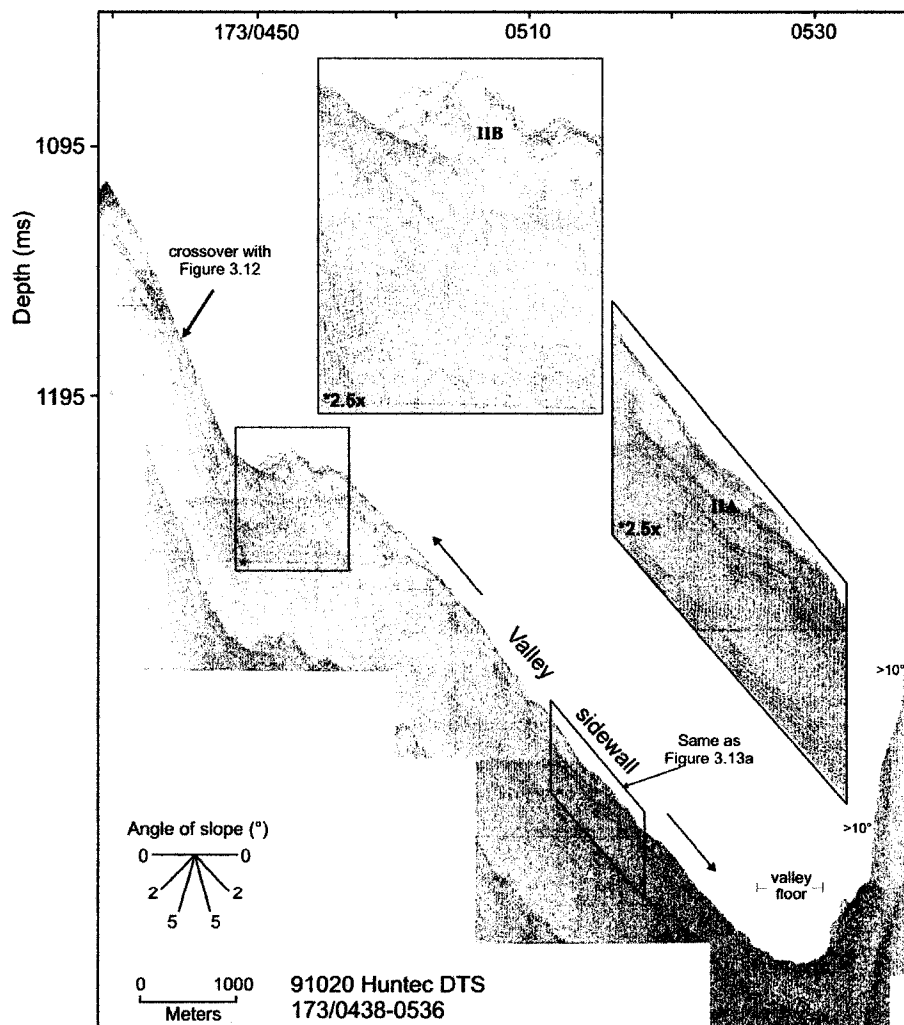


Figure 3.19- Huntec DTS seismic reflection profile showing bodies of subclasses A and B of Class II within a valley.

valleys of Upper Eastern St. Pierre Valley provide a good example of the interaction between subclasses A and B of Class II. Subclass B is prevalent near valley headwalls and at the base of steep slopes (Figures 3.12 and 3.19). Subclass A is common along valley axes downslope of valley heads and along valley sidewalls (Figures 3.13a, b and 3.19). Figure 3.20 provides a magnified plan view of this zone of feeder valleys and the relationship between Figures 3.12, 3.13b and 3.19. The valleys appear to act as

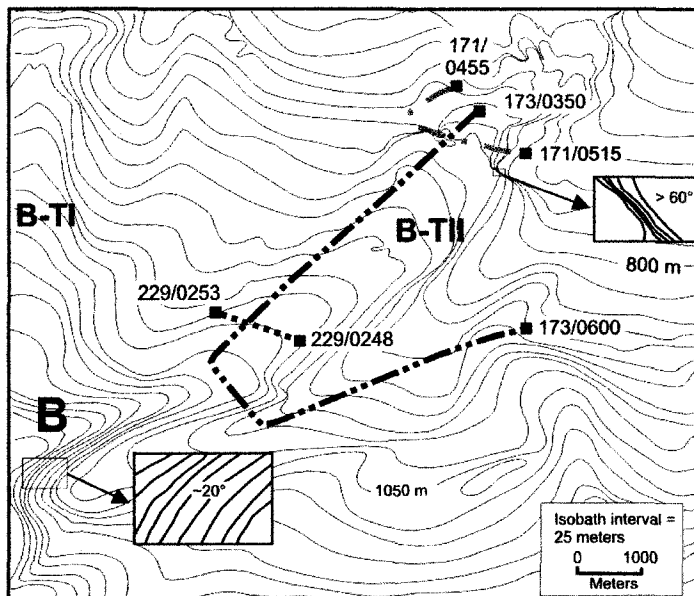


Figure 3.20- Bathymetry map of the upper to middle St. Pierre Slope showing the locations of Figures 3.12, 3.13b and 3.19. Letters are as follows: B = upper Eastern St. Pierre Valley; B-TI = upper Eastern St. Pierre Valley Tributary I; B-TII = upper Eastern St. Pierre Valley Tributary II. Examples of local gradients are shown (insets). Figure location is approximately the same as Figure 3.4.

isolated places near the base of the deposit increases to 10° (Figure 3.10). The other body is on a fairly consistent gradient of 6°. In deeper waters at 1550 mbsl, a body of Class II was documented at the headwall and sidewall of a valley. This body is substantially larger ($>10 \text{ km}^2$) than all other documented bodies of Class II (Figures 3.8 and 3.9) and is on a gradient that varies between 2-5°.

containments for bodies of Class II. Multiple bodies of Class I are present in this zone. Two examples from the headwalls of two spatially close valleys at 900 (Figure 3.10) and 1050 (Figure 3.14) mbsl show respective bodies of 0.69 km^2 and 1.25 km^2 (cross sectional area). Near the headwall of the body in shallower water, the gradient is 3° and in small

Zone 3- locally steep slopes (>10°)

Scarps and scars of Class V, and headwalls and sidewalls of some valleys represent locally steep slopes. This zone does not solely occupy a part of the seabed but is present within other zones, particularly Zone 2, where local gradients reach 60° (Figure 3.20). It usually marks the outer limits of Zones 1 and 3, but is present in places in Zone 1. In seismic reflection profiles, gradients have been measured up to 15° (Figure 3.12). Only bodies of Class I have been documented in a few isolated places in this zone (e.g. Figure 3.10B). Subclass B of Class II is common at the base of these steep slopes. Removal of sediment, revealing previously buried material that may or may not have been subjected to erosional processes, appears to be the dominant sedimentary process.

Zone 4- plateaus

Plateaus are raised areas that typically are bounded by valleys (Figure 3.18). This zone is similar to Zone 1 in morphology but is much smaller in area, which ranges from <1 km² up to 10 km². Class II is the only class documented in these areas, where it forms as thin sheets, a pattern very similar to the one discussed in Zone 1. However, much of these areas preserve the full, undisturbed, stratigraphic record (e.g. Figure 3.5). There seems to be minimal disturbance on and within these areas illustrated, except for converging hyperbolic diffractions thought to represent pockmarks (Figure 3.5; Piper et al., 1999a).

3.6 Volumes of sediment involved in surface failure

3.6.1 Volume of sediment existing as failed bodies at the surface

The total amount of all failed sediment in the study area has been estimated. The data coverage is insufficient to calculate accurate estimate of volumes for each of the defined acoustic classes. Rather, mean thicknesses and area of failed bodies within each slope division (upper, middle, lower and rise) are used to provide an estimate of the total amount of all failed sediment in the study area.

The size of the study area *based on the extent of Hunttec DTS data* (see Figure 2.1) is $3.2 \times 10^8 \text{ m}^2$ for the upper slope, $7.8 \times 10^8 \text{ m}^2$ for the middle slope and $9.1 \times 10^8 \text{ m}^2$ for the lower slope, for a total of **$2.01 \times 10^9 \text{ m}^2$** ($2,000 \text{ km}^2$). The bulk of the Hunttec DTS data shows failed sediment at the surface, suggesting that most of the study area has been affected by sediment failure, with the exception of a few places that show the compete, undisturbed seabed (sidescan sonar data aided in delineating undisturbed seabed). The estimated area of undisturbed seabed within the study area is:

- $1.2 \times 10^8 \text{ m}^2$ in the upper slope
- $1.0 \times 10^8 \text{ m}^2$ of middle slope
- $1.2 \times 10^8 \text{ m}^2$ in the lower slope
- Total area of **$3.4 \times 10^8 \text{ m}^2$** (340 km^2) of sediment that is undisturbed within the study area.

Data coverage on the rise is very sparse and thus, it has not been included in the above area calculations.

Average thickness of failed bodies at the surface have been calculated by taking the mean of the values in Appendix 1 (column titled ‘Thickness of surface MTDs’) and are:

- 6.9 ms (5.2 m) for the upper slope
- 8.5 ms (6.4 m) for the middle slope
- 9.0 ms (6.8 m) for the lower slope

Volumes of failed sediments still present within each slope region are calculated from the above values:

(Total area - undisturbed area) x mean thickness of body = volume of failed sediment (m^3).

$$\text{Upper slope} = (3.2 \times 10^8 \text{ m}^2 - 1.2 \times 10^8 \text{ m}^2) \times 5.2 \text{ m} = 1.04 \times 10^9 \text{ m}^3$$

$$\text{Middle slope} = (7.8 \times 10^8 \text{ m}^2 - 1.0 \times 10^8 \text{ m}^2) \times 6.4 \text{ m} = 4.35 \times 10^9 \text{ m}^3$$

$$\text{Lower slope} = (9.1 \times 10^8 \text{ m}^2 - 1.2 \times 10^8 \text{ m}^2) \times 6.8 \text{ m} = 5.37 \times 10^9 \text{ m}^3$$

Total volume of failed sediment still present in the defined study area is estimated to be **$1.08 \times 10^{10} \text{ m}^3$** .

3.6.2 Total volume of sediment that failed

Average total thickness of sediment that failed has been estimated from Hunttec DTS data. This is the total volume of sediment disturbed during failure, not just the sediment still present after failure, as in 3.6.1. One or two mean thicknesses have been estimated for each slope division, accounting for both shallow failure (labelled ‘a’ below) and sites of thick sediment evacuation and disturbance (labelled ‘b’ below).

In the upper slope - (a) is 12.5 ms (9.4 m) and no value for (b).

In the middle slope - (a) is 12.7 ms (9.5 m) and (b) is 47.7 ms (35.8 m).

In the lower slope – (a) is 10.9 ms (8.2 m) and (b) is 72.9 ms (54.7 m).

The following values are estimates of the total volume of sediment that was disturbed during failure. Italicized values are areas of seabed (primarily around valley headwalls and sidewalls) that experienced thick sediment evacuation and disturbance (typically >30 ms).

$$\text{Upper slope} - 2.0 \times 10^8 \text{ m}^2 \times 9.4 \text{ m} = \underline{1.88 \times 10^9 \text{ m}^3}$$

$$\text{Middle slope} - 3.0 \times 10^7 \text{ m}^2 \times 35.8 \text{ m} = 1.07 \times 10^9 \text{ m}^3$$

$$6.6 \times 10^8 \text{ m}^2 \times 9.5 \text{ m} = 6.26 \times 10^9 \text{ m}^3$$

$$\text{Total for middle slope} = \underline{7.33 \times 10^9 \text{ m}^3}$$

$$\text{Lower slope} - 1.0 \times 10^8 \text{ m}^2 \times 54.68 \text{ m} = 5.47 \times 10^9 \text{ m}^3$$

$$7.3 \times 10^8 \text{ m}^2 \times 8.21 \text{ m} = 6.0 \times 10^9 \text{ m}^3$$

$$\text{Total for lower slope} = \underline{1.147 \times 10^{10}}$$

$$\text{Total estimated thickness of sediment disturbed during failure} = \underline{2.07 \times 10^{10} \text{ m}^3}$$

3.6.3 Total volume of sediment evacuated

The total volume of sediment evacuated is calculated by subtracting the total volume of disturbed bodies remaining on the slope from the total volume of sediment that was disturbed during failure:

$$(\underline{2.07 \times 10^{10} \text{ m}^3}) - (1.08 \times 10^{10} \text{ m}^3) = \underline{0.99 \times 10^{10} \text{ m}^3}$$

3.6.4 Volume estimates applied to the entire region of surface failure

The above calculations are based on the outlined study area. A much larger area assumed to have been affected by surface failure has been estimated from additional

seismic data close to the study area and is $9 \times 10^9 \text{ m}^2$ (9000 km²) (Piper. pers. comm., 2005; see Figure 5.3). The only way to estimate the undisturbed seabed within this larger region is to assume that the proportion of disturbed to undisturbed seabed is similar to that of the study area. An estimate of the undisturbed area existing within the entire region affected by failure is:

$$\text{Study area} = \frac{3.4 \times 10^8 \text{ m}^2}{2.01 \times 10^9 \text{ m}^2 \text{ disturbed}} \quad \text{Entire region} = \frac{x}{9 \times 10^9 \text{ m}^2 \text{ disturbed}}$$

$$2.01 \times 10^9 \text{ m}^2 (x) = 3.06 \times 10^{18} \text{ m}^2 \quad x = 1.52 \times 10^9 \text{ m}^2 \text{ undisturbed seabed}$$

Subtract the undisturbed area from the entire region affected by failure:

$9 \times 10^9 \text{ m}^2 - 1.52 \times 10^9 \text{ m}^2 = 7.48 \times 10^9 \text{ m}^2$ is the total area affected by surface failure.

This value, $7.48 \times 10^9 \text{ m}^2$, multiplied by 8.4 ms (6.3 m); the mean thickness of failed bodies from the upper, middle, and lower slope, gives $4.71 \times 10^{10} \text{ m}^3$ for total volume of failed bodies still present in the entire region after failure. The mean value for thickness of sediment disturbed is 16.7 ms (12.5 m). Doing the same calculation as above gives $9.35 \times 10^{10} \text{ m}^3$ for total volume of sediment that was disturbed during failure.

The total amount of sediment evacuated from the entire region is calculated by subtracting the total volume of failed bodies remaining after failure ($4.71 \times 10^{10} \text{ m}^3$) from total volume of sediment that was disturbed during failure ($9.35 \times 10^{10} \text{ m}^3$) = $4.64 \times 10^{10} \text{ m}^3$.

The values obtained from the entire region show a similar pattern in that the volume of sediment remaining after failure (MTDs) is roughly half of the total volume of sediment that was disturbed during failure.

For further details on how depth, area and volume were calculated were described in Chapter 2 and notes on Appendices 1 and 2.

3.7 Subsurface disturbed bodies

Besides the acoustic classes already recognized at the surface, many subsurface bodies were documented in Huntect DTS data that exhibit properties consistent with Class II. Where bodies could be related to the key reflections, the majority occur a few milliseconds to tens of milliseconds beneath Q91 (Figures 3.9, 3.11 and 3.21). In places in the lower slope, subsurface bodies disrupt the continuity of the green and red reflections (Q97 and Q95), and the accumulation of these bodies over one another in combination with other failure deposits (e.g. turbidites) causes an increase in the depth of

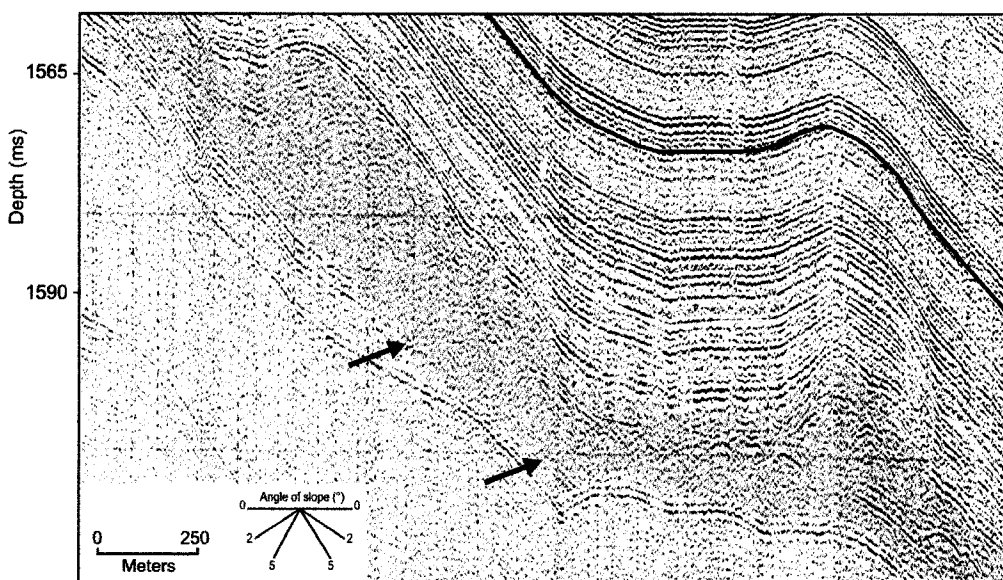


Figure 3.21- An enlarged section of Figure 3.11. Profile shows stacked, internally incoherent bodies with hyperbolic to undulating surface reflections. Underlying continuous reflections are disrupted in places (arrows). blue and yellow (Q93 and Q91). This is shown numerically in Table 3.1, where mean depths for reflections Q91 and Q93 increase by >10 ms from the middle slope to the lower slope.

Acoustic properties of these buried bodies are suggestive of both subclasses of Class II. Morphology of these buried bodies is wedge- and lens-shaped when restricted to valleys and sheet-like on flat to gentle sloping seabed regions. Surface returns from these bodies typically are a combination of weak to strong, undulating and hyperbolic reflections (Figure 3.21). Internally, the bodies are acoustically chaotic. The bases of the bodies overlies and in places interrupt continuous reflections (Figure 3.21). Stacking of bodies, in both valley and flat seabed zones, is common, with bodies being a few to tens of milliseconds thick.

CHAPTER 4

Core data

4.1 Introduction

Eighteen piston cores and, when available, associated trigger weight cores representative of both the undisturbed and disturbed stratigraphy of St. Pierre Slope were studied (Figure 4.1). Eleven cores show the normal stratigraphic succession and the remaining seven cores sampled areas affected by sediment failure. Each core was correlated to the nearest Hunttec DTS high-resolution seismic profile to provide a general understanding of the surface and subsurface acoustic setting (Appendix 2). In a few cases, supplementary 3.5 kHz or 12 kHz profiles were used, as Hunttec DTS data were unavailable at or near the core site. Positions of cores relative to seismic reflection profiles are accurate in most cases to within tens of meters. A few cores did not have complementary seismic data and therefore were projected into the closest seismic reflection profile, giving a station-to-seismic-profile separation of up to 2 km.

All piston and trigger weight cores were visually examined to obtain the stratigraphic succession and for evidence of mass transport deposits (MTDs). Downcore plots showing sediment type and color and, if present, types of MTD facies were completed (Appendix 2). Spectrophotometer analysis accompanies all post-1998 cores and are shown in the downcore plots as L^* , a^* , and b^* color values. A few critical pre-1998 cores were reanalysed for L^* , a^* , and b^* .

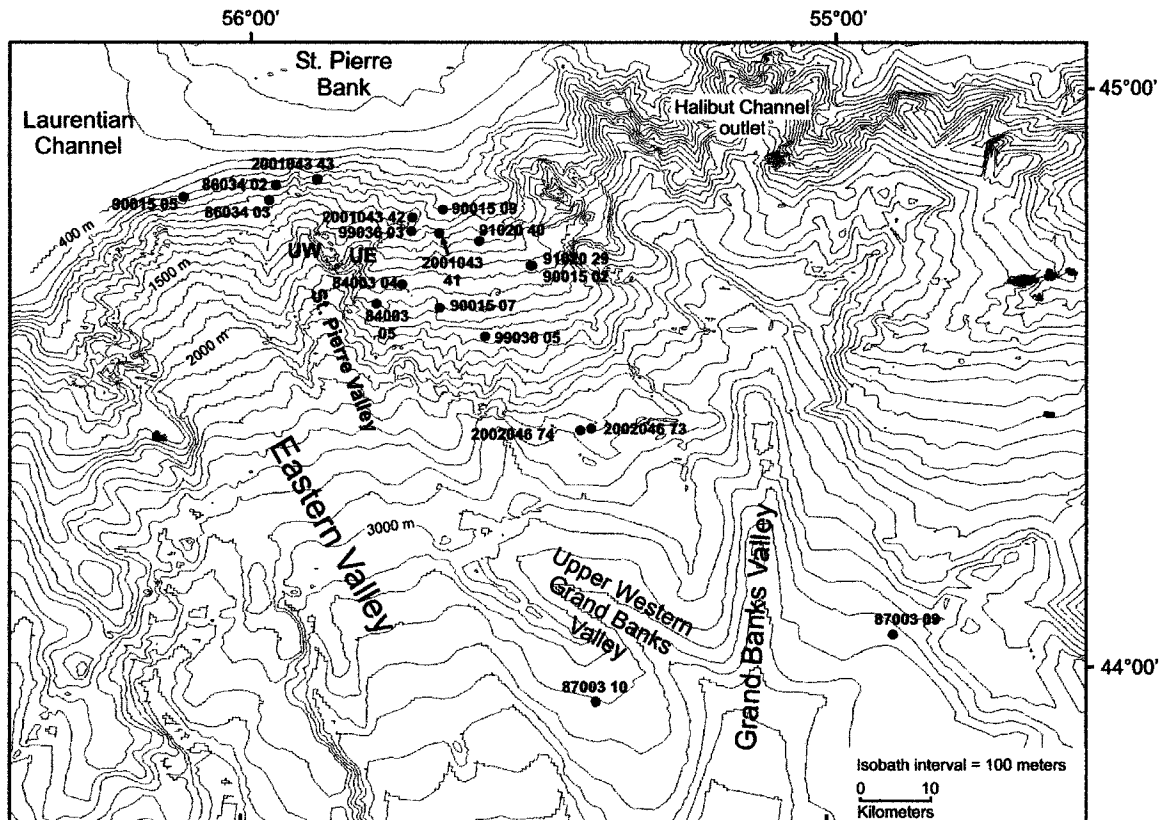


Figure 4.1 - Map of St. Pierre Slope and vicinity showing locations of the eighteen cores (black dots) used for this study (cruise and cores numbers are shown). Major valleys are labelled (UW=upper Western St. Pierre Valley and UE=upper Eastern St. Pierre Valley).

Magnetic susceptibility, velocity, bulk density and shear strength data are available for most cores. In this study, these values, and in particular shear strength, were most useful for recognizing unconformities (e.g. MTD facies boundaries) and for estimating depth of burial prior to failure for cores taken at scarps, using an approach similar to that of Mulder et al. (1997). Each trigger weight core was correlated to its associated piston core to better estimate the correct position of the piston core relative to the seabed. Sediments from cores that sampled failures were interpreted and classified into five facies based on internal character and structure: four MTD facies and an undisturbed facies.

A better understanding of the late Pleistocene and Holocene slope lithostratigraphy and evolution was achieved through examination of the eleven undisturbed cores. Cores that sampled surficial MTDs provide insight into failure dynamics at a mesoscale level (relative to the failures identified in seismic profiles) and provide useful data for comparison with other similar failure complexes, such as MTDs found on the Scotian and the European margins.

4.2 Radiocarbon ages obtained from sediment cores

Seven cores from this study yielded AMS radiocarbon ages ranging from the Late Pleistocene to Holocene (Table 4.1). Only one age, from piston core 90015-07, was obtained specifically for this study. A mollusc shell taken 132 cm downcore yielded a radiocarbon age of 30230 ± 290 radiocarbon years, with a reservoir corrected age of 29820 radiocarbon years. Complementary 3.5 kHz data and high shear strength measures confirm that the core site is from the in-situ stratigraphy (not a resedimented block) at a ~56-m-deep failure plane just below Q91.

All radiocarbon ages are from benthic mollusc samples. The upper and middle slopes are relatively well represented with radiocarbon ages obtained from five cores, in contrast to the lower slope and rise, for which only two radiocarbon ages are available (Table 4.1). Ages from three cores not studied in this thesis are included to aid the establishment of sedimentation history.

Radiocarbon ages mentioned throughout this chapter are non-reservoir corrected conventional ages in radiocarbon years before present.

Cruise-core #	Sample depth in core (cm)	Latitude (dec°)	Longitude (dec°)	Water depth (mbsl)	Conventional ¹⁴ C age (BP)	Reservoir corrected ¹⁴ C age (BP)	Lab N ^o .
86034-PC03	120	44.8185	-55.9673	832	12090 +/-220	11680*	Beta 20734
87003-PC10	110	43.8417	-55.3887	3300	5550 +/-60	5140	TO 7000
90015-PC02	369	44.6837	-55.5225	1300	13400 +/-110	12990	TO 2086
90015-PC02	753	44.6837	-55.5225	1300	15480 +/-140	15070	TO 2087
90015-TWC05	59	44.8115	-56.1270	575	8640 +/-80	8230	TO 4264
90015-PC05	4	44.8115	-56.1270	575	10960 +/-90	10550	TO 4255
90015-PC05	49	44.8115	-56.1270	575	10490 +/-80	10080	TO 4263
90015-PC05	95	44.8115	-56.1270	575	10870 +/-80	10460	TO 4262
90015-PC05	157	44.8115	-56.1270	575	10860 +/-90	10450	TO 4261
90015-PC05	245	44.8115	-56.1270	575	11150 +/-110	10740	TO 4260
90015-PC07	132	44.6085	-55.6860	1621	30230 +/-290	29820	Beta 188399
90015-PC09	2	44.7823	-55.6797	700	10270 +/-80	9860	TO 2391
99036-PC03	600	44.7440	-55.7356	915	14170 +/-120	13760	TO 9095
86034-PC09-a	144	44.7185	-55.5425	1134	15190 +/-130	14780	Beta 28267
84003-PC11-a ⁺	764	44.8353	-55.9017	750	11300 +/-160	10890	Beta 12354
84003-PC13-a	436	44.8327	-55.7347	600	11800 +/-200	11390	Beta 16701

* - The reservoir correction of 410 years is equivalent to a fractionation correction to a base of ¹³C = 0‰. To obtain the reservoir corrected age, subtract 410 years from the given conventional radiocarbon age (Isotrace Radiocarbon Laboratory, 1990).

a - Cores not studied in detail in this thesis but included here to help determine sedimentation history.

⁺ - Same location as core 2001043-43.

Table 4.1 - AMS radiocarbon dates for benthic mollusc samples recovered from St. Pierre Slope shallow sediment cores. Ages quoted as radiocarbon years before present (BP).

4.3 Sedimentary facies

Four sediment types and six colors are recognized within the eighteen cores studied (downcore plots in Appendix 2). The sediment types range from mud to muddy sand and the colors of the sediment are: olive gray, gray, tan, brick red, reddish-brown, and brown. From these types and colors, seven facies (A-G) within the undisturbed cores were distinguished (Table 4.2). The following is a detailed description of the sediment type, color and properties of facies A-G in undisturbed cores. 'MUD' in the following descriptions denotes a mixture of silt and clay. The sequence of sedimentary facies from A-G does not imply relative age. However, facies A and B were normally at the top of the cores and facies C-G in the middle and bottom of the cores.

FACIES A - Olive Gray MUD - Structureless mud is the topmost facies in all trigger weight cores (TWC) and in the majority of piston cores (PC) from the upper slope to rise, with a maximum surface-to-downcore-depth of 700 cm. In the upper and middle slope, this facies contains thin beds (cms) of facies B. Silty patches, mm to cm in size and mud clasts (mostly shades of gray) are rare but when present occur deeper downcore in the facies. Bioturbation, mottling, shell fragments and foraminifera are common, especially near the upper boundary of the facies (or core-top). Burrows, identified as *Zoophycos* traces, are common and in places filled with silt and fine sand. Bulk density measurements from MST vary from 1.8 to 1.9 Mg m⁻³.

The unit also occurs as deeply buried (up to 1230 cm downcore), thin beds (cms) in cores from the lower slope and rise, where it is interbedded with reddish-brown mud of facies E and further downcore, with gray mud of facies D. Bed thickness varies from 5-

Facies	Name	Occurrence	Characteristics and distribution
A	Olive gray MUD	Upper slope to rise	Structureless when the topmost facies. Silty patches are common deeper downcore. Bioturbation, mottling, and foraminifera are fairly common as are <i>Zoophycos</i> burrows that sometimes are sand-filled. The facies is thin (cms) where deeply buried (up to 1230 cm downcore) in deeper water and shows faint color laminations. Topmost facies in all trigger weight cores and in most piston cores from the upper slope to rise.
B	Olive gray MUD with sand	Prevalent in upper slope	Sand as 1-5 cm thick lenses, mm-cm-sized patches and as thin laminae. Primarily restricted to the upper slope with the exception of one thin, gravely sandy bed at 3200 mbsl. IRD and shell fragments are minor.
C	MUD with IRD and patchy sand	Upper to middle slope	Consists of brown and gray mud. This facies is overlain by facies A and in places alternates with both facies A and facies B. Patchy sand and IRD as stones are common. Sand commonly fills burrows and shows a downcore increase in concentration. Bioturbation is moderate, but in places, especially within gray mud, is intense.
D	MUD with color laminations, sparse IRD and little bioturbation	Lower slope to rise	Thick beds of gray mud interbedded in places with thin beds of brown mud that are overlain by structureless olive gray mud of facies A. Silty mud patches, usually shades of the surrounding sediment color, are seen throughout the facies. Mottling of gray and brown mud common as are color laminations of black and red-brown within the gray mud. Color and sediment laminations are distinct and in places on the rise are intense. IRD are sparse and noted in gray mud.
E	Reddish-Brown MUD	Prevalent in lower slope to rise	Reddish-brown mud that is structureless on the middle slope and is color and silt laminated in deeper water cores. Facies thickness increases with depth (~10 cm upslope and upwards of 125cm in deeper water). Laminations of varying color are widespread and typically do not surpass a few mm thick. Mottling is moderate and sandy patches are rare. Bounded above by facies A and below by facies C and or D. Contained within this facies in the lower slope and rise is a thin bed of facies F and multiple thin beds of facies A.
F	Brick Red MUD	Lower slope to rise	The facies has a significant sand fraction and a minor gravel component, and has significant amounts of iron-stained quartz with traces of red siltstone and shale. Facies increases in thickness with water depth and is found within facies E.
G	Tan MUD	Lower slope to rise	Contains a high proportion of detrital calcite and dolomite. Disseminated sand, reactivity to hydrochloric acid and rare gravel also characterize this facies. Facies increases in thickness with water depth. Bounded above and below by olive gray mud of facies A.

Table 4.2 - The seven lithofacies from undisturbed cores on the St. Pierre Slope and rise. IRD refers to ice-rafted detritus.

40 cm. The beds of this facies within the reddish-brown mud of facies E show faint color laminations.

FACIES B- Olive Gray MUD with sand - This facies consists of mud with sand concentrated as 1-5 cm thick lenses, mm-cm-sized patches and as thin laminae. Bulk density measurements from MST vary from $1.9\text{--}2.0 \text{ Mg m}^{-3}$. Facies B occurs as thin beds (cms) within facies A and is almost entirely restricted to cores from the upper slope, with the exception of one thin, gravely sandy bed in core 87003-09 at 3200 mbsl. IRD and shell fragments occur as minor components.

FACIES C- MUD with IRD and patchy sand - This facies consists largely of brown mud but in places is present as thin beds (cms) of gray mud. Silty patches are minor and occur more often as small blebs (mms). Sand commonly fills burrows and shows a downcore increase in concentration. Overall bioturbation is moderate, but in places, especially within gray mud, is intense. P-wave velocity of the brown mud of this facies is relatively uniform at $1500 \text{ to } 1525 \text{ m s}^{-1}$, but varies for the gray mud from $1400 \text{ to } 1600 \text{ m s}^{-1}$. This facies occurs in the upper and middle slope where IRD as gravel-sized stones and patchy sands are common.

FACIES D- MUD with color laminations, sparse IRD, and little bioturbation-

This facies consists of thick beds of gray mud interbedded in places with thin beds of brown mud. Silty mud clasts, usually shades of the surrounding sediment, are seen throughout the facies. Mottling of gray and brown mud, and color laminations of black

and red-brown within the gray mud are common. Laminations picked out by color or sediment grain size are distinct, particular in places on the rise, and might be indicators for turbidite deposition. In gray mud, IRD is sparse and consists of angular stones up to 6 cm in diameter. Bulk density measurements from this facies fluctuate from 1.5 to 1.8 Mg m⁻³, gradually increasing with depth of burial. The facies is restricted to the lower slope and rise.

FACIES E- Reddish-Brown MUD – This facies consists of reddish-brown mud that is structureless on the middle slope, and on the lower slope and rise is silt- and color-laminated and in places has disseminated sand. The silt laminae typically are a few mm thick and generally occur at spacings ≥ 1 cm. In places where the facies is surrounded by brown mud of facies D, the color laminae are black and reddish-brown, and where bounded above and below by gray mud of facies D, the color laminae are olive gray and grayish brown. Mottling is moderate in most of the individual beds. Sandy mud patches are present but not widespread. On the middle slope, the facies is 10-20 cm thick, and in deeper water, facies thickness increases up to 125 cm. Magnetic susceptibility measurements of this facies are fairly constant at 35 SI units, fluctuating ± 2 SI units. In some cores, the reddish color of this facies was very subtle and the ‘a*’ trace was essential to differentiate it from brownish muds.

FACIES F- Brick Red MUD - The brick red color of this facies is distinctive and distinguishes it from all other facies. It has a significant sand fraction and a minor gravel component, and has large amounts of iron-stained quartz with traces of red siltstone and shale. This facies is documented as a single bed of 10 cm in core 99036-05 from the

lower slope and a 15-20 cm bed in four cores (87003-09 and -10, and 2002046-73 and -74) from the rise. Magnetic susceptibility measurements are relatively uniform with an average of 45 SI units. This facies in cores 87003-09 and -10 was previously interpreted to represent 'Brick red mud' unit d (Piper and Skene, 1998 and Skene and Piper, 2003). Piper and Skene (1998) dated this bed on the Scotian margin at 14.4 ka.

FACIES G- Tan MUD – This facies has a distinctive color and contains a high proportion of detrital calcite and dolomite (Skene and Piper, 2003). Disseminated sand, reactivity to dilute hydrochloric acid and rare gravel also characterize this facies. Four cores sampled this facies, all at 1800 mbsl or deeper. In cores 99036-05 and 2002-046-PC73 (1800 and 2600 mbsl) facies thickness is 10 cm and in cores 87003- PC09 and -PC10 (3200 and 3300 mbsl) facies thickness is 15 cm. This facies in cores 87003-09 and -10 was previously interpreted to represent Heinrich event 1 (H1) (Skene and Piper, 2003). A similar facies was previously dated at 14.4 ka in the North Atlantic Ocean (Bond and Lotti, 1995).

4.4 Stratigraphic distribution of sedimentary facies in undisturbed cores

4.4.1 Downcore facies distribution on the slope and rise

On the upper slope, the stratigraphic section is represented in four cores from 550-850 mbsl (Figure 4.2). Two cores (90015-05 and 86034-02) contain a probably correlative bed of facies C that is 2-3 m thick, overlain and underlain by facies A. Beds of facies B, up to 25 cm thick, are interbedded with facies A both below the bed of facies C and above it in the shallower-water core. Core 86034-03 sampled < 2 m of facies A beneath a surface unconformity and likely never penetrated to facies C. Core 90015-09

consists principally of facies C, with thin interbeds of facies A and B. Its lithostratigraphic correlation with the other upper slope cores is uncertain.

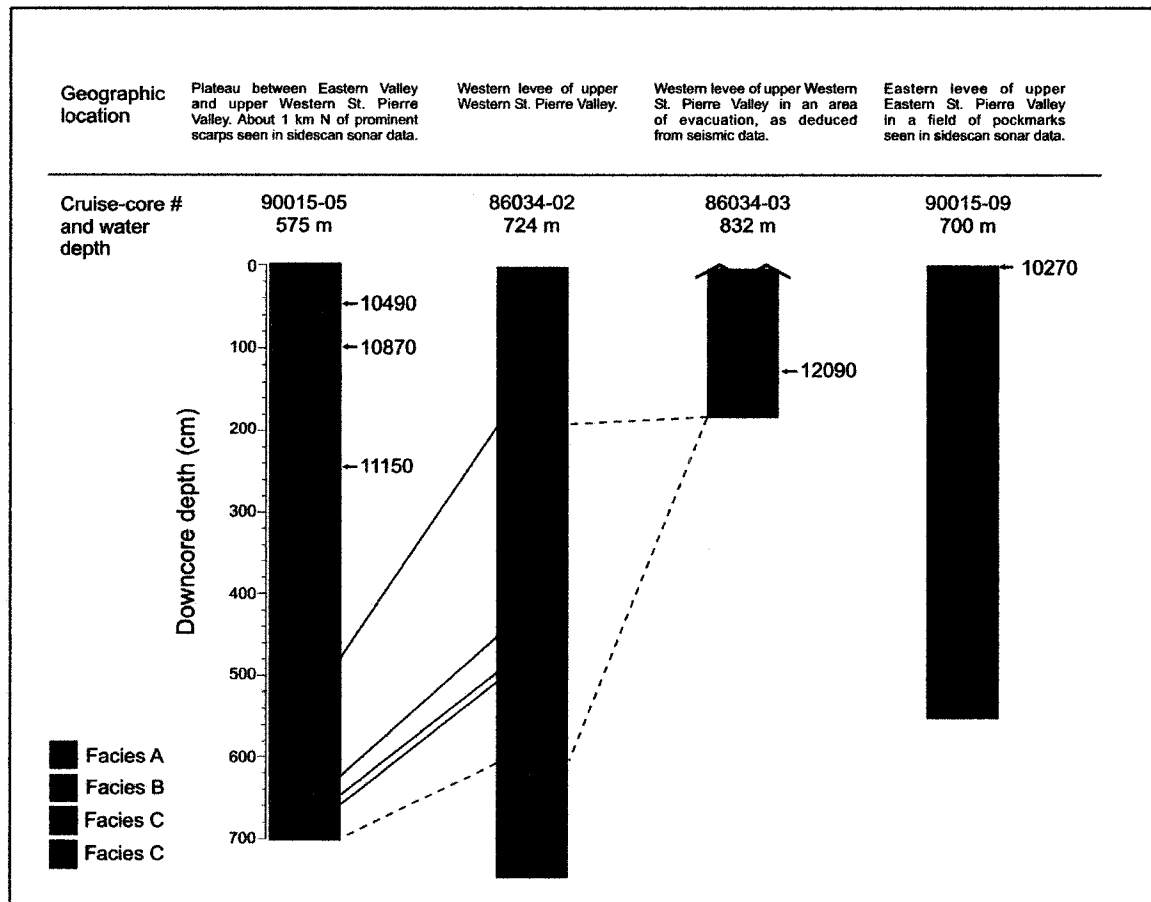


Figure 4.2 – Piston core stratigraphy of the upper St. Pierre Slope. Gray and brown muds of facies C have been distinguished. Solid lines denote confident lithologic correlations and dashed lines denote likely lithologic correlations. Radiocarbon ages are shown beside core at proper stratigraphic interval.

On the middle slope (850-1400 mbsl), three cores (Figure 4.3) show an upper section correlative with that on the upper slope. A 2-3 m thick bed of facies A overlies 3-4 m of brown muds of facies C. In two of the cores, this rests on a distinctive 0.4-0.6 m thick bed of grey mud of facies C that is clearly distinguished by the 'a*' trace in Figure 4.3. Below this grey mud marker bed are several metres of brown mud of facies C, with

interbeds of facies E 0.1-0.4 m thick in core 99036-03. At the base of two cores is another development of structureless olive grey mud of facies A.

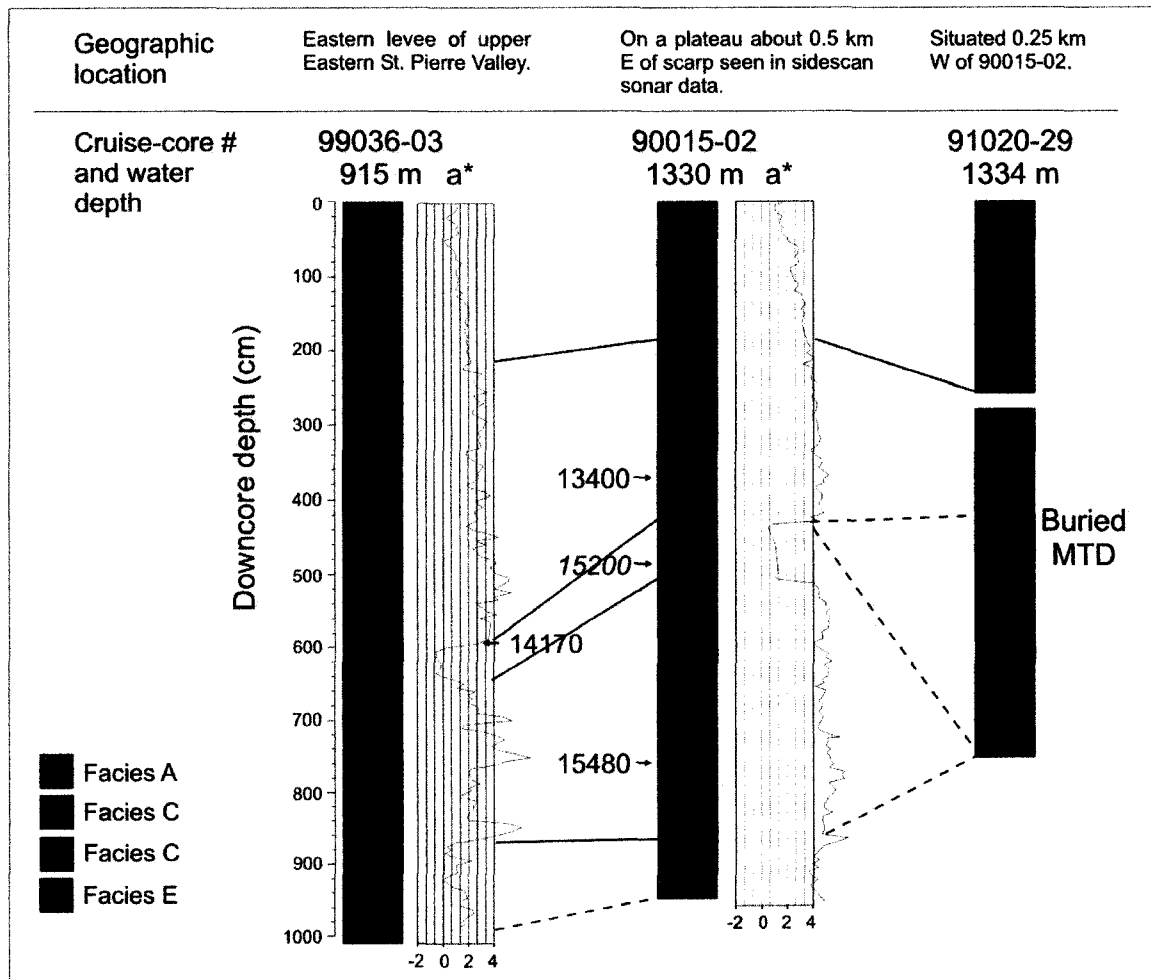


Figure 4.3 – Piston core stratigraphy of the middle St. Pierre Slope. Gray and brown muds of facies C have been distinguished. The 'a' color trace aids correlation and where the trace shows a strong deviation to the right in core 99036-03 (second bed of facies E), might represent traces of facies F. Solid lines denote confident lithologic correlations and dashed lines denote likely lithologic correlations. Age of 15200 is from 86034-09.

The lower slope and rise (1800-3300 mbsl) is represented by five cores (Figure 4.4). Facies A extends from the core-top down to about 250 cm in four of the cores and down to 800 cm in the deepest water core, and overlies a complex sequence of facies D, E, F and A (as deeply-buried thin beds). Facies A is homogeneous except near its lower boundary where a thin bed of facies G is found in four of the cores. Isolated beds of

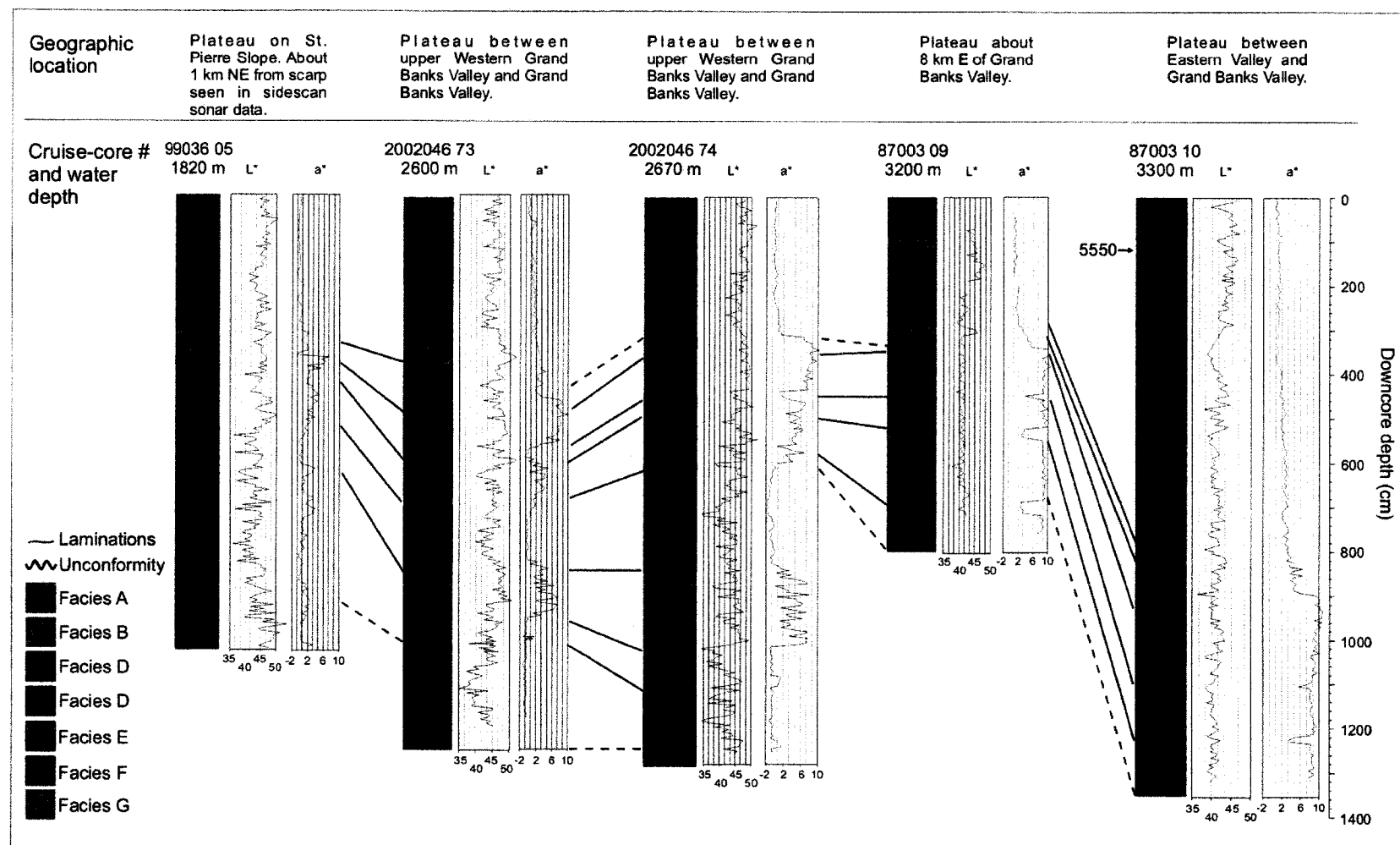


Figure 4.4 - Piston core stratigraphy of the lower St. Pierre slope and rise. Gray and brown muds of facies D have been distinguished. Solid lines denote confident lithologic correlations and dashed lines denote likely lithologic correlations.

facies B interbed with A 100 cm downcore in 87003-09. The typical facies sequence below the topmost facies A for the three shallower water cores is as follows: a thin bed of facies F and multiple beds of facies A are interbedded with structureless to laminated reddish-brown mud of facies E over a thickness of several meters. Facies E is then underlain by a thin bed of brown mud of facies D resting on laminated gray mud of facies D that continues to the core-bottom. Within this gray mud are a few beds of facies A and one thick, laminated bed of facies E (absent in 99036-05). Cores 87003-09 and -10 from the rise show a similar pattern; facies E contains a thin bed of facies F and multiple beds of facies A, but this sequence continues to the core bottom, and the underlying gray and brown mud of facies D does not appear to have been sampled (Figure 4.4). The topmost bed of facies A contains near its lower boundary a 20 cm interval of facies G, compared to the 10 cm thick bed of the same facies in cores 99035-05 and 2002046-73. Facies G, F, and the top and bottom of the main succession of facies E can be used as lithostratigraphic markers (Figure 4.4).

The undisturbed cores show systematic variation with geographic position on the slope and rise. Near the mouth of Laurentian Channel off the western edge of St. Pierre Bank, three cores (A-C in Figure 4.5) are dominated by olive gray mud of facies A and B. Radiocarbon ages in the upper meter are 10.5 to 10.87 ka suggesting low rates of Holocene sedimentation. There is no sign of brown mud of facies C within these three cores, but 1.0- 2.5 m of gray mud of facies C is present in cores 86034-02 and 90015-05. Two meters above this gray mud, facies A is dated at 11.15 ka radiocarbon years (Figure

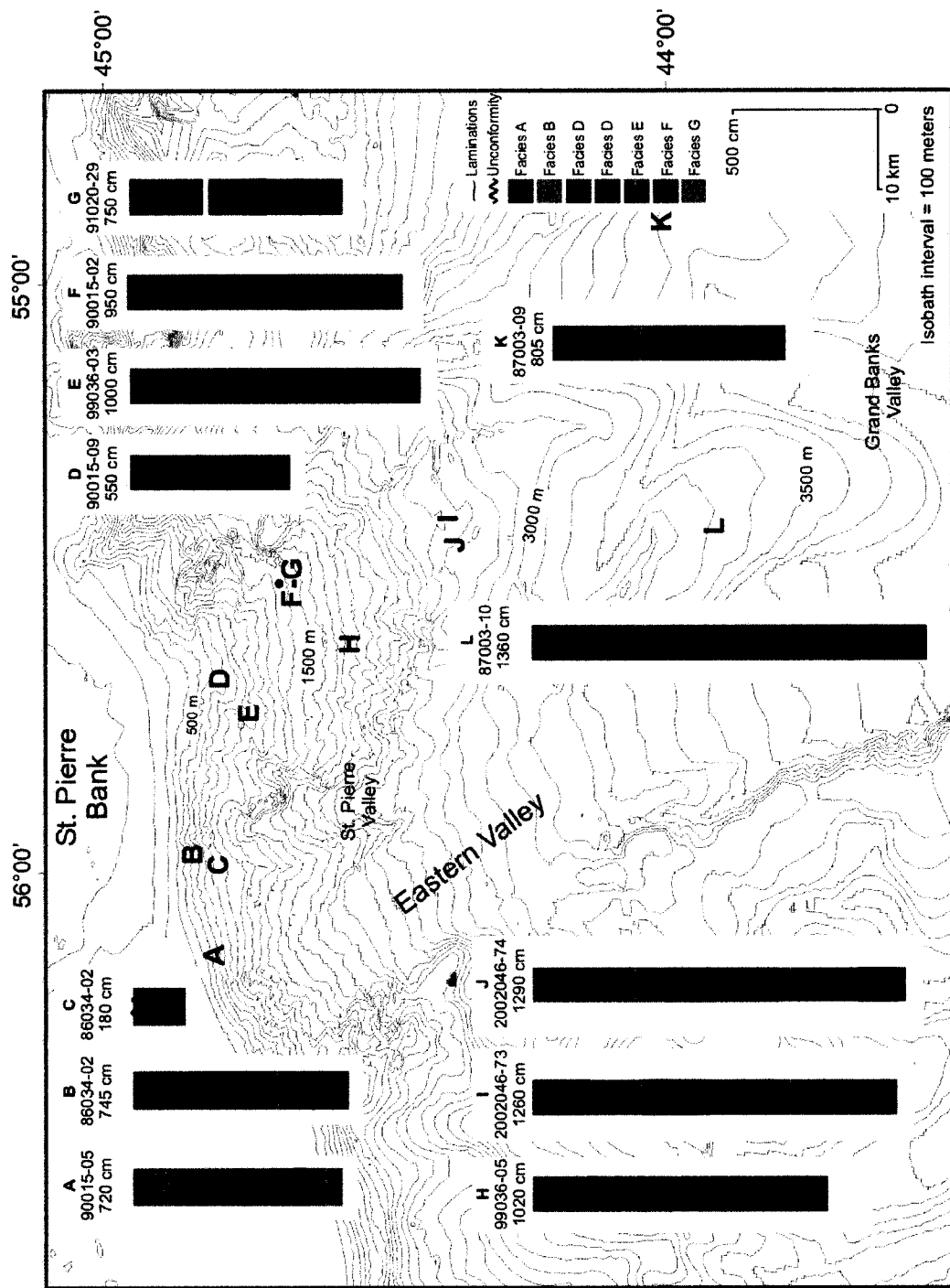


Figure 4.5 - Bathymetry map showing locations and downcore color plots of piston cores that sampled undisturbed sediments. Letters A-L represent core locations. Cruise and core number, and core length in cm are shown above each downcore plot.

4.2). Core 86034-03, about 1.25 km south of 86034-02, sampled olive gray mud of facies A at a ~10-m-deep scarp that at 120 cm downcore yielded a 12.1 ka radiocarbon age. According to Bonifay and Piper (1988), sedimentation rates at this time did not exceed 1

m ky⁻¹. This rate suggests that the gray mud of facies C was likely located below the base of the core in 86034-03.

Thick sequences of Late Pleistocene brown muds of facies C overlain by facies A are observed in cores located off the eastern edge of St. Pierre Bank near the mouth of Halibut Channel (Cores D-G in Figure 4.5). Beds of facies B yielded an age of 10.27 ka (Figure 4.2) radiocarbon years at 2 cm downcore, which suggests a fairly low sedimentation rate, erosion, sample disturbance and or reworking of olive gray mud during this period. Brown mud continues to the bottom of the three cores and in cores 90015-02 and 99036-03 is interrupted by an interval of gray mud of facies C, the top of which is dated at 14.2 ka radiocarbon years in 99036-05. In core 90015-02, the middle and about 0.5 m above this gray mud are dated at 15.2 ka and 13.4 ka radiocarbon years, respectively.

Cores from the lower slope and rise contain considerable thicknesses of Holocene sediments of facies A. Unfortunately, only one radiocarbon age, 5.5 ka at 110 cm downcore in 87003-10, accompanies the five cores representative of this area. However, Facies F and G from cores 87003-09 and -10, which are regional markers dating about 14.4 ka radiocarbon years (Piper and Skene, 1998) provide chronological control for these cores of the lower slope and rise.

4.4.2 Downcore variations in measured physical properties in undisturbed cores

4.4.2.1 Undrained shear strength

Undrained shear strength of the sediment in cores showing a normal stratigraphic succession typically displays a linear downcore increase. Shear strength measurements

A)

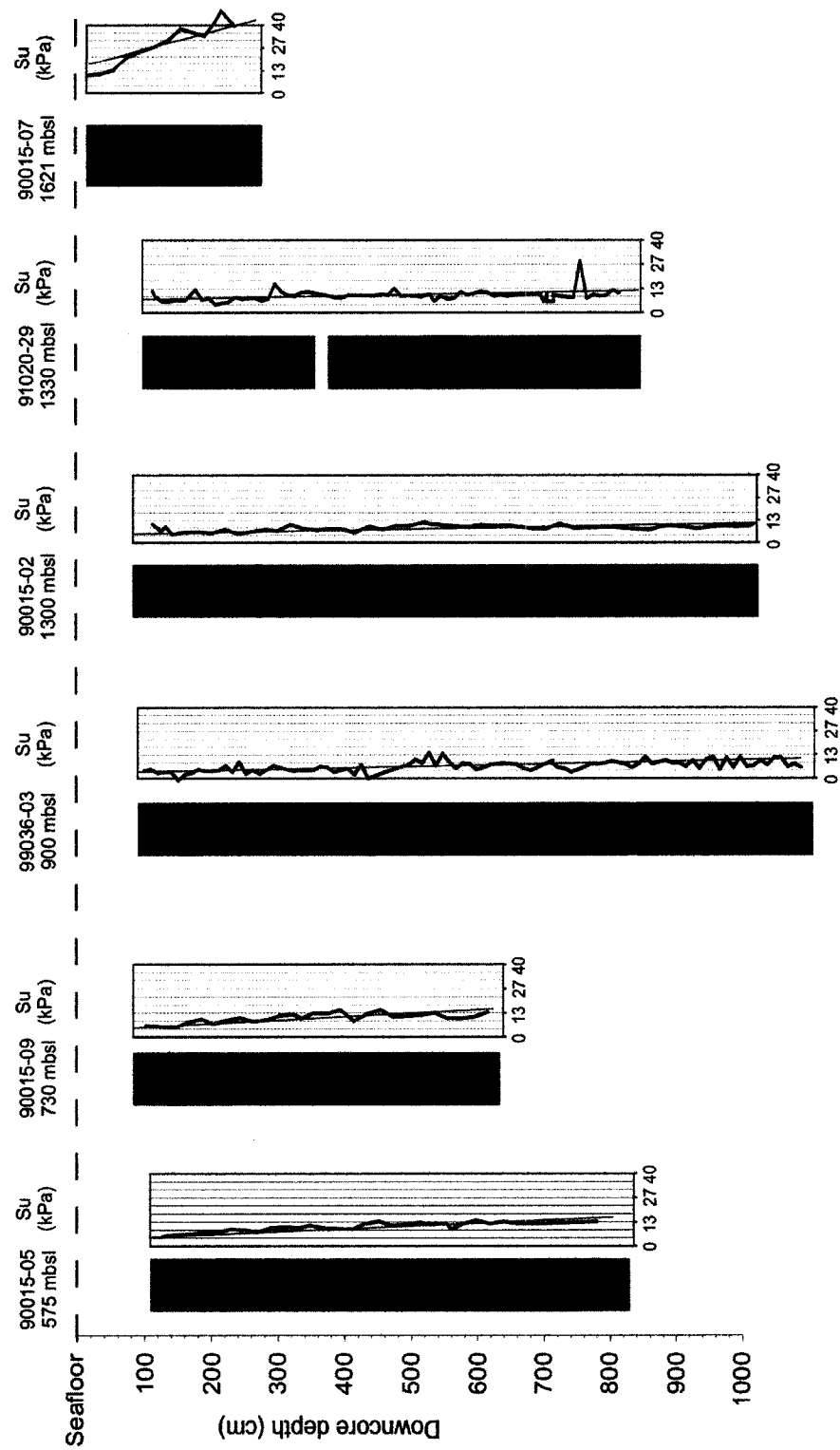
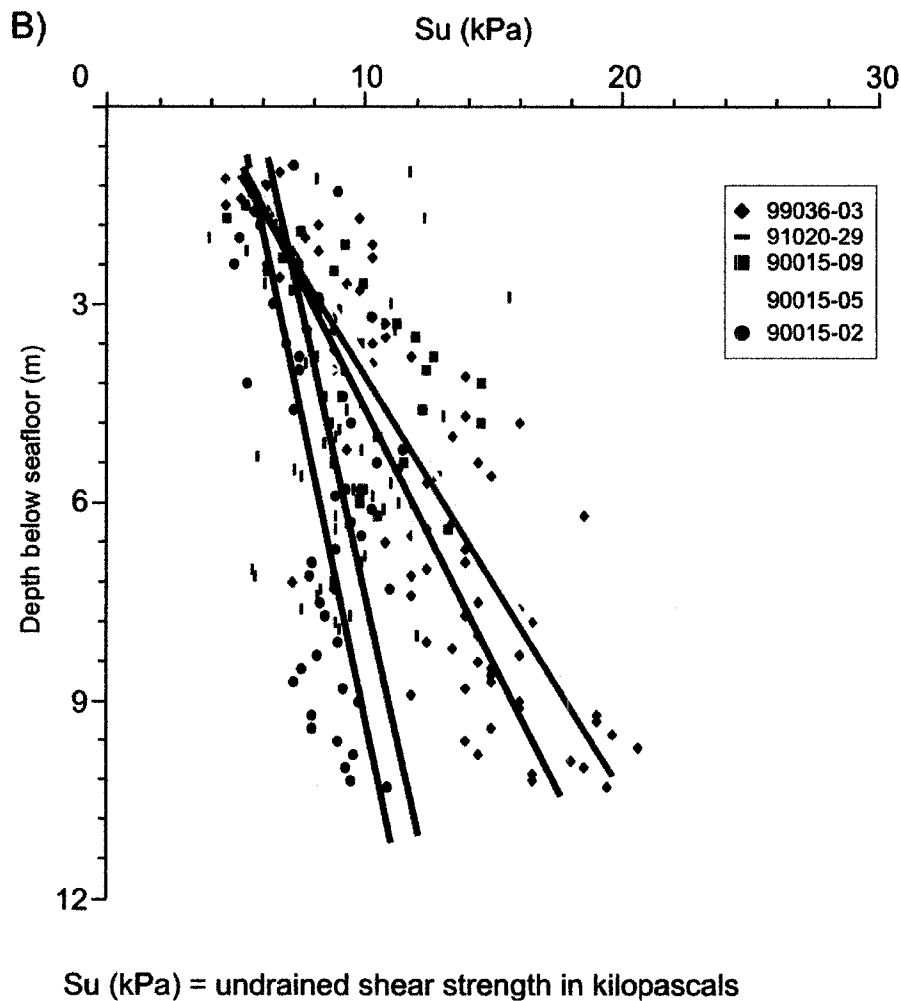
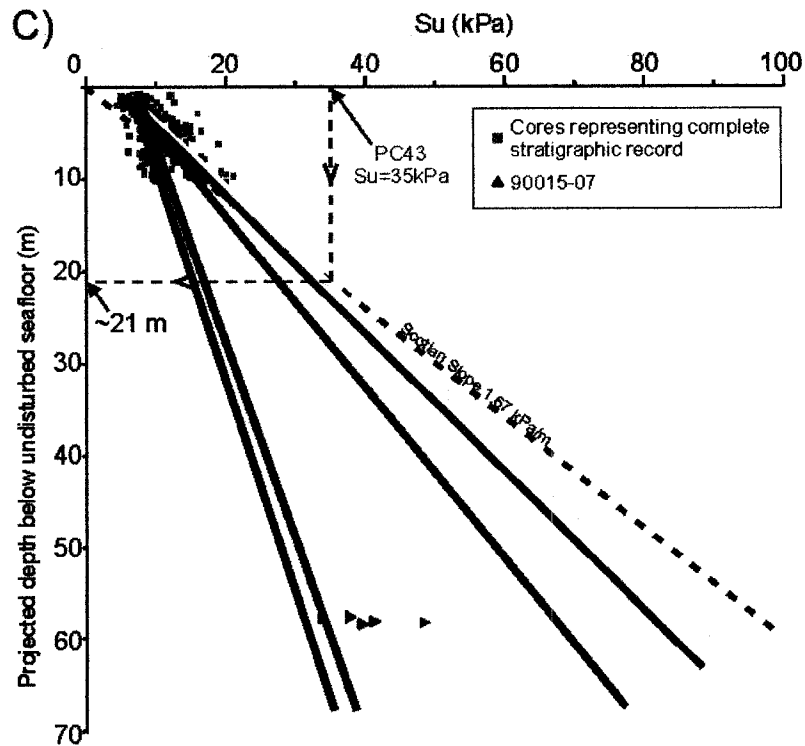


Figure 4.6 – A-(previous page) Five cores representing the undisturbed stratigraphy of St. Pierre Slope and core 90015-07 taken from a ~56-m-deep failure plane. Piston core depths below seafloor estimated through trigger weight core correlation. B) S_u (kPa) vs depth below seafloor (m) for the five undisturbed cores with best-fit lines. C) S_u best-fit lines intersect some S_u values from 90015-07. A S_u increase of 1.67 kPa per meter below seafloor for the Scotian Slope is shown (Campbell, pers. comm., 2005). A 35 kPa S_u value at ~750 cm downcore from disturbed core 2001043-43 when compared to cores from similar water depths suggests that about 21 m of sediment once covered the point where the measurement was taken.





from five undisturbed cores (Figure 4.6-A) have been used to construct a graph relating depth below seafloor (m) to undrained shear strength (S_u in kPa) (Figure 4.6-B). Piston core 90015-07 is from a ~56-m-deep failure plane that at its surface has a thin surficial MTD. Shear strength measurements from the undisturbed section of this core were used in combination with shear strength measurements from the five undisturbed cores to create a graph displaying S_u vs *projected depth below undisturbed seafloor* (Figure 4.6-C).

A general relationship between water depth of the core site and measured S_u is apparent. Extending a best-fit line through S_u values from cores 91020-29 and 90015-02 (~1300 mbsl) shows lower S_u values with depth-below-seafloor in these cores from deeper water. Cores 99036-03 (915 mbsl), 90015-05 (575 mbsl) and -09 (700 mbsl) have S_u values, particularly the latter two, that are similar to the Scotian Slope, where S_u is

estimated to increase at 1.67 kPa per meter below seafloor (Campbell, pers. comm., 2005). Su values from core 90015-07 show an apparent relationship with 91020-29 and 90015-02, as projected best-fit lines are near these values (Figure 4.6-C). The presence of gas, and possibly high sedimentation rates, might account for the higher Su values in the three shallower cores, 99036-03, 99015-05 and -09, as cores 99036-03 and core 90015-09 were obtained from a pockmark-laden seabed, a sign of gas escape.

Shear strength variations within facies A-G of the undisturbed cores are fairly constant with the exception of values obtained from sand- and gravel-laden beds, in which case Su values are not reliable.

4.4.2.2 Color shifts in a^ and b^**

Data from the spectrophotometer provide a quantitative measure of sediment color, giving a numerical value to the white-black (L^*), red-green (a^*), and blue-yellow (b^*) color profiles. Different facies within cores usually show distinctive L^* , a^* , and b^* color values, which in this region may be a proxy for sediment source (Piper and Hundert, 2002). Even where the color of the sediment facies cannot be distinguished visually, slight variations in the spectral data allow for a distinction between specific facies. An increase of 'a' values, an excellent proxy for hematite (Deaton and Balsam, 1990), usually indicates reddish-brown mud and brick red mud facies. The reddish-brown mud facies produces 'a' values of ~5.0-8.0, whereas the brick red mud facies produces 'a' values that surpass 8.0. Only more recent cores have this spectrophotometer data unless specifically reanalyzed for color, as in core 90015-02. Color changes may have taken place during storage of older cores.

4.4.2.3 Cracks associated with gas expansion

Cracks of random orientation with widths of 1 mm up to 2 cm are present in undisturbed cores 86034-02, 90015-02, 90015-09, 91020-29, 99036-03, 99036-05, 2002046-73 and -74. No noticeable disturbance was noted for any of these cores during preliminary examination at sea (e.g. shattered core liner) or during visual examination in the lab that would otherwise explain these cracks. The cracks are concentrated fairly deep within all the cores. In the upper slope west of upper Western St. Pierre Valley, cracks were noted in one core only in a 15 cm interval of facies A and B. East of this site, at the base of four cores from 700-1400 mbsl, cracks are widespread in brown mud of facies C and in lesser concentrations in facies E and a basal bed of facies A. In the lower slope, core 99036-05 shows cracks in gray and brown mud of facies D, and in facies A at the core bottom. Cores 2002046-73 and -74 from the rise have two intervals of cracks. The first interval of 50 cm begins at about 800 cm downcore and is in gray mud of facies D. The second begins around 950 cm downcore and is in facies E.

The presence of gas was noted in all of these cores either while at sea or during physical examination in the lab. Gas samples taken from the bottom of cores 99036-03 (915 mbsl) and -05 (1800 mbsl) yielded 0.37% and 0.3% methane in headspace gas analysis. A previous study on cores collected from the upper St. Pierre Slope documented methane (up to 3%) and small amounts of propane, ethane and butane (0.08%), possibly petroliferous in origin (Piper et al., 1984). Sidescan sonar images collected over core sites from the upper slope show common pockmarks, inferred to be a sign of gas escape (Piper et al., 1999a).

4.4.2.4 Magnetic susceptibility

Magnetic susceptibility is a measured response of the sediment to an induced magnetic field, generally a function of the quantity of iron-bearing minerals present. This measurement can indicate different sediment sources. For this study, magnetic susceptibility measures were used as a supplementary identifier for Heinrich layers (facies G), specifically Heinrich event 1 (H1), as these layers usually show a strong increase in magnetic susceptibility in addition to the signature identifiers of detrital carbonates, tan mud color, and reactivity to dilute hydrochloric acid.

4.5 Core sampling disturbed sediments

4.5.1 Introduction

Seven of the studied cores sampled areas affected by mass transport processes: four sampled disturbed sediments underlain by undisturbed sediments, two are entirely comprised of MTDs and one (86034-03) sampled undisturbed sediments at a scarp and thus has been included in the undisturbed core section. The MTDs have been distinguished principally by direct visual observation of contained structures (e.g. soft-sediment deformation such as contorted beds) and facies relationships (bedding contacts, sediment color shifts). Four disturbed facies have been identified: Facies I, Facies II, Facies III and Facies IV (Table 4.3). Undisturbed sediments, which can be classified as Facies A-G according to Table 4.2, are here grouped as Facies V.

Facies	Facies description	Environment of deposition (a) and sedimentary process (b)
I	Structureless mud occasionally with disseminated sand. Mud matrix with mud clasts up to 5 cm. Typically, mud clasts are similar in color to surrounding matrix. IRD are common and up to 4 cm. Sandy lenses are sparse and a few cm.	(a) Flat to gentle slopes (<2°). On plateaus and is the topmost deposit in cores. (b) Mud clast conglomerates
II	Mud with cm-mm thick sandy and silty mud beds that dip up to 40°. The sandy muds are medium to coarse grained and contain abundant shell fragments. Recumbent folds and overturned beds are common and in places have sandy mud laminations (mm thick). Contacts between sediment facies dip 15-25°. When present, laminations follow this degree of dipping.	(a) Gentle slopes (typically not exceeding 5°). Near and on valley walls. (b) Slumps
III	Mud with mm-cm, sub-horizontal to horizontal sandy and silty mud laminations, beds and lenses. Contact between sediment facies are distinct and approach but do not surpass 15°. Basal glide plane is distinct and identified by abrupt change in sediment facies. Disseminated sand and IRD are common (1 to 4 cm).	(a) Gentle slopes (<5°). On plateaus near valleys and on gentle valley walls. (b) Glides
IV	Well-laminated silty sandy mud that can be tilted a few degrees. Defined by fining upward sequence, rhythmic banding and sharp basal contact that is marked by a gravel lag.	(a) In valley floors. (b) Turbidity currents or possibly bottom currents
V	In-situ sediments. Show the same stratigraphic sequence when compared to undisturbed cores from similar location. Basal plane of the above facies represent topmost limit of this facies in cores.	(a) Underlies surficial MTDs. (b) Undisturbed sediments

Table 4.3- Classification of sediments from cores that sampled areas affected by sediment failure.

Facies I is identified in cores based on the following criteria: (1) sharp upper and lower contacts, (2) 'floating' mud clasts, (3) moderate to high muddy matrix content and (4) absence of internal structures (e.g. sandy and silty beds). Facies II is identified by: (1)

soft-sediment folds (e.g. recumbent and overturned), (2) truncated stratification, (3) steeply dipping beds (up to 45°) and (4) basal (primary) and internal (secondary) glide planes typically dipping >10°. Facies III is identified by (1) basal (primary) glide planes that dip a few degrees, (2) principally horizontal to sub-horizontal (<10°) internal bedding structures and (3) a largely intact normal stratigraphy. The presence of a basal planar glide plane was key in the recognition of this facies. Facies IV is identified by (1) a fining upward sequence, (2) sharp basal contact (marked by a lag of coarse sand and or gravel and (3) sediment grain size and color laminae. Facies V represents the undisturbed stratigraphy that underlies the above facies. It is identified by (1) gradational contacts between different lithologies, (2) sharp upper contacts against disturbed sediments, (3) undeformed internal bedding structures and (4) a normal downcore color and sediment scheme when compared to an undisturbed core from a similar water depth and stratigraphic interval.

4.5.2 Descriptions of cores containing disturbed sediments

Detailed descriptions of the variability encountered in the six piston cores containing MTD facies are presented below in order of increasing water depth (Table 4.3). Approximate location of each core within Hunttec DTS, 3.5 kHz or 12 kHz profiles is shown in Appendix 2. Some piston cores have complementary sidescan data over the core site that expands the understanding of topography and surrounding features. Trigger weight cores and piston cores were correlated to determine a more precise thickness of the topmost MTD facies. Certain physical properties are mentioned within the disturbed core descriptions that add to the understanding of the dynamics of facies distribution and

formation. For example, high shear strength measurements of in-situ sediments of facies V could be an indication that the sediments previously had a thick sediment cover.

The downcore facies distribution of facies V generally follows a similar pattern as the undisturbed cores, provided that the core does not sample a zone where evacuation of large amounts of sediment has occurred (e.g. in excess of 10 m stratigraphic thickness).

2001043- PC43

Piston core (PC) 43 was obtained at 747 mbsl on the bank between upper Western and upper Eastern St. Pierre Valleys (Figure 4.1). The piston core sampled three of the defined facies down to 440 cm. Correlation of the trigger weight core (TWC) revealed at least 50 cm of sediment missing from the top of the PC.

Facies I - 0-24 cm in PC - Structureless olive gray to gray mud matrix with disseminated silt and sand, and mud clasts of varying shades of gray dispersed throughout. Total thickness of this facies is 74 cm. Sharp contact below with facies III.

Facies III - 24-320 cm - Thin (mm-2 cm) sub-horizontal silty and sandy mud beds and lenses (tilted a few degrees) within gray mud. The individual beds extend 5 to 10 cm (entire width) across the width of the PC and increase in quantity down-facies. Shell fragments are documented from 24-50 cm and bioturbation is slight, except that it is intense from 180-218 cm. Contact with underlying facies II is distinct and evident from abrupt change in orientation of silty beds.

Facies II - 320-440 cm- Gray mud with steeply dipping thin silty and sandy mud laminations (~2-6 cm wide, < 1 cm thick) that define the boundary with facies III above (Figure 4.7-A). Shell fragments exist at 360-363 cm and bioturbation is slight from 430-440 cm.

Glide plane - 440-448 cm – An 8 cm thick bed of sub-horizontal silty laminations is the glide plane of the MTD complex that marks the boundary between the disturbed facies and facies V. Sediments underlying this plane are undisturbed as no deformed features were seen to suggest otherwise.

The dominant sediment facies underlying most MTD facies (some cores sampled only MTDs, thus the underlying sediment was unknown) is grayish mud similar to facies C in the undisturbed cores. The color shifts from a dark olive gray to a dark gray mud around 440 cm downcore corresponding to the transition from disturbed facies to underlying undisturbed facies V. Shear strength values are high, follow a relatively linear path downcore and by about 750 cm downcore reach upwards of 35 kPa. Comparing S_u values of facies V to other PC from similar water depths suggests that the undisturbed sediments of the PC were previously buried under approximately 18 m of sediment (Figure 4.6-C). SeaMARC I sidescan sonar data shows the core site is located downslope of a failure scarp (see Appendix 2).

2001043- PC42

Piston core 2001043-42 contains facies I and II. It was taken from the valley floor in a tributary of upper Eastern St. Pierre Valley at 970 mbsl (Figure 4.1). No confident correlation of the TWC to the PC was achieved because of the absence of prominent correlatable features, e.g. contact between facies. An attempt was made to correlate the two cores based on the ‘a*’ and ‘b*’ values but to no effect. Bulk density values suggest that no sediment is missing from the PC top. Conversely, 130 cm of sediment could be missing from the top of the PC if the total length of the TWC is taken into account.

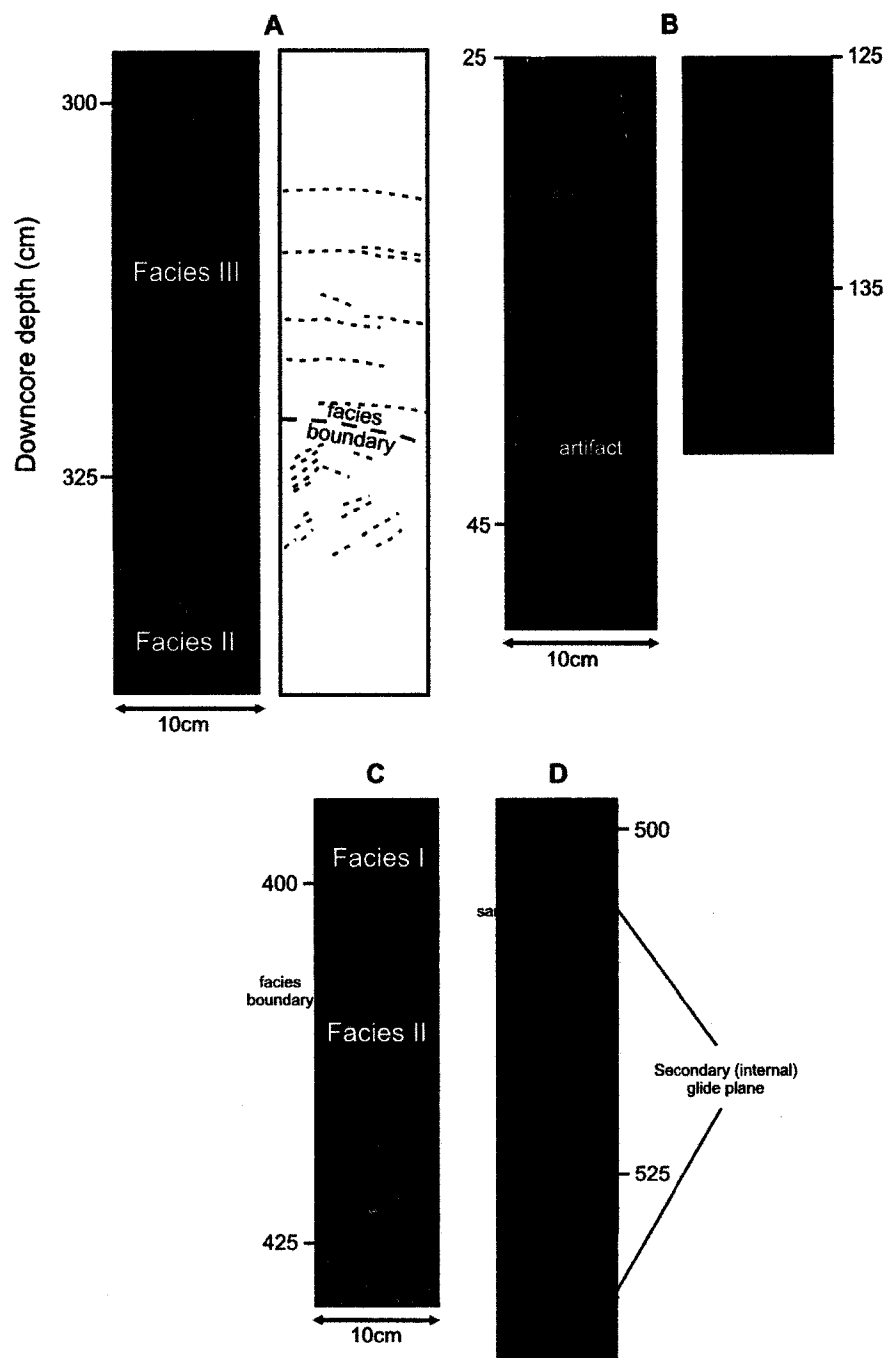


Figure 4.7 – Downcore photos of sediment cores from St. Pierre Slope. A) Facies III in contact with underlying facies II from 2001043 PC 43. Within the mud are mm thick horizontal to sub-horizontal silt beds (illustrated to the right). B) Facies I from 2001043 PC42 showing mud clasts ('a') within a dominant mud matrix. C) Sharp contact between facies I and II from 2001043 PC 42 dips at 23°. D) Recumbent folds and overturned beds at about 520-530 cm from 2001043 PC42 within facies II. Contact between contiguous facies shows some mixing.

Facies I - 0-400 cm in PC - Gray mud matrix with grayish mud clasts dispersed throughout and IRD as angular to sub-angular stones from 0-35 cm (Figure 4.7-B). Variable shell fragments (one complete bivalve half at 83 cm). Intercalated sandy mud lenses are common and 5-8 cm wide. Total thickness of this facies could either be 400 cm (nothing missing from PC top) or 530 cm (if total length of TWC is taken into account). Contact with facies II below is distinct (Figure 4.7-C).

Facies II - 400-680 cm – Alternating beds (upwards of 100 cm thick) of color laminated light and dark gray mud show distinct contacts dipping 15-25° that might represent secondary glide planes with slight shear mixing of adjacent facies (Figure 4.7-C and D). Laminations show a similar dip and increase in concentration downcore. These laminations are similar to those of facies IV but fining upward grain-size sequences are absent, a characteristic of facies IV. This facies may be a combination of facies II and IV, with facies II being a secondary feature developed after the deposition of facies IV. Sandy mud (up to 4 cm thick) and silty beds (~1 cm) dipping as much as 40° are quite common. The sandy mud is medium to coarse grained and contains abundant shell fragments. Recumbent folds (Figure 4.7-D) and overturned beds are composed of light and dark gray muds and in places have intercalated sandy muds (mm thick).

At about 400 cm downcore at the boundary between facies I and II, shear strength values increase from 9.5 to 25 kPa over an interval of 20 cm and continue to fluctuate between 13-27 kPa to the core-bottom. Magnetic susceptibility and bulk density readings also increase dramatically at 400 cm, but seem to return to a linear downcore pattern after the 20 cm interval. Although coarse-grained sandy lenses at about 400 cm downcore could potentially account for the high magnetic susceptibility and bulk density values, it

does not explain the irregular shear strength values. Su and bulk density values markedly increase in zones of recumbent folds and overturned beds. Cracks documented from 655-680 cm may be associated with gas expansion, as gas was detected in the core.

2001043- PC41

Piston core 41 sampled facies III and is located on a plateau between upper Eastern St. Pierre Valley and upper Grand Banks Valley at 980 mbsl (Figure 4.1). Correlating thin (mm-cm), sandy mud laminations and beds of both the TWC and PC suggest about 50 cm missing from the top of the PC.

Facies III - 0-135 cm – Grayish brown mud with slightly dipping (a few degrees) mm-cm thick, sandy mud laminations and beds. IRD sampled by both the TWC and PC but are larger and more abundant in the TWC. Facies contact with underlying gray mud bed is sharp, approaches 15° and is slightly concave-up (Figure 4.8). Total thickness of the facies is 185 cm.

The facies terminates sharply at a gray mud bed at 135 cm. The gray mud continues downcore to 180 cm, where transition to brown mud is gradual (Figure 4.8). These muds represent facies V. They resemble facies D of the undisturbed cores in many respects (e.g. color laminations, sandy patches and cracking) except that bioturbation within these sediments can at times be fairly intense, a characteristic common of facies C.

Su measurements from the core-top to 145 cm are between 4-5 kPa. At 145 to 200 cm downcore, values fluctuate between 10-13 kPa and follow a fairly linear downcore trend to the end of the core, where values approach 25 kPa. The initial Su increase to 10-13 kPa roughly corresponds to the boundary between facies III and the underlying gray

mud bed. Performing the same Su calculations as was done above for 2001043-PC43 and comparing the values to cores obtained in similar water depths suggests that the undisturbed sediments of the PC were previously buried under about 7-8 m of sediment.

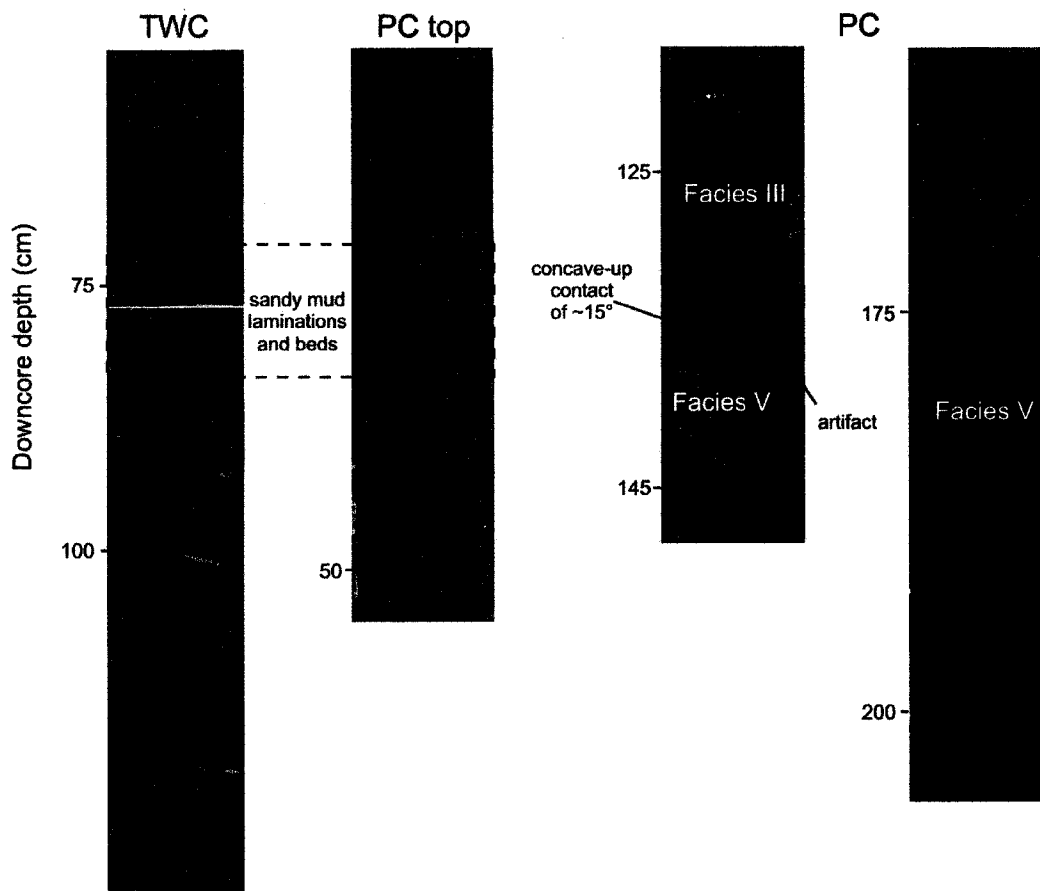


Figure 4.8 - Downcore photos of sediment cores 2001043-TWC41 and PC41 from St. Pierre Slope. Correlation of TWC and PC using sandy mud laminations and beds (dashed box) reveals at least 50 cm missing from PC top. Contact between facies III and V approaches 15°. Contact between gray and laterally mixed gray and brown muds of facies V is gradational.

91020- PC40

Piston core 40 samples facies I at 1062 mbsl on the same plateau as and approximately 6 km ESE of core 2001043- 41. No structural features were seen in the PC and TWC to allow for a confident correlation. Instead, correlation of ammonium (NH_4^+), sulphate (SO_4^{++}) and pE (oxidizing or reducing capacity of an environment) values, in which SO_4^{++} and pE degrade with depth downcore and NH_4^+ increases with depth (Cranston, 1991 and 1999), revealed at least an additional 135 cm missing from the top of the PC (Table 4.4).

Facies I - 0-110 in PC – A matrix of olive gray and brown mud with a gradual transition to brown mud at 30 cm. Disseminated sand throughout the brown mud becomes increasingly sandy at 90-110 cm downcore and in places is concentrated as small (mm) patches. Dark brown mud clasts are common and an isolated red mud clast is noted at 95 cm. An abrupt change in lithology at 110 cm downcore is marked by a sharp

Downcore depth (cm)	TWC			PC		
	SO_4^{++} (mM)	NH_4^+ (mM)	pE	SO_4^{++} (mM)	NH_4^+ (mM)	pE
0	28	0	5.5	28	0.28	4.9
5	28	0	4.9	28	0.44	4.9
10	28	0	5.1	25	0.85	4.3
20	28	0.07	5.1	12	1.3	4.6
40	28	0.15	5.4	12	1.8	4.4
60	28	0.16	5.4	11	1.9	4.4
80	28	0.28	4.9	6	2	4.4
100	28	0.32	4.6	2	2.3	4.4
140	28	0.4	4.9	n/a	n/a	n/a
150	n/a	n/a	n/a	0	2.4	4.1

Table 4.4 – Analyses for SO_4^{++} , NH_4^+ and pE from 91020 TWC- and PC-40. Correlating similar values (gray areas) suggests that at least 135 cm is missing from the top of the PC.

contact, this represents the basal plane of facies I. Total thickness of this facies is 245 cm.

Both the brown and gray mud and muddy sands of facies I, and the underlying sediments of facies V are similar to facies C of the undisturbed cores. Facies V shows gradual contacts between contiguous under- and overlying sediments and a downcore color sequence typical of undisturbed cores from similar water depths (e.g. 91020-29). Sandy and silty patches, lenses and IRD are common from 380 cm to the bottom of the core. IRD increases in quantity with depth downcore.

Su values in the PC near the surface are about 5.5 kPa and show a relatively linear downcore trend. The values are fairly high (12 kPa) at about 110 cm downcore and might be an indication that the undisturbed sediments sampled by the PC were at one time under a few meters of sediment. Su values surpass 20 kPa at about 400 cm but the significance of this is unknown.

84003- PC05

Core 05 is located 1537 mbsl about 3.5 km from the eastern flank of St. Pierre Valley. The core was selected for study because of its relative position within corresponding SeaMARC I sidescan sonar and Hunttec DTS data (Figure 4.9-A and B). The Hunttec DTS profile shows a deposit with numerous hyperbolic diffractions at its surface near the headwall, consistent with bodies of acoustic Class I. Further from the headwall, surface reflections are undulating and interrupted in places by hyperbolic diffractions and may represent a body of acoustic Class II. SeaMARC I sidescan images show parallel, nearly linear ridges bounded upslope by arcuate headscarps. The core

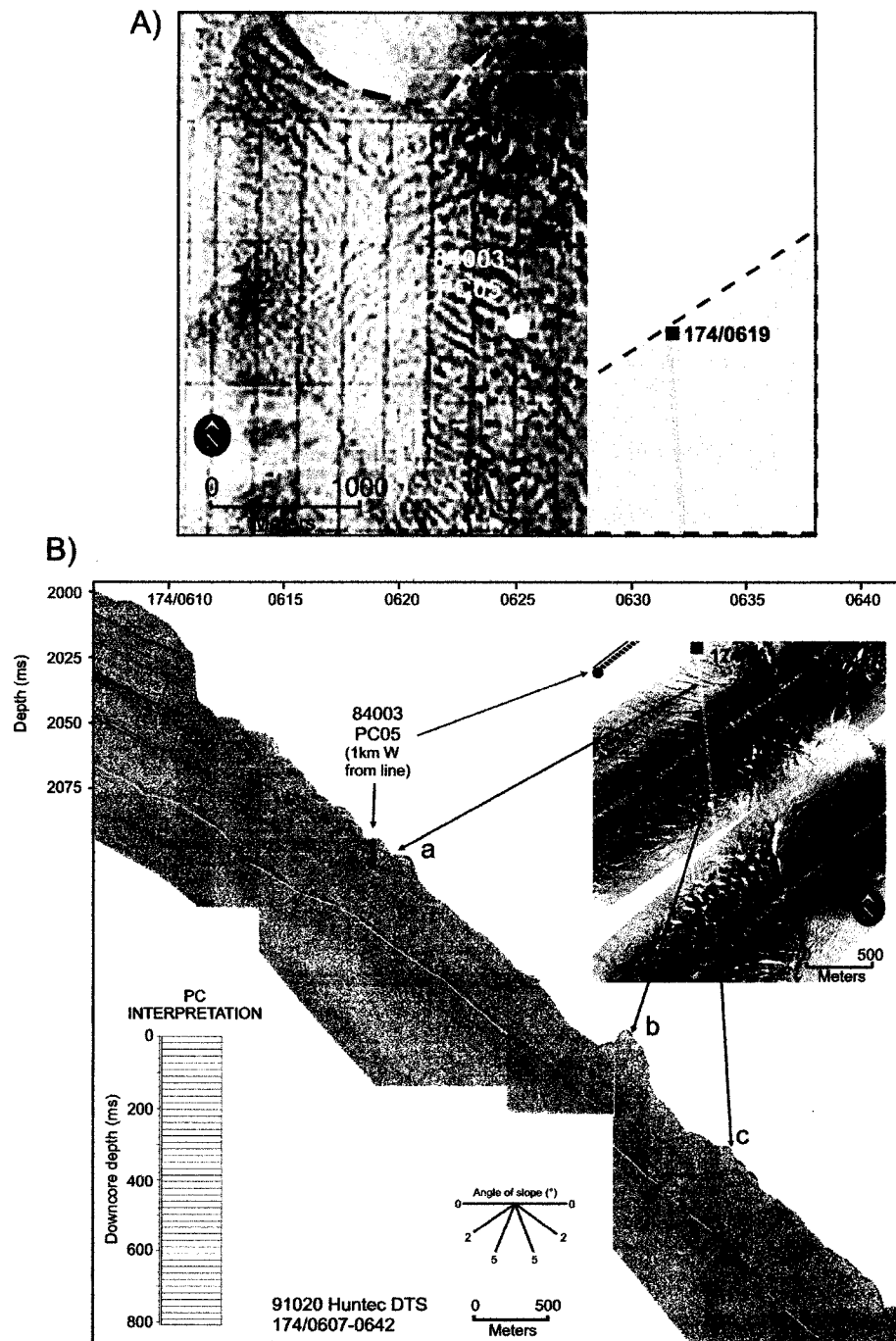


Figure 4.9 - A) SeaMARC I sidescan sonar image showing piston core 84003 05 within a field of linear ridges. Approximate position of SAR sidescan image and Hunttec DTS line in relation to SeaMARC I are shown. B) Hunttec DTS profile and associated SAR sidescan sonar images showing location of PC05 within hyperbolic diffractions that in SAR are represented as parallel, fairly linear ridges ('a'). Due to the size of the deposit, the offset between the core and Hunttec line is acceptable. Figure (B-only seismic section) is a modification of Figure 3.7a. Reflections Q100-Q91 and PC failure interpretation are shown.

appears to sample these parallel ridges and in Hunttec DTS appears to penetrate acoustic Class I. SAR sidescan images correlate better to the Hunttec DTS data than the SeaMARC I data due to improved navigation methods (as discussed in Ch.2). The Hunttec DTS profile demonstrates nicely the acoustic appearance of the parallel ridges near the headwall ('a' in Figure 4.9-B). In places further from the headwall, surface hyperbolae are concentrated ('b' and 'c' in Figure 4.9-B and appear as irregular ridges in sidescan sonar images.

Correlation of the TWC to the PC was not possible due to the TWC being lost during acquisition at sea.

Facies III - 0-809 cm – Olive gray mud from the top of the PC down to 120 cm, where transition to brown mud is gradual. Brown mud constitutes the remainder of the core except at 480 cm where contact above with a reddish-brown mud bed of 10 cm is sharp and approaches 5°. The transition back to the underlying brown mud at 490 cm is gradual. Disseminated sand is throughout the 100-380 cm interval and at 380 cm a thin (~5 cm thick) sandy mud bed dips at ~10°. Small, sandy clasts are sparse (6 in total). IRD (1-4 cm) are in the top and bottom of the facies and are concentrated between 100-170 cm. No mud clasts were noted. Bioturbation and mottling are common throughout the core, especially near the core-top. Consolidation test results show that the core at a depth of 600 cm is overconsolidated (Marsters, 1986).

Shear strength values do not follow any obvious downcore trend. Instead, they fluctuate randomly, particularly in the upper 250 cm, with values ranging between 2-16 kPa.

90015- PC07

Piston core 07 is located 1621 mbsl on the floor of a small, unnamed valley between St. Pierre Valley and Grand Banks Valley (Figure 4.1). The TWC and PC contain multiple, thin deposits of facies IV. Correlation of the two cores was difficult and not achieved, and therefore an unknown amount of sediment could be missing from the top of the PC.

Facies IV - 0-26 cm in TWC and 0-110 cm in PC- The facies sequence of the two cores is suggestive of multiple episodes of facies deposition. In the TWC olive gray mud with bands of reddish-brown mud dip a few degrees. Muds become siltier near the bottom of the unit and have well-defined laminations that appear 'wispy'. A sharp contact at 10 cm is marked by a gravel lag that represents the basal plane of the topmost MTD facies. Olive gray mud grades to gray mud below the sharp contact and is laminated and bioturbated parallel to bedding planes.

The PC is characterized by greenish gray to gray laminated muds that show gradational contacts to 60 cm downcore. Four fining-upward sequences exist between 60-75 cm that show rhythmic banding and have sharp basal contacts. From 75-110 cm, structureless gray mud increases in sand and gravel content with depth. A sharp contact marked by a gravel lag is noted at 110 cm and represents the basal plane of the bottommost MTD facies. Beds (<10 cm) of gray to darker gray stone-rich, sandy mud become prevalent downcore. Bioturbation is minor throughout the core.

The topmost Facies IV in the TWC (0-10 cm) is similar to facies D as it has sediment laminations and is likely a mixture of facies A and E due to the olive gray and reddish-brown sediments. The underlying gray muds of the remaining deposits of facies

IV in both the TWC and PC and the undisturbed sediment of facies V in the PC resemble facies D of the undisturbed cores.

Shear strength values in the TWC are high after 10 cm downcore and by about 60 cm downcore in the PC are 22 kPa and at 200 cm are 50 kPa. Low Su values in the upper part of the TWC (0-10 cm) suggest that the topmost facies IV in the TWC was not previously buried under a substantial amount of sediment. Unusually high Su values in the PC and in the lower part of the TWC suggest that the other deposits of facies IV were likely buried under a substantial amount of sediment at one point in time and likely represent older failure events, exhumed by younger erosion.

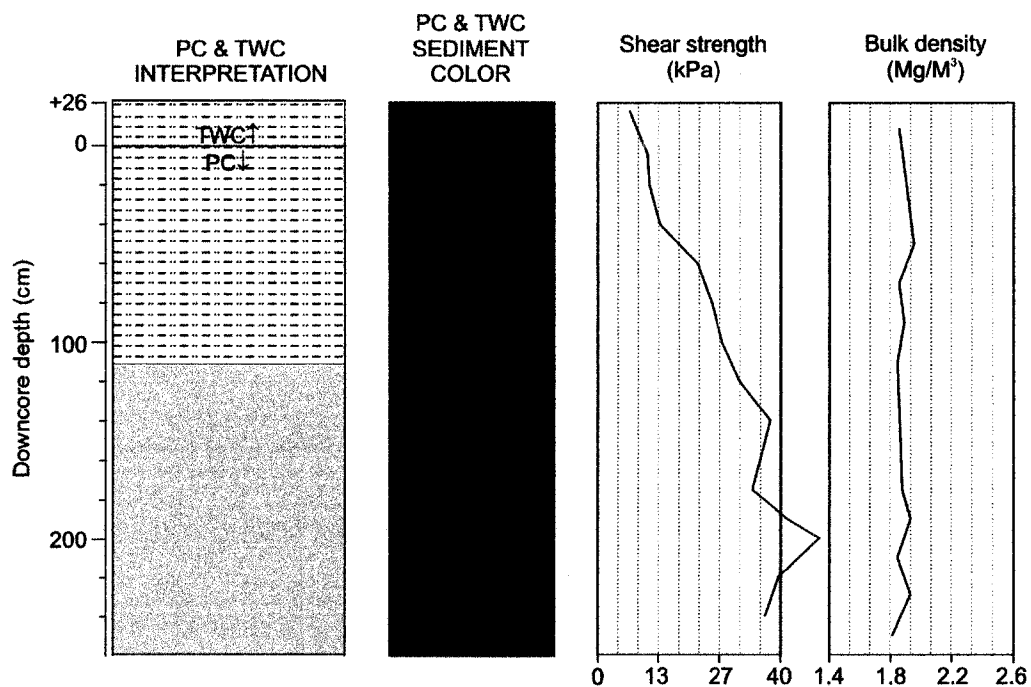


Figure 4.10 - Downcore plots for piston core 90015-07. Shear strength values in the PC increase sharply after about 40 cm downcore. This suggests that this area might have been previously under substantial sediment cover at one time.

CHAPTER 5

Discussion

5.1 Introduction

This chapter will present an integration of data from Chapters 3 and 4 to arrive at an understanding of the dynamics of surface failure on the St. Pierre Slope. The documented surface failures are assumed to be a consequence of the 1929 event. The integration will achieve the following: a) a regional sedimentation model will be established based on measured radiocarbon ages, established acoustic and core stratigraphy, and probable sediment sources. This model will provide the necessary foundation to begin to address the focus of this thesis: the style of surface failure on the St. Pierre Slope; b) set up an architectural framework of failure distribution. This includes i) core projection into seismic profiles, ii) analysis of the sediment budget from calculated volumes, iii) distribution of defined failure types with emphasis on gradients, and iv) evolution and progression of failure. Comparisons with nearby and international margins subjected to similar styles of failures will be drawn, mainly the Scotian margin, and briefly to European studies (e.g. COSTA Europe and Eurostrataform).

5.2 Integration of seismic and core data

5.2.1 Age model for key reflections

Two radiocarbon ages have been used to constrain reflection Q99. A radiocarbon age of 15.5 ka from core 90015-02 about 1.5 m below and a radiocarbon age of 15.2 ka from 86034-09 about 1.0 m above reflection Q99 allow for an extrapolated radiocarbon age of about 15.3 ka radiocarbon years for reflection Q99. This age of 15.3 ka and a 30.2

ka radiocarbon age from core 90015-07 just below reflection Q91 allow for the extrapolation of radiocarbon ages (assuming similar sedimentation styles between reflections) for reflection Q97 of about 20.5 ka, reflection Q95 of about 23.0 ka, reflection Q93 of about 26.3 ka and reflection Q91 of about 29.2 ka, (Figure 5.1). On the upper slope, three of the key reflections show a relationship to acoustically incoherent units that pinch out downslope. These units, of which there are three (labelled I-III in Figure 5.1), are similar in morphology and downslope extent (none extend past the 550-m isobath) to units described by Piper and MacDonald (2002) and Piper et al. (2005) on the upper St. Pierre Slope as 'till tongues' (TT). An alternate interpretation that these units are MTDs is not supported as these units extend up onto the outer shelf and show acoustic properties consistent with units recognized by King and Fader (1986) as till. Reflection Q91 terminates at the downslope limit of till tongue II, bounding TTII to a basal age of 30 ka. Reflection Q93 lies at the surface of till tongue II, extending upslope past the 500-m isobath, suggesting that the ice-margin at 30 ka was fairly far down the slope and retreated fairly rapidly as the till tongue is overlain by continuous, coherent reflections by 26 ka. Reflection Q95 is about 10 ms below the base of till tongue I. Although reflections Q99 and Q97 were not traced upslope of the 700-m isobath due to disturbance from sediment failure, Q97 likely lies just beneath or at the downslope limit of and Q99 overtop of till tongue I, as a mollusc shell ~2-3 m above the surface of till tongue I was dated at 11.8 ka radiocarbon years (Bonifay and Piper, 1988).

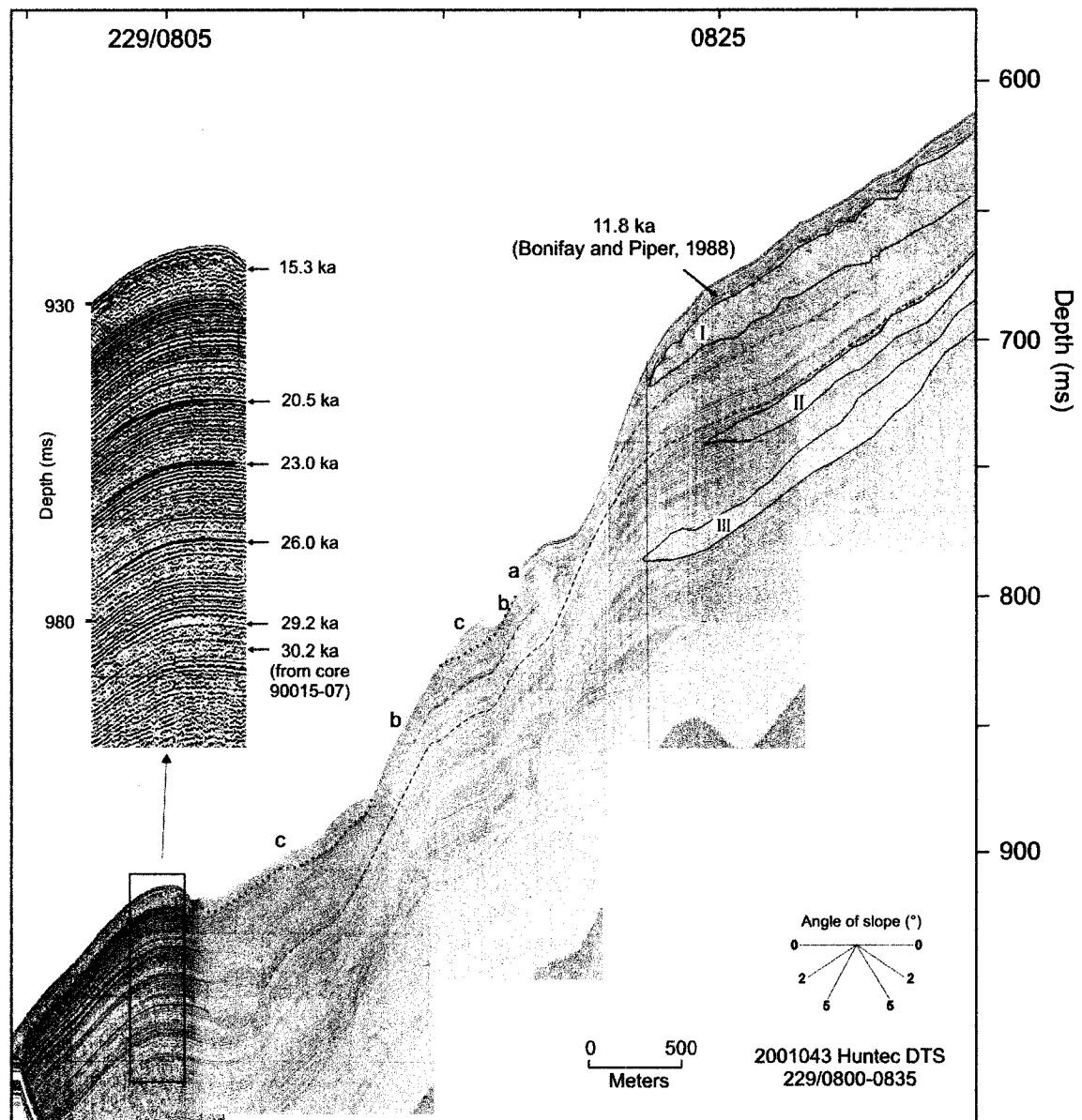


Figure 5.1 – Hunttec DTS seismic reflection profile of the upper and mid St. Pierre Slope showing extrapolation of radiocarbon dates for the key reflections. Till tongues I-III pinch out at the ~550-m-isobath. Scarps (a), scars (b) and MTDs (c) are labelled.

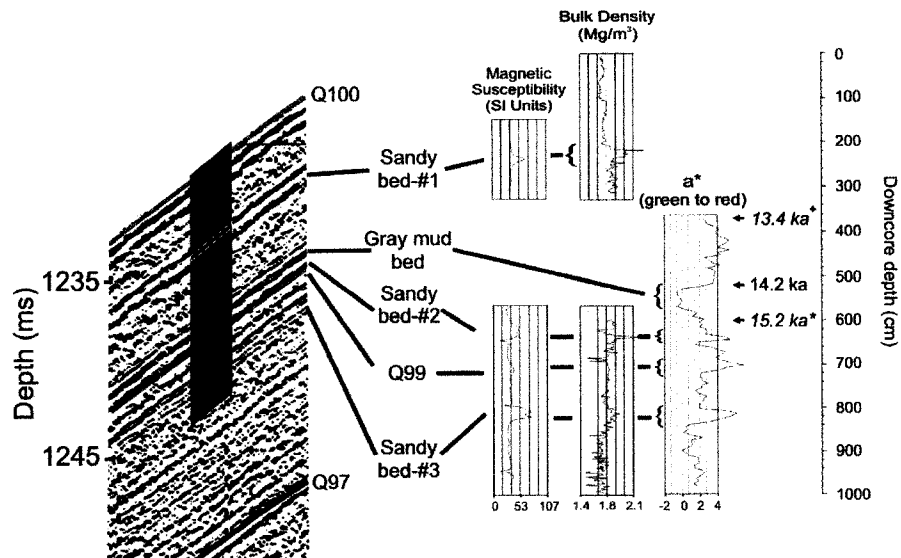
On the mid to lower slope and rise, chronological control is by facies F and G of the undisturbed cores. Facies F is dated at about 14.4 ka radiocarbon years and

interpreted as representing BRM-d (Piper and Skene, 1998). Facies G is dated at 14.4 ka radiocarbon years and interpreted as representing DC1 of Labrador Sea (Andrews et al., 1993) and Heinrich event H1 of the North Atlantic (Bond and Lotti, 1995). None of the key reflections were correlated into these core-site seismic profiles and thus cannot be related to the established seismic stratigraphy of this study.

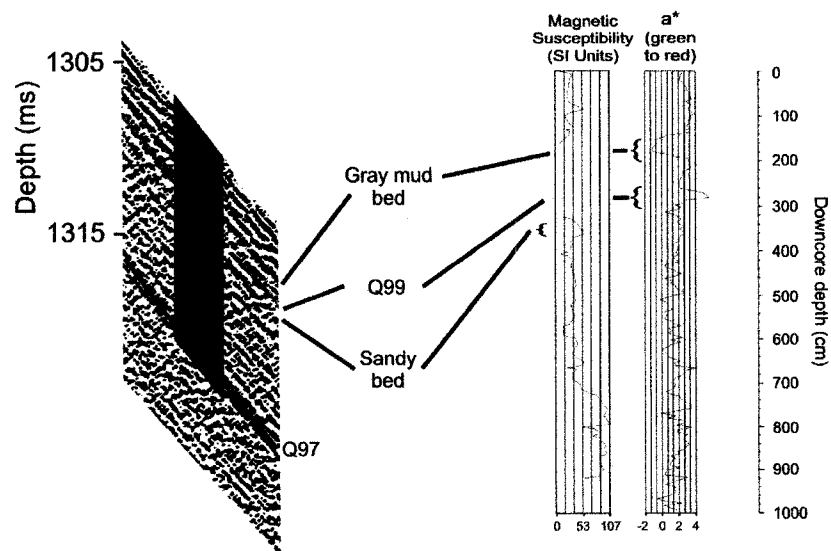
5.2.2 Core stratigraphy related to key reflections

Cores from the upper slope penetrated reflection Q100 but did not penetrate down to any of the other key reflections. Two cores from the middle slope have been projected into seismic reflection profiles (Figure 5.2). Core 99036-03 sampled the undisturbed seabed to just below reflection Q99 (Figure 5.2). Olive gray mud of facies A represents reflection Q100. Below this, brown mud of facies C is interrupted in places by sandy mud beds of facies E and a gray mud bed of facies C. Three of the sandy mud beds (#1-3 in Figure 5.2A) have high magnetic susceptibility and bulk density measurements compared to the surrounding sediment. These sandy mud beds are both above and below reflection Q99 and may even represent the reflection event. These sandy beds appear to be captured in the seismic reflection profile as a contrast in the acoustic impedance and are represented by a high amplitude reflection. Core 2001043-41 sampled MTD facies III to just above the gray mud bed, and below this, undisturbed sediments and reflections Q99 and Q97 (Figure 5.2B). The gray mud bed and Q99 sampled by this core have been correlated to core 99036-03. Below reflection Q99, the sediment is dark greenish gray mud that resembles both facies A and D, interrupted in places by thin beds of gray mud

A) Core 99036-03 (915 mbsl)



B) Core 2001043-041 (980 mbsl)



■ Facies A

■ Facies C/D

■ Facies F

Figure 5.2- Seismic reflection and core data integration showing the sediment equivalent for reflections Q97, Q99 and Q100 (A, B). Note the sandy mud beds close to the orange reflection (Q99) (A, B). Note in (A): ka^+ - radiocarbon age from 86034-09 and ka^* from 90015-PC02.

of facies C. The core sampled reflection Q97 at its bottom. Magnetic susceptibility measurements are very high from 7 m to the core bottom at 9 m, approaching 110 SI units, indicating a high ferromagnetic mineral content within the sediment.

On the lower slope, core 90015-07 sampled stiff dark gray mud of facies D at a ~56-m-deep failure plane just below reflection Q91. Due to poor seismic coverage, no key reflections could be correlated to any other core sites further down on the lower slope and rise.

Key reflections, therefore, have a sediment equivalent in cores. The sediment equivalent of reflection Q100 is olive gray mud of facies A that in places has thin sandy beds (Facies B). Brown to reddish-brown sandy mud of facies C and E represent reflection Q99 and associated reflections (± 2 ms vertically). Dark greenish gray mud with a high ferromagnetic mineral content surrounds reflection Q97 and stiff dark gray mud is just below reflection Q91.

5.3 Undisturbed sediment facies related to facies from other studies

The undisturbed sediments from cores of this study show a relationship to documented lithofacies from previous studies of this region, both in lithologic properties and chronology (or time of deposition) (Table 5.1). On the upper slope near the eastern edge of the mouth of Laurentian Channel, both facies A and B are a mix of units A and B of Bonifay and Piper (1988). A radiocarbon date of 11.15 ka about 2.0 m above the gray mud of facies C at this location likely correlates to units B and C of Bonifay and Piper (1988). Facies D, E, F and G are restricted to the middle slope to rise and thus have no upper slope counterparts.

Sediment lithofacies from this study St. Pierre Slope and Rise		Sediment lithofacies from other studies correlated to defined facies A-G					
		Bonifay and Piper (1988) Upper St. Pierre Slope		Piper and Skene (1998) Scotian Margin and Laurentian Fan		Skene and Piper (2003) Laurentian Fan (>3000 mbsl)	
Facies	Age	UNITS	Age	Facies	Age	Lithofacies	Age
A (olive gray mud)	5.5 to 10.5 ka* 10.5 to >15.5 ka	A and B (A-olive gray mud with local sand beds)	Holocene to 11.0 ka	Olive gray mud with some silt and sand beds	Holocene to latest Pleistocene	Ila and Ib (Ila- olive gray mud; Ib- olive gray silt and sand laminated mud)	Holocene (and up to 16.1 ka as deeply buried thin marker beds)
B (olive gray mud with sand)	10.27 to <11.15 ka	A and B (B- bioturbated olive gray silty mud)	Holocene to 11.0 ka	Olive gray mud with some silt and sand beds	Holocene to latest Pleistocene	n/a	n/a
C (mud with IRD and patchy sand)	~11.15 to >15.5 ka	B and or C (C- olive gray to gray silty mud, in places is laminated)	11.2 ka	Brownish & grayish mud, some sand	Date from middle of facies- 14.9 ka	n/a	n/a
D (mud with color laminations, sparse IRD and little bioturbation)	>14.4 to ?	n/a	n/a	Brownish & grayish mud	Date from middle of facies- 14.9 ka	IV (brown silty mud)	14.4 to 14.5 ka
E (reddish-brown mud)	14.4 to ?	n/a	n/a	Red-brown clay turbidites	top of unit = 14.9 to 15.6 ka	Mix of III and Ia (III- reddish-brown & olive gray color laminated mud; Ia- silt laminated mud)	14.4 to 16.1 ka
F (brick red mud)	14.4 ka	n/a	n/a	Brick red mud or gravelly sandy mud	14.4 to 14.5 ka	Vb (red sandy, gravelly mud)	14.4 ka
G (tan mud)	14.4 ka	n/a	n/a	Sandy mud rich in detrital carbonate	14.4 ka	Va (gray sandy, gravelly mud)	14.4 ka

Table 5.1- Lithostratigraphic and chronologic relationship shown by sediments from undisturbed cores of this study to documented lithofacies from previous studies of this region.

On the lower St. Pierre Slope and rise, facies A correlates to olive gray silty and sandy mud of lithofacies described by Piper and Skene (1998) and Skene and Piper (2003) (Table 5.1). Facies D correlates to lithofacies IV of Skene and Piper (2003) from Laurentian Fan and to brown and grayish mud of Piper and Skene (1998) from the Scotian Margin. Facies E correlates to a mix of lithofacies III and Ia of Skene and Piper (2003) and to red-brown clay turbidites of Piper and Skene (1998). Facies F and G are volumetrically minor on both the Newfoundland and Scotian margins but provide the most accurate chronological control. Facies F correlates across the Scotian margin to a sediment bed identified as brick red sandy mud 'd' and to facies Vb on Laurentian Fan (Skene and Piper, 2003). Facies G correlates to detrital carbonate beds as far west as the Scotian Slope south of Sable Island and to the northeast in the Labrador Sea. Age constraints of these carbonate beds suggest a correlation with Heinrich event H1 in the North Atlantic Ocean (Bond and Lotti, 1995; Dowdeswell et al., 1995) and DC-1 of the Labrador Sea (Andrews et al., 1993).

The clear similarities between the facies described by previous authors and facies of this study indicate that similar geologic processes were occurring along the entire SE Canadian margin at similar times; primarily glacial processes, i.e. glacial advance and retreat, ice margin sedimentation and calving of the ice margin.

5.4 Source area and transportation for sediment facies from undisturbed cores

The main transportation mode of coarse-grained sediments (i.e. IRD) delivered to the lower slope and rise would have been ice-rafting (Skene and Piper, 2003), which is the product of iceberg calving at the ice margin front. Subglacial and coastal meltwaters

likely played a major role in sediment delivery to the upper and mid slope. Ice is thought to have persisted at the mouth of Laurentian Channel until ~14.2 ka (Piper and MacDonald, 2002) providing the setting for iceberg calving from the ice-margin front, before retreating rapidly up the channel (Josenhans and Lehman, 1999). Glacial tills from the Gulf of St. Lawrence area typically contain at least 40% sand and gravel. The predominance of muds and relatively minor amounts of sand and gravel from cores of this study suggest that ice margin processes segregated the sand and gravel component. Other transportation and erosional mechanisms that could account for the high mud component include plume fallout and turbidity current deposition.

Sediments recovered by shallow piston and trigger weight cores provide evidence for a likely source area. The brick red mud (Facies F) and reddish-brown muds (Facies E) sampled by cores are likely the result of glacial erosion of Carboniferous-Permian redbeds that underlie the Gulf of St. Lawrence and surrounding lowlands (Piper and Slatt, 1977), delivered to the open sea through Laurentian Channel following the LGM at ~18 ka (Figure 5.3). In addition, redbed sediments of probable Devonian age from southeast of the Avalon Peninsula (King et al., 1985) could also be a source for reddish sediments. Brown sediments point towards a source area from Carboniferous rocks of Placentia and Fortune Bays, with the likely conduit being Halibut Channel. Gray sediments suggest siltstones of Ordovician, Silurian and Devonian age derived from SE of the Avalon Peninsula delivered to the slope via Haddock Channel.

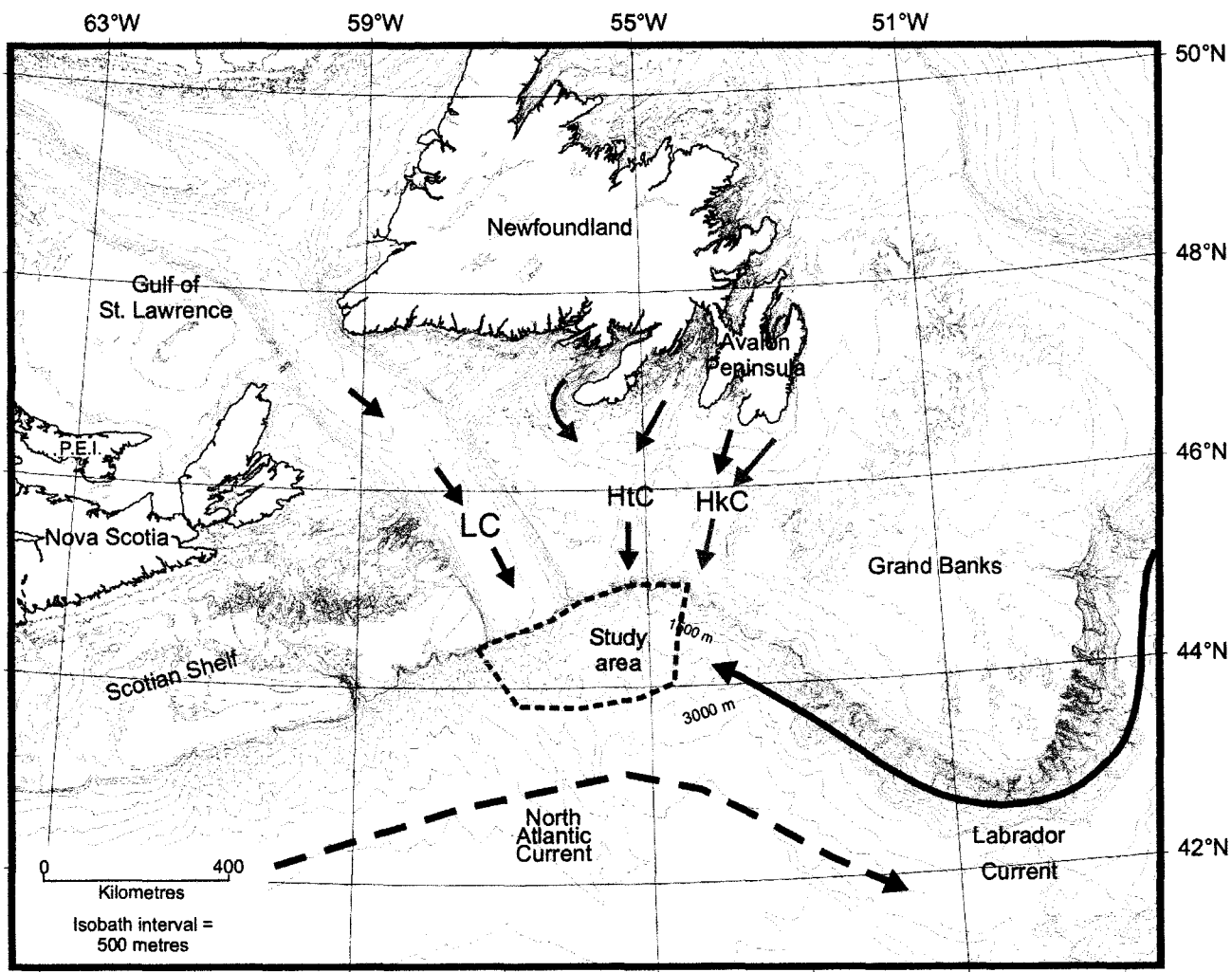


Figure 5.3- Regional map of eastern Canadian margin showing likely source areas for sediment sampled by cores from St. Pierre Slope and rise. LC = Laurentian Channel; HtC = Halibut Channel, HkC = Haddock Channel. Colored arrows signify sediment color. Dashed line (blue) outlines entire area believed to have been affected by the 1929 event.

The brick red muds (BRM) were previously documented in deep waters on

Laurentian Fan (>3000 mbsl) (Skene and Piper, 2003) (see Figure 4.4- cores 87003-09

and -10). No previous study has documented these muds in water depths shallower than 3000 m on Laurentian Fan or St. Pierre Slope. It has been suggested that the Labrador Current transported the source icebergs and related reddish sediments to the Scotian Slope (Piper and Skene, 1998), away from the study area. However, cores 99036-05 (1820 mbsl), 2002046-73 (2600 mbsl) and 2002046-74 (2670 mbsl) (Figure 4.4) contain these BRM beds, suggesting two possible scenarios: a) calving of icebergs from the glacial margin at the Laurentian Channel outlet (around 14.4 ka) carried BRM sediments (e.g. IRD or ice-rafted detritus) to the open sea and were subsequently deposited (likely from iceberg melting, dumps and 'flips'). Surface winds are believed to have flowed along the slope break in a WSW to ENE trend (opposite the Labrador Current) (de Vernal and Hillaire-Marcel, 1987), possibly moving icebergs in the NE direction, allowing for the deposition of BRM beds in shallower water, before the Labrador Current had a chance to transport the icebergs towards the Scotian margin or b) that redbed sediments from southeast of the Avalon Peninsula incorporated into the Laurentide ice sheet during glacial activity, were deposited into the open sea during calving of the ice margin. Ice is thought to have occupied Halibut Channel until 12.4 ka (Moran and Fader, 1997), and is assumed to have occupied Haddock Channel. The Labrador Current, with an east-west flow path along the Newfoundland shelf break (Smith and Schwing, 1991), carried these calved icebergs, which deposited their load onto the St. Pierre Slope.

The reddish-brown muds (Facies E) likely were delivered to the slope in a surface plume through Laurentian Channel via subglacial meltwater following the LGM at ~18 ka. The sediments would have experienced similar transport by currents as the BRM (Facies F). The absence of IRD within Facies E suggests deposition by plume fallout,

accounting for the location of the facies high on the slope (in shallow water). The apparent color layering and silt laminations of this facies on the lower slope and rise suggest deposition from turbidity currents. The increase in thickness downslope further supports turbidity current deposition, as decreasing gradients downslope would cause a concurrent decrease in velocity of the turbidity current (see Figure 4.4).

From core data, brown muds are restricted to the eastern side of Eastern Valley. After deposition into the open sea via subglacial meltwater from Halibut Channel, these brown muds would have been transported westward by the Labrador Current. However, since the ice sheet is thought to have crossed St. Pierre Bank at about 12.4 ka (Bonifay and Piper, 1988), subglacial (below the ice sheet) and deglacial (on the ice sheet) meltwater from the ice margin could have forced the Labrador Current farther offshore, in effect ‘pushing’ the brown sediments away from the Eastern Valley area. This effect would have affected any sediment supply from Haddock Channel as well.

As mentioned above, gray muds have a likely source from the siltstones from the SE Avalon Peninsula, delivered to the slope via subglacial and deglacial meltwaters (Figure 5.3). It is possible that the gray muds of facies C and D are the product of diagenesis of reddish-brown sediments, but this process would likely be dependant on sedimentation rate and is unlikely to have affected all cores at the same stratigraphic intervals.

Olive gray muds (facies A and B) are primarily restricted to the Holocene and very Late Pleistocene, and are synchronous to facies II of Skene and Piper (2003). Facies A represents hemipelagic and pelagic deposition after 12 ka, which explains the absence of IRD. Elsewhere on the continental slope, a facies described by Hill (1984) has been

correlated to facies A and is interpreted as representing hemipelagic sedimentation. Facies B, with its high concentration of sands and relatively recent age within the stratigraphic record, suggests a relationship to storminess events during the Younger Dryas (10 to 11 ka). It is thought there was an increase of sand deposition in marine environments due to erosion of banks (and any other raised subsurface areas), in this case, erosion of St. Pierre and Green Banks. Events of storminess have been documented from Emerald Basin in the Younger Dryas (Piper and Fehr, 1991) and elsewhere in the North Atlantic (Mayewski et al., 1993).

Thin olive gray beds underlying facies F (BRM) and facies G (H1) suggest a pre-14 ka radiocarbon age and have been correlated (Figure 4.4) to similar layers that Skene and Piper (2003) interpreted as turbidite deposits. Two components within this facies, clean quartz and green amphibole (Skene and Piper, 2003), suggest an Appalachian source, likely Newfoundland (Piper and Slatt, 1977).

5.5 Sedimentation rates

On the lower slope and rise, the gray and brown muds of facies D lie beneath facies F (dated at 14.4 ka radiocarbon years) (Figure 4.4). Due to the absence of radiocarbon dates within these brown and gray muds, no sedimentation rates were estimated. Facies E is immediately above and below facies F. This facies (E) thickens downslope and in places contains interbedded thin beds of facies A (Figure 4.4), which act as time markers (Skene and Piper, 2003). On the rise, facies E is close to 5 metres thick and thins to about 1 metre at 1800 mbsl on the lower slope. Skene and Piper (2003) estimated that similar reddish-brown muds accumulated on the order of 10 m kyr^{-1} and

the thin intervals of facies A at 70-140 cm kyr⁻¹ between LGM (~18 ka) and 14 ka. The thickening downslope of facies E likely relates to the gradient shift, as the rise is of a gentler gradient compared to the lower slope. This would cause the velocity of turbidity currents to decrease, resulting in turbidite accumulation to thicken downslope. In addition, there would have been more sediment available for deposition as the turbidity current swept downslope, as it would have entrained and eroded sediments progressively. Reflections Q93 and Q91 further support the thickening downslope assumption as they increase in depth below seafloor from the middle to lower slope by 16 ms and 12 ms respectively. This depth increase likely was caused by multiple, downslope sweeping turbidity currents that deposited their sediment loads as gradients decreased progressively downslope.

A radiocarbon date of 30 ka from core 90015-07 taken from a ~56-metre-deep failure plane, together with the known age of reflection Q99 of ~15.3 ka, allow for the extrapolation of sedimentation rates of a fairly thick subsurface portion of the seabed on the slope (Figure 5.4). This gives a sedimentation rate of 3.15 m kyr⁻¹ for a period of 14.9 ka radiocarbon years (30.2 to 15.3 ka radiocarbon years). Turbidites are known to accumulate at a fairly high rate of sedimentation in this area (Skene and Piper, 2003) and are documented in many cores from this study (e.g. Figures 4.4 and 4.10). Multiple episodes of turbidite deposition in the upper section of core 90015-07 document turbidity currents in this area as far back as 30 ka radiocarbon years. Thus, it is presumed that this sedimentation rate is not one of constant sediment accumulation, but that there were intervals of very high sediment accumulation on the order of something similar to that of

facies E (10 m kyr^{-1}) with intervals of relatively low sedimentation rates, similar to that of facies A of $\sim 0.7\text{--}1.0 \text{ m kyr}^{-1}$.

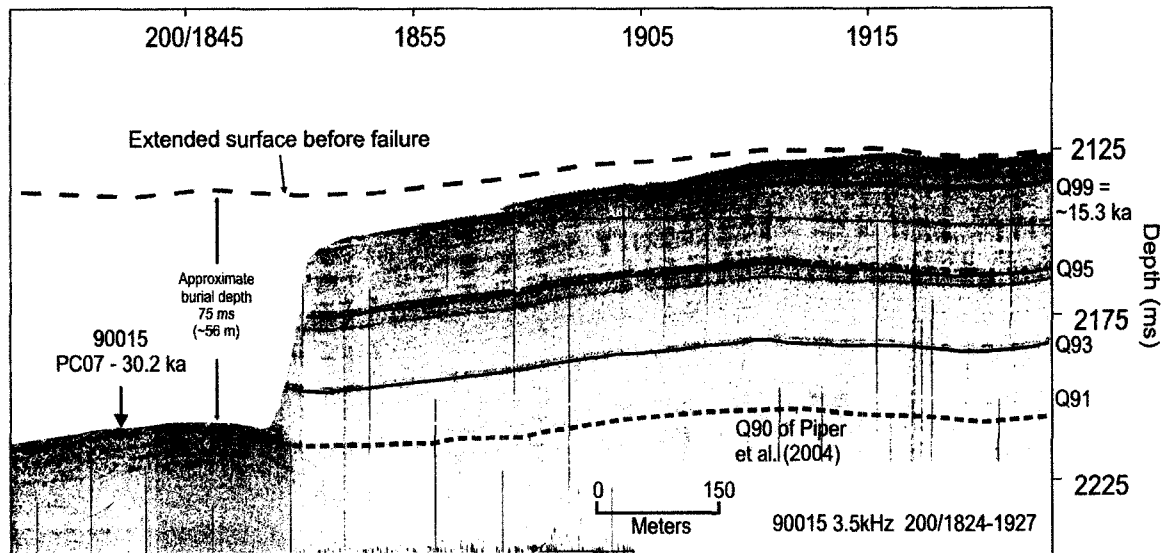


Figure 5.4- Reflection Q99 at $\sim 7.3 \text{ m}$ subsurface has a radiocarbon age of 15.3 ka and at 1.5 m below the failure plane a radiocarbon age of 30.2 ka . This gives an estimated sedimentation rate of 3.15 m kyr^{-1} .

On the middle slope, brown mud and gray mud of facies C from core 90015-02 (Figure 4.3) dated at 13.4 ka at 3.5 m and 15.4 ka at 7.5 m downcore, give a sedimentation rate of 2.0 m kyr^{-1} . Extrapolation of radiocarbon ages of 15.2 ka from core 86034-09 suggests that sedimentation rates for the brown mud of facies C under the distinct gray mud bed (Figure 4.3) were on the order of 9.6 m kyr^{-1} . The high sedimentation rates for the brown mud could represent major pulses of deglacial meltwater out of Halibut Channel. An age of 14.2 ka at the top of the distinct gray mud bed and 15.2 ka near the base of the same bed suggest sedimentation rates $< 1 \text{ m kyr}^{-1}$. The apparent low rates of sedimentation for the distinct gray mud bed, with a likely source out of Haddock Channel, point towards a period of decreased meltwater from the ice margin, and cessation of deposition of brown muds.

On the upper slope, radiocarbon dates from core 90015-05 (Figure 4.2) indicate that rates of sedimentation during the latest Pleistocene could have exceeded 5 m kyr^{-1} . This high rate of sedimentation may be due in part to increased sand deposition during the Younger Dryas, and from coastal meltwater influxes off St. Pierre Bank, as the ice is believed to have crossed St. Pierre Bank around 12 ka (Bonifay and Piper, 1988). No piston core yielded dates from the Holocene. Trigger weight core 90015-05 yielded a radiocarbon age of 8.6 ka. If this core is taken as representing the full stratigraphic record, it suggests that sedimentation rates during the Holocene have been quite low, around 0.07 m kyr^{-1} .

5.6 Mass Transport Deposits: core-seismic integration

Each core that sampled disturbed sediments has been placed into a corresponding seismic reflection profile (Appendix 2). Each profile shows an acoustic class (es), relative position of the core within the stratigraphic record and the failure interpretation of the core. Core facies have been interpreted as follows based on internal structure (as described in Ch.4): Facies I- mud clast conglomerate (MCGL); Facies II- glide block; Facies III- slump block; Facies IV- turbidity current (TB); and Facies V- not an MTD but an eroded surface and or basal failure plane. The disturbed facies sampled by the cores are compared with the acoustic class imaged by Huntect DTS (Table 5.2). Two scales of failure are recognized: a *mesoscale* disturbed facies sampled by cores and a *macroscale* disturbed facies imaged by Huntect DTS. The following describes the similarities and variability between the sampled and imaged disturbed sediment at each core site (*see Appendix 2 for figures of integration of cores and seismic profiles*).

Cruise-core #	Disturbed facies from cores (core top to core bottom)	Corresponding acoustic class
2001043-43	Facies I - MCGL Facies III - Glide Facies II - Slump	?- Likely Class II - Mass flow (see text)
2001043-42	Facies I - MCGL Facies II - Slump	Class II - Mass Flow
2001043-41	Facies III - Glide	Class V - Erosional or evacuation surface
91020-40	Facies I - MCGL	Class II - Mass Flow
90015-07	Facies IV - TB	Class V - Erosional or evacuation surface
84003-05	Facies III - Glide	Class I - Rotational slump

Table 5.2- Comparison of MTD facies sampled by cores to MTDs imaged by seismic data.

Core 2001043-43 -

The closest seismic profile to the position of this core is approximately 1 km to the north. Complementary SeaMARC I sidescan data over the core site sheds light on the surface character of the seabed (pg. 225) but does not further the knowledge of the subsurface setting, thus the integration between core and seismic reflection profile is unreliable.

Core 2001043-42 -

The seismic profile over the core site (a valley) shows stacked mass flow deposits of Class II (Figure 5.5). The top of the core to about 4 metres downcore is a mud clast

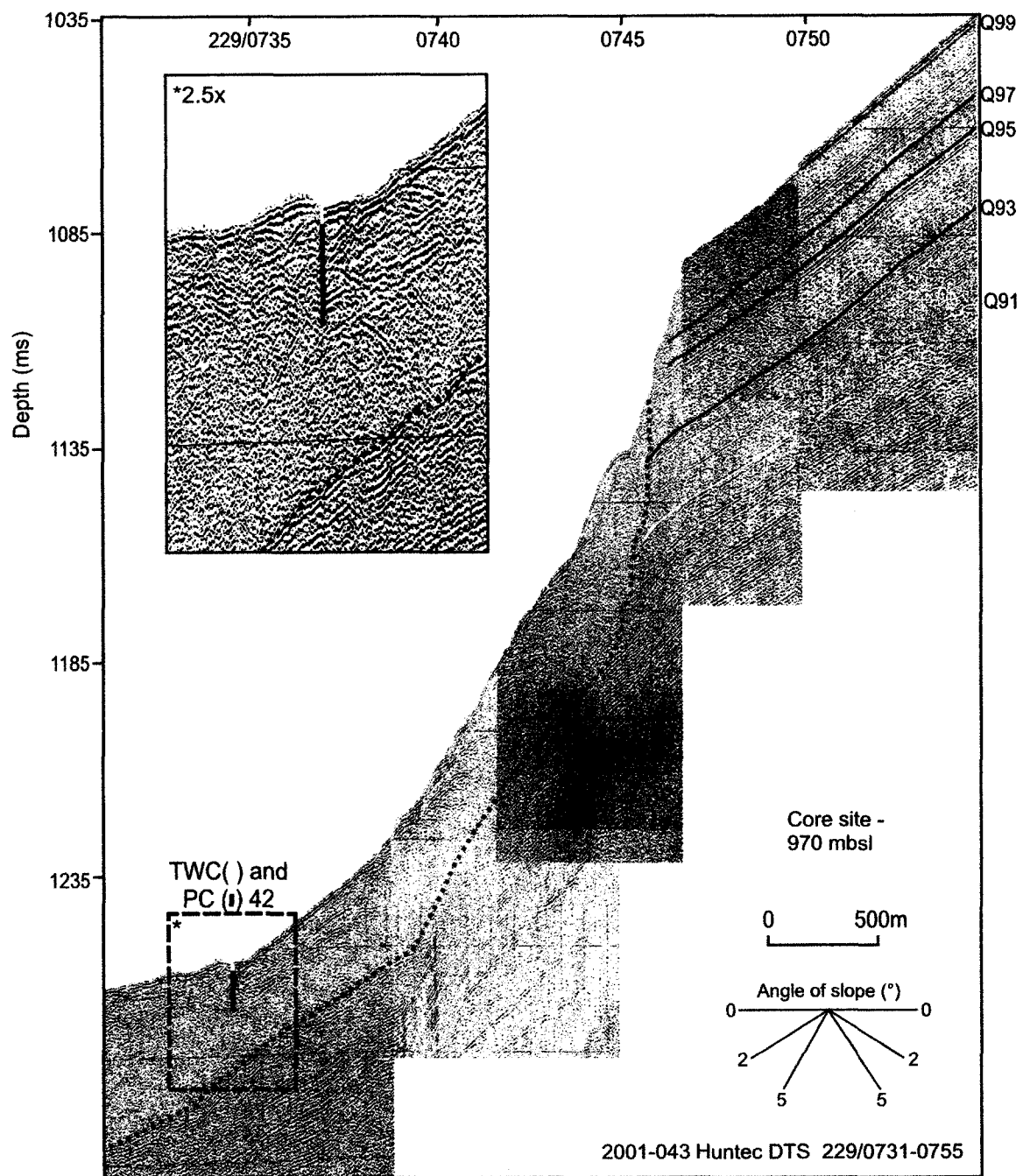


Figure 5.5- Integration of cores and seismic data. Multiple MTD events appear to be separated by continuous, coherent subsurface reflections. The core samples hyperbolic reflections characteristic of both acoustic Class I (slump) and subclass IIA (blocky mass flow) of acoustic Class II (inset). The former corresponds to Facies II (slump) as described in the core. The basal failure plane is outlined (dashed turquoise line).

conglomerate and from about 4 metres to the core bottom is a slump deposit (Figure 4.7B-D). This failure boundary at 4 metres is shown by irregular shear strength measurements (pg. 223). Normally, a core will show a shear strength increase with burial depth due to compaction and consolidation (Mosher et al., 1994). These irregular readings are likely the result of the reorganization and reconsolidation of sediments during transport.

Two scenarios of failure are possible. First, initial large-scale failure occurred, depositing the bottommost mass flow (Class II) (basal plane outlined in turquoise in Figure 5.5). This was followed by subsequent small-scale (or thin skinned) mass flow failure that in places covered the initial mass flow. Acoustic evidence for multiple failures is from the semi-continuous reflections that separate the mass flows (Figure 5.5). These reflections may represent a drape overlying the bottommost mass flow and could signify that this mass flow is an old failure not initiated by the 1929 event. However, the absence of overlying drape (with a seismic appearance of original undisturbed stratigraphy) on this mass flow upslope suggests that it is a recent deposit (Figure 5.5). The core sediments show a stratigraphy typical of disturbed sediments, especially at the surface where no internal structures are present. A second scenario for failure is that during initial break-up of the original seabed, some parts of the sediment might have remained intact and been transported as blocks or slabs within a mud matrix. Structure within the core supports this scenario and MTD complexes like this are well documented (e.g. Moore et al., 1994; Masson et al., 1998). This mechanism would account for the continuous reflections observed within the mass flow, explaining the slump deposit sampled by the core. This scenario is supported by both the core and seismic data.

Examining the seismic profile away from the core-sampling-spot shows extensive, lateral, undulating, subsurface reflections that support the first scenario of thin skinned mass flows. It appears then, that there was a large scale mass flow with sediment slabs as well as thin skinned mass flows.

Core 2001043-41 -

The seismic profile over the core site shows a seabed of continuous, parallel reflections in places interrupted by hyperbolic diffractions, caused by a scar (acoustic Class V) (Figure 5.6). Five of the reflections have been carried through the site with the

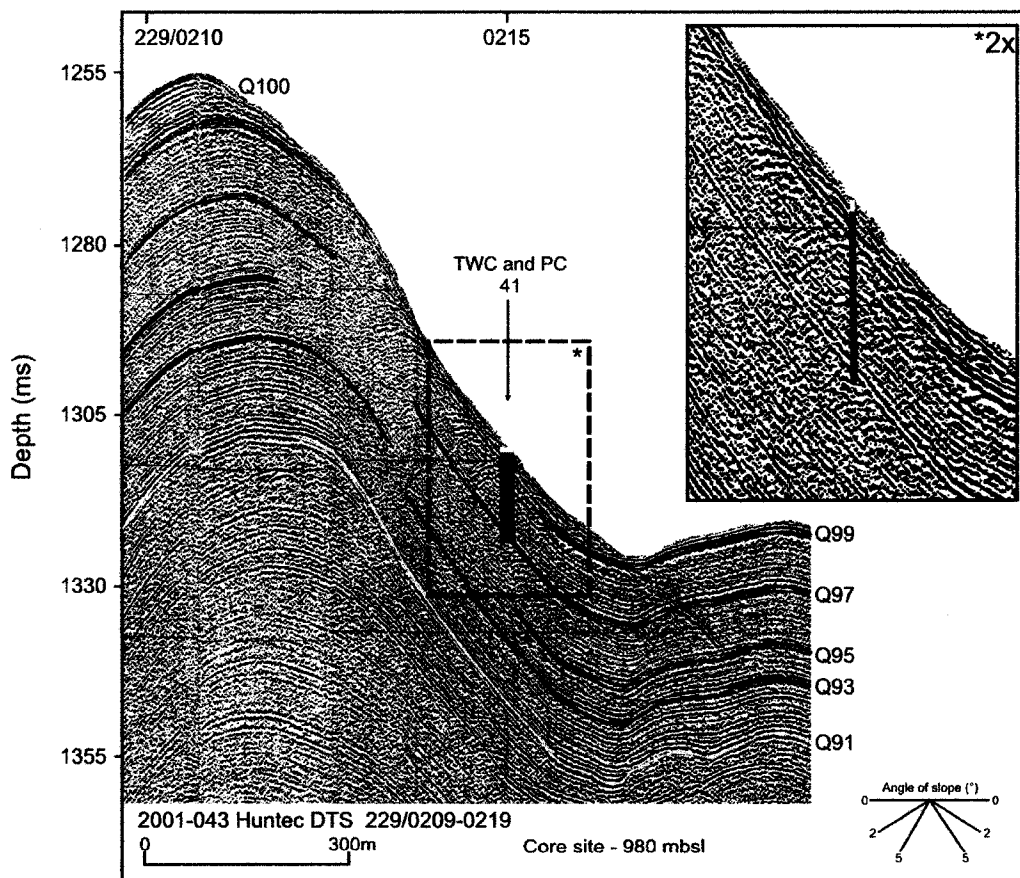


Figure 5.6- Integration of cores and seismic data. The core samples a stripped-off seabed evident from the absence of the brown reflection (Q100) and hyperbolic diffractions indicative of a scar of acoustic Class V. The two cores (red is PC, yellow is TWC) sample Facies III (a glide), and the coincident seismic data shows coherent, semi-continuous reflections that likely represent acoustic Class IV (a glide).

exception of reflection Q100, which is absent and has been stripped away. The piston and trigger weight cores show the upper 1.85 metres to be a glide (Facies III) (Figure 4.8). It is probable that this glide is a remnant sediment block that has been only displaced slightly downslope during removal of the overlying sediment. Alternatively, the glide could be a marginal glide block marking the transition between an undisturbed seabed to a mass flow. The sharp basal contact of the glide block with the underlying gray mud facies represents the basal failure plane. Shear strength measurements from the core show an increase of values at the basal failure surface and suggest removal of about 7-8 metres of sediment, which is consistent with the seismic profile that shows a stripped-off seabed.

Core 91020-40 -

The seismic profile near the core site shows a mass flow deposit (subclass A of Class II) (Figure 5.7) and the piston and trigger weight cores sampled sediments classified as a mud clast conglomerate (Facies I) (pg. 215). This class and facies are synonymous and represent the same type of failure process. The thickness of the deposit from seismic reflection data is about 5.3 metres, whereas its thickness recovered in the two cores is about 2.45 metres, roughly half the estimated thickness from seismic data. Two possible scenarios could account for this inconsistency in deposit thickness. The seismic profile is known to be located about a couple of hundred metres to the south of the core site and thus it is possible that either 1) the deposit thickens downslope or 2) that the core site and seismic profile sampled two entirely different deposits. The latter seems unlikely as SeaMARC I sidescan data over the core site show a smooth seabed with no ridges or scarps suggestive of multiple, independent failure deposits. Rather, the smooth

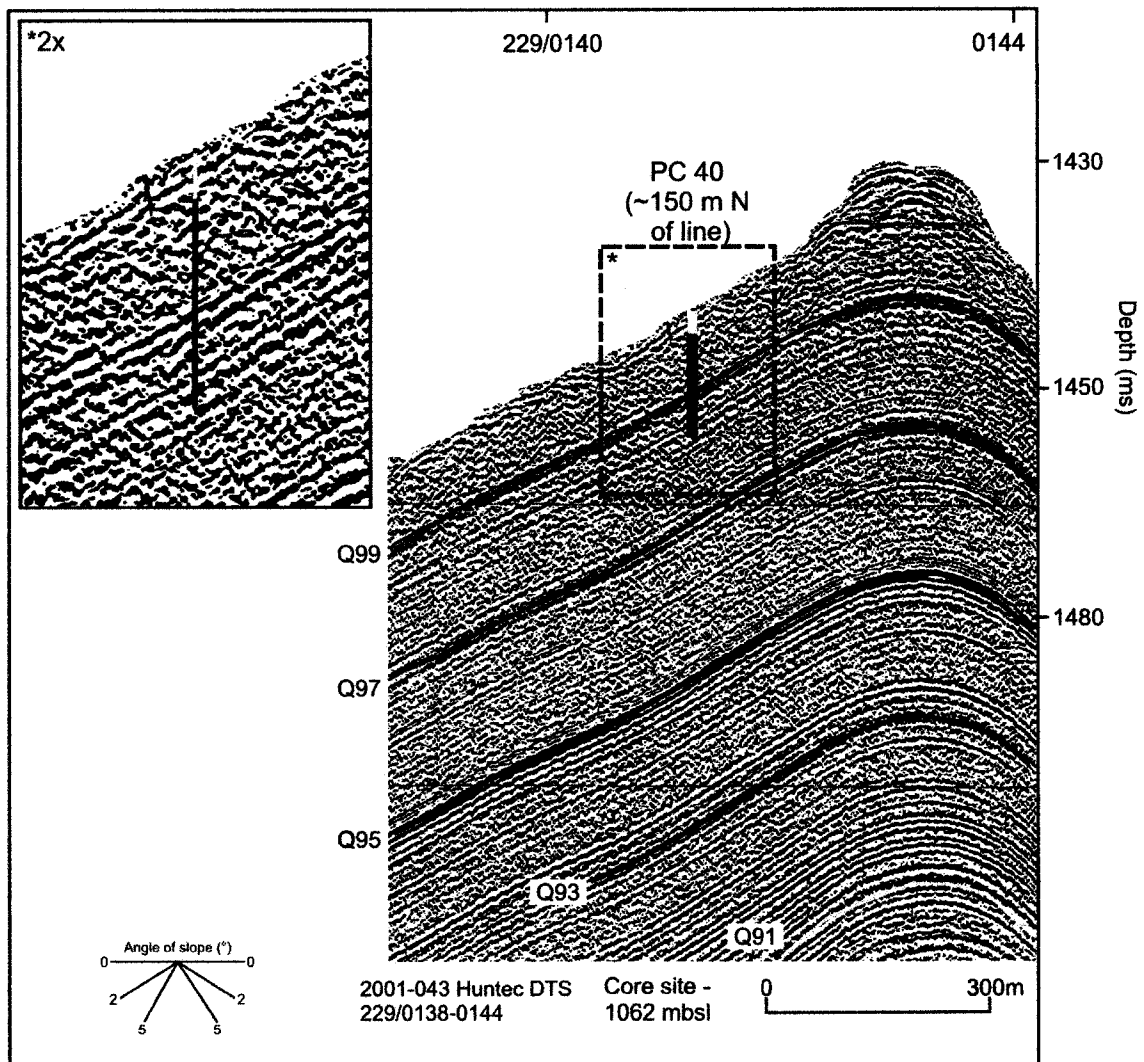


Figure 5.7- Integration of cores and seismic data. The MTD sampled by the core (mud clast conglomerate of Facies I) and imaged by the seismic (smooth mass flow of Class II, base of MTD is orange reflection) are synonymous. A noted discrepancy is that the core deposit is roughly half that of the seismically imaged MTD, likely due to slight offsets in sampling locations.

topography from complementary seismic data suggest one failure deposit. A third possibility is that the basal boundary of the mud clast conglomerate does not contact the normal undisturbed stratigraphy but that this underlying sequence is a 'floating' sediment block within the mass flow that has not broken up during transport of the main sediment mass. With this underlying sequence being about 6 metres thick, no apparent distortion to

the internal structure and a fairly linear shear strength downcore suggest that this latter scenario is unlikely.

Core 84003-05 -

SeaMARC I and SAR sidescan data over the core site show a seabed composed of parallel, arcuate ridges that in seismic profile are represented as overlapping hyperbolae (Figure 4.9), interpreted as a rotational slump deposit (Class I). The sheer size of this slump deposit (10 km²) makes positioning errors associated with core placement in the seismic and sidescan data relatively minor. The core interpretation conflicts slightly with the acoustic class, as the core sampled a glide (Facies III). This interpretation is based on the preservation of internal structure, i.e. where the bedding plane contacts dip at 5° and a single bed dips at 10°, which is near the transition when a sediment body is classified into either a slump or glide (pg. 92-93). The slight dips of structure indicate that movement of the sediment did occur but did not completely destroy the internal character and stratigraphic succession. Shear strength readings do not follow any linear downcore trend indicative of undisturbed sediments, further suggesting that the sediments were somewhat disturbed and reorganized to produce the erratic shear strength measurements.

It is likely then, that the core sampled the top of a block where the angle of tilt was not very high and disruption of the stratigraphy was relatively minor, as compared to a mass flow where a major loss of internal structure occurs. Figure 5.8 is a schematic of the core site showing the most likely part of the slump sampled by the core. The placement of the core on the 'top' ('a') of the slump shows that tilting of the strata would be minor. If the core had sampled a shear surface ('b'), the dip of the strata would be

much greater and the stratigraphic succession would not be similar to the succession shown by nearby undisturbed cores.

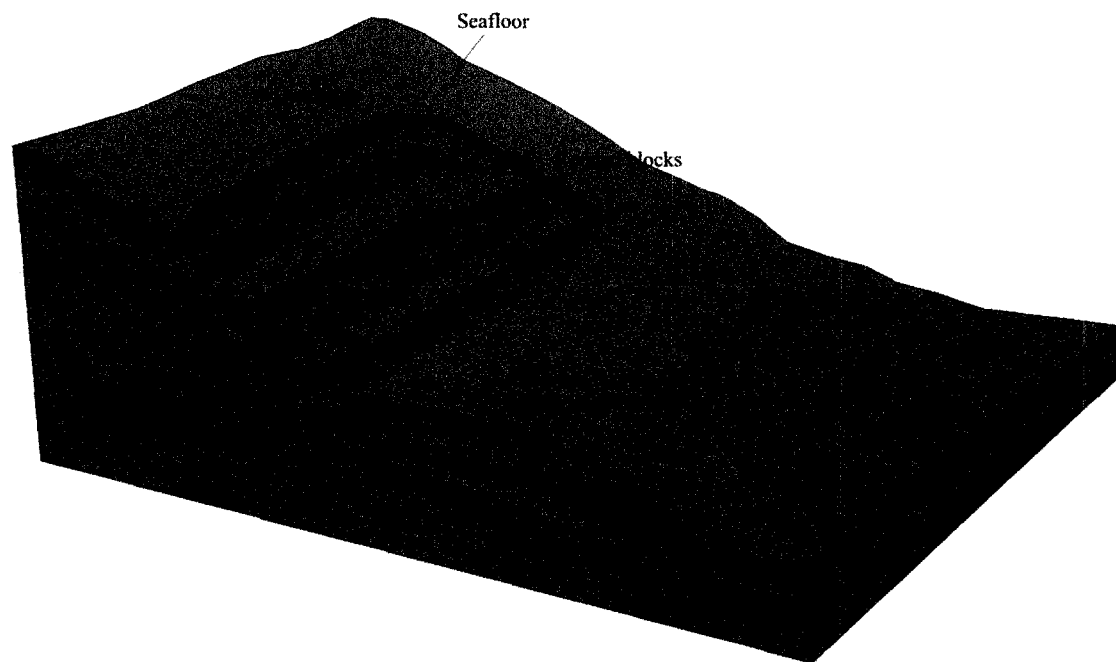


Figure 5.8- Cartoon of a rotational slump deposit (acoustic Class I) showing likely (a) and unlikely (b) sampling point for core 84003-05.

Core 90005-07 –

The seismic profile over the core site shows an area that has undergone removal of about 56 metres of sediment (Figure 5.4). The seabed shows no acoustic evidence for deposition of MTDs. Instead, the seabed consists of parallel, continuous reflections representing a scar of acoustic Class V. Core data reveals multiple episodes of either bottom current or turbidity current deposition (Facies IV) from the seabed to about 1.4 metres downcore (PC-110cm and TWC-26cm) (Figure 4.10). The topmost deposit of facies IV fines upwards and is marked by a gravel lag at its base. The possibility of this gravel lag representing gravel waves described by Piper et al. (1985) is discarded as the waves are 2-5 metres in height compared to the lag which is a few cms thick only. The

sequence overlying this gravel lag is a turbidite, deposited from the 1929 turbidity current that swept down the slope to the Sohm Abyssal Plain. Immediately below the gravel lag are more deposits of Facies IV. Shear strength measurements from these deposits are relatively high, an indication that these deposits were at one time buried, then exposed during evacuation of overlying sediments and subsequently covered by the ensuing turbidity current of 1929.

5.7 Observed failure types in seismic reflection data

5.7.1 Gradients and distribution

The general distribution of documented surface failures on the St. Pierre Slope is illustrated in Figure 5.9. Failure initiation and deposition correlate closely with gradients (e.g. valley walls, gentle slopes). Acoustic Class I is mainly found on gradients of or exceeding 5° and acoustic Class II on gradients $<5^{\circ}$, except for subclass IIB, which is prominent at and partially on the base of steep gradients. Acoustic Classes III and IV are documented in areas of gradients $<5^{\circ}$. Acoustic Class V represents a surface of irregular reflections such as scars and erosional surfaces, and has a wide range of gradients from a few degrees up to 60° . Class I and subclass IIB of Class II occur primarily near or on valley headwalls and sidewalls where gradients surpass 5° (Figure 5.10).

In general, as gradients increase, the subsurface depth of failure planes increases as well. This is illustrated nicely in Figure 3.10. Where the slope surpasses 10° , the seabed has been stripped off to just above the red reflection (Q95) and no visible acoustic

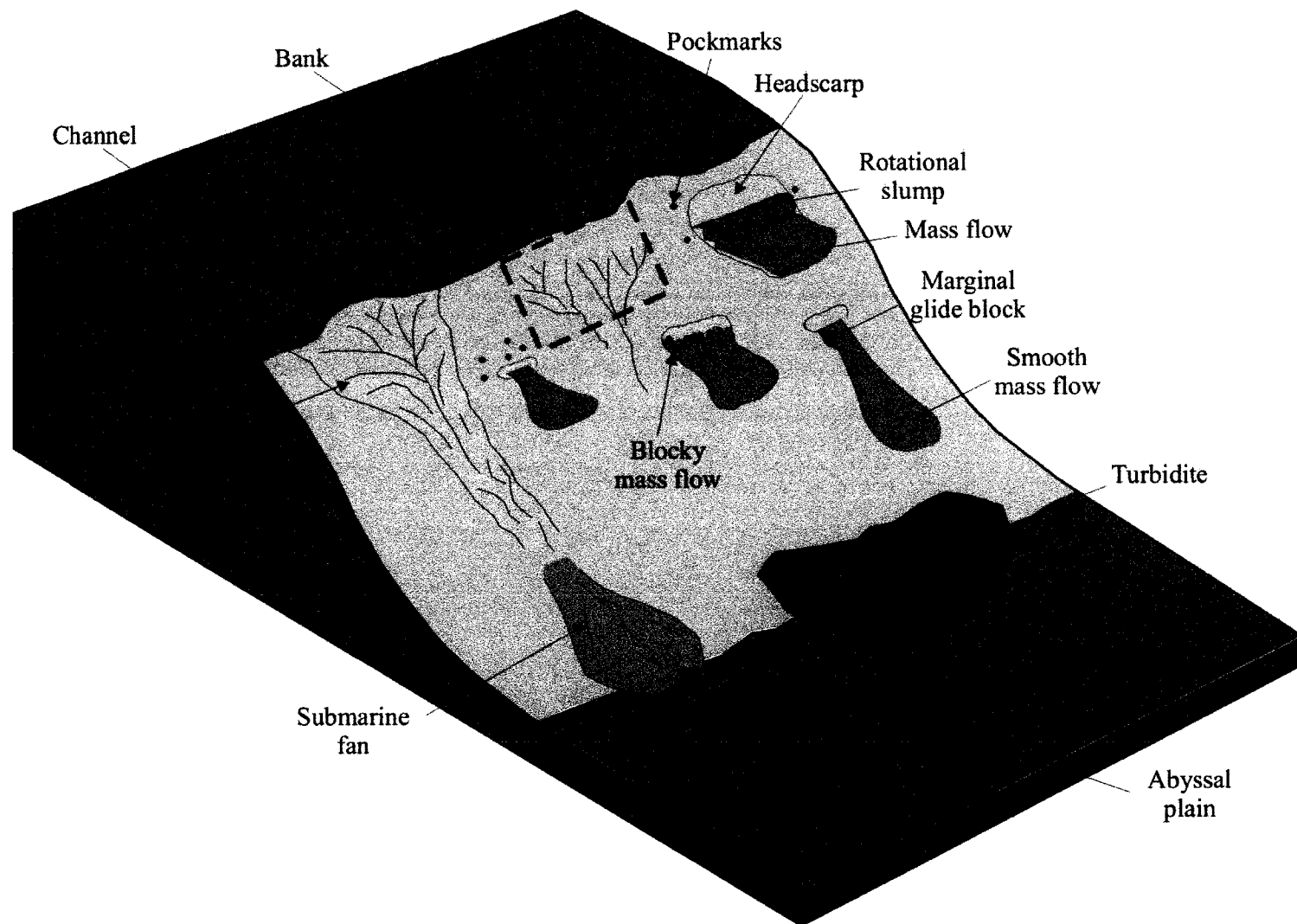


Figure 5.9- Cartoon of the mass transport deposits documented on the St. Pierre Slope from Huntect DTS seismic reflection data, with the exception of the turbidite. The dashed box outlines Figure 5.10.

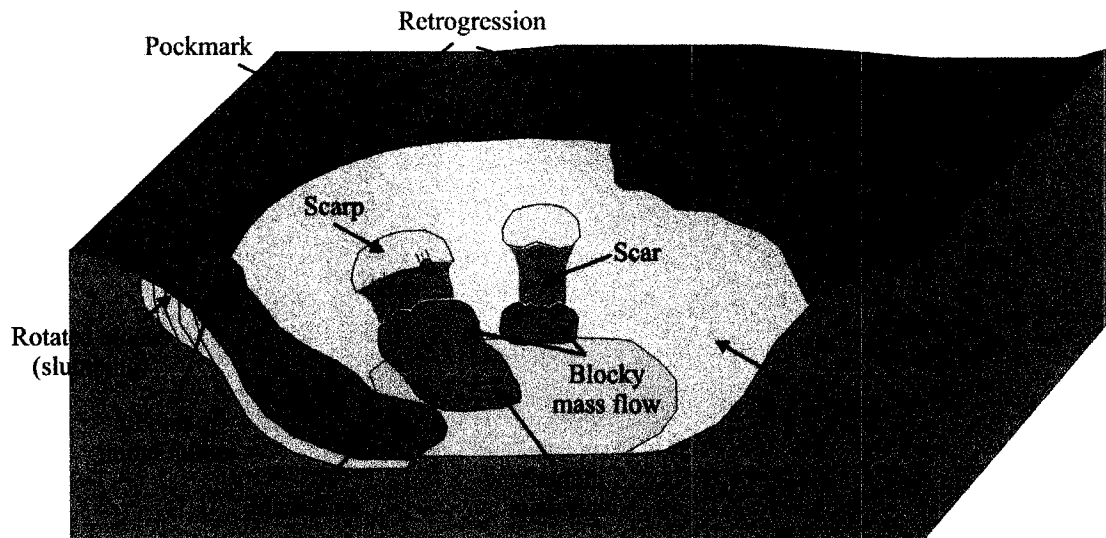


Figure 5.10- Cartoon of mass transport deposits documented on or near valley walls. Note that retrogression occurs up the steep walls and that no failures are seen high up on the walls, except for slumping.

deposits remain, rather the seabed shows signs of erosion likely from mobilized sediment and is represented by a scar (Class V). In the middle of the profile, a mass flow deposit (Class II) rests on a slope of 1-2°. It is uncertain whether failure occurred here. It is possible that the mass flow has an upslope source and that the deposit moved downslope stripping off a few metres of seabed at this location before coming to rest. Only the top few metres of sediment appear to be missing, as suggested by the position of the underlying reflections (the orange reflection (Q99) is close to its subsurface average depth in the undisturbed stratigraphy). To the east, a slump deposit (Class I) on a gradient of 5° has affected the seabed to about half way between the green (Q97) and red (Q95) reflections. One exception is shown in figure 3.8. The failure plane of this deposit in places extends down to the yellow reflection (Q91). However, because the profile obliquely transects the deposit, the gradient appears lower than the true value of more than 5°.

There appears to be no significant deposition of sediment on gradients that surpass 10° , only scars and scarps remain (e.g. Figures 3.10 and 3.19). Creep-like deformation is limited to a gradient of 4° and has affected the stratigraphy to about the red reflection (Q95) (Figure 3.15). The one example of a glide is on a gentle slope of 2° , with the base of the deposit about 2-3 metres above the orange reflection (Q99).

Wherever gradients do not surpass $3-4^\circ$ there seems to be preferential failure along or a few ms above or below the orange reflection (Q99). The sediment equivalent to the orange reflection (Q99) is a succession of sandy mud and mud layers (Figure 5.2). This relationship between failure and the orange reflection (Q99) is dominant in areas of low gradients ($\sim 1-2^\circ$). It is probable that during seismic shaking from the 1929 event, earthquake-induced ground accelerations caused liquefaction of sandy layers, providing the ideal setting for failure along these sandier intervals. This failure along the orange reflection and its associated reflections seems too widespread to be random. In the Verrill Canyon area of the Scotian Slope, Campbell (2000) found that failure planes appear to be restricted to specific horizons (or acoustic reflections) that correlate with sandy to silty intervals. It has been surmised (e.g. Atkinson, 1985) that earthquake-induced horizontal ground accelerations (and possibly gas escape) can cause liquefaction of thin sandy-silty intervals, resulting in failure along such horizons. Excess pore pressures generated in a sand layer that liquefies can be trapped and form a water film below a less permeable layer (Kokusho, 1999). It is known that gas charged sediment exist on the St. Pierre Slope, mostly from core analyses and from the widespread presence of pockmarks. Eight of the cores contain detectable gas (pg. 90) and cores 2001043-41 and 99036-03 show

cracking near the orange reflection (Q99) (sandy bed), providing a suitable zone for failure.

5.7.2 MTD Lithology

The majority of sediments sampled by the cores from MTDs are muds of a glacial origin, as failure involved predominantly Late Pleistocene sediment overlain by Holocene sediments. In places, the muds are intermixed with sands and IRD, to a degree that reflects the MTD type. For example, a mud clast conglomerate has experienced a high degree of mixing, apparent from the mud to muddy sand matrix, and the deposit lacks original internal structure. In contrast, glide deposits retain most of their internal structure with little mixing, if any, of adjacent lithologies; bedding plane contacts are in place and are rarely disturbed, and mud is the major constituent. Intermediate between these two deposits are slumps. The bedding plane contacts are usually distorted and intermixing of adjacent lithologies appears to reflect the degree of transportation, and just as with glides, mud is the major constituent (see Figure 4.7).

5.8 Evolution and progression of failure types

The turbidity current caused by the 1929 event has been intensely studied (e.g. Piper et al., 1988, 1999a) and a linkage has been presumed between the widespread failure of sediment on the continental slope and initiation of turbidity current (Piper et al., 1999a), similar to mechanisms proposed by Hampton (1972) for the transformation of debris flows into turbidity currents. It has been proposed that rotational failures (slumping) evolved downslope, through hydraulic jumps, into debris flows that if

entrained with sufficient water, and with adequately steep gradients, evolved into turbidity currents.

This section will attempt an explanation on evolution of failure (acoustic Classes I-IV) on the St. Pierre Slope, with particular emphasis on the influence that gradients had on MTDs, particularly how local changes in gradient influenced the type of MTDs that resulted. Other factors contributing to failure besides gradients include: sediment type, the stratigraphic location of this sediment, and the presence of gas. It is assumed that the ground accelerations associated with the 1929 earthquake triggered initial surface failure, both during the initial and the two subsequent shocks.

For the remainder of the chapter, the four classes will be referred by their assigned MTD name: Class I- rotational slumps, Class II- mass flow deposits (IIA- smooth and IIB blocky), Class III- creep deformation, and Class IV- glide block.

Smooth mass flows usually are stacked in valleys (Figures 3.13a, b and 3.19) and exist as thin sheets on gentle slopes ($<2^\circ$) (Figures 3.11 and 3.16). Where other deposits exist, smooth mass flows are in direct contact (e.g. overlying, laterally) with blocky mass flows, slumps and glides, and in places are located immediately downslope of blocky mass flows and slumps. In the one area where creep-like deformation exists, a smooth mass flow deposit is at the surface. A pattern of deposition and apparent failure evolution, thus, has been recognized. From both seismic and sidescan data, smooth mass flows exist at the distal ends of slumps and blocky mass flows. This transition downslope is apparent in Figures 3.10 and 3.14. Sidescan sonar data shows sub parallel, arcuate ridges terminating upslope at a headscarp that pass downslope into seemingly smooth terrain. Coincident seismic data show this smooth terrain to be a smooth mass flow. Determining

what occurred first is the dilemma. The initial failure likely was a slump with the distal portion of the deposit becoming a mass flow as it progressed downslope causing disintegration of internal structure (Figures 5.8 and 5.10). The successive overlapping of ridges, similar to that described in Piper et al. (1999a), is proof of retrogression, a process that has occurred here. Initial failure probably was at the first block (Figure 5.10), with subsequent retrogressive blocks occurring upslope from progressive loss of sediment integrity as sediments are exposed (e.g. excess pore pressures). If gradients downslope of this initial failure were high, simultaneous disintegration would have occurred (Figure 5.10). In an isolated area near the slump headscarp is a glide block ('a' in Figures 3.11, 3.14 and 3.16). This glide block deposit may mark the transition of the undisturbed stratigraphy to that of a mass flow. The acoustic character of this deposit is similar to that of the adjacent stratigraphy except that there are some surface and subsurface hyperbolic diffractions. At the surface these diffractions probably represent erosion as some of the overlying material has been removed, whereas in the subsurface, they likely represent a disintegration of internal stratigraphy, leading to a complete loss of internal structure as the MTD complex progressed downslope. Similar marginal transitional glide blocks have been documented on the Scotian margin by Mosher et al. (1994), marking the transition of an undisturbed zone to a disturbed zone. The lack of sub parallel ridges at the surface of this glide block suggests that this specific location was not subjected to slumping. The most probable scenario for this is that gradients were not sufficient to induce slumps but that the sediment was subjected to slow translation movement on a gradient of 2-3°.

Figure 3.8 displays a few types of MTDs as it obliquely transects multiple failures. First, there appears to have been regional failure with the failure plane a few

milliseconds above the yellow reflection (Q91) (Figure 5.11). The internal structure of this body shows both incoherent and prominent, coherent reflections (Q93) suggesting movement of a lesser magnitude, as significant internal structure remains intact, similar to the glide block of class IV. Near and at the surface other MTD classes are represented. Downslope from the headscarp (1-3km), parts of the surface resemble smooth and blocky mass flow deposits. The boundary between the lower glide-like deposit and the apparent surface MTDs is unclear. It is possible that they form a single, complex deposit. Upslope of these smooth and blocky mass flows, the deposit is smooth and could be a smooth mass flow or an erosional pathway as suggested by the sidescan sonar image (Figure 5.11). Within 1 km of the headscarp, the surface deposit was originally classified as a rotational slump (Figures 3.8, 5.8), but upon further inspection an alternate hypothesis is presented here. Tracing the prominent reflections of the upper hyperbolic deposit suggests that the blocks are imbricated in an upslope direction, the opposite direction expected for a retrogressive, rotational slump (Figure 5.11C- compare with Figures 3.8, 5.8 and 5.10). A similar situation is documented in the Titanic area where blocks dip upslope and these upslope blocks are emplaced over those downslope (Savoye et al., 1990, Figures 5, 6, and 13). Also, due to the fact that the seismic profile obliquely transects the MTD (Figure 5.11B), the apparent upslope imbrication may be misleading. It is possible that the failure imaged in Huntet DTS (Figure 5.11A) is coming through the page, towards the reader. Further investigation would be required to resolve this uncertainty (e.g. seismic data that runs parallel with direction of transport).

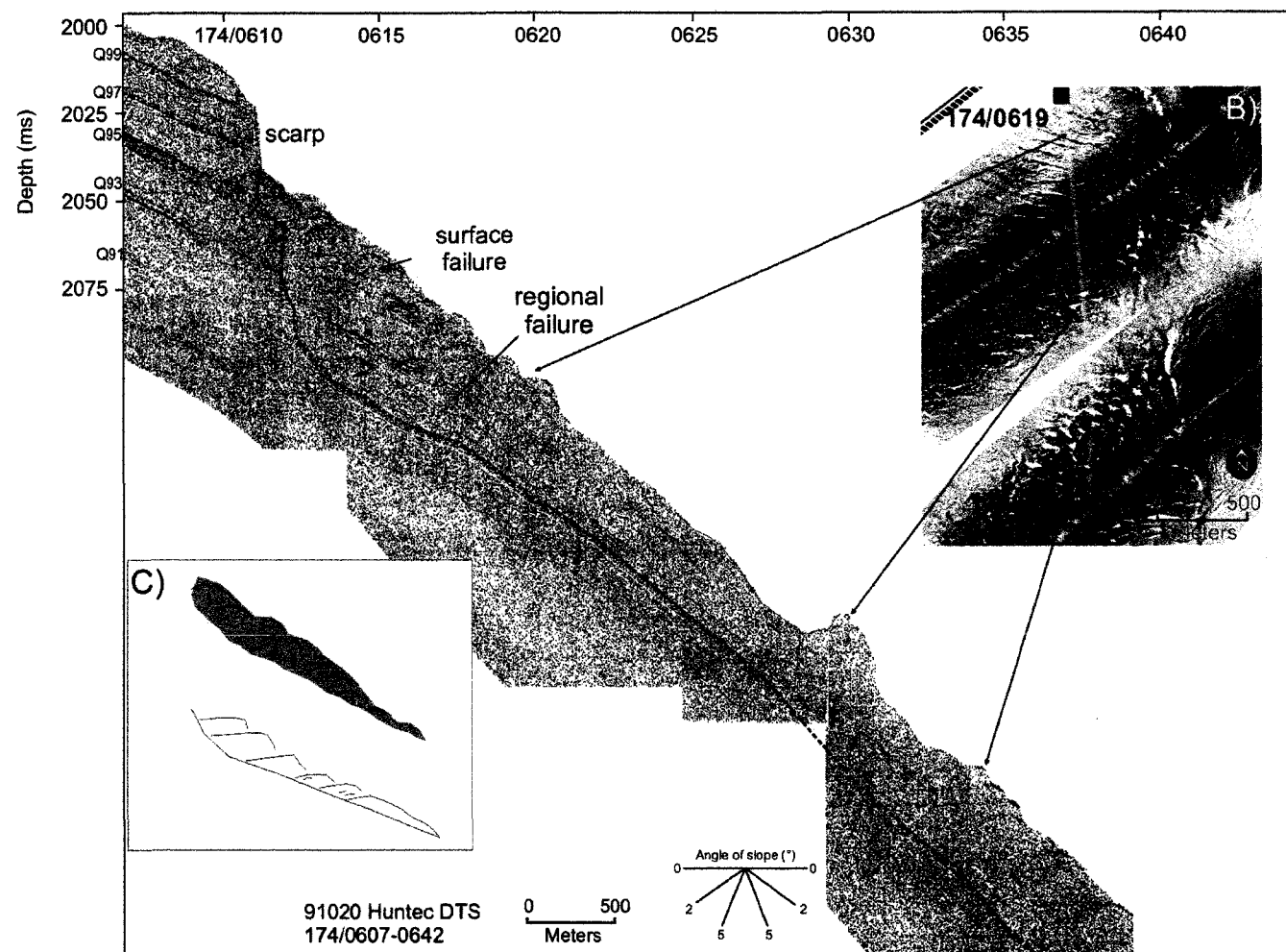


Figure 5.11- Huntec DTS seismic reflection profile of multiple failures. The regional failure appears to be a glide block (Class IV) (black dashed line marks failure plane) with overlying failure deposits of Class I and II. Appearance of these surface deposits is shown in (B). The orientation of the blocks near the headscarp suggests the blocks are imbricated in an upslope direction, the opposite of what is expected for slumps (C).

5.9 Sediment budget from failure volumes

The amount of sediment speculated to have been mobilized and reworked as a result of the 1929 event has been poorly studied, with previous values (e.g. Piper and Aksu, 1987) being merely estimates based on small amounts of data. This study examined ~1000 line-km of seismic data to arrive at an estimate of the amount of sediment that was affected by the 1929 event.

The turbidity current deposit has been conservatively estimated to have a volume 175 km^3 of sediment and is thought to have been initiated by failure of 100 km^3 of sediment (Piper and Aksu, 1987). This study suggests that the volume of sediment involved in initial failure was 93.5 km^3 ($9.35 \times 10^{10} \text{ m}^3$) over the entire region (see Figure 5.3- blue dashed line); 6.5 km^3 less than the Piper and Aksu (1987) estimate of 100 km^3 . The total volume of sediment remaining in the entire region as failed deposits is estimated at 47.1 km^3 ($4.71 \times 10^{10} \text{ m}^3$), mostly as mass flow deposits. This means that 46.4 km^3 ($4.64 \times 10^{10} \text{ m}^3$) of sediment evacuated from the entire region, presumably travelling downslope, transforming into the turbidity current as failure progressed. Thus, this 46.4 km^3 was the initial evacuated sediment that entrained and eroded about 130 km^3 of sediment as the failure progressively grew downslope through erosion of valley floors, likely Eastern Valley, St. Pierre Valley and its tributaries, and Grand Banks Valley to the west.

Failure has been shown to have involved mostly muds, with an estimated content of 30% gravel, sand and coarse silt (Piper et al., 1999a). The turbidity current is known to contain about 10 km^3 ($1 \times 10^{10} \text{ m}^3$) of mud (fine silt and clay). Taking the observed volume of evacuated sediment during initial failure of 46.4 km^3 (with 70% being mud), it

is suggested that a lot of this mud was not deposited on the Sohm Abyssal Plain but it was transported by ocean currents. Transport would have been in two directions: mud in suspension on the slope and upper rise would have been transported westward by the Labrador Current and any mud that made it to depths of the lower rise and Abyssal Plain would have been transported westward by the Western Boundary Undercurrent. In addition, if the turbidity current consisted of so little mud (10 km^3), had such a large total volume of sediment (175 km^3), and with so little amount of available coarse sediments from the slope, this further suggests that the most of the coarse sediment that comprises the deposit was derived from the valley floors through erosion, as suggested by Piper et al. (1988).

5.10 Implications for tsunami modelling

Failure thickness and volumes estimates from this study will allow for better numerical modelling of landslide-generated tsunamis, particularly for studies currently being conducted in this area and waiting further data (e.g. Fine et al., 2005). The total amount of sediment involved in initial failure from the 1929 event has been calculated at 93.5 km^3 . The size of the study area is about 2000 km^2 and the entire region (see Figure 5.3) is about 9000 km^2 . Fine et al. (2005) estimated the entire region thought to be affected by the earthquake-induced ground accelerations to be $20,000 \text{ km}^2$, a little more than twice the size of the region estimated to have been affected by failure from this study (9000 km^2).

A note of caution is advised as these volume estimates, although based on all available data, are from 2D and bathymetry data. Through acquisition of 3D and swath bathymetric data, volume estimates would be more accurate.

5.11 Comparisons with other similar failure complexes

5.11.1 Eastern Canadian Margin with emphasis on the Scotian Slope

Quaternary failures on the eastern Canadian margin are numerous and widespread, extending from the upper slope down to the rise (e.g. Mosher et al., 1994; Mulder et al., 1997; Piper et al., 1999b). Failure types are relatively easy to categorize in terms of geophysical character and range from slides to debris flows (Mosher et al, 2004). The cause of these failures, however, is often disputed and more often speculated. It is the unique circumstance to know the cause of failure on St. Pierre Slope: ground accelerations due to seismic activity. Most of the observed failure complexes on the eastern Canadian margin occurred before modern record keeping and invention of appropriate detection instruments. A clear cause of most failures on the margin is unknown but has been speculated to have been caused by one or a combination of the following mechanisms: high sedimentation rates during deglaciation (thus sediment overloading at glaciated margins), seismic activity, excess pore pressures, and in the isolated case of Makkovik Bank, boulder dumps (ice-rafted boulders) (Table 5.3).

Debris flows are by and far the most well represented class of MTDs on the Scotian margin (Table 5.3), a characteristic shared with the St. Pierre Slope, where mass flow deposits (Class II) comprise the majority of failure observed, both volumetrically and areally. Gradients at the source area for debris flows along the margin compare well to the same criteria from the St. Pierre Slope (Table 5.3). Triggering mechanisms for debris flows along the Scotian margin are unknown and in the absence of slides or debris flows are attributed to seismic activity or sediment overloading. In areas where slides and slumps accompany debris flows, it is thought that progressive loss of sediment cohesion

during initial failure of sediment transforms into debris flows, a situation very similar to failure on the St. Pierre Slope. Two particular areas, SE of Grand Banks (Titanic Area, Savoye et al., 1990) and the Labrador Slope (e.g. Hesse et al., 2001), show this type of failure scenario: slide and slumps with mass flows located immediately downslope and resting on a lesser gradient than the upslope slides and slumps.

5.11.2 European and Mediterranean Margins

No in depth comparison has been made here, but a brief mention of a well known failure is warranted. The Storegga Slide, one of the world's largest submarine slides (e.g. Bunz, 2004; Jung, 2003), is speculated as being caused by earthquakes together with the release of gas hydrates. Pockmarks, identified by bathymetry and acoustic seafloor images, are present near and in the failure area, just as they are on the St. Pierre Slope. Also, areas that lack evidence of gas (from core and absence of pockmarks) remain stable, similar areas on the St. Pierre Slope have been identified. Further study of the St. Pierre Slope regarding gas hydrates would likely show striking similarities between these two massive submarine MTD complexes. Studies of this nature are current and ongoing for the Storegga Slide.

Haflidason et al. (2004) estimated that the minimum volume of sediments displaced was 2400 km³ and the maximum was 3200 km³ for the Storegga Slide. This is of a much larger magnitude than the Grand Banks slide as discovered in this study, approximately 10-14 fold. The headscarp extends about 290 km, commonly is 30-50 m in height but that can reach 120 meters. Altogether, the slide complex is vast but the

Geographic Location	Environment	Gradient source : run out	Type of Failure	Cause or Contributory Conditions	Sources
<i>St. Pierre Slope, offshore Newfoundland</i>	<i>continental slope</i>	<i>2- >20° : 2- 10°</i>	<i>retrogressive rotational slumps and debris flows</i>	<i>Ground accelerations related to the 1929 Grand Banks earthquake</i>	<i>Piper et al. (1999); Hughes Clarke et al. (1989); Piper et al. (1988); Piper and Aksu (1987); Piper et al. (1985);</i>
West Scotian Rise	upper continental rise	~1° : ~1°	slide, MTDs	Unknown	Piper (2001); Hughes Clarke et al. (1992)
West Scotian Slope	upper continental slope	5°- 10° : 3°	slumping, slides and debris flows	Unknown; likely high sedimentation rates (rapid loading)	Hill and Bowen (1983)
Albatross Area, Central Scotian Slope	continental slope and rise	~4° : <1°	Initial failure unknown, created debris flows	Unknown; possibly seismic activity and or ice loading/bearing capacity failure	Piper (2001); Gauley (2001); Piper and Skene (1998); Mulder et al. (1997)
Mohican Channel, Central Scotian Slope	continental slope and rise	~5° : ~2.5°	debris flows	Unknown	Mulder et al. (1997); McCall (unpublished)
East of Mohican Channel, Central Scotian Slope	continental slope and rise	~5° : ~2.5°	retrogressive, rotational slumps and debris flows	Unknown	Unpublished seismic data
Mohican Channel area, Central Scotian Slope	middle and lower continental rise	~2.5° : ~2.5°	debris flows	Unknown	Swift (1985)
Verrill Canyon area, Central Scotian Slope	continental slope and upper rise	~5° : ~2.5°	retrogressive rotational slumps, debris flows, turbidity currents	Unknown; possibly seismic activity, also excess pore pressures from shallow gas and/or high sediment- ation rates during deglaciation	Mulder and Moran (1995); Mosher et al. (1994); Baltzer et al. (1994); Mosher (1987); Piper et al. (1985)
Scotian Rise, South of Western, Emerald and Sable Island Banks	continental rise	~2.5° : ~2.5°	debris flows, rotational slumps	Unknown; possibly excess pore pressures due to shallow gas (sublimation of gas hydrate)	Piper et al. (1999); McCall (unpublished)

Table 5.3- Characteristics of MTDs documented on the eastern Canadian margin. Compare and contrast to MTDs from St. Pierre Slope.

Geographic Location	Environment	Gradient source : run out	Type of Failure	Cause or Contributory Conditions	Sources
Central Scotian Slope	continental slope		MTDs	Unknown	McCall (unpublished)
East Scotian Rise, South of Banquereau	continental rise	~2.5° : ~2.5°	debris flows	Unknown; possibly excess pore pressure due to shallow gas (sublimation of gas hydrate)	Piper et al. (1999)
East Scotian Rise	continental rise	~2.5° : ~2.5°	debris flow	Unknown	Piper (1991)
Southeast of Grand Banks, Newfoundland (Titanic Area)	continental rise with valleys	~10° : ~1°	slide followed slumps, debris flows, turbidity currents	Unknown	Savoie et al. (1990); Cochonat et al. (1989); Cochonat and Ollier (1987)
Offshore Grand Banks and Flemish Cap area	continental slope	?	debris flows and slumps	Unknown	McCall (unpublished)
Flemish Pass, East of Newfoundland	continental slope	~2° : ~2.0°	debris flows	Unknown; possibly seismic activity and or excess pore pressures	Campbell (2002)
Western flank of Flemish Cap	continental slope	?	debris flows	Unknown	McCall (unpublished)
Orphan Basin	continental slope and rise	~1.5° : ?	mostly debris flows	Unknown	McCall (unpublished)
Orphan Basin	continental slope and rise	~1.5° : ?	MTDs	Unknown	McCall (unpublished)
Orphan Basin	continental slope	~1.5° : ~0.6°	debris flows	Unknown; possibly sediment over- loading from high sedimentation rates at the margin during deglaciation	Hiscott and Aksu (1996); Aksu and Hiscott (1992)

Table 5.3- continued.

Geographic Location	Environment	Gradient source : run out	Type of Failure	Cause or Contributory Conditions	Sources
Orphan Basin	continental slope	~1.5° : ?	MTDs	Unknown	McCall (unpublished)
SE flank of Orphan Knoll	continental rise		MTDs	Seismic activity	Toews and Piper (2002)
Labrador Slope seaward of Makkovik Bank	continental slope	~20° : ~8°	slumps and debris flow	Unknown; interpreted as impact by ice-rafted boulders (boulder dumps)	Josenhans et al. (1986)
Labrador Slope	continental slope	~2° : ~1°	slides, slumps, and debris flows	Slides and slumps? high sediment- ation rates on slope; debris flows due to progressive loss of cohesion in material of some slump and slide masses	Hesse et al. (2001); Hesse (1995)
Southern Labrador Slope and rise	continental slope and rise	~2.0° : ?	debris flows	Unknown	McCall (unpublished)
Baffin Bay	continental slope	~2.0° : ~0.2°	slides, MTDs	Unknown; possibly sediment over- loading from high sedimentation rates at the margin during deglaciation	Hiscott and Aksu (1994); Aksu and Hiscott (1989)

Table 5.3- continued.

mechanisms of failure are very comparable to that of the St. Pierre Slope.

CHAPTER 6

Conclusions

The character of the mass transport deposits from the 1929 Grand Banks earthquake and of the undisturbed stratigraphy on and around St. Pierre Slope has been studied in detail over 2000 km² and more generally over 9000 km² using Huntect DTS seismic reflection, sidescan sonar and core data.

The following conclusions have been drawn from the preceding chapters:

- 1) A stratigraphic framework has been established through correlation of Huntect DTS profiles and cores. Six key reflections, Q91-Q100, have been recognized and dated, and have been related to till tongues, failures and core sediments. Dates are as follows: Q91 ~29.2 ka and Q99 ~15.3 ka, with interpolated ages for reflections Q93 of 26.3 ka, Q95 ~23 ka and Q97 ~20.5 ka.
- 2) Sediments on the upper slope are ice margin muds with minor sands from the Younger Dryas, on the middle slope are plume fallout muds, and on the lower slope and rise are dominated by turbidite deposition.
- 3) A radiocarbon date of 30 ka from core 90015-07 taken from a ~56-metre-deep failure plane together with an age of reflection Q99 of ~15.3 ka allow for the extrapolation of a sedimentation rate of a fairly thick subsurface portion of the seabed at 3.15 m kyr⁻¹, which was likely influenced by turbidite deposition.
- 4) On the upper slope, till tongues document advance and retreat of the ice margin. Key reflections correlated to these till tongues provide approximate ages for these events: 30 ka for maximum downslope extent of till tongue II (TTII) and a total

retreat of the ice margin front at 26 ka lasting until the Last Glacial Maximum, represented by TTI, at 21 ka. By 11.8 ka, ice margin sedimentation had ceased on the slope, replaced by a drape of mud, silt and occasional sand layers.

- 5) Sediments from cores document sediment sources from the Gulf of St. Lawrence and the Avalon Peninsula delivered to the slope via Laurentian, Halibut and Haddock Channels from processes related to glaciation. The different sources are distinguished by the characteristic colour of muddy sediment.
- 6) Sedimentation rates on the slope in water depths of 1650 m have been calculated at 3.15 m kyr^{-1} . These high rates are influenced by the rapid deposition of turbidites, known elsewhere to accumulate as rapidly as 10 m kyr^{-1} . Intermittent periods of low and high sedimentation rates in shallower water as documented by gray and brown mud respectively, suggest decreased meltwater out of Haddock Channel and periods of major pulses of deglacial meltwater out of Halibut Channel. During the late Pleistocene, sedimentation rates on the upper slope may have exceeded 3 m kyr^{-1} , due to increased sand deposition during the Younger Dryas and from meltwater influxes from ice on St. Pierre Bank. Sedimentation rates on the upper slope during the Holocene are quite low, about 0.07 m kyr^{-1} .
- 7) Reddish-brown muds of Facies E are thickest on the rise due to downslope flow of turbidity currents, and in places are interrupted by thin mud beds of facies A suggesting periods of non-turbidite deposition. The presence of similar reddish-brown mud on the middle slope is credited to plume fallout from subglacial meltwater out of Laurentian Channel, as it is structureless.

- 8) Four types of surficial MTDs based on seismic criteria are identified on the St. Pierre Slope: the most abundant are mass flows, followed by slumps, glides and creep deformation. The majority of mass flows, glides, and creep are found on gentle slopes of $<5^\circ$. Blocky mass flows and slumps are found primarily near or on valley headwalls and sidewalls where gradients surpass 5° . In most cases, as gradient increases so too does subsurface depth of the basal failure plane.
- 9) Smooth mass flows, wherever found directly downslope of slumps, are the direct consequence of disintegration of sediment blocks from slumps. A glide block (Figures 3.14 and 3.16) may mark the transition from undisturbed stratigraphy to mass flow failure.
- 10) Widespread mass flow failure along the orange reflection (Q99) (which corresponds to sandy mud beds) documents a probable link between sandy mud beds, earthquake induced ground accelerations and failure.
- 11) The total volume of sediment involved in initial failure in the 1929 earthquake has been calculated at 93.5 km^3 : 47.1 km^3 remaining on the slope as MTDs and 46.4 km^3 of sediment evacuated from the slope and contributing to the 1929 turbidite. The estimated volume of 175 km^3 of the turbidite together with the 47.1 km^3 of MTDs on the slope, suggests that about 225 km^3 of sediment was eroded and displaced during the 1929 event.
- 12) Comparison of information on MTDs derived from cores and from high-resolution seismic-reflection profiles shows an inherent variability between instruments that sample mesoscale (core) to macroscale (seismic reflection), not only in size of the sample but in relating the two samples spatially.

13) Applications of this study to specific sectors include, but are not limited to, the following:

- a. **Geological**- provides information for understanding the relationship between failure dynamics and gradients.
- b. **Public safety**- volume estimates can be used in failure and tsunami modeling. Also, known variables from this study can be compared to other similar margins to assess the possibility of future failure (applies to c and d also).
- c. **Petroleum Industry**- interpretations and data can be used in combination with other data (e.g. engineering) to determine the risk associated with drilling into the subsurface sediments.
- d. **Telecommunication Industry**- future risk evaluation for submarine cables on the eastern Canadian margin.

14) Throughout the thesis, all surface failures mentioned are assumed to be wholly attributed to occurring during and immediately after the 1929 event and including up to the present day based on the following:

- a. It is believed that instantaneous deep-sea cable breaks occurred in response to widespread sediment failure within 100km of the earthquake epicentre.
- b. Failed sediments subsequently evolved into a turbidity current that broke more cables as the current traveled downslope, finally depositing its load on the Sohmi Abyssal Plain.

- c. Cores that penetrate failure deposits show no evidence of major biological recolonization and bioturbation. This is further supported by pictures from Pisces IV dive #1643 (Hughes Clarke et al., 1989) over a Class I slump deposit (Figures 3.8 and 4.9) showing a 'fresh', uninhabited surface. It is possible that some of these 'fresh' surfaces represent 'readjustment' of failure blocks as sediment failure continued years after the 1929 event, in isolated instances.
- d. Virtually no shallow buried failures are documented on the slope between reflections Q100 and Q91. A few are seen below reflection Q91 (see Figure 3.11) but their extent is localized. This suggests that major failure events were rare in the study area during the Quaternary period, thus large failure events before 1929 appear unlikely.

It is apparent from this study that *local gradient changes* (thus a diverse, complex topographic terrain) play an essential role in failure development and evolution. Along with this is the *type of sediment* that is being disturbed, i.e. thin sandy mud beds that appear to provide a preferential 'weak zone' for which sediment packages fail along; these thin beds essentially become basal failure planes.

Areas on the Scotian Slope (e.g. Mosher et al. 1994) and Labrador Slope (e.g. Hesse et al. 2001) have been subjected to similar failure mechanisms (slumps, debris flows), but source area and run out gradients are of a lesser magnitude, $\sim 2\text{-}5^\circ$ and $\sim 1\text{-}3^\circ$ respectively. In contrast, on the St. Pierre Slope, failure complexity is related to, and thus exemplified by, topographic complexity.

REFERENCES

- Aksu, A.E. and Hiscott, R.N., 1989. Slides and debris flows on the high-latitude continental slopes of Baffin Bay. *Geology*, v. 17, p. 885-888.
- Aksu, A.E. and Hiscott, R.N., 1992. Shingled Upper Quaternary debris flow lenses on the NE Newfoundland slope. *Sedimentology*, v. 39, p. 193-206.
- Andrews, J.T., Tedesco, K. and Jennings, A.E., 1993. Heinrich events: Chronology and processes, east-central Laurentide Ice Sheet and NW Labrador Sea. In: W.R. Peltier, ed., *Ice in the Climate System*. Springer-Verlag, Berlin Heidelberg, p. 167-186.
- Ascoli, P., 1976. Foraminiferal and ostracod biostratigraphy of the Mesozoic-Cenozoic, Scotian Shelf, Atlantic Canada. *Maritime Sediments Special Publication*, no. 1, p. 653-771.
- Atkinson, G.M., 1985. Seismic liquefaction probability for Canadian offshore regions. *Canadian Journal of Civil Engineering*, 12, p.920-926.
- Balter, A., Cochonat, P. and Piper, D.J.W., 1994. In situ geotechnical characterization of sediments on the Scotian Slope, eastern Canadian continental margin. *Marine Geology*, v. 120, p. 291-308.
- Barss, M.S., Bujak, J.P. and Williams, G.L., 1979. Palynological zonation and correlation of sixty-seven wells, eastern Canada. *Geological Survey of Canada, Paper 78-24*, 188p.
- Bond, G.C. and Lotti, R., 1995. Iceberg discharges into the North Atlantic on millennial time scales during the last glaciation. *Science*, v. 267, p. 1005-1010.
- Bonifay, D. and Piper, D.J.W., 1988. Probable Late Wisconsinan ice margin on the upper continental slope off St. Pierre Bank, eastern Canada. *Canadian Journal of Earth Sciences*, 25, p. 853-865.
- Boulanger, E., 2000. Comportement cyclique des sediments de la marge continentale de La riviere Eel: une explication possible pour le peu de glissements sous-marin superficiels dans cete region. M.Sc. thesis, Department of Geology and Geological Engineering, Laval University, Sainte Foy, Quebec.
- Buckley, D.E., MacKinnon, W.G., Cransto, R.E. and Christian, H.A., 1994. Problems with piston core sampling: Mechanical and geochemical diagnosis. *Marine Geology*, v. 117, p. 95-106.
- Campbell, D.C., 2000. Relationship of sediment properties to failure horizons for a small area of the Scotian Slope. *Current Research 2000D*, Geological Survey of Canada, 9p.
- Coakley, J.P. and Syvitski, J.P.M., 1991. SediGraph technique. In: J.P.M. Syvitski, (ed), *Principles, Methods, and Application of Particle Size Analysis*, Cambridge University Press, p. 129-142.
- Cochonat, P. and Ollier, G., 1987. Geological interpretation of images "SAR": Towed Acoustic system. Data of the Titanic operation.
- Cochonat, P., Ollier G. and Michel J.-L., 1989. Evidence for slope instability and current-induced sediment transport: the R.M.S. Titanic wreck search area, Newfoundland Rise. *Geo-Marine Letters*, v. 9, p. 145-152.
- Christian, H., Piper, D.J.W. and Armstrong, R., 1991. Geotechnical properties of seabed

- sediments from Flemish Pass. *Deep Sea Research*, 38, p. 663-676.
- de Vernal, A. and Hillaire-Marcel, C., 1987. Paleoenvironments along the Laurentide Ice Sheet margin and timing of the last ice maximum and retreat. *Géographie Physique et Quaternaire*, v. 4, p. 265-278.
- de Vernal, A., Hillaire-Marel, C. and Bilodeau, G., 1996. Reduced meltwater outflow from the Laurentide ice margin during the Young Dryas, *Nature*, v. 381, p. 774-777.
- Dewey, J.W. and Gordon, D.W., 1984. Map Showing Recomputed Hypocenters of Earthquakes in the Eastern and Central United States and Adjacent Canada, 1925-1980, U.S. Geological Survey Misc. Field Studies, Map MF-1699.
- Doxsee, W.W., 1948. The Grand Banks Earthquake of November 18, 1929. Publications of the Dominion Observatory, Canada Department of Mines and Technical Surveys, Ottawa, Ontario, v. 7, no. 7, p. 323-335.
- Embley, R.W., 1976. New evidence for occurrence of debris flow deposits in the deep sea, *Geology*, v. 4, p. 371-374.
- Fader, G.B., King, E., Gillespie, R. and King, L.H., 1988. Surficial geology of Georges Bank, Browns Bank, and the southeastern Gulf of Maine. Geological Survey of Canada, 2p.
- Fader, G.B., King, L.H. and Josenhans, H.W., 1982. Surficial geology of the Laurentian Channel and the western Grand Banks of Newfoundland. Geological Survey of Canada, Paper 81-22, 37p and map.
- Fader, G.B., King, L.H. and MacLean, B., 1977. Surficial geology of the eastern Gulf of Maine and Bay of Fundy. Marine Sciences, Paper 19. Geological Survey of Canada, Paper 76-17, 23p.
- Fine, I.V., Rabinovich, A.B., Bornhold, B.D., Thomson, R.E. and Kulikov, E.A., 2005. The Grand Banks landslide-generated tsunami of November 18, 1929: preliminary analysis and numerical modeling. *Marine Geology*, v. 215, no. 1-2, p. 45-57.
- Fruth, L.S. 1965. The 1929 Grand Banks turbidite and the sediments of the Sohm Abyssal Plain. M.Sc. thesis, Columbia University, New York City, New York, 257p.
- Gauley, B.J.L., 2001. Lithostratigraphy and sediment failure on the central Scotian Slope. M.Sc. thesis, Dalhousie University, Halifax, Nova Scotia, 214 p.
- Grant, A.C., McAlpine, K.D. and Wade, J.A., 1986. The continental margin of eastern Canada: Geological framework and petroleum potential. In: M.T. Halbouty (ed), *Future Petroleum Provinces of the World*, American Association of Petroleum Geologists, Memoir 40, p. 177-205.
- Given, M.M., 1977. Mesozoic and Cenozoic geology of offshore Nova Scotia. *Bulletin of Canadian Petroleum Geology*, 25, p. 63-91.
- Hampton, M.A., 1972. The role of subaqueous debris flow in generating turbidity currents. *Journal of Sedimentary Research*, v. 42, no. 4, p. 775-793.
- Hesse, R., 1995. Continental slope and basin sedimentation adjacent to an ice-margin: a continuous sleeve gun profile across the Labrador slope, rise and basin. In: Pickering, K.T., Ricci Lucchi, F., Smith, R.D.A., Kenyon, N.H. and Hiscott, R.N. (eds), *Atlas of Deep Water Environments*. Chapman and Hall, p. 14-17.

- Hesse, R., Klaucke, I., Khodabakhsh, S., Ryan, W.B.F., Piper, D.J.W. and the NAMOC Study Group, 2001. Sandy submarine braid plains: potential deep-water reservoirs in subpolar settings. *American Association of Petroleum Geologists Bulletin*, v. 85, p. 1499-1521.
- Heezen, B.C. and Drake, C.L., 1964. Grand Banks slump. *Geological Society of America, Bulletin*, v. 48, no. 2, p. 221-225.
- Heezen, B.C. and Ewing, M., 1952. Turbidity currents and submarine slumps and the 1929 Grand Banks earthquake. *American Journal of Science*, 250, p. 849-873.
- Hill, P.R. and Bowen A.J., 1983. Modern sediment dynamics at the shelf slope boundary off Nova Scotia. In: Stanley, D.J. & Moore, G.T. (eds), *The Shelfbreak. Critical Interface on Continental Margins*. Society of Economic Palaeontologists & Mineralogists Special Publication, no. 33, p. 265-276.
- Hiscott, R.N. and Aksu, A.E., 1994. Submarine debris flows and continental slope evolution in front of Quaternary ice sheets, Baffin Bay, Canadian Arctic. *Bulletin of American Association of Petroleum Geology*, v. 78, p. 445-460.
- Hiscott, R.N. and Aksu, A.E., 1996. Quaternary sedimentary processes and budgets in Orphan Basin, southwestern Labrador Sea. *Quaternary Research*, v. 45, p. 160-175.
- Howie, R.D. and Barss, M.S., 1975. Upper Paleozoic rocks of the Atlantic Provinces, Gulf of St. Lawrence and adjacent continental shelf. In: W.J.M. van der Linden and J.A. Wade (eds), *Offshore geology of eastern Canada*, Geological Survey of Canada, Paper 74-30, 28p.
- Hughes Clarke, J.E., 1988. The geological record of the 1929 'Grand Banks' earthquake and its relevance to deep-sea clastic sedimentation. Ph.D. thesis, Dalhousie University, Halifax, Nova Scotia.
- Hughes Clarke, J.E., 1990. Late stage slope failure in the wake of the 1929 Grand Banks earthquake. *Geo-Marine Letters*, 10, p. 69-80.
- Hughes Clarke, J.E., Mayer, L.A., Piper, D.J.W. and Shor, A.N., 1989. Pisces IV submersible operations in the epicentral region of the 1929 Grand Banks earthquake. Geological Survey of Canada, Paper 88-20, 12p.
- Hughes Clarke, J.E., Shor, A.N., Piper, D.J.W. and Mayer, L.A., 1990. Large-scale current-induced erosion and deposition in the path of the 1929 Grand Banks turbidity current. *Sedimentology*, 37, p. 613-629.
- Hundert, T., 2003. Western Scotian Slope stratigraphy: insights into late Quaternary deglaciation of the western Scotian Shelf, eastern Canada. MSc thesis, Dalhousie University, 154p.
- Jansa, L.F. and Wade, J.A., 1975. Geology of the continental margin off Nova Scotia and Newfoundland. In: W.J.M. van der Linden and J.A. Wade (eds), *Offshore geology of eastern Canada*, Regional Geology, Geological Survey of Canada, Paper 74-30, 56p.
- Josenhans, W.H. and Lehman, S., 1999. Late Glacial stratigraphy and history of the Gulf of St. Lawrence, Canada. *Canadian Journal of Earth Science*, v. 36, p. 1327-1345.
- Josenhans, W.H., Klassen R.A. and Zevenhuizen, J., 1986. Quaternary geology of the Labrador Shelf. *Canadian Journal of Earth Sciences*, v. 23, p. 1190-1213.
- Keppie, J.D., 1989. Northern Appalachian terranes and their accretionary history. *Geological Society of America, Special Paper 230*, p. 159-192.

- King, L.M., 1970. Surficial geology of the Halifax-Sable Island map area. *Maritime Science*, Paper, no. 1, 16p.
- King, L. H. and Fader, G. B. J., 1986. Wisconsinan glaciation of the southeastern Canadian Continental Shelf. *Geological Survey of Canada Bulletin* 363.
- King, L.H., Fader, G.B., Poole, W.H. and Wantess, R.K., 1985. Geological setting and age of the Flemish Cap granodiarite, east of the Grand Banks of Newfoundland. *Canadian Journal of Earth Science*, v. 22, p. 1286-1298.
- Kokusho, T., 1999. Formation of water film in liquefied sand and its effect on lateral spread. *Journal of Geotechnical and Geoenvironmental Engineering*. American Society of Civil Engineers, vol. 125, no.10, p.817-826.
- Kosalos, J.G. and Chayes, D.N., 1983. A portable system for ocean bottom imaging and charting: *Proceedings Oceans '83* (Los Angeles), p. 649-656.
- Kvalstad, T.J., Gauer, P., Kayina, A.M., Nadim, F. and Bryn, P., 2002. Slope stability at Ormen Lange. In: *Offshore Site Investigation and Geotechnics*, *Proceedings of an International Conference held in London, UK*, Society for Underwater Technology, p. 233-250.
- Lee, S.H. and Chough, S.K., 2001. High-resolution (2–7 kHz) acoustic and geometric characters of submarine creep deposits in the South Korea Plateau, East Sea. *Sedimentology*, v. 48, p. 629–644.
- Lee, S.H., Chough, S.K., Back, G.G. and Kim, Y.B., 2002. Chirp (2-7-kHz) echo characters of the South Korea Plateau, East Sea: styles of mass movement and sediment gravity flow. *Marine Geology*, v. 184, no. 3, p. 227-247.
- Locat, J. and Lee, H.J., 2002. Submarine landslides: advances and challenges. *Canadian Geotechnical Journal*, 39, p. 193-212.
- Locat, J., Martin, F., Locat, P., Leroueil, S., Levesque, C., Konrad, J.-M., Urgeles, R., Canals, M. and Duchesne, M.J., 2003. Submarine mass movements in the Upper Saguenay Fjord, (Quebec, Canada), triggered by the 1663 earthquake. In: J. Locat and J. Mienert (eds), *Submarine Mass Movements and Their Consequences*. Kluwer, Dordrecht, p. 509-519.
- Long, D., Stevenson, A.G., Wilson, C.K. and Bulat, J., 2003. Slope failures in the Faroe-Shetland channel. In: J. Locat and J. Mienert (eds), *Submarine Mass Movements and Their Consequences*. Kluwer, Dordrecht, p. 281-289.
- Lykousis, V., Sakellariou, D. and Roussakis, G., 2003. Prodelta slope stability and associated coastal hazards in tectonically active margins: Gulf of Corinth (NE Mediterranean). In: J. Locat and J. Mienert (eds), *Submarine Mass Movements and Their Consequences*. Kluwer, Dordrecht, p. 433-440.
- MacDonald, A.W., 2001. Late Cenozoic geological framework of St. Pierre Slope offshore eastern Canada. B.Sc. thesis, Saint Mary's University, Halifax, Nova Scotia.
- MacLean, B. and King, L.H., 1971. Surficial geology of the Banquereau and Misaine Bank map area. *Marine Sciences*, Paper 3. Geological Survey of Canada, Paper 71-52, 19p.
- MacLean, B.A. and Wade, J.A., 1992. Petroleum geology of the continental margin south of the islands of St. Pierre and Miquelon, offshore eastern Canada. *Bulletin of Canadian Petroleum Geology*, vol. 40, no. 3, p. 222-253.
- Marsters, J.C., 1986. Geotechnical analysis of sediments from the eastern Canadian

- continental slope, south of the St. Pierre Bank. M.Eng thesis, Technical University of Nova Scotia, Halifax, Nova Scotia.
- Masson, D.G., Canals, M., Alonso, B., Urgeles R., and Huhnerbach V., 1998. The Canary Debris flow: Source area morphology and failure mechanisms, *Sedimentology*, v. 45, p. 411-432.
- Masson, D.G., Gardner, J.V., Parson, L.M. and Field, M.E, 1985. Morphology of Upper Laurentian Fan using GLORIA long-range side-scan sonar. *AAPG Bulletin*, v. 69, no. 6, p. 950-959.
- Mayewski, P.A., Meeker, L.D., Whitlow, S., Twicker, M.S., Morrison, M.C., Alley, R.B., Bloomfield, P. and Taylor, K. 1993. The atmosphere during the Younger Dryas. *Science*, v. 262, p. 195-197.
- McCall, C., Morrison, M.L. and Piper, D.J.W., 2005. Geological data from the epicentral region of the 1929 Grand Banks earthquake. Geological Survey of Canada Open File 4879.
- McIver, N.L., 1972. Cenozoic and Mesozoic Stratigraphy of the Nova Scotia Shelf. *Canadian Journal of Earth Science*, 9, p. 54-70.
- Moore, J.G., Normark, W.R. and Holcomb, R.T., 1994. Giant Hawaiian landslides, *Annual Reviews of Earth and Planetary Sciences*, v. 22, p. 119-144.
- Moran, K., Keen, M.J., Piper, D.J.W. and Adams, J., 1990. Slope stability. In: M.J.Keen and G.L.Williams (eds), *Geology of the continental margin off eastern Canada*, Geological Survey of Canada, *Geology of Canada*, no. 2, p. 798-802.
- Moran, K. and Fader, G.B.J., 1997. Glacial and glaciomarine sedimentation: Halibut Channel, Grand Banks of Newfoundland. In: T.A. Davies et al., ed., *Glaciated Continental Margins, an Atlas of Acoustic Images*. Chapman and Hall, London, UK, p. 217-271.
- Morrison, M.L., 1998. Late Glacial-Holocene, St. Pierre Slope. Incomplete Ph.D. thesis, Memorial University of Newfoundland.
- Mosher, D.C. and Simpkin, P.G., 1999. Environmental Marine Geoscience 1. Status and trends of marine high-resolution seismic reflection profiling: data acquisition. *Geoscience Canada*, v. 26, p. 174-188.
- Mosher, D.C., Moran, K. and Hiscott, R.N., 1994. Late Quaternary sediment, sediment mass flow processes and slope stability on the Scotian Slope, Canada. *Sedimentology*, 41, p. 1039-1061.
- Mosher, D.C., Piper, D.J.W., Campbell, D.C. and Jenner, K.A., 2004. Near surface geology and sediment failure geohazards of the Scotian Slope. *American Association of Petroleum Geologists Bulletin* 88, p. 705-723.
- Mudie, P.J., Piper, D.J.W., Rideout, K., Robertson, K.R., Schafer, C.T., Vilks, G. and Hardy, I.A., 1984. Standard methods for collecting, describing and sampling Quaternary sediments at the Atlantic Geoscience Center. Geological Survey of Canada, Open File 1044.
- Mulder, T. and Cochonat, P., 1996. Classification of offshore mass movements. *Journal of Sedimentary Research*, v. 66, p. 43-57.
- Mulder, T. and Moran, K., 1995. Relationship among submarine instabilities, sea-level variations and the presence of an ice sheet on the continental shelf: an example from the Verrill Canyon area, Scotian Shelf. *Paleoceanography*, 10, p. 137-154.

- Mulder, T., Berry, J.A. and Piper, D.J.W., 1997. Links between geomorphology and geotechnical characteristics of large debris flow deposits in the Albatross area on the Scotian slope (eastern Canada). *Marine Georesources and Geotechnology*, v. 15, p. 253-281.
- Nardin, T.R., Hein, F.J., Gorsline, D.S. and Edwards, B.D., 1979. A review of mass movement processes, sediment and acoustic characteristics, and contrasts in slope and base-of-slope systems versus canyon-fan-basin systems. In: *Geology of Continental Slopes*. Edited by L.J. Doyle and O.H. Pilkey, Jr. Society of Economic Paleontologists and Mineralogists, Special Publication, p. 2761-2773.
- Pe-Piper, G., 2002. Progress report on Cretaceous rocks onshore Nova Scotia and their relevance to understanding sources, diagenesis and reservoir properties of Offshore sedimentary rocks. For: Petroleum Research Atlantic Canada (Project 02), 29p.
- Pe-Piper, G. and Jansa, L.F., 1999. Pre-Mesozoic basement rocks offshore Nova Scotia, Canada: new constraints on the origin and Paleozoic accretionary history of the Meguma Terrane. *Geological Society of America Bulletin*, 111, p. 1773-1791.
- Pe-Piper, G. and Loncarevic, B.D., 1989. Offshore continuation of Meguma Terrane, southwestern Nova Scotia. *Canadian Journal of Earth Sciences*, 26, p. 176-191.
- Piper, D.J.W., 1988. Glaciomarine sediments on the continental slope off eastern Canada. *Geoscience Canada*, 15, p. 23-28.
- Piper, D.J.W., 1991. Surficial geology and physical properties 6: deep-water surficial geology. In: *East Coast Basin Atlas Series: Scotian Shelf*; Atlantic Geoscience Center, Geological Survey of Canada, p. 121-122.
- Piper, D.J.W., 2001. The geological framework of sediment instability on the Scotian Slope: studies to 1999. Geological Survey of Canada, Open File 3920.
- Piper, D.J.W. and Aksu, A.E., 1987. The source and origin of the 1929 Grand Banks turbidity current inferred from sediment budgets. *Geo-Marine Letters*, v. 7, p. 177-182.
- Piper, D.J.W. and Fehr, S.D., 1991. Radiocarbon chronology of Late Quaternary sections on the inner and middle Scotian Shelf, south of Nova Scotia. In: *Current Research, Part E*, Geological Survey of Canada, Paper 91-1E, p. 321-325.
- Piper, D.J.W. and Hundert, T., 2002. Provenance of distal Sohm Abyssal Plain sediments: history of supply from the Wisconsinan glaciation in eastern Canada. *Geo-Marine Letters*, v. 22, no. 2, p. 75-85.
- Piper, D.J.W. and MacDonald, A.W., 2002. Timing and position of late Wisconsinan ice Margins on the upper slope seaward of Laurentian Channel. *Geographie Physique et Quaternaire*, 55, p. 131-150.
- Piper, D.J.W. and McCall, C.W., 2003. A synthesis of the distribution of submarine mass movements on the eastern Canadian margin. In: J. Locat and J. Mienert (eds), *Submarine Mass Movements and Their Consequences*. Kluwer, Dordrecht, p. 291-298.
- Piper, D.J.W. and Normark, W.R., 1989. Late Cenozoic sea-level changes and the onset of glaciation: impact on continental slope progradation off eastern Canada. *Marine and Petroleum Geology*, v. 6, p. 336-348.

- Piper, D.J.W. and Skene, K.I., 1998. Latest Pleistocene ice-rafting events on the Scotian Margin (eastern Canada) and their relationship to Heinrich events. *Paleoceanography*, v. 13, p. 205-214.
- Piper, D.J.W. and Slatt, R.M., 1977. Late Quaternary clay-mineral distribution on the eastern continental margin of Canada. *Geological Society of America Bulletin*, v. 88, no.2, p. 267-272.
- Piper, D.J.W., Cochonat, P. and Morrison, M.L., 1999a. The sequence of events around the epicenter of the 1929 Grand Banks earthquake: initiation of debris flows and turbidity current inferred from sidescan sonar. *Sedimentology*, 46, p. 79-97.
- Piper, D.J.W., MacDonald, A., Ingram, S., Williams G.L. and McCall, C.W., 2005. Late Cenozoic architecture of the St. Pierre Slope. *Canadian Journal of Earth Science*, v. 42, no. 11, p. 1987-2000.
- Piper, D.J.W., Mosher, D.C., Gauley, B.J., Jenner, K. and Campbell, D.C., 2003. The chronology and recurrence of submarine mass movements on the continental slope off southeastern Canada. In: J. Locat and J. Mienert (eds), *Submarine Mass Movements and Their Consequences*. Kluwer, Dordrecht, p. 299-306.
- Piper, D.J.W., Shor, A.N., Farre, J.A., O'Connell, S. and Jacobi, R. 1985. Sediment slides around the epicenter of the 1929 Grand Banks earthquake. *Geology*, 13, p. 538-541.
- Piper, D.J.W., Shor, A.N. and Hughes Clarke, J.E., 1988. The 1929 "Grand Banks" earthquake: slump and turbidity current. *Geological Society of America, Special Paper on Catastrophic Events in Geology*, no. 229, p. 77-92.
- Piper, D.J.W., Skene, K.I. and Morash, N., 1999b. History of major debris flows on the Scotian Rise, offshore Nova Scotia. *Current Research 1999-E*, p. 203-212.
- Piper, D.J.W., Stow, D.A.V.A.V., and Normark, W.R., 1984. The Laurentian Fan; Sohm abyssal plain. *Geo-Marine Letters*, v. 3, no. 2-4, p. 141- 146.
- Savoye, B., Cochonat, P. and Piper, D.J.W., 1990. Seismic evidence for a complex slide near the wreck of the Titanic: Model of an instability corridor for non-channelled gravity events. *Marine Geology*, v. 91, p. 281-298.
- Skene, K.I. and Piper, D.J.W., 2003. Late Quaternary stratigraphy of Laurentian Fan: a record of events off the eastern Canadian continental margin during the last deglacial period. *Quaternary International*, v. 99-100, p. 135-152.
- Skinner, L. and McCave, I.N., 2003. Analysis and modeling of gravity- and piston coring based on soil mechanics. *Marine Geology*, v. 199, p. 181-204.
- Stuiver M., Reimer, P.J., Bard, E., Beck, J.W., Burr, G.S., Hughen, K.A., Kromer, B., McCormac, G., van der Plicht, J. and Spurk, M., 1998. *INTCAL98 Radiocarbon Age Calibration, 24000-0 cal BP Radiocarbon*, v. 40, no. 3, p. 1041-1083.
- Smith, P.C. and F.B. Schwing., 1991. Mean circulation and variability on the eastern Canadian continental shelf. *Continental Shelf Research*, v. 11, p. 977-1012.
- Swift, S. A. 1985. Late Pleistocene sedimentation on the continental slope and rise off western Nova Scotia. *Geological Society of America Bulletin* Year, v. 96, no. 7, p. 832-841.
- Syvitski, J.P.M, Burrell, D.C. and Skei, J.M., 1987. *Fjords: Processes and Products*, Springer Verlag, NY, 379p.

- Toews, M.W. and Piper D.J.W., 2002. Recurrence interval of seismically-triggered mass-transport deposition at Orphan Knoll, continental margin off Newfoundland and Labrador. Geological Survey of Canada, Current Research 2002-E17, 7p.
- Trincardi, F., Cattaneo, A., Correggiari, A., Mongardi, S., Breda, A. and Asioloi, A., 2003. Submarine slides during relative sea level rise: Two examples from the eastern Tyrrhenian margin. In: J. Locat and J. Mienert (eds), *Submarine Mass Movements and Their Consequences*. Kluwer, Dordrecht, p. 469-478.
- Tripsanas, E.K., Bryant, W.R., Prior, D.B. and Phaneuf, B.A., 2003. Interplay between salt activities and slope instabilities, Bryant Canyon area, Northwest Gulf of Mexico. In: J. Locat and J. Mienert (eds), *Submarine Mass Movements and Their Consequences*. Kluwer, Dordrecht, p. 307-316.
- Urgeles, R., Masson, D.G., Canals, M., Watts, A.B. and Le Bas, T., 1999. Recurrent large-scale landsliding on the west flank of La Palma, Canary Islands. *Journal of Geophysical Research*, v. 104, p. 25331-25348.
- Wade, J.A., 1990. The geology of the southeastern margin of Canada, Chapter 5, Part 1: The stratigraphy of Georges Bank Basin and relationships to the Scotian Basin. In: M.J. Keen and G.L. Williams (eds), *Geology of the continental margin of eastern Canada*, Geological Survey of Canada, *Geology of Canada*, no. 2, p. 169-190.
- Wade, J.A. and MacLean, B.C., 1990. The geology of the southeastern margin of Canada, Chapter 5, Part 2: Aspects of the geology of the Scotian Basin from recent seismic and well data. In: M.J. Keen and G.L. Williams (eds), *Geology of the continental margin of eastern Canada*, Geological Survey of Canada, *Geology of Canada*, no. 2, p. 190-238.
- Wade, J.A., Grant, A.C., Sanford, B.V. and Barss, M.S., 1977. Basement structure eastern Canada and adjacent areas. Geological Survey of Canada, Map 1400A, 4 sheets, Scale 1:2,000,000.

APPENDIX 1

This appendix shows the measured depth in milliseconds from the seafloor of the six defined reflections. Measurements were taken on paper copies of seismic reflection data at 1-10 minute intervals, depending on the morphology of the seabed: i.e. if the seabed was smooth for many kilometres, measurements were taken every 5-10 minutes, and if the seabed was highly irregular, measurements were taken every 1-2 minutes. Measurements were done by a ruler and subsequently converted into milliseconds using the 'sweep' rate obtained from the seismic reflection record.

Thicknesses of MTD acoustic facies at the surface, estimated total thickness failed and depth from sea-level to pre-failure seafloor have been included as well. The beginning and end of each MTD was recorded, and in most cases, two thickness measurements of the MTD were completed to provide a fairly good 2D estimate of the dimensions of the deposit.

Depth to the pre-failure seafloor is calculated as follows (described in detail in Chapter 2 (section 2.5)):

Here is an example from row 2 of Appendix 1.

Depth from sea-level to seafloor = 2134ms

Surface MTD thickness = 22.05 ms

Estimated total thickness failed = 70.56 ms

$$= 2134 + 22.05 - (70.56) = 2085.49 \text{ ms}$$

Seafloor character was noted and the following abbreviations apply:

1st Term denotes measured gradient:

F = flat seabed (0-2°); G = gentle seabed (>2-5°); S = steeper seabed (>5°)

2nd Term denotes if seabed is disturbed or undisturbed:

U = undisturbed seabed; D = disturbed seabed

3rd Term denotes surface expression of seabed:

s = smooth surface; u = undulating; h = hummocky to hyperbolic surface

4th Term denotes the type of acoustic facies encountered:

gl = glide; sl = slump; mf = mass flow; c = creep; sc = scar*;

sp = scarp*

* Class V

For example – G-D-h-sl = gentle sloping, disturbed seabed with a hummocky to hyperbolic surface expression that represents a slump deposit

Cruise #	Day/time (Huntec)	Day/time (Ship)	Latitude of ship (dec deg)	Longitude of ship (dec deg)	DTS (ms)	Depth from seafloor to reflections (ms)						Thickness of surface MTDs (ms)	Estimated total thickness failed (ms)	Depth to pre- failure seafloor from sea-level (ms)	Seafloor Character
						Q100	Q99	Q97	Q95	Q93	Q91				
2003033	1700111	1700110	44.6220	-55.8218	2200							0.00	71.05	2128.95	G-D-s-sp
2003033	1700116	1700115	44.6230	-55.8108	2134							22.05	70.56	2085.49	G-D-h-sl
2003033	1700120	1700119	44.6238	-55.8023	2092							44.10	71.05	2065.05	G-D-h-sl
2003033	1700122	1700121	44.6244	-55.7981	2096							44.10	69.58	2070.52	F-D-h-sl
2003033	1700124	1700123	44.6248	-55.7935	2085							46.55	70.56	2060.99	F-D-h-sl
2003033	1700128	1700127	44.6254	-55.7850	2074							52.92	71.54	2055.38	F-D-h-sl
2003033	1700130	1700129	44.6258	-55.7808	2088							27.00	69.58	2045.42	G-D-h-sl
2003033	1700131	1700130	44.6260	-55.7785	2110							8.33	68.56	2049.77	F-D-h-mf
2003033	1700134	1700133	44.6270	-55.7715	2128							14.70	69.58	2073.12	G-D-h-sl
2003033	1700136	1700135	44.6276	-55.7668	2115							24.50	68.12	2071.38	G-D-h-sl
2003033	1700140	1700139	44.6281	-55.7578	2118							27.00	68.12	2076.88	G-D-h-sl
2003033	1700141	1700140	44.6282	-55.7558	2138							0.00	51.00	2087.00	G-D-h-sl
2003033	1700146	1700145	44.6291	-55.7453	2092		0.00	10.78	24.00	41.65		0.00	12.74	2079.26	G-D-s-mf
2003033	1700148	1700147	44.6295	-55.7412	2063		11.27	22.54	35.77	53.41		7.84	9.80	2061.04	G-D-s-mf
2003033	1700152	1700151	44.6302	-55.7325	2042		13.23	24.00	37.24	56.35		9.80	7.84	2043.96	G-D-s-mf
2003033	1700156	1700155	44.6310	-55.7235	2077		7.84	16.17	30.70	50.00		7.84	12.74	2072.10	G-D-s-mf
2003033	1700158	1700157	44.6315	-55.7188	2074		14.70	22.05	35.77	56.35		14.70	9.80	2078.90	G-D-s-mf
2003033	1700200	1700159	44.6320	-55.7141	2081							0.00	8.82	2072.18	G-D-s-mf
2003033	1700210	1700209	44.6337	-55.6929	2130										G-D-s-mf
2003033	1700216	1700215	44.6352	-55.6798	2050			2.45	10.78	28.42		0.00	19.60	2030.40	G-D-s-mf
2003033	1700220	1700219	44.6362	-55.6712	2032		3.92	14.70	32.83	51.45		3.92	12.25	2023.67	G-D-s-mf
2003033	1700224	1700223	44.6368	-55.6627	2029		3.43	15.68	28.42	48.02		3.43	12.25	2020.18	G-D-s-mf
2003033	1700228	1700227	44.6377	-55.6541	2009		10.78	22.05	36.25	55.86		10.78	12.50	2007.28	G-D-s-mf
2003033	1700232	1700231	44.6382	-55.6453	2022		4.90	17.15	30.38	51.45		4.90	12.25	2014.65	G-D-s-mf
2003033	1700240	1700239	44.6393	-55.6276	2005		6.86	19.11	32.34	53.41		6.86	12.50	1999.36	G-D-s-mf
2003033	1700244	1700243	44.6400	-55.6185	2009		7.84	20.58	34.40	55.86		7.84	11.76	2005.08	G-D-s-mf
2003033	1700248	1700247	44.6404	-55.6093	2008		3.92	17.15	30.38	52.43		3.92	12.50	1999.42	G-D-s-mf
2003033	1700252	1700251	44.6409	-55.6001	2010		12.25	25.00	38.22	61.25		12.25	11.76	2010.49	G-D-s-mf
2003033	1700255	1700254	44.6414	-55.5939	2020		3.92	17.15	29.90	55.86		3.92	12.25	2011.67	G-D-s-mf
2003033	1700302	1700301	44.6425	-55.5790	2042		4.41	17.40	30.38	54.39		4.41	12.50	2033.91	G-D-s-mf
2003033	1700305	1700304	44.6429	-55.5727	2018		11.76	25.00	36.26	58.80		7.35	7.84	2017.51	G-D-s-mf
2003033	1700310	1700309	44.6434	-55.5620	2015		11.50	24.50		56.84		2.94	2.94	2015.00	G-D-s-mf
2003033	1700314	1700313	44.6442	-55.5531	2038		10.29	23.52		50.96		0.00	0.00	2038.00	G-D-s-mf

Cruise #	Day/time (Huntec)	Day/time (Ship)	Latitude of ship (dec deg)	Longitude of ship (dec deg)	DTS (ms)	Depth from seafloor to reflections (ms)						Thickness of surface MTDs (ms)	Estimated total thickness failed (ms)	Depth to pre- failure seafloor from sea-level (ms)	Seafloor Character
						Q100	Q99	Q97	Q95	Q93	Q91				
2003033	1700315	1700314	44.6442	-55.5509	2042	0.00	11.76	26.00		53.90					F-U-s
2003033	1700318	1700317	44.6446	-55.5442	2050	0.00	12.25	25.00		56.35					F-U-s
2003033	1700321	1700320	44.6451	-55.5374	2055		11.76	24.50		61.25		0.00	0.00	2055.00	G-D-s-mf
2003033	1700323	1700322	44.6454	-55.5329	2070		12.00	25.00		50.47		4.41	4.41	2070.00	G-D-s-mf
2003033	1700324	1700323	44.6455	-55.5306	2069		11.76	22.54		49.49		0.00	0.00	2069.00	G-D-s-mf
2003033	1700330	1700329	44.6463	-55.5172	2044	0.00	11.76	24.50		50.47					F-U-s
2003033	1700335	1700334	44.6471	-55.5057	2032	0.00	10.78	24.00		50.72					F-U-s
2003033	1700340	1700339	44.6479	-55.4945	2033	0.00	11.76	25.97		57.33					F-U-s
2003033	1700345	1700344	44.6484	-55.4835	2063	0.00	11.76	26.00		56.35					F-U-s
2003033	1700350	1700349	44.6492	-55.4728	2088	0.00	10.29	25.48		51.94					F-U-s
2003033	1700354	1700353	44.6499	-55.4638	2080	0.00	9.80	23.52		58.80					F-U-s
2003033	1700613	1700612	44.6364	-55.4581	2285	0.00	12.72			63.70	83.30				G-U-s
2003033	1700615	1700614	44.6346	-55.4618	2215	0.00	10.29			53.90	71.05				G-U-s
2003033	1700620	1700619	44.6300	-55.4692	2212	0.00	9.80			58.80	73.97				G-U-s
2003033	1700624	1700623	44.6261	-55.4753	2186	0.00	10.00			59.00	74.48				G-U-s
2003033	1700630	1700629	44.6199	-55.4853	2281	0.00	11.76			61.25	77.91				G-U-s
2003033	1700635	1700634	44.6147	-55.4937	2268	0.00	11.27			64.68	82.81				G-U-s
2003033	1700640	1700639	44.6089	-55.5027	2295	0.00	12.74			83.79					G-U-s
2003033	1700645	1700644	44.6037	-55.5112	2320		7.35			57.82		0.00	0.00	2320.00	G-D-s-mf
2003033	1700648	1700647	44.6009	-55.5151	2330		8.82			61.25		8.82	13.23	2325.59	G-D-s-mf
2003033	1700652	1700651	44.5943	-55.5131	2372		2.45			54.88		2.45	13.50	2360.95	G-D-s-mf
2003033	1700656	1700655	44.5922	-55.5050	2393		1.47			55.37		0.00	13.23	2379.77	G-D-s-mf
2003033	1700657	1700656	44.5920	-55.5031	2393	0.00	11.27			66.15					F-U-s
2003033	1700701	1700700	44.5919	-55.4956	2380	0.00	11.27			65.17					F-U-s
2003033	1700705	1700704	44.5916	-55.4882	2387	0.00	11.27			73.50					F-U-s
2003033	1700710	1700709	44.5907	-55.4777	2415	0.00	12.25			75.95					F-U-s
2003033	1700715	1700714	44.5898	-55.4669	2409	0.00	11.00			77.42					F-U-s
2003033	1700716	1700715	44.5896	-55.4647	2417	0.00	11.00			77.42		0.00	0.00	2417.00	F-U-s
2003033	1700720	1700719	44.5889	-55.4562	2471					63.70		7.35	15.19	2463.16	F-D-s-mf
2003033	1700724	1700723	44.5881	-55.4479	2500							13.72	14.70	2499.02	F-D-s-mf
2003033	1700727	1700726	44.5876	-55.4418	2560							0.00	0.00	2560.00	F-D-s-mf
2003033	1700728	1700727	44.5874	-55.4399	2580							0.00	0.00	2580.00	F-D-s-mf

Cruise #	Day/time (Huntec)	Day/time (Ship)	Latitude of ship (dec deg)	Longitude of ship (dec deg)	DTS (ms)	Depth from seafloor to reflections (ms)						Thickness of surface MTDs (ms)	Estimated total thickness failed (ms)	Depth to pre- failure seafloor from sea-level (ms)	Seafloor Character
						Q100	Q99	Q97	Q95	Q93	Q91				
2003033	1700730	1700729	44.5872	-55.4360	2590							17.15	42.14	2565.01	F-D-s-mf
2003033	1700732	1700731	44.5868	-55.4321	2595							11.76	40.00	2566.76	F-D-s-mf
2003033	1700733	1700732	44.5866	-55.4301	2597							0.00	42.00	2555.00	F-D-s-mf
2001043	2281945	2281944	44.2143	-55.5452	4162							19.60	Indeterminate	Indeterminate	F-D-s-mf
2001043	2281950	2281949	44.2195	-55.5450	4141							21.07	"	"	F-D-s-mf
2001043	2281955	2281954	44.2274	-55.5448	4125							17.15	"	"	F-D-s-mf
2001043	2282000	2281959	44.2353	-55.5448	4108							20.00	"	"	F-D-s-mf
2001043	2282005	2282004	44.2428	-55.5447	4082							23.52	"	"	F-D-s-mf
2001043	2282010	2282009	44.2507	-55.5446	4064							16.17	"	"	F-D-s-mf
2001043	2282015	2282014	44.2586	-55.5446	4040							14.70	"	"	F-D-s-mf
2001043	2282020	2282019	44.2672	-55.5443	4014							13.72	"	"	F-D-s-mf
2001043	2282021	2282020	44.2689	-55.5443	4013							0.00	"	"	F-D-s-mf
2001043	2282115	2282114	44.3545	-55.5430	3657							0.00	"	"	F-D-u-mf
2001043	2282118	2282117	44.3593	-55.5430	3635							8.82	"	"	F-D-u-mf
2001043	2282120	2282119	44.3625	-55.5429	3620							11.22	"	"	F-D-u-mf
2001043	2282125	2282124	44.3705	-55.5426	3600							5.86	"	"	F-D-u-mf
2001043	2282127	2282126	44.3737	-55.5425	3583							0.00	"	"	F-D-u-mf
2001043	2282236	2282235	44.4828	-55.5409	3000							0.00	"	"	G-D-s-mf
2001043	2282241	2282240	44.4898	-55.5407	2950							5.88	"	"	G-D-s-mf
2001043	2282246	2282245	44.4969	-55.5406	2895							0.00	"	"	G-D-s-mf
2001043	2282253	2282252	44.5073	-55.5408	2825							0.00	"	"	G-D-s-mf
2001043	2282256	2282255	44.5121	-55.5404	2785							9.31	"	"	G-D-s-mf
2001043	2282303	2282302	44.5227	-55.5404	2730							4.90	"	"	F-D-s-mf
2001043	2282305	2282304	44.5256	-55.5402	2703		0.00		49.00	72.55	109.80	4.90	12.68	2695.22	F-D-s-mf
2001043	2282310	2282309	44.5328	-55.5400	2667		8.82		57.84	82.35	119.61	8.82	12.68	2663.14	F-D-s-mf
2001043	2282315	2282314	44.5401	-55.5401	2640		5.88		55.39	79.41	117.65	5.88	13.16	2632.72	F-D-s-mf
2001043	2282320	2282319	44.5473	-55.5397	2608		2.94		50.00	73.53	108.82	2.94	12.68	2598.26	G-D-s-mf
2001043	2282327	2282326	44.5577	-55.5398	2562		4.90		50.00	71.08	106.37	4.90	13.65	2553.25	G-D-s-mf
2001043	2282330	2282329	44.5622	-55.5397	2540		5.88			71.57	104.90	5.88	12.68	2533.20	F-D-s-mf
2001043	2282336	2282335	44.5712	-55.5395	2510		7.84		50.50	72.06	105.88	6.86	12.68	2504.18	F-D-s-mf
2001043	2282338	2282337	44.5740	-55.5395	2490		1.96		45.10	66.18	99.51	0.00	11.70	2478.30	F-D-s-mf
2001043	2282340	2282339	44.5767	-55.5394	2465		0.00		38.24	56.86	87.26	0.00	12.68	2452.32	G-D-s-mf

Cruise #	Day/time (Huntec)	Day/time (Ship)	Latitude of ship (dec deg)	Longitude of ship (dec deg)	DTS (ms)	Depth from seafloor to reflections (ms)						Thickness of surface MTDs (ms)	Estimated total thickness failed (ms)	Depth to pre- failure seafloor from sea-level (ms)	Seafloor Character
						Q100	Q99	Q97	Q95	Q93	Q91				
2001043	2282346	2282345	44.5849	-55.5392	2410		3.43		42.65	62.26	90.20	3.43	13.65		G-D-s-mf
2001043	2282348	2282347	44.5877	-55.5392	2395		4.90	19.61	45.10	63.73	91.67	4.90	13.16		G-D-s-mf
2001043	2282351	2282350	44.5918	-55.5392	2373		5.88			64.22	92.16	5.88	12.19		G-D-s-mf
2001043	2282353	2282352	44.5945	-55.5392	2350		10.29			63.73	90.20	10.29	14.63		G-D-s-mf
2001043	2282355	2282354	44.5973	-55.5392	2335		11.76			64.71	90.20	11.76	13.65		G-D-s-mf
2001043	2282358	2282357	44.6015	-55.5391	2305		12.74			66.67	92.16	12.74	12.74		G-D-s-mf
2001043	2290001	2290000	44.6059	-55.5389	2270		10.29			59.80	84.80	10.29	13.16		G-D-s-mf
2001043	2290005	2290004	44.6116	-55.5388	2235		5.39			59.80	84.31	5.39	13.65		G-D-s-mf
2001043	2290009	2290008	44.6175	-55.5389	2215		0.00			50.98	74.51	0.00	10.73		G-D-s-mf
2001043	2290013	2290012	44.6233	-55.5386	2163		2.45			51.96	74.51	0.00	9.26		G-D-s-mf
2001043	2290015	2290014	44.6263	-55.5385	2142		16.18			67.65	89.22	5.88	5.88		G-D-s-mf
2001043	2290020	2290019	44.6339	-55.5386	2105	0.00	14.95			70.59	89.22	0.00	0.00		G-D-s-mf
2001043	2290022	2290021	44.6371	-55.5386	2080	0.00	15.20			63.73	80.88				G-U-s
2001043	2290024	2290023	44.6405	-55.5384	2063		14.71	30.39		68.63	86.77	0.00	0.00		F-D-s-mf
2001043	2290027	2290026	44.6456	-55.5382	2050		13.73	27.45		66.18	84.31	4.90	0.00		F-D-s-mf
2001043	2290028	2290027	44.6474	-55.5382	2040		12.25	25.49		58.33	74.51	0.00	0.00		F-D-s-mf
2001043	2290034	2290033	44.6578	-55.5381	1950	0.00	12.75	25.49	36.77	58.82	73.53				F-D-s-mf
2001043	2290037	2290036	44.6631	-55.5380	1925	0.00	14.70	26.47		59.80	75.98	0.00	0.00	1925.00	F-D-s-mf
2001043	2290040	2290039	44.6684	-55.5379	1900		14.21	26.47	37.26	57.84	74.02	8.82	8.82	1900.00	F-D-s-mf
2001043	2290045	2290044	44.6774	-55.5379	1865		9.31	21.57	31.37	48.53	63.23	8.33	10.20	1863.13	F-D-s-mf
2001043	2290049	2290048	44.6846	-55.5378	1830		7.84	20.59	29.41	44.12	58.33	6.86	11.70	1825.16	G-D-s-mf
2001043	2290052	2290051	44.6900	-55.5376	1785		5.39	17.35	25.98	38.23	52.94	5.39	11.21	1779.18	G-D-s-mf
2001043	2290053	2290052	44.6918	-55.5376	1757	0.00	11.76	22.55	29.90	42.65	57.84	2.94	13.16	1746.78	G-D-s-mf
2001043	2290055	2290054	44.6954	-55.5374	1730	0.00	10.78	22.06	32.84	47.55	61.76				G-U-s
2001043	2290100	2290059	44.7043	-55.5373	1675	0.00	10.67	22.35	36.27	49.55	65.69				G-U-s
2001043	2290105	2290104	44.7109	-55.5417	1623	0.00	9.31	20.88	34.51	45.92	59.80				F-U-s
2001043	2290110	2290109	44.7131	-55.5521	1604	0.00	9.61	20.39	33.33	46.12	59.80	0.00	0.00	1604.00	F-D-s-mf
2001043	2290111	2290110	44.7135	-55.5542	1607		7.06	18.63	31.86	46.12	60.00	4.41	5.88	1605.53	F-D-s-mf
2001043	2290115	2290114	44.7156	-55.5622	1590		8.33	20.59	33.33	46.31	64.22	7.06	8.33	1588.73	F-D-s-mf
2001043	2290120	2290119	44.7166	-55.5725	1578		8.33	20.59	32.35	46.31	63.73	6.86	9.31	1575.55	F-D-s-mf
2001043	2290125	2290124	44.7194	-55.5831	1553		6.86	18.63	30.88	44.35	61.76	5.39	8.82	1549.57	F-D-s-mf
2001043	2290128	2290127	44.7207	-55.5891	1537		9.80	21.57	35.29	49.25	67.65	9.80	9.80	1537.00	F-D-s-mf

Cruise #	Day/time (Huntec)	Day/time (Ship)	Latitude of ship (dec deg)	Longitude of ship (dec deg)	DTS (ms)	Depth from seafloor to reflections (ms)						Thickness of surface MTDs (ms)	Estimated total thickness failed (ms)	Depth to pre- failure seafloor from sea-level (ms)	Seafloor Character
						Q100	Q99	Q97	Q95	Q93	Q91				
2001043	2290135	2290134	44.7232	-55.6031	1495		8.82	21.08	35.29	48.08	67.65	8.82	10.29	1493.53	F-D-s-mf
2001043	2290140	2290139	44.7256	-55.6136	1467		7.16	18.82	32.55	45.63	61.96	7.16	9.80	1464.36	F-D-s-mf
2001043	2290144	2290143	44.7270	-55.6214	1475		5.29	20.88	29.41	41.22	55.88	5.29	7.84	1472.45	G-D-s-mf
2001043	2290150	2290149	44.7295	-55.6339	1492		5.39	18.33	32.84	43.10	66.67	4.90	9.80	1487.10	F-D-s-mf
2001043	2290155	2290154	44.7317	-55.6447	1465		7.25	21.57	36.77	50.53	71.76	6.37	9.31	1462.06	G-D-s-mf
2001043	2290200	2290159	44.7339	-55.6554	1414		6.86	20.59	35.29	48.57	68.82	4.90	6.86	1412.04	G-D-s-mf
2001043	2290205	2290204	44.7360	-55.6659	1375		5.88	20.59	36.27	48.47	70.78	3.14	5.88	1372.26	G-D-s-mf
2001043	2290207	2290206	44.7369	-55.6701	1331		2.45	18.14	32.35	46.12	68.63	0.00	3.92	1327.08	G-D-s-sc
2001043	2290210	2290209	44.7382	-55.6764	1272	0.00	8.82	19.61	33.82	48.12	61.76				F-U-s
2001043	2290211	2290210	44.7386	-55.6783	1278	0.00	5.39	15.69	28.43	40.24	51.96	0.00	0.00	1278.00	G-D-s-mf
2001043	2290213	2290212	44.7395	-55.6822	1300		0.00	10.29	26.47	32.39	39.71	1.96	9.80	1292.16	G-D-s-sc
2001043	2290215	2290214	44.7403	-55.6861	1333		1.96	11.47	21.57	28.47	36.27	5.39	9.80	1328.59	G-D-s-sc
2001043	2290216	2290215	44.7407	-55.6880	1340		0.00	8.82	18.43	25.53	32.35	0.00	8.62	1331.38	G-D-s-sc
2001043	2290219	2290218	44.7416	-55.6940	1319		0.00	9.02	17.65	26.51	33.82				F-D-s-sc
2001043	2290222	2290221	44.7428	-55.7002	1370		0.00	12.75	21.08	29.39	38.23				F-D-s-sc
2001043	2290225	2290224	44.7444	-55.7064	1345		0.00	13.72	25.00	32.35	41.67				F-D-s-sc
2001043	2290233	2290232	44.7476	-55.7230	1188	0.00	9.31	21.08	32.55	44.61	63.73				F-U-s
2001043	2290236	2290235	44.7489	-55.7290	1200	0.00	11.27	23.53	34.31	46.77	65.69				F-U-s
2001043	2290240	2290239	44.7506	-55.7373	1212	0.00	7.84	18.63	28.63	40.20	55.88				F-U-s
2001043	2290241	2290240	44.7510	-55.7393	1225	0.00	3.92	13.73	23.53	34.31	48.53				G-U-s
2001043	2290245	2290244	44.7527	-55.7475	1345							0.00	Indeterminate	Indeterminate	G-D-u-sc
2001043	2290246	2290245	44.7531	-55.7495	1395							24.50	"	"	G-D-u-sc
2001043	2290250	2290249	44.7545	-55.7575	1403							23.52	"	"	F-D-s-mf
2001043	2290252	2290251	44.7555	-55.7616	1394							0.00	"	"	G-D-h-mf
2001043	2290254	2290253	44.7564	-55.7657	1353							0.00	8.82	1344.18	G-D-h-mf
2001043	2290255	2290254	44.7568	-55.7677	1345		8.82		33.81			5.88	8.82	1342.06	G-D-h-mf
2001043	2290257	2290256	44.7576	-55.7716	1337		8.82		31.36			5.88	9.80	1333.08	F-D-s-mf
2001043	2290300	2290259	44.7580	-55.7774	1350		8.82		32.34			6.37	12.74	1343.63	F-D-s-mf
2001043	2290303	2290302	44.7570	-55.7827	1382							6.37	15.68	1372.69	F-D-s-mf
2001043	2290304	2290303	44.7568	-55.7847	1405							0.00	16.00	1389.00	G-D-s-mf
2001043	2290305	2290304	44.7568	-55.7867	1428										G-D-s-sc
2001043	2290307	2290306	44.7563	-55.7908	1475							0.00	0.00	1475.00	G-D-u-sc

Cruise #	Day/time (Huntec)	Day/time (Ship)	Latitude of ship (dec deg)	Longitude of ship (dec deg)	DTS (ms)	Depth from seafloor to reflections (ms)						Thickness of surface MTDs (ms)	Estimated total thickness failed (ms)	Depth to pre- failure seafloor from sea-level (ms)	Seafloor Character
						Q100	Q99	Q97	Q95	Q93	Q91				
2001043	2290310	2290309	44.7550	-55.7968	1530							15.20	49.00	1496.20	F-D-h-mf
2001043	2290311	2290310	44.7546	-55.7989	1537							10.78	48.02	1499.76	F-D-h-mf
2001043	2290312	2290311	44.7543	-55.8010	1537							7.35	48.02	1496.33	F-D-h-mf
2001043	2290314	2290313	44.7540	-55.8053	1545							18.14	48.51	1514.63	F-D-h-mf
2001043	2290315	2290314	44.7539	-55.8075	1542							8.82	46.06	1504.76	F-D-h-mf
2001043	2290318	2290317	44.7532	-55.8137	1565							11.27	51.94	1524.33	F-D-h-mf
2001043	2290320	2290319	44.7526	-55.8177	1570							3.92	49.00	1524.92	G-D-h-mf
2001043	2290322	2290321	44.7519	-55.8217	1562							9.80	46.06	1525.74	G-D-h-mf
2001043	2290325	2290324	44.7511	-55.8279	1535							24.51	49.00	1510.51	F-D-h-mf
2001043	2290327	2290326	44.7507	-55.8321	1530							28.92	48.02	1510.90	F-D-h-mf
2001043	2290329	2290328	44.7504	-55.8363	1540							33.33	48.02	1525.31	F-D-h-mf
2001043	2290330	2290329	44.7503	-55.8382	1545					42.14		38.23	49.00	1534.23	F-D-h-mf
2001043	2290331	2290330	44.7500	-55.8401	1547					33.81		30.39	49.00	1528.39	F-D-h-mf
2001043	2290332	2290331	44.7496	-55.8419	1535					30.38		0.00	38.22	1496.78	G-D-h-mf
2001043	2290333	2290332	44.7492	-55.8438	1520		0.00	17.64		45.08		0.00	11.76	1508.24	F-D-u-mf
2001043	2290337	2290336	44.7482	-55.8515	1521		8.82	25.97	49.00	61.74		8.82	9.80	1520.02	F-D-u-mf
2001043	2290339	2290338	44.7477	-55.8554	1519		15.19		52.92	68.60		15.19	15.19	1519.00	F-D-u-mf
2001043	2290343	2290342	44.7464	-55.8624	1520		12.25		49.00	61.74		12.25	12.25	1520.00	F-D-u-mf
2001043	2290350	2290349	44.7375	-55.8611	1555		12.75	29.40	48.02	59.78		12.75	12.75	1555.00	F-D-u-mf
2001043	2290355	2290354	44.7302	-55.8608	1585		11.27	29.40	45.08	57.33		11.27	12.25	1584.02	F-D-u-mf
2001043	2290400	2290359	44.7239	-55.8596	1615		10.78	26.46	46.06	57.33		10.78	12.74	1613.04	F-D-u-mf
2001043	2290405	2290404	44.7177	-55.8599	1642		10.78		45.08	55.86		10.78	13.72	1639.06	F-D-u-mf
2001043	2290407	2290406	44.7151	-55.8596	1640		12.25		49.49	60.76		12.25	12.25	1640.00	F-D-u-mf
2001043	2290412	2290411	44.7089	-55.8585	1665		6.36	21.07	33.81	45.08		5.39	9.80	1660.59	F-D-u-mf
2001043	2290416	2290415	44.7040	-55.8585	1678		0.00	12.74	26.00	37.24		0.00	9.80	1668.20	F-D-u-mf
2001043	2290418	2290417	44.7016	-55.8582	1663				19.60	28.43					G-D-u-mf
2001043	2290420	2290419	44.6991	-55.8580	1658				23.04	32.84					G-D-u-mf
2001043	2290423	2290422	44.6951	-55.8577	1634	0.00	5.40	18.63	29.90	40.20					G-D-u-mf
2001043	2290424	2290423	44.6939	-55.8568	1640	0.00	6.37	19.61	33.33	43.38					F-D-s-mf
2001043	2290425	2290424	44.6933	-55.8547	1670	0.00	5.39	19.61	30.78	42.16					G-D-s-sc
2001043	2290447	2290446	44.6808	-55.8073	1680		9.80	18.63							S-U-s
2001043	2290448	2290447	44.6804	-55.8049	1680		12.74	25.50							G-U-s

Cruise #	Day/time (Huntec)	Day/time (Ship)	Latitude of ship (dec deg)	Longitude of ship (dec deg)	DTS (ms)	Depth from seafloor to reflections (ms)						Thickness of surface MTDs (ms)	Estimated total thickness failed (ms)	Depth to pre- failure seafloor from sea-level (ms)	Seafloor Character
						Q100	Q99	Q97	Q95	Q93	Q91				
2001043	2290449	2290448	44.6797	-55.8027	1720		10.03	20.10							S-U-s
2001043	2290450	2290449	44.6791	-55.8005	1762		0.00								S-MD-s-sp
2001043	2290452	2290451	44.6779	-55.7959	1784		0.00	13.72		35.29	40.20	0.00	8.82	1775.18	G-D-u-mf
2001043	2290455	2290454	44.6761	-55.7892	1768		6.37	16.67	28.43	39.70	55.40	4.90	8.82	1764.08	F-D-u-mf
2001043	2290458	2290457	44.6743	-55.7826	1782		7.35	20.09	30.39	41.67	58.82	5.10	9.80	1777.30	F-D-u-mf
2001043	2290500	2290459	44.6732	-55.7782	1795		1.47	18.63	29.40	40.19	57.35	1.47	7.84	1788.63	F-D-u-mf
2001043	2290503	2290502	44.6716	-55.7718	1815		0.00	13.23	25.00	34.80	53.43	0.00	10.78	1804.22	F-D-u-mf
2001043	2290504	2290503	44.6711	-55.7697	1810		0.00	13.72	25.49	35.78	52.94	0.00	8.33	1801.67	F-D-u-mf
2001043	2290507	2290506	44.6693	-55.7633	1820		4.90	17.65	28.92	38.23	55.39	4.41	9.80	1814.61	F-D-u-mf
2001043	2290529	2290528	44.6652	-55.7238	1925		2.45	15.19	28.43	41.67	62.74	1.96	8.81	1918.15	G-D-s-mf
2001043	2290533	2290532	44.6692	-55.7293	1885		0.00	13.72	24.90	34.31	52.45	0.00	8.33	1876.67	G-D-s-mf
2001043	2290537	2290536	44.6741	-55.7340	1810		0.00	10.29	22.55	30.39	47.06	0.00	9.80	1800.20	S-D-s-sc
2001043	2290540	2290539	44.6792	-55.7332	1740		4.90	17.65	28.43	40.69	60.29	3.92	10.78	1733.14	S-D-s-sc
2001043	2290545	2290544	44.6865	-55.7335	1675		6.86	18.63	31.37	48.04	63.73	5.88	9.31	1671.57	G-D-u-mf
2001043	2290548	2290547	44.6907	-55.7331	1640		10.78	22.55	36.27	47.06	66.67	9.80	12.25	1637.55	G-D-u-mf
2001043	2290549	2290548	44.6921	-55.7328	1622		3.92	16.67	27.94	36.76	53.92	0.00	4.90	1617.10	S-D-u-mf
2001043	2290550	2290549	44.6934	-55.7328	1605		3.92	15.68	27.45	35.78	51.47	0.00	6.37	1598.63	S-D-u-mf
2001043	2290555	2290554	44.7000	-55.7338	1570		5.88	17.16	28.43	41.17	60.78	2.94	7.84	1565.10	G-D-u-mf
2001043	2290600	2290559	44.7070	-55.7335	1518		4.90	16.67	28.43	40.19	60.29	3.92	9.80	1512.12	G-D-s-mf
2001043	2290605	2290604	44.7142	-55.7335	1455		8.33	19.61	32.35	44.61	67.65	4.90	9.31	1450.59	G-D-s-mf
2001043	2290607	2290606	44.7170	-55.7335	1420		6.37	18.63	30.39	45.16	64.22	5.39	9.80	1415.59	G-D-s-mf
2001043	2290608	2290607	44.7184	-55.7336	1408	0.00	12.75	24.02	36.27	48.53	71.08	0.00	0.00	1408.00	G-D-s-mf
2001043	2290610	2290609	44.7212	-55.7336	1390	0.00	12.50	24.51	36.27	48.53	71.08				F-U-s
2001043	2290612	2290611	44.7241	-55.7337	1395	0.00	11.76	23.04	35.29	47.06	71.57	0.00	0.00	1395.00	F-U-s
2001043	2290613	2290612	44.7255	-55.7336	1410	0.00	7.35	18.63	30.88	42.65	65.19	3.92	5.88	1408.04	F-D-s-mf
2001043	2290614	2290613	44.7269	-55.7336	1375		4.90	16.67	28.92	40.67	62.75	0.00	3.92	1371.08	G-D-s-mf
2001043	2290615	2290614	44.7284	-55.7336	1345		0.98	10.29	23.53	34.31	49.02				S-D-s-sc
2001043	2290616	2290615	44.7298	-55.7336	1330		0.98	12.25	24.02	34.80	50.98	0.00	3.92	1326.08	S-D-s-sc
2001043	2290620	2290619	44.7353	-55.7337	1285		8.82	20.59	32.35	43.63	61.76	7.35	9.80	1282.55	G-D-u-mf
2001043	2290621	2290620	44.7366	-55.7337	1275		5.39	17.16	28.43	40.20	56.86	3.92	10.30	1268.62	G-D-u-mf
2001043	2290622	2290621	44.7380	-55.7336	1257	0.00	9.31	21.08	32.35	44.12	62.25	0.00	0.00	1257.00	G-D-u-mf
2001043	2290625	2290624	44.7422	-55.7336	1230	0.00	11.76	22.55	33.82	46.09	64.71				F-U-s

Cruise #	Day/time (Huntec)	Day/time (Ship)	Latitude of ship (dec deg)	Longitude of ship (dec deg)	DTS (ms)	Depth from seafloor to reflections (ms)						Thickness of surface MTDs (ms)	Estimated total thickness failed (ms)	Depth to pre- failure seafloor from sea-level (ms)	Seafloor Character
						Q100	Q99	Q97	Q95	Q93	Q91				
2001043	2290630	2290629	44.7493	-55.7337	1200	0.00	11.27	22.06	32.35	44.61	61.76				F-U-s
2001043	2290633	2290632	44.7533	-55.7332	1205	0.00	7.35	16.18	25.49	37.25	50.98				F-U-u
2001043	2290637	2290636	44.7578	-55.7277	1192	0.00	3.92	11.27	19.61	31.37	42.16				F-U-u
2001043	2290640	2290639	44.7612	-55.7237	1180	0.00	2.94	10.78			34.31				F-U-u
2001043	2290643	2290642	44.7647	-55.7197	1172	0.00	3.92	7.84			27.45				F-U-u
2001043	2290646	2290645	44.7671	-55.7150	1110	0.00	1.96	10.78		23.04	35.78				S-D-s-sc
2001043	2290647	2290646	44.7669	-55.7132	1095	0.00	4.41	14.71	20.10	31.18	45.10				S-D-s-sp
2001043	2290648	2290647	44.7662	-55.7117	1100	0.00	5.69	16.47	25.49	37.25	53.92				F-U-s
2001043	2290650	2290649	44.7641	-55.7102	1125	0.00	7.35	19.61	31.96	45.10	65.20				G-U-s
2001043	2290655	2290654	44.7584	-55.7100	1185	0.00	10.78	23.53		44.12	64.22				G-U-s
2001043	2290659	2290658	44.7536	-55.7097	1227	0.00	11.76	25.49		50.49	67.65				G-U-s
2001043	2290701	2290700	44.7511	-55.7097	1245		6.86	18.63	27.45	43.14	57.84				G-D-s-mf
2001043	2290703	2290702	44.7486	-55.7098	1275		2.94	14.71	25.49	37.25	49.51				S-D-s-mf
2001043	2290708	2290707	44.7426	-55.7129	1350										S-D-s-sc
2001043	2290711	2290710	44.7409	-55.7176	1290										S-D-s-sc
2001043	2290714	2290713	44.7417	-55.7229	1220	0.00	10.29	22.55	34.31	46.08	63.73				G-U-s
2001043	2290717	2290716	44.7451	-55.7265	1208	0.00	11.76	23.53	35.29	47.55	67.16				F-U-s
2001043	2290720	2290719	44.7486	-55.7307	1200	0.00	11.27	23.04	33.82	46.27	64.90				F-U-s
2001043	2290723	2290722	44.7524	-55.7337	1210	0.00	7.84	17.65	27.94	39.31	54.90				F-U-s
2001043	2290727	2290726	44.7587	-55.7339	1315							0.00	Indeterminate	Indeterminate	S-D-s-sp
2001043	2290729	2290728	44.7615	-55.7339	1320							33.33	"	"	F-D-s-mf
2001043	2290730	2290729	44.7628	-55.7338	1315							32.35	"	"	F-D-s-mf
2001043	2290733	2290732	44.7668	-55.7336	1310							31.37	"	"	F-D-s-mf
2001043	2290739	2290738	44.7756	-55.7341	1275							29.41	"	"	S-D-h-mf
2001043	2290740	2290739	44.7771	-55.7341	1260							32.35	"	"	S-D-h-mf
2001043	2290741	2290740	44.7785	-55.7340	1245							28.43	"	"	S-D-h-mf
2001043	2290745	2290744	44.7847	-55.7342	1190							33.33	"	"	S-D-s-sp
2001043	2290746	2290745	44.7862	-55.7342	1152			22.00	34.50	38.73	44.10		10.00	1142.00	G-D-s-sc
2001043	2290747	2290746	44.7877	-55.7341	1140			19.70	35.00	39.71	46.10		10.00	1130.00	G-D-s-sc
2001043	2290751	2290750	44.7938	-55.7340	1080		1.00	20.25	33.70	39.71	44.10		10.00	1070.00	G-D-s-sc
2001043	2290755	2290754	44.8000	-55.7340	1045		1.00	20.25	34.50	35.30	44.10		11.00	1034.00	G-D-s-sc
2001043	2290800	2290759	44.8077	-55.7340	968		1.00	19.20	35.00	35.30	44.10		11.00	957.00	G-D-s-sc

Cruise #	Day/time (Huntec)	Day/time (Ship)	Latitude of ship (dec deg)	Longitude of ship (dec deg)	DTS (ms)	Depth from seafloor to reflections (ms)						Thickness of surface MTDs (ms)	Estimated total thickness failed (ms)	Depth to pre- failure seafloor from sea-level (ms)	Seafloor Character
						Q100	Q99	Q97	Q95	Q93	Q91				
2001043	2290804	2290803	44.8138	-55.7339	943		1.00	19.20	34.00	35.30	44.10		11.00	932.00	G-D-s-sc
2001043	2290805	2290804	44.8153	-55.7339	945		1.00	19.20	35.00	35.30	44.10	7.35	9.80	942.55	F-D-u-mf
2001043	2290807	2290806	44.8182	-55.7339	930		1.00	19.20	35.00	35.30	44.10	5.88	9.31	926.57	F-D-u-mf
2001043	2290811	2290810	44.8240	-55.7339	890				35.75			0.00	1.96	888.04	F-D-u-mf
2001043	2290813	2290812	44.8270	-55.7339	845				35.75						G-D-h-mf
2001043	2290814	2290813	44.8284	-55.7339	835				34.50			0.00	11.76	823.24	G-D-h-mf
2001043	2290815	2290814	44.8298	-55.7339	830							8.33	14.70	823.63	G-D-h-mf
2001043	2290817	2290816	44.8327	-55.7338	800							0.00	4.90	795.10	G-D-u-sp
2001043	2290820	2290819	44.8371	-55.7340	755										G-D-u-sc
2001043	2291941	2291940	44.8585	-55.9411	815										G-D-u-sc
2001043	2291945	2291944	44.8538	-55.9418	876										G-D-u-sc
2001043	2291950	2291949	44.8476	-55.9417	971										G-D-u-sc
2001043	2291955	2291954	44.8414	-55.9427	1042										G-D-u-sc
2001043	2292000	2291959	44.8355	-55.9428	1122										G-D-u-sc
2001043	2292005	2292004	44.8293	-55.9434	1183										G-D-u-sc
2001043	2292010	2292009	44.8231	-55.9439	1237							0.00	Indeterminate	Indeterminate	G-D-u-sl
2001043	2292012	2292011	44.8208	-55.9441	1256							4.90	"	"	G-D-u-sl
2001043	2292015	2292014	44.8173	-55.9445	1289							12.25	"	"	G-D-u-sl
2001043	2292018	2292017	44.8137	-55.9448	1316							0.00	"	"	G-D-u-sl
2001043	2292021	2292020	44.8100	-55.9452	1350							0.00	"	"	F-D-h-mf
2001043	2292023	2292022	44.8077	-55.9454	1348							22.05	"	"	F-D-h-mf
2001043	2292025	2292024	44.8054	-55.9456	1358							24.50	"	"	F-D-h-mf
2001043	2292030	2292029	44.7997	-55.9441	1397							29.89	"	"	G-D-h-mf
2001043	2292032	2292031	44.7991	-55.9400	1435							0.00	"	"	G-D-h-mf
2001043	2292033	2292032	44.7987	-55.9381	1470							0.00	"	"	G-D-h-mf
2001043	2292035	2292034	44.7977	-55.9345	1495							14.70	"	"	F-D-h-mf
2001043	2292038	2292037	44.7962	-55.9294	1511							12.25	"	"	F-D-h-mf
2001043	2292040	2292039	44.7955	-55.9258	1530							9.80	"	"	F-D-h-mf
2001043	2292045	2292044	44.7939	-55.9167	1528							19.60	"	"	F-D-h-mf
2001043	2292047	2292046	44.7930	-55.9132	1534							0.00	"	"	F-D-h-mf
2001043	2292049	2292048	44.7920	-55.9095	1491							0.00	"	"	F-D-h-mf
2001043	2292050	2292049	44.7916	-55.9077	1492							9.80	"	"	F-D-h-mf

Cruise #	Day/time (Huntec)	Day/time (Ship)	Latitude of ship (dec deg)	Longitude of ship (dec deg)	DTS (ms)	Depth from seafloor to reflections (ms)						Thickness of surface MTDs (ms)	Estimated total thickness failed (ms)	Depth to pre- failure seafloor from sea-level (ms)	Seafloor Character
						Q100	Q99	Q97	Q95	Q93	Q91				
2001043	2292055	2292054	44.7897	-55.8986	1483							7.84	"	"	F-D-h-mf
2001043	2292058	2292057	44.7886	-55.8931	1482							0.00	"	"	F-D-h-mf
2001043	2292103	2292102	44.7864	-55.8839	1502							0.00	"	"	F-D-h-mf
2001043	2292105	2292104	44.7857	-55.8801	1488							14.70	"	"	F-D-h-mf
2001043	2292106	2292105	44.7853	-55.8783	1462							0.00	"	"	F-D-h-mf
2001043	2292107	2292106	44.7849	-55.8764	1448							0.00	"	"	F-D-s-mf
2001043	2292108	2292107	44.7845	-55.8745	1445							4.90	"	"	F-D-s-mf
2001043	2292109	2292108	44.7841	-55.8726	1444							3.92	"	"	F-D-s-mf
2001043	2292110	2292109	44.7838	-55.8707	1442							6.86	"	"	F-D-s-mf
2001043	2292111	2292110	44.7834	-55.8689	1434							0.00	"	"	F-D-s-mf
2001043	2292114	2292113	44.7821	-55.8633	1332							0.00	14.63	1317.37	G-D-h-mf
2001043	2292116	2292115	44.7812	-55.8597	1303							5.88	20.48	1288.40	G-D-h-mf
2001043	2292118	2292117	44.7802	-55.8558	1302										F-D-s-sc
2001043	2292119	2292118	44.7799	-55.8537	1320							0.00	30.23	1289.77	F-D-s-mf
2001043	2292120	2292119	44.7796	-55.8517	1327							6.37	33.15	1300.22	F-D-s-mf
2001043	2292121	2292120	44.7792	-55.8497	1332							8.29	35.10	1305.19	F-D-s-sc
2001043	2292122	2292121	44.7789	-55.8476	1331										F-D-s-sc
2001043	2292125	2292124	44.7759	-55.8448	1357										G-D-s-sc
2001043	2292130	2292129	44.7689	-55.8470	1400										G-D-s-sc
2001043	2292131	2292130	44.7673	-55.8474	1407							16.67	33.15	1390.52	G-D-s-sp
2001043	2292135	2292134	44.7615	-55.8489	1445							15.69	34.13	1426.56	G-D-s-mf
2001043	2292140	2292139	44.7543	-55.8510	1477							14.71	34.13	1457.58	G-D-s-mf
2001043	2292144	2292143	44.7486	-55.8526	1519							9.80	37.05	1491.75	G-D-s-mf
2001043	2292145	2292144	44.7473	-55.8529	1521							11.76	36.56	1496.20	G-D-s-mf
2001043	2292148	2292147	44.7431	-55.8539	1528							9.31	34.13	1503.18	G-D-s-mf
2001043	2292151	2292150	44.7396	-55.8573	1550							11.27	37.05	1524.22	G-D-s-mf
2001043	2292153	2292152	44.7403	-55.8613	1544							12.75	35.10	1521.65	G-D-s-mf
2001043	2292155	2292154	44.7427	-55.8653	1532							9.80	33.15	1508.65	G-D-s-mf
2001043	2292159	2292158	44.7468	-55.8738	1500							0.00	38.00	1462.00	G-D-s-mf
2001043	2292200	2292159	44.7476	-55.8761	1480							0.00	34.13	1445.87	G-D-s-mf
2001043	2292203	2292202	44.7504	-55.8833	1475							5.88	36.08	1444.80	G-D-s-mf
2001043	2292206	2292205	44.7536	-55.8893	1486							0.00	30.23	1455.77	G-D-s-mf

Cruise #	Day/time (Huntec)	Day/time (Ship)	Latitude of ship (dec deg)	Longitude of ship (dec deg)	DTS (ms)	Depth from seafloor to reflections (ms)						Thickness of surface MTDs (ms)	Estimated total thickness failed (ms)	Depth to pre- failure seafloor from sea-level (ms)	Seafloor Character
						Q100	Q99	Q97	Q95	Q93	Q91				
2001043	2292213	2292212	44.7599	-55.9035	1780							0.00	Indeterminate	Indeterminate	F-D-h-mf
2001043	2292215	2292214	44.7616	-55.9074	1759							14.71	"	"	F-D-h-mf
2001043	2292216	2292215	44.7625	-55.9094	1752							13.72	"	"	F-D-h-mf
2001043	2292218	2292217	44.7644	-55.9133	1750							10.78	"	"	F-D-h-mf
2001043	2292220	2292219	44.7662	-55.9173	1750							0.00	"	"	F-D-h-mf
2001043	2292222	2292221	44.7680	-55.9213	1740							0.00	"	"	F-D-h-mf
2001043	2292223	2292222	44.7689	-55.9233	1733							10.78	"	"	F-D-h-mf
2001043	2292224	2292223	44.7698	-55.9253	1729							15.69	"	"	F-D-h-mf
2001043	2292225	2292224	44.7707	-55.9273	1728							17.16	"	"	F-D-h-mf
2001043	2292226	2292225	44.7716	-55.9293	1724							0.00	"	"	F-D-h-mf
2001043	2292227	2292226	44.7725	-55.9313	1700							0.00	"	"	S-D-s-sc
2001043	2292230	2292229	44.7753	-55.9372	1640							18.63	"	"	G-D-h-mf
2001043	2292235	2292234	44.7799	-55.9470	1580							33.33	"	"	G-D-h-mf
2001043	2292236	2292235	44.7808	-55.9489	1570							30.39	"	"	G-D-h-mf
2001043	2292238	2292237	44.7824	-55.9528	1530							50.98	"	"	S-D-s-mf
2001043	2292239	2292238	44.7832	-55.9548	1516							40.20	"	"	S-D-s-mf
2001043	2292242	2292241	44.7860	-55.9607	1448							0.00	"	"	S-D-s-mf
2001043	2292245	2292244	44.7889	-55.9666	1385							21.57	"	"	S-D-s-mf
2001043	2292250	2292249	44.7932	-55.9766	1354							23.53	"	"	S-D-s-mf
2001043	2292252	2292251	44.7950	-55.9806	1328							0.00	"	"	G-D-s-sc
2001043	2292255	2292254	44.7979	-55.9868	1295							0.00	"	"	G-D-s-sp
2001043	2292257	2292256	44.7999	-55.9911	1245							23.53	"	"	G-D-s-mf
2001043	2292300	2292259	44.8031	-55.9974	1218							29.41	"	"	G-D-s-mf
2001043	2292303	2292302	44.8082	-55.9987	1172							30.39	"	"	G-D-s-mf
2001043	2292305	2292304	44.8115	-55.9990	1150							19.61	"	"	G-D-s-mf
2001043	2292306	2292305	44.8130	-55.9993	1135							0.00	"	"	G-D-s-mf
2001043	2292309	2292308	44.8176	-55.9998	1090										G-D-s-sc
99036	2322258	2322257	44.7990	-55.6146	955							5.88	8.78	952.10	S-D-s-mf
99036	2322259	2322258	44.7979	-55.6135	962							4.41	8.78	957.63	S-D-s-mf
99036	2322301	2322300	44.7952	-55.6111	980							1.96	6.34	975.62	S-D-s-mf
99036	2322303	2322302	44.7932	-55.6095	1002							0.00	2.92	999.08	S-D-s-mf
99036	2322310	2322309	44.7849	-55.6024	1085							0.00	0.00	1085.00	G-D-s-sc

Cruise #	Day/time (Huntec)	Day/time (Ship)	Latitude of ship (dec deg)	Longitude of ship (dec deg)	DTS (ms)	Depth from seafloor to reflections (ms)						Thickness of surface MTDs (ms)	Estimated total thickness failed (ms)	Depth to pre- failure seafloor from sea-level (ms)	Seafloor Character
						Q100	Q99	Q97	Q95	Q93	Q91				
99036	2322313	2322312	44.7816	-55.5995	1110		15.69	25.49	41.18	55.39	73.53				G-D-s-sc
99036	2322315	2322314	44.7793	-55.5974	1132		14.22	24.51	41.18	54.90	68.63				G-D-s-sc
99036	2322320	2322319	44.7735	-55.5924	1168		8.82	18.14	34.80	48.04	61.76				G-D-s-sc
99036	2322323	2322322	44.7699	-55.5894	1190		8.82	20.09	36.75	49.00	65.17				G-D-s-sc
99036	2322325	2322324	44.7676	-55.5874	1212		8.33	16.67	33.33	46.08	62.75				G-D-s-sc
99036	2322327	2322326	44.7644	-55.5845	1232		7.64	16.66	34.30	46.55	64.68				G-D-s-sc
99036	2322329	2322328	44.7630	-55.5833	1250		7.84	18.13	37.00	49.49	70.07				G-D-s-sc
99036	2322330	2322329	44.7618	-55.5823	1252	0.00	11.76	21.56	41.16	52.92	74.48				G-D-s-sc
99036	2322331	2322330	44.7607	-55.5812	1255	0.00	11.76	21.08	40.20	52.94	73.53				G-U-s
99036	2322332	2322331	44.7595	-55.5803	1265	0.00	10.78	22.55	40.20	53.43	72.55				G-U-s
99036	2322333	2322332	44.7580	-55.5789	1282		7.35	16.67	32.84	46.08	69.12	0.00	2.73	1279.27	G-U-s
99036	2322334	2322333	44.7572	-55.5782	1287		10.78	21.08	35.78	49.02	69.61	4.90	7.31	1284.59	F-D-u-mf
99036	2322335	2322334	44.7560	-55.5773	1284		8.33	16.67	34.31	45.10	65.69	0.00	6.34	1277.66	F-D-u-mf
99036	2322336	2322335	44.7541	-55.5756	1277		8.33	16.18	31.37	44.12	62.75				G-D-s-sc
99036	2322337	2322336	44.7538	-55.5753	1273		7.35	15.20	32.35	45.10	64.71				G-D-s-sc
99036	2322338	2322337	44.7526	-55.5744	1286		8.33	16.18	34.31	48.04	66.18				S-D-s-sp
99036	2322340	2322339	44.7503	-55.5725	1345							11.70	8.78	1347.92	F-D-h-mf
99036	2322342	2322341	44.7480	-55.5705	1354		18.14	29.41				12.16	8.29	1357.87	F-D-h-mf
99036	2322343	2322342	44.7470	-55.5695	1352	0.00	14.71	25.50	42.65	57.84	77.45	0.00	0.00	1352.00	F-D-h-mf
99036	2322345	2322344	44.7442	-55.5669	1359	0.00	13.72	25.00	41.66	55.88	76.00				F-U-s
99036	2322348	2322347	44.7412	-55.5644	1416		0.00	13.24		39.22	58.82	0.00	9.26	1406.74	S-D-s-sc
99036	2322350	2322349	44.7387	-55.5623	1415		10.78	21.57	39.71	52.94	71.57	10.78	14.63	1411.15	F-D-s-mf
99036	2322355	2322354	44.7328	-55.5571	1456		8.33	19.61	37.35	52.00	72.55	8.33	15.11	1449.22	G-D-s-mf
99036	2322359	2322358	44.7281	-55.5533	1460		6.37	16.67	34.31	47.55	63.73	6.37	14.14	1452.23	G-D-s-mf
99036	2330002	2330001	44.7245	-55.5500	1507		0.00	11.76		37.25	53.00	0.00	12.68	1494.32	G-D-s-mf
99036	2330004	2330003	44.7221	-55.5479	1517	0.00	9.80	21.08	37.25	51.00	67.65				F-U-s
99036	2330007	2330006	44.7183	-55.5446	1542	0.00	8.82	18.63	33.36	46.08	62.75				G-U-s
99036	2330015	2330014	44.7088	-55.5364	1646	0.00	7.84	23.52	46.08	60.30	68.63	0.00	9.26	1636.74	S-D-s-mf
99036	2330016	2330015	44.7076	-55.5354	1659		2.94	16.67	39.73	54.90	64.71	2.94	8.78	1653.16	S-D-s-mf
99036	2330020	2330019	44.7030	-55.5316	1695		9.80	21.57	37.25	50.50	59.80	9.80	10.73	1694.07	G-D-s-mf
99036	2330025	2330024	44.6974	-55.5265	1730		8.82	19.61	30.88	45.59	54.90	8.82	10.24	1728.58	G-D-s-mf
99036	2330026	2330025	44.6962	-55.5255	1735	0.00	9.80	22.06		48.04	56.86	9.75	9.75	1735.00	G-U-s

Cruise #	Day/time (Huntec)	Day/time (Ship)	Latitude of ship (dec deg)	Longitude of ship (dec deg)	DTS (ms)	Depth from seafloor to reflections (ms)						Thickness of surface MTDs (ms)	Estimated total thickness failed (ms)	Depth to pre- failure seafloor from sea-level (ms)	Seafloor Character
						Q100	Q99	Q97	Q95	Q93	Q91				
99036	2330031	2330030	44.6897	-55.5199	1762	0.00	10.78	22.06	32.84	50.00	65.69				G-U-s
99036	2330035	2330034	44.6860	-55.5168	1794	0.00	10.78	22.55	32.35	50.50	64.71				G-U-s
99036	2330041	2330040	44.6791	-55.5108	1865	0.00	11.76	25.00	31.37	46.00	66.18				G-U-s
99036	2330050	2330049	44.6691	-55.5021	1922	0.00	12.75	26.96		53.92	75.50				G-U-s
99036	2330055	2330054	44.6635	-55.4971	1959	0.00	12.25	26.47							G-U-s
99036	2330100	2330059	44.6581	-55.4918	2005	0.00	12.45	25.50			72.54				G-U-s
99036	2330105	2330104	44.6524	-55.4865	2040	0.00	12.25	26.47							G-U-s
99036	2330115	2330114	44.6418	-55.4767	2107	0.00	11.00			53.40	68.63				F-U-s
99036	2330120	2330119	44.6364	-55.4715	2159	0.00	9.80			53.92	69.61				F-U-s
99036	2330125	2330124	44.6309	-55.4665	2223	0.00	7.84			51.00	65.37				F-D-s-sc
99036	2330135	2330134	44.6202	-55.4564	2306	0.00	11.76			53.92					F-U-s
91020	1700312	1700311	44.8115	-55.6880	855		0.00	5.11	14.31	26.06		0.00	4.08	850.92	S-D-s-mf
91020	1700313	1700312	44.8104	-55.6866	843		7.15	13.29	23.00	34.75		7.15	8.16	841.99	G-D-s-mf
91020	1700314	1700313	44.8094	-55.6853	840	0.00	8.18	15.84	26.57	38.00					G-U-s
91020	1700315	1700314	44.8083	-55.6839	838	0.00	9.20	19.93	31.17	42.41					G-U-s
91020	1700317	1700316	44.8062	-55.6813	833	0.00	10.20	20.95	32.70	45.48					G-U-s
91020	1700323	1700322	44.8005	-55.6734	842	0.00	16.35	28.60	43.44	55.70					G-U-s
91020	1700325	1700324	44.7985	-55.6706	855	0.00	14.30	27.59	41.39	55.19					G-U-s
91020	1700330	1700329	44.7932	-55.6637	892	0.00	14.30	28.11	41.39	55.19					G-U-s
91020	1700335	1700334	44.7878	-55.6572	932	0.00	13.29	26.57	38.84	53.14					G-U-s
91020	1700336	1700335	44.7868	-55.6558	948		8.18	21.46	33.22	44.97		4.60	8.16	944.44	S-D-h-mf
91020	1700340	1700339	44.7822	-55.6507	1016		4.60	15.84				2.56	8.67	1009.89	S-D-h-mf
91020	1700343	1700342	44.7788	-55.6470	1064		10.22	20.44	32.70	46.00		6.13	10.71	1059.42	G-D-s-mf
91020	1700345	1700344	44.7765	-55.6445	1074		7.15	16.86	27.59	40.88		3.58	9.69	1067.89	G-D-s-mf
91020	1700346	1700345	44.7752	-55.6433	1082		5.11	14.30	25.55	38.84		3.58	7.14	1078.44	G-D-s-mf
91020	1700347	1700346	44.7741	-55.6422	1108		2.55	10.22	23.50	35.77		2.55	7.67	1102.88	S-D-s-sc
91020	1700348	1700347	44.7729	-55.6410	1140			7.67	24.32			3.58	8.20	1135.38	S-D-s-sc
91020	1700350	1700349	44.7709	-55.6382	1205		6.13	19.42				3.07	8.67	1199.40	S-D-s-er
91020	1700355	1700354	44.7644	-55.6325	1254		11.24	25.55	36.28	49.06		6.13	11.22	1248.91	G-D-h-mf
91020	1700358	1700357	44.7608	-55.6290	1286		7.67	20.95	34.24	46.00		4.09	8.67	1281.42	G-D-h-mf
91020	1700401	1700400	44.7572	-55.6256	1307		7.67	21.46	33.73	46.00		3.27	8.16	1302.11	F-D-u-mf
91020	1700405	1700404	44.7531	-55.6211	1322		6.13	17.37	29.64	41.39		6.13	12.24	1315.89	F-D-u-mf

Cruise #	Day/time (Huntec)	Day/time (Ship)	Latitude of ship (dec deg)	Longitude of ship (dec deg)	DTS (ms)	Depth from seafloor to reflections (ms)						Thickness of surface MTDs (ms)	Estimated total thickness failed (ms)	Depth to pre- failure seafloor from sea-level (ms)	Seafloor Character
						Q100	Q99	Q97	Q95	Q93	Q91				
91020	1700410	1700409	44.7471	-55.6151	1323		7.67	17.37	29.64	40.88		3.78	10.71	1316.07	F-D-u-mf
91020	1700412	1700411	44.7447	-55.6126	1336		5.62	16.86	29.13	40.88		3.07	9.69	1329.38	F-D-u-mf
91020	1700415	1700414	44.7411	-55.6090	1372		8.18	19.42	32.70	43.95		5.11	9.69	1367.42	F-D-u-mf
91020	1700420	1700419	44.7348	-55.6028	1419		4.60	16.35	29.13	41.90		4.60	11.73	1411.87	F-D-u-mf
91020	1700425	1700424	44.7287	-55.5970	1465		7.15	19.21	31.68	43.74		7.15	11.73	1460.42	F-D-u-mf
91020	1700428	1700427	44.7249	-55.5935	1500		5.11	17.89	30.15	42.41		5.11	11.22	1493.89	F-D-u-mf
91020	1700435	1700434	44.7159	-55.5865	1563		6.64	17.37	30.66	42.41		6.64	12.24	1557.40	F-D-u-mf
91020	1700440	1700439	44.7092	-55.5829	1622		5.11	15.33	27.08	41.39		5.11	13.26	1613.85	F-D-u-mf
91020	1700445	1700444	44.7025	-55.5798	1681		4.60	15.33	26.57	41.08		4.60	11.73	1673.87	F-D-u-mf
91020	1700450	1700449	44.6994	-55.5727	1718		2.56	14.30		37.30		2.56	9.69	1710.87	G-D-h-mf
91020	1700455	1700454	44.7034	-55.5649	1668		4.60	15.33	27.08	39.86		4.60	8.67	1663.93	S-D-s-mf
91020	1700459	1700458	44.7063	-55.5575	1659		4.60	15.84	27.59	39.86		4.60	9.18	1654.42	G-D-s-mf
91020	1700502	1700501	44.7088	-55.5524	1639		5.11	18.40	34.75			0.00	8.16	1630.84	G-D-s-mf
91020	1700509	1700508	44.7138	-55.5393	1585										G-D-s-sc
91020	1700515	1700514	44.7179	-55.5280	1663										G-D-s-sc
91020	1700524	1700523	44.7100	-55.5263	1638										G-D-s-sc
91020	1700530	1700529	44.7033	-55.5330	1695	0.00	10.20	18.36		41.82					G-U-s
91020	1700535	1700534	44.7059	-55.5383	1670	0.00	10.20	19.38	32.64	46.92					G-U-s
91020	1700540	1700539	44.7111	-55.5444	1630	0.00	10.20	17.34	30.60	42.84					G-U-s
91020	1700545	1700544	44.7168	-55.5505	1582	0.00	9.18	20.40	32.64	44.88					G-U-s
91020	1700548	1700547	44.7202	-55.5541	1555		5.10	19.38	31.62	43.86		5.10	8.16	1551.94	F-D-s-mf
91020	1700549	1700548	44.7213	-55.5554	1552		6.12	19.38	33.66	46.92		4.08	9.18	1546.90	F-D-s-mf
91020	1700550	1700549	44.7225	-55.5566	1542		4.08	19.38	35.70	47.94		4.08	8.16	1537.92	F-D-s-mf
91020	1700552	1700551	44.7248	-55.5590	1525				20.40						S-D-s-sc
91020	1700555	1700554	44.7282	-55.5625	1450				22.44						G-D-s-mf
91020	1700557	1700556	44.7306	-55.5649	1425	0.00	8.16	16.32	32.64	43.86					G-U-s
91020	1700559	1700558	44.7329	-55.5672	1408	0.00	8.16	18.36	33.66	47.94					G-U-s
91020	1700602	1700601	44.7364	-55.5708	1385	0.00	7.75	20.40	36.72	51.00					G-U-s
91020	1700605	1700604	44.7399	-55.5744	1363	0.00	8.57	19.38	32.64	47.94					G-U-s
91020	1700610	1700609	44.7457	-55.5801	1338	0.00	6.53	16.32	28.56	41.82					G-U-s
91020	1700612	1700611	44.7481	-55.5823	1330		5.71	15.00	28.56	40.80		4.08	6.12	1327.96	G-D-s-mf
91020	1700614	1700613	44.7503	-55.5844	1320		3.06	12.65	26.52	40.80		3.06	7.55	1315.51	G-D-s-mf

Cruise #	Day/time (Huntec)	Day/time (Ship)	Latitude of ship (dec deg)	Longitude of ship (dec deg)	DTS (ms)	Depth from seafloor to reflections (ms)						Thickness of surface MTDs (ms)	Estimated total thickness failed (ms)	Depth to pre- failure seafloor from sea-level (ms)	Seafloor Character
						Q100	Q99	Q97	Q95	Q93	Q91				
91020	1700615	1700614	44.7515	-55.5855	1310		4.08	14.28	29.00	41.82		4.08	7.14	1306.94	G-D-s-mf
91020	1700617	1700616	44.7537	-55.5880	1292		5.92	17.14	29.58	41.82		2.04	5.71	1288.33	G-D-s-mf
91020	1700620	1700619	44.7546	-55.5929	1290		5.50	14.28	28.56	42.84		2.04	5.10	1286.94	F-D-s-mf
91020	1700625	1700624	44.7573	-55.5979	1256		7.75	16.32	32.64	47.94		2.04	4.08	1253.96	G-D-s-mf
91020	1700628	1700627	44.7590	-55.5931	1245		9.18	18.36	32.65	48.55		2.04	4.08	1242.96	G-D-s-mf
91020	1700630	1700629	44.7572	-55.5905	1260		8.16	14.69	30.60	46.92		3.06	6.12	1256.94	G-D-s-mf
91020	1700635	1700634	44.7500	-55.5873	1329		4.08	13.87	26.11	38.76		4.08	13.26	1319.82	G-D-s-mf
91020	1700640	1700639	44.7428	-55.5832	1373		3.47	12.24	26.11	38.76		3.47	9.18	1367.29	G-D-s-mf
91020	1700642	1700641	44.7401	-55.5816	1395				17.34	28.56		17.34	8.16	1404.18	G-D-s-sp
91020	1700645	1700644	44.7361	-55.5795	1422				11.22	20.40		11.22	30.60	1402.62	G-D-h-sl
91020	1700650	1700649	44.7295	-55.5761	1478				14.28	23.46		14.28	29.58	1462.70	G-D-h-sl
91020	1700655	1700654	44.7224	-55.5723	1532				22.44	26.52		22.44	37.74	1516.70	G-D-h-sl
91020	1700659	1700658	44.7168	-55.5696	1573		6.53	18.36	30.60	40.80		6.53	10.20	1569.33	G-D-s-mf
91020	1700705	1700704	44.7082	-55.5652	1632		5.71		25.50	37.74		5.71	9.18	1628.53	G-D-s-mf
91020	1700710	1700709	44.7013	-55.5617	1685		8.16	16.32	27.54	40.80		8.16	10.20	1682.96	G-D-s-mf
91020	1700715	1700714	44.6943	-55.5593	1748		5.10	15.30	27.54			5.10	9.18	1743.92	G-D-s-mf
91020	1700720	1700719	44.6872	-55.5578	1793		8.16	19.79	31.00	46.92		8.16	11.22	1789.94	G-D-s-mf
91020	1700725	1700724	44.6801	-55.5559	1818		6.12	18.36	31.62	49.00		6.12	9.18	1814.94	G-D-s-mf
91020	1700730	1700729	44.6729	-55.5546	1848		11.83	24.48	35.70	55.08		8.16	10.20	1845.96	G-D-s-mf
91020	1700735	1700734	44.6657	-55.5529	1890		10.61	24.48	34.68	53.04		3.67	6.12	1887.55	G-D-s-mf
91020	1700740	1700739	44.6589	-55.5513	1941		14.28					0.00	0.00	1941.00	G-D-s-mf
91020	1700745	1700744	44.6519	-55.5523	1985		10.20	21.42	32.64	50.59					G-D-s-mf
91020	1700750	1700749	44.6450	-55.5538	2026		12.24	24.48		48.96					G-D-s-mf
91020	1700755	1700754	44.6381	-55.5558	2068		10.20	24.48		51.00		0.00	3.06	2064.94	G-D-s-mf
91020	1700757	1700756	44.6354	-55.5567	2080		14.28	27.54				5.10	5.10	2080.00	G-D-s-mf
91020	1700800	1700759	44.6313	-55.5578	2095		12.24					0.00	0.00	2095.00	G-D-s-mf
91020	1710444	1710443	44.8094	-55.7029	945							25.63	Indeterminate	Indeterminate	G-D-h-mf
91020	1710446	1710445	44.8076	-55.7061	1006							22.04	"	"	G-D-h-mf
91020	1710448	1710447	44.8058	-55.7094	978							19.48	"	"	G-D-h-mf
91020	1710449	1710448	44.8049	-55.7109	972							0.00	3.06	968.94	S-D-s-mf
91020	1710452	1710451	44.8023	-55.7157	1005							5.64	5.64	1005.00	S-D-s-mf
91020	1710454	1710453	44.8006	-55.7189	1042							6.15	6.15	1042.00	S-D-s-mf

Cruise #	Day/time (Huntec)	Day/time (Ship)	Latitude of ship (dec deg)	Longitude of ship (dec deg)	DTS (ms)	Depth from seafloor to reflections (ms)						Thickness of surface MTDs (ms)	Estimated total thickness failed (ms)	Depth to pre- failure seafloor from sea-level (ms)	Seafloor Character
						Q100	Q99	Q97	Q95	Q93	Q91				
91020	1710455	1710454	44.7997	-55.7205	1060							0.00	5.10	1054.90	S-D-s-sc
91020	1710458	1710457	44.7969	-55.7253	1100		2.05	10.25	18.45	33.83		0.00	7.65	1092.35	F-D-s-mf
91020	1710501	1710500	44.7942	-55.7301	1095		9.74	17.94	26.14	42.03		7.18	7.18	1095.00	G-D-s-mf
91020	1710503	1710502	44.7919	-55.7311	1115		9.74	16.61	26.63	41.51		7.18	7.18	1115.00	G-D-s-mf
91020	1710505	1710504	44.7905	-55.7286	1138		0.00	4.10	12.30	26.65		0.00	7.14	1130.86	S-D-s-sp
91020	1710506	1710505	44.7937	-55.7357	1169							21.53	Indeterminate	Indeterminate	F-D-h-mf
91020	1710507	1710506	44.7898	-55.7251	1181							29.73	"	"	F-D-h-mf
91020	1710510	1710509	44.7884	-55.7195	1180							9.22	"	"	F-D-h-mf
91020	1710511	1710510	44.7880	-55.7175	1186							7.18	"	"	F-D-h-mf
91020	1710513	1710512	44.7870	-55.7137	1159							0.00	"	"	G-D-s-mf
91020	1710520	1710519	44.7837	-55.7004	967	0.00	5.64	14.86	30.75	42.03					F-U-s
91020	1710525	1710524	44.7828	-55.6902	958	0.00	8.71	18.96	37.41	49.71					F-U-s
91020	1710530	1710529	44.7826	-55.6806	953	0.00	9.74	20.50	38.95	51.25					F-U-s
91020	1710535	1710534	44.7819	-55.6713	958	0.00	11.28	21.53	39.98	51.76					F-U-s
91020	1710540	1710539	44.7812	-55.6621	968	0.00	10.25	21.53	39.46	51.25					F-U-s
91020	1710542	1710541	44.7810	-55.6584	992		0.00		28.70			0.00	6.63	985.37	S-D-s-sp
91020	1710544	1710543	44.7807	-55.6546	1025				34.85			7.18	12.75	1019.43	G-D-s-mf
91020	1710545	1710544	44.7806	-55.6528	1045		5.64	18.45	31.26	43.05		4.10	9.69	1039.41	G-D-s-mf
91020	1710548	1710547	44.7802	-55.6472	1049	0.00	8.20	17.43	31.78	42.54		0.00	9.18	1039.82	G-D-s-mf
91020	1710550	1710549	44.7800	-55.6434	1035	0.00	11.79	18.96	33.83	45.10					G-U-s
91020	1710552	1710551	44.7797	-55.6396	1030	0.00	11.79	18.96	33.83	45.10		0.00	0.00	1030.00	F-D-s-sp
91020	1710553	1710552	44.7796	-55.6377	1037		7.69	16.40	29.73	42.54		4.10	8.16	1032.94	G-D-s-sc
91020	1710555	1710554	44.7793	-55.6339	1059			11.79	25.63	35.88		5.13	9.18	1054.95	G-D-s-sc
91020	1710558	1710557	44.7789	-55.6282	1090			11.28	23.58	33.83		4.61	9.18	1085.43	G-D-s-sc
91020	1710559	1710558	44.7788	-55.6262	1098			10.25	24.09	34.85		3.07	9.18	1091.89	G-D-s-sc
91020	1710600	1710559	44.7786	-55.6242	1120				5.13	14.35		5.13	30.60	1094.53	G-D-s-sc
91020	1710602	1710601	44.7784	-55.6203	1139				8.20	18.96	31.78	3.08	27.54	1114.54	G-D-h-mf
91020	1710604	1710603	44.7781	-55.6164	1140				11.28	22.55	39.00	5.64	25.50	1120.14	F-D-h-mf
91020	1710605	1710604	44.7780	-55.6143	1122		4.10	12.30	26.65	37.93	55.35	3.06	6.12	1118.94	F-D-s-sp
91020	1710607	1710606	44.7777	-55.6104	1120	0.00	8.20	16.40	31.78	42.54	58.94	2.20	5.10	1117.10	F-D-s-mf
91020	1710608	1710607	44.7776	-55.6084	1117	0.00	10.20	17.40	32.78	43.98	59.87	1.00	1.00	1117.00	F-D-s-mf
91020	1710609	1710608	44.7774	-55.6065	1118		9.23	17.43	32.78	43.98	62.25	3.06	3.06	1118.00	F-D-s-mf

Cruise #	Day/time (Huntec)	Day/time (Ship)	Latitude of ship (dec deg)	Longitude of ship (dec deg)	DTS (ms)	Depth from seafloor to reflections (ms)						Thickness of surface MTDs (ms)	Estimated total thickness failed (ms)	Depth to pre- failure seafloor from sea-level (ms)	Seafloor Character
						Q100	Q99	Q97	Q95	Q93	Q91				
91020	1710610	1710609	44.7773	-55.6045	1121			15.38	31.26	42.03	61.00	6.67	8.16	1119.51	F-D-s-mf
91020	1710611	1710610	44.7771	-55.6025	1129	0.00	9.23	18.45	34.34	45.61	65.60	0.00	0.00	1129.00	F-U-s
91020	1710612	1710611	44.7770	-55.6006	1140	0.00	7.18	17.94	34.85	46.13	69.70	0.00	3.06	1136.94	F-U-s
91020	1710615	1710614	44.7765	-55.5946	1167		6.67	17.22	32.80	44.08	71.75	2.87	5.10	1164.77	F-D-s-mf
91020	1710616	1710615	44.7762	-55.5927	1170	0.00	8.20	19.48	34.85	47.15	67.65	0.00	1.53	1168.47	F-D-s-mf
91020	1710619	1710618	44.7737	-55.5905	1180	0.00	8.20	19.48	34.85	47.15	67.65				F-U-s
91020	1710620	1710619	44.7729	-55.5912	1179	0.00	8.20	19.48	34.85	47.15	67.65	0.00	0.00	1179.00	F-D-s-gl
91020	1710624	1710623	44.7716	-55.5963	1179		9.23	20.50	35.88	47.66	70.73	4.41	0.00	1183.41	F-D-s-gl
91020	1710626	1710625	44.7703	-55.5997	1180	0.00	10.25	21.53	36.90	47.66	69.70	0.00	0.00	1180.00	F-U-s
91020	1710628	1710627	44.7691	-55.6033	1182	0.00	9.74	20.50	34.85	45.61	67.65				F-U-s
91020	1710632	1710631	44.7669	-55.6101	1201	0.00	8.71	18.45	32.80	43.56	63.55	20.50	20.50	1201.00	G-D-h-sl
91020	1710635	1710634	44.7655	-55.6151	1238				16.40	26.65	42.03	6.15	21.42	1222.73	G-D-h-sl
91020	1710637	1710636	44.7647	-55.6184	1265				27.68	34.85	51.25	12.30	13.77	1263.53	G-D-h-mf
91020	1710639	1710638	44.7637	-55.6216	1282				21.00	32.29	54.33	10.25	23.97	1268.28	G-D-h-mf
91020	1710641	1710640	44.7627	-55.6246	1272		8.20	20.50	34.34	46.13	69.19	4.10	5.61	1270.49	F-D-h-mf
91020	1710645	1710644	44.7603	-55.6308	1282		10.25	22.55	36.39	48.18	67.65	6.15	6.15	1282.00	F-D-h-mf
91020	1710650	1710649	44.7550	-55.6341	1335		7.18	20.50		37.41	57.40	4.10	5.10	1334.00	G-D-s-mf
91020	1710652	1710651	44.7526	-55.6350	1345		6.15	17.93		40.00	59.45	2.26	4.08	1343.18	G-D-s-mf
91020	1710654	1710653	44.7503	-55.6360	1367		5.64	18.45		41.51	63.55	0.00	3.06	1363.94	G-D-s-mf
91020	1710656	1710655	44.7480	-55.6372	1372		4.61	16.91	30.24	41.00	64.58	0.00	2.04	1369.96	F-D-s-mf
91020	1710701	1710700	44.7426	-55.6411	1390		7.18	19.48	34.34	45.10	68.68	2.05	4.08	1387.97	G-D-s-mf
91020	1710705	1710704	44.7381	-55.6440	1420		5.64	16.40	31.78	42.03	62.53	2.05	4.08	1417.97	G-D-s-mf
91020	1710710	1710709	44.7324	-55.6470	1452		8.20	20.50	34.85	46.13	68.68	3.59	5.10	1450.49	F-D-s-mf
91020	1710715	1710714	44.7267	-55.6505	1479		6.15	18.96	32.80	44.08	64.06	5.64	8.16	1476.48	G-D-s-mf
91020	1710720	1710719	44.7211	-55.6539	1530		7.18	20.50	34.85	45.61	63.03	7.18	10.20	1526.98	G-D-s-mf
91020	1710725	1710724	44.7155	-55.6574	1562							3.08	7.65	1557.43	G-D-s-mf
91020	1710730	1710729	44.7102	-55.6606	1585							0.00	8.25	1576.75	G-D-s-mf
91020	1710830	1710829	44.6639	-55.7280	1917		6.67	19.48		46.13	67.65	6.67	9.18	1914.49	F-D-s-mf
91020	1710832	1710831	44.6624	-55.7303	1920		6.15	19.48	33.83	47.15	70.21	6.15	8.67	1917.48	F-D-s-mf
91020	1710835	1710834	44.6604	-55.7338	1928		5.64	17.94	30.75	43.05	65.60	5.64	7.65	1925.99	F-D-s-mf
91020	1710837	1710836	44.6589	-55.7362	1938		6.15	18.66	31.78	45.61	68.68	6.15	8.16	1935.99	F-D-s-mf
91020	1710840	1710839	44.6568	-55.7398	1950		5.64	17.43		44.59	66.63	5.64	9.18	1946.46	F-D-s-mf

Cruise #	Day/time (Huntec)	Day/time (Ship)	Latitude of ship (dec deg)	Longitude of ship (dec deg)	DTS (ms)	Depth from seafloor to reflections (ms)						Thickness of surface MTDs (ms)	Estimated total thickness failed (ms)	Depth to pre- failure seafloor from sea-level (ms)	Seafloor Character
						Q100	Q99	Q97	Q95	Q93	Q91				
91020	1710845	1710844	44.6531	-55.7454	1970		5.13	18.45		39.00	63.55	5.13	9.18	1965.95	F-D-s-mf
91020	1710846	1710845	44.6524	-55.7465	1975		4.51	15.38	28.19	42.00	66.11	4.51	7.14	1972.37	F-D-s-mf
91020	1710850	1710849	44.6494	-55.7511	1980		3.59	14.86	27.68	42.00	65.09	3.59	7.14	1976.45	F-D-s-mf
91020	1710855	1710854	44.6485	-55.7583	1980		5.13	16.91	29.73	43.05	65.60	5.13	8.16	1976.97	G-D-s-mf
91020	1710901	1710900	44.6549	-55.7564	1952		4.10	15.89	28.19	41.51	64.06	4.10	9.18	1946.92	F-D-s-mf
91020	1710905	1710904	44.6531	-55.7513	1962		3.08	15.38	27.68	42.00	68.68	3.08	9.18	1955.90	F-D-s-mf
91020	1710910	1710909	44.6482	-55.7469	1994		6.15	16.40	32.29	46.64	73.29	6.15	10.71	1989.44	F-D-s-mf
91020	1710912	1710911	44.6462	-55.7452	2007		4.61	16.40		45.10	68.68	4.61	10.20	2001.41	F-D-s-mf
91020	1710913	1710912	44.6451	-55.7444	2011		4.10	15.38	29.21	43.05	66.63	4.10	8.16	2006.94	F-D-s-mf
91020	1710915	1710914	44.6431	-55.7426	2015		3.08	15.38	27.68	42.00	64.58	3.08	8.16	2009.92	F-D-s-mf
91020	1710920	1710919	44.6380	-55.7376	2019		10.25	22.04	33.31	49.20	71.75	10.25	10.25	2019.00	F-D-s-mf
91020	1710925	1710924	44.6328	-55.7326	2034		12.30	24.60	36.39	53.30	75.85	10.25	10.25	2034.00	F-D-s-mf
91020	1710927	1710926	44.6307	-55.7306	2042	0.00	10.25	22.04	34.34	51.76	73.80	0.00	0.00	2042.00	F-U-s
91020	1710928	1710927	44.6297	-55.7296	2050	0.00	9.74	21.53	32.80	49.71	71.75				F-U-s
91020	1710930	1710929	44.6276	-55.7276	2062	0.00	10.25	21.53	32.29	52.28	71.75				G-D-s-sp
91020	1710932	1710931	44.6255	-55.7257	2090					37.93		0.00	12.24	2077.76	G-D-s-sc
91020	1710934	1710933	44.6233	-55.7236	2115		9.23					6.15	8.16	2112.99	G-D-s-mf
91020	1710935	1710934	44.6223	-55.7227	2122		7.18					2.05	8.16	2115.89	G-D-s-mf
91020	1710937	1710936	44.6201	-55.7207	2139		6.15					0.00	4.08	2134.92	G-D-s-mf
91020	1710940	1710939	44.6170	-55.7175	2160		4.10		24.60	48.69	69.70				G-D-s-mf
91020	1710943	1710942	44.6139	-55.7143	2184		0.00		24.60	47.15	72.78	0.00	9.18	2174.82	G-D-s-mf
91020	1710945	1710944	44.6118	-55.7121	2197		7.00		29.21	51.25	76.88	7.00	12.24	2191.76	G-D-s-mf
91020	1710946	1710945	44.6108	-55.7109	2205						71.75	0.00	8.16	2196.84	G-D-s-mf
91020	1710948	1710947	44.6087	-55.7088	2235						34.85	11.28	61.20	2185.08	S-D-s-sp
91020	1710950	1710949	44.6068	-55.7064	2280						30.75	30.75	73.44	2237.31	G-D-h-mf
91020	1711840	1711839	44.6928	-55.5221	1760	0.00	11.22	24.48	36.23	48.96	59.12				S-U-s
91020	1711845	1711844	44.6849	-55.5222	1810	0.00	11.22	23.46	38.76	50.00	60.69				S-U-s
91020	1711850	1711849	44.6771	-55.5221	1857	0.00	10.71	22.44		50.00	59.67				S-U-s
91020	1711855	1711854	44.6692	-55.5223	1895	0.00	12.75	25.50	35.70		65.28				G-U-s
91020	1711856	1711855	44.6676	-55.5223	1902		13.77	26.52	37.23			0.00	0.00	1902.00	G-D-s-mf
91020	1711858	1711857	44.6644	-55.5224	1915		15.81	28.00	38.25			6.12	6.12	1915.00	G-D-s-mf
91020	1711900	1711859	44.6612	-55.5224	1935		11.22	23.46				0.00	0.00	1935.00	G-D-s-mf

Cruise #	Day/time (Huntec)	Day/time (Ship)	Latitude of ship (dec deg)	Longitude of ship (dec deg)	DTS (ms)	Depth from seafloor to reflections (ms)						Thickness of surface MTDs (ms)	Estimated total thickness failed (ms)	Depth to pre- failure seafloor from sea-level (ms)	Seafloor Character
						Q100	Q99	Q97	Q95	Q93	Q91				
91020	1711902	1711901	44.6581	-55.5224	1960	0.00	9.18	22.44							G-U-s
91020	1711905	1711904	44.6534	-55.5224	1998	0.00	10.20	22.44							G-U-s
91020	1711910	1711909	44.6456	-55.5224	2052	0.00	12.24								S-U-s
91020	1711915	1711914	44.6379	-55.5223	2137	0.00	13.77								G-U-s
91020	1711917	1711916	44.6348	-55.5222	2153		14.28					6.12	8.67	2150.45	G-D-u-mf
91020	1711919	1711918	44.6316	-55.5220	2172		10.20					7.65	8.67	2170.98	G-D-u-mf
91020	1711920	1711919	44.6301	-55.5220	2182		12.24					6.63	8.67	2179.96	G-D-u-mf
91020	1711922	1711921	44.6270	-55.5219	2198	0.00	13.77					0.00	1.02	2196.98	G-D-u-mf
91020	1711925	1711924	44.6223	-55.5217	2214	0.00	14.28								G-U-s
91020	1711926	1711925	44.6207	-55.5216	2221	0.00	14.28								G-U-s
91020	1711927	1711926	44.6190	-55.5216	2233		0.00					0.00	14.28	2218.72	G-D-s-sp
91020	1711935	1711934	44.6064	-55.5212	2290							13.04	14.28	2288.76	G-D-s-mf
91020	1711940	1711939	44.5984	-55.5213	2340							6.52	12.24	2334.28	G-D-s-mf
91020	1711945	1711944	44.5904	-55.5212	2409		15.30					4.89	5.10	2408.79	G-D-s-mf
91020	1711950	1711949	44.5824	-55.5212	2440		17.34					20.65	13.26	2447.39	F-D-s-mf
91020	1711954	1711953	44.5761	-55.5215	2451		11.22					16.31	14.28	2453.03	F-D-s-mf
91020	1712010	1712009	44.5509	-55.5211	2613		11.22								G-D-u-mf
91020	1712016	1712015	44.5416	-55.5212	2653		0.00					0.00	9.18	2643.82	G-D-u-mf
91020	1712020	1712019	44.5355	-55.5209	2688		8.71					8.71	10.20	2686.51	G-D-u-mf
91020	1712029	1712028	44.5220	-55.5207	2717		0.00					0.00	0.00	2717.00	G-D-u-mf
91020	1712030	1712029	44.5355	-55.5209	2720	0.00	9.18								G-U-s
91020	1712040	1712039	44.5122	-55.5226	2756	0.00	9.18								G-U-s
91020	1712045	1712044	44.5168	-55.5281	2742	0.00	10.20								F-U-s
91020	1712049	1712048	44.5181	-55.5345	2750		0.00					0.00	9.18	2740.82	F-D-s-mf
91020	1712050	1712049	44.5187	-55.5361	2758		5.13					5.13	11.73	2751.40	F-D-s-mf
91020	1712051	1712050	44.5188	-55.5376	2760		5.13					0.00	0.00	2760.00	F-D-s-mf
91020	1712055	1712054	44.5196	-55.5443	2752	0.00	10.20								F-D-u-mf
91020	1712340	1712339	44.5830	-55.7986	2335							0.00	37.74	2297.26	F-D-h-sl
91020	1712343	1712342	44.5837	-55.7941	2316							22.44	74.46	2263.98	F-D-h-sl
91020	1712345	1712344	44.5833	-55.7905	2317							22.44	76.50	2262.94	F-D-h-sl
91020	1712350	1712349	44.5828	-55.7804	2311							16.32	74.46	2252.86	F-D-h-sl
91020	1712355	1712354	44.5821	-55.7702	2310							18.36	73.44	2254.92	F-D-h-sl

Cruise #	Day/time (Huntec)	Day/time (Ship)	Latitude of ship (dec deg)	Longitude of ship (dec deg)	DTS (ms)	Depth from seafloor to reflections (ms)						Thickness of surface MTDs (ms)	Estimated total thickness failed (ms)	Depth to pre- failure seafloor from sea-level (ms)	Seafloor Character
						Q100	Q99	Q97	Q95	Q93	Q91				
91020	1720000	1712359	44.5816	-55.7599	2395							8.16	81.60	2321.56	F-D-s-mf
91020	1720005	1720004	44.5812	-55.7495	2391							5.10	73.44	2322.66	F-D-s-mf
91020	1720010	1720009	44.5811	-55.7394	2372							17.34	87.72	2301.62	F-D-h-sl
91020	1720015	1720014	44.5801	-55.7290	2381							21.42	81.60	2320.82	G-D-h-sl
91020	1720020	1720019	44.5793	-55.7187	2441							10.20	75.48	2375.72	G-D-s-gl
91020	1720022	1720021	44.5792	-55.7145	2472							0.00	77.52	2394.48	G-D-s-gl
91020	1720023	1720022	44.5791	-55.7124	2483							0.00	102.00	2381.00	G-D-h-mf
91020	1720024	1720023	44.5790	-55.7103	2510							24.48	85.68	2448.80	G-D-h-mf
91020	1720025	1720024	44.5789	-55.7082	2493							22.44	75.48	2439.96	G-D-h-mf
91020	1720030	1720029	44.5785	-55.6976	2360							44.88	91.80	2313.08	S-D-h-sp
91020	1720031	1720030	44.5784	-55.6943	2338										F-U-s
91020	1720033	1720032	44.5783	-55.6913	2354							38.76	87.72	2305.04	S-D-s-sp
91020	1720035	1720034	44.5781	-55.6871	2407							30.60	83.64	2353.96	F-D-h-mf
91020	1720037	1720036	44.5779	-55.6829	2419							20.40	87.72	2351.68	F-D-h-mf
91020	1720038	1720037	44.5778	-55.6808	2431							0.00	75.48	2355.52	F-U-s
91020	1720045	1720044	44.5794	-55.6669	2348				26.52	36.72		0.00	10.20	2337.80	S-D-s-sp
91020	1720050	1720049	44.5820	-55.6571	2315				34.68	44.88		4.08	12.24	2306.84	G-D-s-mf
91020	1720055	1720054	44.5836	-55.6467	2298					48.96		5.10	12.24	2290.86	F-D-s-mf
91020	1720100	1720059	44.5833	-55.6358	2309					51.00		5.10	14.28	2299.82	F-D-s-mf
91020	1720110	1720109	44.5827	-55.6143	2328				39.78	53.04		4.08	16.32	2315.76	F-D-s-mf
91020	1720112	1720111	44.5827	-55.6100	2329				36.72	51.00		0.00	10.20	2318.80	F-D-s-mf
91020	1720115	1720114	44.5826	-55.6036	2370				27.54	44.88		0.00	8.16	2361.84	F-D-s-mf
91020	1720120	1720119	44.5830	-55.5929	2366				41.82	57.12		7.14	14.28	2358.86	F-D-s-mf
91020	1720125	1720124	44.5832	-55.5823	2390				41.82	57.12		6.12	12.24	2383.88	F-D-s-mf
91020	1720130	1720129	44.5833	-55.5716	2390		4.08		40.80	57.12		4.08	14.28	2379.80	F-D-s-mf
91020	1720135	1720134	44.5832	-55.5611	2421		4.08			55.08		4.08	11.22	2413.86	F-D-s-mf
91020	1720140	1720139	44.5834	-55.5503	2397		7.14		44.88	63.24		3.68	7.14	2393.54	F-D-s-mf
91020	1720145	1720144	44.5834	-55.5397	2418		3.06		42.84	61.20		3.06	10.20	2410.86	F-D-s-mf
91020	1720148	1720147	44.5834	-55.5333	2424				38.76	56.10		0.00	8.57	2415.43	F-D-s-mf
91020	1720149	1720148	44.5835	-55.5312	2429					54.00		0.00	8.16	2420.84	F-D-s-mf
91020	1720150	1720149	44.5835	-55.5291	2426					56.10		4.08	10.20	2419.88	F-D-s-mf
91020	1720153	1720152	44.5836	-55.5231	2432							16.32	17.34	2430.98	F-D-s-mf

Cruise #	Day/time (Huntec)	Day/time (Ship)	Latitude of ship (dec deg)	Longitude of ship (dec deg)	DTS (ms)	Depth from seafloor to reflections (ms)						Thickness of surface MTDs (ms)	Estimated total thickness failed (ms)	Depth to pre- failure seafloor from sea-level (ms)	Seafloor Character
						Q100	Q99	Q97	Q95	Q93	Q91				
91020	1720155	1720154	44.5837	-55.5191	2437							17.34	17.34	2437.00	F-D-s-mf
91020	1720200	1720159	44.5840	-55.5092	2452							4.08	13.87	2442.21	F-D-s-mf
91020	1720205	1720204	44.5837	-55.4995	2449							10.20	12.24	2446.96	F-D-h-mf
91020	1720206	1720205	44.5836	-55.4975	2448	0.00	12.24					0.00	0.00	2448.00	F-D-h-mf
91020	1720210	1720209	44.5843	-55.4899	2428	0.00	10.20								F-U-s
91020	1720215	1720214	44.5809	-55.4856	2448	0.00	11.22								F-U-s
91020	1720220	1720219	44.5785	-55.4870	2461	0.00	11.22								F-U-s
91020	1720225	1720224	44.5808	-55.4918	2447	0.00	10.20								F-U-s
91020	1720230	1720229	44.5841	-55.4991	2447	0.00	11.22								F-U-s
91020	1720231	1720230	44.5845	-55.5006	2445	0.00	11.22					0.00	0.00	2445.00	F-U-s
91020	1720232	1720231	44.5850	-55.5021	2446							10.20	10.20	2446.00	F-D-s-mf
91020	1720235	1720234	44.5864	-55.5069	2449					48.96		5.10	20.40	2433.70	F-D-s-mf
91020	1720240	1720239	44.5901	-55.5145	2407		3.06			48.00		3.06	14.28	2395.78	F-D-s-mf
91020	1720245	1720244	44.5941	-55.5222	2364					51.00		5.10	16.32	2352.78	F-D-s-mf
91020	1720250	1720249	44.5981	-55.5304	2327		3.06			54.06		3.06	12.24	2317.82	F-D-s-mf
91020	1720255	1720254	44.6022	-55.5380	2306		4.08			56.10		4.08	11.22	2298.86	F-D-s-mf
91020	1720256	1720255	44.6031	-55.5396	2295	0.00	12.24			61.20		12.24	12.24	2295.00	F-D-s-mf
91020	1720259	1720258	44.6055	-55.5443	2262	0.00	13.26			58.14					F-U-s
91020	1720301	1720300	44.6069	-55.5473	2251	0.00	13.26			62.22		0.00	8.16	2242.84	F-U-s
91020	1720302	1720301	44.6077	-55.5489	2250		5.71			56.10		5.71	12.65	2243.06	F-D-s-mf
91020	1720305	1720304	44.6102	-55.5535	2240		3.06			52.02		3.06	12.24	2230.82	F-D-s-mf
91020	1720310	1720309	44.6142	-55.5614	2224		3.06			54.67		3.06	14.28	2212.78	F-D-s-mf
91020	1720315	1720314	44.6183	-55.5692	2197		3.06			47.94		3.06	15.30	2184.76	F-D-s-mf
91020	1720320	1720319	44.6224	-55.5769	2147		2.04	15.91	29.58	61.20		2.04	16.32	2132.72	F-D-s-mf
91020	1720325	1720324	44.6264	-55.5848	2100		4.08	17.34	30.60	59.16		4.08	12.65	2091.43	F-D-s-mf
91020	1720330	1720329	44.6304	-55.5925	2059		8.16	20.40	34.68	61.20		8.16	14.28	2052.88	F-D-s-mf
91020	1720335	1720334	44.6342	-55.6006	2044		6.12	18.36	31.62	56.50		6.12	13.26	2036.86	F-D-s-mf
91020	1720340	1720339	44.6381	-55.6086	2021		6.12	19.38	31.62	54.06		6.12	11.22	2015.90	F-D-s-mf
91020	1720345	1720344	44.6419	-55.6166	2000		9.18	21.42	33.66	56.10		9.18	13.26	1995.92	F-D-s-mf
91020	1720350	1720349	44.6456	-55.6247	1973		6.12	18.36	30.60	51.00		6.12	14.28	1964.84	F-D-s-mf
91020	1720355	1720354	44.6496	-55.6327	1962		5.71	17.34	29.58	47.94		5.71	13.87	1953.84	F-D-s-mf
91020	1720400	1720359	44.6535	-55.6410	1950		5.10	17.34	30.60	48.96		5.10	13.26	1941.84	F-D-s-mf

Cruise #	Day/time (Huntec)	Day/time (Ship)	Latitude of ship (dec deg)	Longitude of ship (dec deg)	DTS (ms)	Depth from seafloor to reflections (ms)						Thickness of surface MTDs (ms)	Estimated total thickness failed (ms)	Depth to pre- failure seafloor from sea-level (ms)	Seafloor Character
						Q100	Q99	Q97	Q95	Q93	Q91				
91020	1720405	1720404	44.6578	-55.6489	1914		4.08	14.28	28.56	43.86		4.08	12.24	1905.84	F-D-s-mf
91020	1720410	1720409	44.6619	-55.6570	1902		4.08	15.30	30.60	44.88		4.08	12.24	1893.84	F-D-s-mf
91020	1720415	1720414	44.6659	-55.6653	1896		4.08	15.30		42.84		4.08	10.20	1889.88	F-D-s-mf
91020	1720420	1720419	44.6708	-55.6724	1858		4.90	16.32	28.56	45.90		4.90	12.24	1850.66	F-D-s-mf
91020	1720425	1720424	44.6766	-55.6786	1838		2.45	14.28	24.48	38.76		2.45	11.22	1829.23	F-D-s-mf
91020	1720430	1720429	44.6821	-55.6844	1800		2.45	14.28	26.52	40.80		2.45	11.22	1791.23	F-D-s-mf
91020	1720435	1720434	44.6870	-55.6897	1760		3.06	16.32		38.76		3.06	12.24	1750.82	F-D-s-mf
91020	1720440	1720439	44.6914	-55.6951	1726		4.08	15.30		41.82		4.08	12.24	1717.84	F-D-s-mf
91021	1720455	1720454	44.7061	-55.7138	1535							0.00	11.22	1523.78	G-D-s-mf
91020	1720458	1720457	44.7093	-55.7179	1490	0.00	10.20	20.80	36.72	51.00					G-U-s
91020	1720500	1720459	44.7113	-55.7206	1463	0.00	11.22	22.44	37.74	48.96					G-U-s
91020	1720510	1720509	44.7220	-55.7342	1401	0.00	11.22	22.44	35.70	46.92					G-U-s
91020	1720511	1720510	44.7231	-55.7356	1407		9.18	18.36	33.66	44.88		9.18	9.18	1407.00	F-D-s-mf
91020	1720512	1720511	44.7242	-55.7368	1419		6.53	16.32	30.60	41.82		6.53	12.24	1413.29	F-D-s-mf
91020	1720514	1720513	44.7265	-55.7394	1420		0.00	10.20	23.46			0.00	6.12	1413.88	F-D-s-mf
91020	1720515	1720514	44.7276	-55.7408	1383		0.00	8.16	20.40	29.58		0.00	8.16	1374.84	G-D-s-sc
91020	1720520	1720519	44.7332	-55.7474	1330		4.08	14.28	27.54	37.74		3.06	10.20	1322.86	G-D-s-mf
91020	1720523	1720522	44.7366	-55.7515	1305		4.08	13.26	24.48	34.68		4.08	12.24	1296.84	G-D-s-mf
91020	1720524	1720523	44.7378	-55.7529	1310		0.00	8.16	20.40	27.54		0.00	12.24	1297.76	G-D-s-mf
91020	1720526	1720525	44.7401	-55.7557	1356							35.70	53.05	1338.65	G-D-s-sc
91020	1720528	1720527	44.7424	-55.7583	1425							22.44	42.84	1404.60	S-D-s-sc
91020	1720530	1720529	44.7448	-55.7611	1444							20.40	40.80	1423.60	F-D-u-mf
91020	1720535	1720534	44.7508	-55.7678	1430							24.48	39.78	1414.70	F-D-u-mf
91020	1720536	1720535	44.7519	-55.7692	1398		5.10	12.24	22.44			5.10	8.57	1394.53	S-D-s-sc
91020	1720540	1720539	44.7566	-55.7746	1352		8.16	14.28	25.90	36.11		8.16	11.22	1348.94	F-D-s-mf
91020	1720543	1720542	44.7598	-55.7795	1345			5.13	16.32	26.52		5.13	13.26	1336.87	F-D-s-mf
91020	1720545	1720544	44.7623	-55.7813	1370				7.14	15.30		0.00	14.28	1355.72	G-D-s-mf
91020	1720546	1720545	44.7635	-55.7827	1382							4.08	20.40	1365.68	G-D-s-mf
91020	1720548	1720547	44.7657	-55.7855	1382			0.00				6.12	22.44	1365.68	G-D-s-mf
91020	1720550	1720549	44.7679	-55.7883	1351			8.16	20.40	30.60		8.16	18.36	1340.80	F-D-s-mf
91020	1720552	1720551	44.7702	-55.7911	1349			0.00	12.24	23.46		0.00	20.40	1328.60	F-D-s-mf
91020	1720553	1720552	44.7713	-55.7925	1355				0.00	8.16		16.32	40.80	1330.52	G-D-s-sp

Cruise #	Day/time (Huntec)	Day/time (Ship)	Latitude of ship (dec deg)	Longitude of ship (dec deg)	DTS (ms)	Depth from seafloor to reflections (ms)						Thickness of surface MTDs (ms)	Estimated total thickness failed (ms)	Depth to pre- failure seafloor from sea-level (ms)	Seafloor Character
						Q100	Q99	Q97	Q95	Q93	Q91				
91020	1720555	1720554	44.7735	-55.7955	1387							18.36	51.00	1354.36	G-D-s-sp
91020	1720600	1720559	44.7788	-55.8027	1408							30.60	61.20	1377.40	F-D-u-mf
91020	1720603	1720602	44.7821	-55.8070	1383							22.44	61.20	1344.24	G-D-h-mf
91020	1720605	1720604	44.7842	-55.8099	1368							20.40	57.12	1331.28	G-D-h-mf
91020	1720606	1720605	44.7853	-55.8115	1364							14.28	59.16	1319.12	G-D-h-mf
91020	1720608	1720607	44.7874	-55.8144	1336							34.68	61.20	1309.48	G-D-h-mf
91020	1720610	1720609	44.7896	-55.8171	1300							42.84	72.00	1270.84	G-D-h-mf
91020	1720611	1720610	44.7909	-55.8186	1265							44.88	76.00	1233.88	G-D-h-mf
91020	1720612	1720611	44.7921	-55.8200	1238		9.80	17.34	25.50	34.68		8.16	9.87	1236.29	S-D-s-sp
91020	1720615	1720614	44.7956	-55.8239	1225		12.24	22.44	30.60	41.82		10.20	11.22	1223.98	F-D-s-mf
91020	1720616	1720615	44.7968	-55.8253	1220		12.24	21.42	32.64	42.84		10.20	11.22	1218.98	F-D-s-mf
91020	1720620	1720619	44.8017	-55.8309	1201		5.06	15.30	26.52	39.78		3.06	10.20	1193.86	G-D-s-mf
91020	1720622	1720621	44.8043	-55.8316	1177		5.06	15.30	24.48	36.72		3.06	10.70	1169.36	G-D-s-mf
91020	1720624	1720623	44.8055	-55.8289	1142		12.24	22.44	34.27	44.88		10.20	11.63	1140.57	G-D-s-mf
91020	1720625	1720624	44.8056	-55.8272	1140		11.22	23.36	32.64	42.24		9.79	11.22	1138.57	G-D-s-mf
91020	1720630	1720629	44.8059	-55.8174	1103		12.24	22.44	34.68	42.12		10.20	11.22	1101.98	G-D-s-mf
91020	1720631	1720630	44.8061	-55.8153	1109		11.22	21.42	25.76	41.76		9.79	10.20	1108.59	S-D-s-sp
91020	1720632	1720631	44.8062	-55.8133	1146							16.00	19.30	1142.70	S-D-s-sp
91020	1720634	1720633	44.8065	-55.8093	1230							18.32	19.57	1228.75	S-D-h-mf
91020	1720635	1720634	44.8066	-55.8075	1250							18.36	19.43	1248.93	F-D-h-mf
91020	1720638	1720637	44.8070	-55.8015	1248							3.06	11.22	1239.84	F-D-s-mf
91020	1720640	1720639	44.8072	-55.7978	1253							0.00	11.63	1241.37	F-D-s-mf
91020	1720641	1720640	44.8072	-55.7960	1250							0.00	11.22	1238.78	F-D-s-mf
91020	1720642	1720641	44.8074	-55.7941	1239							12.24	10.20	1241.04	G-D-u-mf
91020	1720643	1720642	44.8075	-55.7923	1229							0.00	11.22	1217.78	S-D-s-sc
91020	1720644	1720643	44.8076	-55.7904	1200							0.00	11.22	1188.78	S-D-s-sc
91020	1720645	1720644	44.8077	-55.7886	1170							15.30	18.00	1167.30	S-D-s-mf
91020	1720646	1720645	44.8078	-55.7867	1128							13.26	15.45	1125.81	S-D-s-mf
91020	1720647	1720646	44.8081	-55.7848	1092							7.18	11.22	1087.96	S-D-s-mf
91020	1720648	1720647	44.8084	-55.7831	1055							10.20	11.22	1053.98	S-D-s-mf
91020	1720649	1720648	44.8086	-55.7813	1140		9.79		24.48	37.74		9.79	11.22	1138.57	S-D-s-sp
91020	1720650	1720649	44.8089	-55.7793	1033		10.20		30.60	44.88		10.20	11.22	1031.98	F-D-s-mf

Cruise #	Day/time (Huntec)	Day/time (Ship)	Latitude of ship (dec deg)	Longitude of ship (dec deg)	DTS (ms)	Depth from seafloor to reflections (ms)						Thickness of surface MTDs (ms)	Estimated total thickness failed (ms)	Depth to pre- failure seafloor from sea-level (ms)	Seafloor Character
						Q100	Q99	Q97	Q95	Q93	Q91				
91020	1720652	1720651	44.8095	-55.7758	1049		10.20		32.64	48.96		10.20	11.22	1047.98	G-D-s-mf
91020	1720653	1720652	44.8098	-55.7741	1060							9.79	11.22	1058.57	G-D-s-mf
91020	1720654	1720653	44.8101	-55.7723	1071							10.20	10.20	1071.00	F-D-s-mf
91020	1720655	1720654	44.8104	-55.7705	1067							3.67	11.22	1059.45	F-D-s-mf
91020	1720659	1720658	44.8110	-55.7630	1014				21.42	33.66		7.14	24.48	996.66	G-D-s-mf
91020	1720701	1720700	44.8111	-55.7592	994				23.46	35.70		6.12	20.40	979.72	G-D-s-mf
91020	1720702	1720701	44.8113	-55.7575	980				17.34			2.06	18.36	963.70	G-D-s-sp
91020	1720704	1720703	44.8116	-55.7536	932			8.16	21.42	34.68		5.10	13.26	923.84	G-D-s-mf
91020	1720705	1720704	44.8118	-55.7518	920		6.12	13.26	26.93	40.40		5.10	12.24	912.86	F-D-s-mf
91020	1720710	1720709	44.8125	-55.7424	937		9.18	18.36	35.70	46.92		5.10	12.24	929.86	F-D-s-mf
91020	1720711	1720710	44.8127	-55.7406	940	0.00	10.20	20.40	35.70	48.96					F-D-s-mf
91020	1720715	1720714	44.8128	-55.7330	947	0.00	9.18	18.36	33.66	47.94		0.00	8.16	938.84	F-D-s-mf
91020	1720717	1720716	44.8126	-55.7293	979			8.16	21.42	37.74		7.14	18.36	967.78	G-D-s-mf
91020	1720718	1720717	44.8126	-55.7275	980							0.00	18.36	961.64	F-D-s-mf
91020	1720720	1720719	44.8125	-55.7235	955				10.20	26.52		0.00	12.24	942.76	S-D-s-sc
91020	1720723	1720722	44.8123	-55.7178	912		6.53	14.28	26.93	40.40		4.90	14.28	902.62	F-D-s-mf
91020	1720725	1720724	44.8123	-55.7138	903		8.16	14.69	26.93	43.86		4.08	8.16	898.92	F-D-s-mf
91020	1720726	1720725	44.8124	-55.7118	915		0.00	7.14	22.44	35.70		0.00	6.12	908.88	F-D-s-mf
91020	1720728	1720727	44.8124	-55.7050	960										F-D-s-sc
91020	1720732	1720731	44.8125	-55.6999	900										F-D-s-sc
91020	1720733	1720732	44.8125	-55.6980	923							20.40	44.88	898.52	F-D-s-mf
91020	1720735	1720734	44.8125	-55.6939	935							22.44	46.00	911.44	F-D-s-mf
91020	1720736	1720735	44.8126	-55.6918	935							22.44	48.96	908.48	F-D-s-mf
91020	1720738	1720737	44.8125	-55.6882	862							12.24	40.80	833.44	S-D-s-mf
91020	1720740	1720739	44.8124	-55.6842	818			11.22	21.42	33.66		8.16	20.40	805.76	S-D-s-mf
91020	1720745	1720744	44.8126	-55.6744	784		8.16	14.29	31.62	44.47		8.16	10.20	781.96	F-D-u-mf
91020	1720750	1720749	44.8129	-55.6644	773		11.22	19.38	35.70	50.00		7.14	7.14	773.00	F-D-u-mf
91020	1720755	1720754	44.8133	-55.6543	778		8.16	17.34	31.62	44.88		3.06	3.06	778.00	F-D-u-mf
91020	1720759	1720758	44.8134	-55.6462	777			21.42	36.72	50.00		12.24	12.24	777.00	F-D-u-mf
91020	1720802	1720801	44.8137	-55.6398	792			15.30	30.60	43.86		0.00	0.00	792.00	F-D-u-mf
91020	1720805	1720804	44.8137	-55.6336	810			16.32	31.62	44.88					F-D-u-mf
91020	1720806	1720805	44.8138	-55.6317	819				22.44	36.72		22.44	30.60	810.84	F-D-u-mf

Cruise #	Day/time (Huntec)	Day/time (Ship)	Latitude of ship (dec deg)	Longitude of ship (dec deg)	DTS (ms)	Depth from seafloor to reflections (ms)						Thickness of surface MTDs (ms)	Estimated total thickness failed (ms)	Depth to pre- failure seafloor from sea-level (ms)	Seafloor Character
						Q100	Q99	Q97	Q95	Q93	Q91				
91020	1720810	1720809	44.8139	-55.6231	845			12.24	24.48	37.74		12.24	20.40	836.84	F-D-u-mf
91020	1720813	1720812	44.8138	-55.6168	870		18.36	31.62	47.94	66.30		12.24	14.28	867.96	F-D-u-mf
91020	1720815	1720814	44.8139	-55.6125	905		4.50	14.28	28.56	38.76		4.50	17.34	892.16	F-D-u-mf
91020	1720817	1720816	44.8139	-55.6084	904			26.93	36.72	46.92		13.26	22.44	894.82	F-D-u-mf
91020	1720818	1720817	44.8140	-55.6063	900	0.00	11.22	21.42	30.60	43.25		0.00	0.00	900.00	F-D-u-sp
91020	1720820	1720819	44.8140	-55.6021	890	0.00	11.42	22.00	31.21	43.86					F-U-s
91020	1720822	1720821	44.8140	-55.5979	899	0.00	12.24	20.40	28.56	40.80					F-U-s
91020	1720824	1720823	44.8141	-55.5938	908							22.44	22.44	908.00	F-D-s-sc
91020	1720825	1720824	44.8145	-55.5918	928					30.60		30.60	46.92	911.68	F-D-s-mf
91020	1720830	1720829	44.8196	-55.5897	902					26.52		26.52	31.62	896.90	G-D-u-mf
91020	1720835	1720834	44.8239	-55.5947	850					17.34		17.34	28.56	838.78	G-D-u-mf
91020	1720840	1720839	44.8239	-55.6021	808					40.80		40.80	40.80	808.00	F-D-u-mf
91020	1720845	1720844	44.8217	-55.6090	842							27.54	32.64	836.90	G-D-s-mf
91020	1720850	1720849	44.8156	-55.6099	885				33.66			12.24	16.32	880.92	G-D-s-mf
91020	1720855	1720854	44.8098	-55.6121	950				32.64			4.08	16.32	937.76	G-D-s-mf
91020	1720859	1720858	44.8049	-55.6128	971				43.86			4.08	8.16	966.92	F-D-s-mf
91020	1720902	1720901	44.8014	-55.6134	968		14.69	24.48	41.82	56.03		4.08	10.20	961.88	F-D-s-mf
91020	1720905	1720904	44.7978	-55.6146	958	0.00	18.00	29.58	47.94	62.22		0.00	0.00	958.00	F-U-s
91020	1720909	1720908	44.7931	-55.6153	985	0.00	14.28	26.52	42.84	57.12					G-U-s
91020	1720912	1720911	44.7894	-55.6155	1016		8.16	20.40	36.72	50.00					G-D-s-sp
91020	1720913	1720912	44.7883	-55.6156	1028			10.20	25.50	38.76		0.00	12.24	1015.76	G-D-s-sc
91020	1720915	1720914	44.7859	-55.6158	1055			10.20	24.48	37.74		5.13	12.24	1047.89	G-D-s-sc
91020	1720917	1720916	44.7835	-55.6161	1075			8.16	23.36	36.72		3.00	14.36	1063.64	G-D-s-sc
91020	1720918	1720917	44.7824	-55.6164	1083			18.36	28.15	44.88		4.08	15.30	1071.78	G-D-s-gl
91020	1720919	1720918	44.7813	-55.6165	1096		4.08	18.36	28.56	46.92		4.08	12.34	1087.74	G-D-s-gl
91020	1720920	1720919	44.7801	-55.6168	1107		4.08	18.36	28.56	46.92		4.08	12.24	1098.84	G-D-s-sc
91020	1720921	1720920	44.7790	-55.6172	1121				8.16	22.44					G-D-s-sc
91020	1720922	1720921	44.7777	-55.6175	1150				8.16	22.44					G-D-s-sc
91020	1720925	1720924	44.7742	-55.6181	1200				6.53	20.40					G-D-s-sc
91020	1720929	1720928	44.7712	-55.6189	1255			6.13	14.28	27.54		0.00	35.70	1219.30	G-D-s-sc
91020	1720930	1720929	44.7683	-55.6193	1255			9.79	21.42	35.70		8.16	28.56	1234.60	F-D-h-mf
91020	1720931	1720930	44.7671	-55.6195	1258			12.24	23.46	37.74		10.20	16.28	1251.92	G-D-h-mf

Cruise #	Day/time (Huntec)	Day/time (Ship)	Latitude of ship (dec deg)	Longitude of ship (dec deg)	DTS (ms)	Depth from seafloor to reflections (ms)						Thickness of surface MTDs (ms)	Estimated total thickness failed (ms)	Depth to pre- failure seafloor from sea-level (ms)	Seafloor Character
						Q100	Q99	Q97	Q95	Q93	Q91				
91020	1720933	1720932	44.7647	-55.6198	1268			17.34	28.56	41.82		10.20	15.26	1262.94	G-D-h-mf
91020	1720935	1720934	44.7624	-55.6203	1280			24.48	36.72	51.00		12.24	11.22	1281.02	G-D-h-mf
91020	1720940	1720939	44.7568	-55.6215	1305			19.38	33.66	46.92		8.16	10.20	1302.96	G-D-s-mf
91020	1720945	1720944	44.7513	-55.6228	1331			16.32	32.00	44.88		0.00	3.06	1327.94	G-D-s-mf
91020	1720948	1720947	44.7478	-55.6238	1350			15.30	26.52	38.76					G-D-s-mf
91020	1720950	1720949	44.7457	-55.6249	1367			15.91	28.56	41.82		0.00	3.06	1363.94	G-D-s-mf
91020	1720955	1720954	44.7458	-55.6315	1405			10.20	26.52	38.76		6.12	14.69	1396.43	F-D-s-mf
91020	1720957	1720956	44.7481	-55.6324	1392					41.82		4.08	12.24	1383.84	G-D-s-mf
91020	1720958	1720957	44.7492	-55.6317	1385				21.42	34.68		0.00	10.20	1374.80	G-D-s-mf
91020	1721001	1721000	44.7524	-55.6282	1350			12.24	26.52	38.76		0.00	7.55	1342.45	G-D-s-mf
91020	1721005	1721004	44.7561	-55.6220	1310		5.10	16.32	30.60	44.88	60.18	5.10	10.20	1304.90	G-D-s-mf
91020	1721008	1721007	44.7590	-55.6172	1286			26.52	40.80	53.00	67.32	16.32	12.24	1290.08	G-D-s-mf
91020	1721010	1721009	44.7610	-55.6141	1261				20.40	32.64	40.80	4.08	7.14	1257.94	G-D-h-sl
91020	1721012	1721011	44.7629	-55.6110	1231			6.12	21.42	33.66	44.88	6.12	10.20	1226.92	G-D-h-sl
91020	1721013	1721012	44.7639	-55.6093	1214							15.30	15.30	1214.00	G-D-h-sl
91020	1721014	1721013	44.7649	-55.6077	1205	0.00	7.14	18.36	30.60	44.88	57.12				F-U-s
91020	1721015	1721014	44.7658	-55.6061	1200	0.00	8.16	18.36	31.00	45.90	59.16				F-U-s
91020	1721018	1721017	44.7688	-55.6013	1190	0.00	9.18	19.38	34.68	48.96	63.24				F-U-s
91020	1721019	1721018	44.7698	-55.5997	1184		8.16	18.36	31.62	46.92	61.20	3.06	6.12	1180.94	F-D-s-gl
91020	1721023	1721022	44.7744	-55.5962	1166		8.16	18.36	34.68	48.96	65.28	4.08	8.16	1161.92	F-D-s-gl
91020	1721025	1721024	44.7762	-55.5980	1152		8.16	18.36	34.68	48.96	65.28	4.08	8.16	1147.92	F-D-s-gl
91020	1721027	1721026	44.7766	-55.6009	1143		7.14	17.34	32.64	46.00	65.28	0.00	4.08	1138.92	F-U-s
91020	1721028	1721027	44.7765	-55.6024	1138	0.00	8.16	19.38	34.68	49.00	67.32	0.00	0.00	1138.00	F-U-s
91020	1721030	1721029	44.7761	-55.6055	1131		7.14	16.32	31.62	45.90		4.08	4.08	1131.00	F-D-s-mf
91020	1721032	1721031	44.7757	-55.6087	1139		4.10	13.26	28.56	41.82		2.04	8.16	1132.88	F-D-s-mf
91020	1721034	1721033	44.7755	-55.6121	1149			8.16	22.44	37.74		8.16	13.87	1143.29	F-D-s-sp
91020	1721035	1721034	44.7757	-55.6137	1167				10.20	24.48		0.00	25.50	1141.50	F-D-s-sc
91020	1721039	1721038	44.7760	-55.6203	1188				6.12	20.40					F-D-s-sc
91020	1721041	1721040	44.7761	-55.6236	1180							0.00	26.52	1153.48	G-D-s-mf
91020	1721045	1721044	44.7763	-55.6299	1163							4.08	25.50	1141.58	G-D-s-mf
91020	1721047	1721046	44.7766	-55.6333	1136							4.08	19.38	1120.70	G-D-s-sp
91020	1730449	1730448	44.6998	-55.7058	1245							0.00	Indeterminate	Indeterminate	F-D-u-mf

Cruise #	Day/time (Huntec)	Day/time (Ship)	Latitude of ship (dec deg)	Longitude of ship (dec deg)	DTS (ms)	Depth from seafloor to reflections (ms)						Thickness of surface MTDs (ms)	Estimated total thickness failed (ms)	Depth to pre- failure seafloor from sea-level (ms)	Seafloor Character
						Q100	Q99	Q97	Q95	Q93	Q91				
91020	1730455	1730454	44.7061	-55.7138	1258							25.62	"	"	F-D-u-mf
91020	1730459	1730458	44.7727	-55.7407	1272							34.85	"	"	G-D-u-mf
91020	1730503	1730502	44.7684	-55.7450	1300							41.00	"	"	G-D-u-mf
91020	1730506	1730505	44.7649	-55.7484	1325							42.03	"	"	G-D-u-mf
91020	1730510	1730509	44.7608	-55.7526	1350							35.88	"	"	G-D-u-mf
91020	1730515	1730514	44.7558	-55.7579	1395							26.65	"	"	G-D-u-mf
91020	1730518	1730517	44.7525	-55.7613	1415							23.58	"	"	G-D-u-mf
91020	1730525	1730524	44.7492	-55.7649	1460							22.55	"	"	G-D-s-mf
91020	1730530	1730529	44.7448	-55.7611	1476							23.58	"	"	F-D-s-mf
91020	1730532	1730531	44.7472	-55.7638	1455							15.25	"	"	F-D-s-mf
91020	1730535	1730534	44.7338	-55.7599	1380			0.00	9.22			0.00	15.30	1364.70	S-D-s-mf
91020	1730538	1730537	44.7350	-55.7547	1325		4.10					4.10	9.18	1319.92	G-D-s-mf
91020	1730540	1730539	44.7365	-55.7515	1308		5.13	14.35	27.16			5.13	10.20	1302.93	G-D-s-mf
91020	1730542	1730541	44.7381	-55.7480	1285	0.00	8.20	18.45	30.75	41.51		0.00	5.10	1279.90	S-D-s-sp
91020	1730543	1730542	44.7389	-55.7463	1273	0.00	8.40	18.45	31.78	43.05					G-U-s
91020	1730545	1730544	44.7401	-55.7427	1260	0.00	10.25	18.45	31.78	43.87					G-U-s
91020	1730550	1730549	44.7431	-55.7337	1232	0.00	11.79	21.53	34.85	47.66					G-U-s
91020	1730555	1730554	44.7461	-55.7248	1205	0.00	11.79	21.53	35.88	48.18					G-U-s
91020	1730557	1730556	44.7474	-55.7215	1202		4.10	13.84	27.16	40.00					F-u-s
91020	1730602	1730601	44.7504	-55.7141	1257							0.00	2.04	1254.96	F-D-s-mf
91020	1730603	1730602	44.7509	-55.7127	1260							6.66	9.18	1257.48	G-D-s-mf
91020	1730605	1730604	44.7522	-55.7100	1240							8.71	10.71	1238.00	G-D-s-mf
91020	1730606	1730605	44.7528	-55.7086	1233							2.05	8.67	1226.38	G-D-s-mf
91020	1730607	1730606	44.7535	-55.7070	1225							0.00	6.12	1218.88	S-D-s-sc
91020	1730609	1730608	44.7546	-55.7044	1195				24.60			0.00	6.63	1188.37	S-D-s-sc
91020	1730615	1730614	44.7579	-55.6962	1132				33.83			7.00	10.20	1128.80	G-D-s-mf
91020	1730620	1730619	44.7609	-55.6890	1105				33.31			7.18	10.71	1101.47	G-D-s-mf
91020	1730625	1730624	44.7637	-55.6822	1078							2.56	10.20	1070.36	G-D-s-mf
91020	1730630	1730629	44.7664	-55.6752	1060							2.56	6.12	1056.44	G-D-s-mf
91020	1730635	1730634	44.7689	-55.6686	1032							2.56	7.18	1027.38	F-D-s-mf
91020	1730640	1730639	44.7715	-55.6619	1038							3.08	5.10	1035.98	F-D-s-mf
91020	1730645	1730644	44.7742	-55.6551	1042							3.08	5.10	1039.98	F-D-s-mf

Cruise #	Day/time (Huntec)	Day/time (Ship)	Latitude of ship (dec deg)	Longitude of ship (dec deg)	DTS (ms)	Depth from seafloor to reflections (ms)						Thickness of surface MTDs (ms)	Estimated total thickness failed (ms)	Depth to pre- failure seafloor from sea-level (ms)	Seafloor Character
						Q100	Q99	Q97	Q95	Q93	Q91				
91020	1730753	1730752	44.7746	-55.6239	1213							4.61	28.05	1189.56	F-D-s-mf
91020	1730755	1730754	44.7748	-55.6280	1210							2.56	25.50	1187.06	F-D-s-mf
91020	1730756	1730755	44.7749	-55.6302	1209							0.00	22.44	1186.56	F-D-s-mf
91020	1730800	1730759	44.7746	-55.6386	1140		0.00	4.61		28.70					F-D-s-sc
91020	1730801	1730800	44.7738	-55.6402	1132		0.00	4.61	15.89	28.70		0.00	7.65	1124.35	G-D-s-sp
91020	1730805	1730804	44.7720	-55.6474	1105		10.25	20.50	32.80	51.76		4.61	5.10	1104.51	G-D-s-mf
91020	1730807	1730806	44.7739	-55.6495	1079		9.74	19.48	33.83	49.20		5.13	5.13	1079.00	G-D-s-mf
91020	1730810	1730809	44.7773	-55.6472	1071		13.12	22.00	35.88	50.75		8.00	6.12	1072.88	F-D-s-mf
91020	1730811	1730810	44.7784	-55.6460	1067	0.00	10.25	18.96	33.83	48.18		4.10	7.14	1063.96	F-D-h-mf
91020	1730813	1730812	44.7803	-55.6430	1035	0.00	11.28	16.91	32.29	46.64					G-U-h
91020	1730814	1730813	44.7806	-55.6411	1023	0.00	10.25	17.43	30.75	45.61					G-U-h
91020	1730816	1730815	44.7802	-55.6372	1022	0.00	5.64	12.30	26.65	42.54		2.05	5.10	1018.95	G-D-s-sp
91020	1730818	1730817	44.7798	-55.6332	1050		4.61	12.30	25.11	40.00		2.05	7.14	1044.91	G-D-s-sc
91020	1730820	1730819	44.7797	-55.6295	1068		3.59	12.30	23.58	38.95		2.05	7.14	1062.91	G-D-s-sc
91020	1730823	1730822	44.7796	-55.6249	1084		4.10	13.33	24.60	38.95		4.10	8.67	1079.43	G-D-s-sc
91020	1730825	1730824	44.7795	-55.6216	1107				5.13	17.94		5.13	27.03	1085.10	F-D-s-sc
91020	1730826	1730825	44.7795	-55.6201	1110				4.10	18.96		4.10	27.03	1087.07	F-D-s-sc
91020	1730827	1730826	44.7795	-55.6185	1113		5.13	14.04	25.63	42.00		5.13	11.22	1106.91	F-D-s-mf
91020	1730828	1730827	44.7795	-55.6170	1119				7.68	22.55		4.10	28.56	1094.54	F-D-s-sc
91020	1730829	1730828	44.7795	-55.6155	1118		5.13	13.84	26.65	42.54		3.08	8.16	1112.92	F-D-s-mf
91020	1730830	1730829	44.7794	-55.6139	1116		6.36	16.40	29.73	46.13		3.59	7.14	1112.45	F-D-s-mf
91020	1730831	1730830	44.7794	-55.6124	1115		6.15	15.38	29.73	46.13		3.08	6.63	1111.45	F-D-s-mf
91020	1730833	1730832	44.7793	-55.6093	1105	0.00	9.23	18.45	31.78	47.15	65.60	0.00	3.06	1101.94	F-D-s-mf
91020	1730835	1730834	44.7792	-55.6062	1102	0.00	8.71	18.45	32.80	48.69	67.65				F-U-s
91020	1730837	1730836	44.7789	-55.6031	1112		5.13	14.60	30.75	45.10	67.14	0.00	2.55	1109.45	F-D-h-sp
91020	1730840	1730839	44.7786	-55.5984	1138		9.00	20.50	35.88	51.76	73.29	4.61	7.14	1135.47	F-D-s-mf
91020	1730845	1730844	44.7753	-55.5945	1160		8.61	19.48	34.34	49.20	68.16	4.61	6.12	1158.49	F-D-s-mf
91020	1730849	1730848	44.7717	-55.5985	1175		8.20	18.45	32.80	48.18	66.63	3.59	6.12	1172.47	F-D-s-mf
91020	1730850	1730849	44.7710	-55.6000	1174	0.00	9.74	20.71	34.85	49.20	64.58				F-U-h
91020	1730855	1730854	44.7671	-55.6072	1190	0.00	8.71	18.45	32.29	44.59	60.48				F-U-h
91020	1730857	1730856	44.7656	-55.6099	1200				30.75	44.08	58.43	21.00	24.48	1196.52	G-D-h-sl
91020	1730900	1730859	44.7634	-55.6143	1246				14.35	27.68		5.13	20.40	1230.73	G-D-h-sl

Cruise #	Day/time (Huntec)	Day/time (Ship)	Latitude of ship (dec deg)	Longitude of ship (dec deg)	DTS (ms)	Depth from seafloor to reflections (ms)						Thickness of surface MTDs (ms)	Estimated total thickness failed (ms)	Depth to pre- failure seafloor from sea-level (ms)	Seafloor Character
						Q100	Q99	Q97	Q95	Q93	Q91				
91020	1730903	1730902	44.7613	-55.6190	1280		18.96	27.68	43.56	57.91		18.96	11.22	1287.74	F-D-h-mf
91020	1730905	1730904	44.7611	-55.6226	1292		3.59	12.81	27.68	42.00		3.59	9.18	1286.41	F-D-h-mf
91020	1730910	1730909	44.7650	-55.6285	1263		10.25	20.50	33.83	49.71	69.70	5.13	8.16	1259.97	F-D-s-mf
91020	1730912	1730911	44.7674	-55.6273	1252		9.23	18.45	32.29	47.97	66.63	3.08	6.12	1248.96	F-D-s-mf
91020	1730914	1730913	44.7700	-55.6261	1250		8.20	16.91	28.19	41.51		2.56	8.16	1244.40	F-D-s-mf
91020	1730915	1730914	44.7713	-55.6259	1247		9.43	17.43	31.78	47.15		4.10	10.20	1240.90	G-D-h-mf
91020	1730917	1730916	44.7741	-55.6257	1231				2.05						S-D-s-sc
91020	1730918	1730917	44.7755	-55.6256	1200				4.10						S-D-s-sc
91020	1730919	1730918	44.7770	-55.6256	1160				5.13						S-D-s-sc
91020	1730920	1730919	44.7784	-55.6255	1125				19.48			0.00	16.32	1108.68	S-D-s-sp
91020	1730922	1730921	44.7813	-55.6254	1066		5.13	13.33	27.68			5.13	12.24	1058.89	S-D-s-sc
91020	1730925	1730924	44.7856	-55.6251	1015		10.25	20.00	35.88	47.66		6.15	7.14	1014.01	G-D-s-mf
91020	1730927	1730926	44.7885	-55.6247	998		9.74	21.00	34.85	49.71		4.61	5.10	997.51	G-D-s-mf
91020	1730930	1730929	44.7902	-55.6207	1002		10.25	22.55	37.41	51.76		6.15	7.14	1001.01	G-D-s-mf
91020	1730933	1730932	44.7873	-55.6178	1036			8.20	22.00	36.90		5.13	7.14	1033.99	G-D-s-gl
91020	1730935	1730934	44.7848	-55.6170	1064			9.23	23.58	37.41		4.10	15.30	1052.80	G-D-s-gl
91020	1730939	1730938	44.7795	-55.6155	1114			10.25	23.58	36.39		0.00	10.20	1103.80	G-D-s-gl
91020	1730940	1730939	44.7781	-55.6157	1138				7.69	23.58					G-D-s-sp
91020	1730942	1730941	44.7756	-55.6167	1173				7.69	23.58					G-D-s-sc
91020	1730943	1730942	44.7744	-55.6171	1198				7.69	23.58					G-D-s-sc
91020	1730945	1730944	44.7717	-55.6180	1230				8.20	22.55	36.39				G-D-s-sc
91020	1730946	1730945	44.7704	-55.6184	1245				9.23	24.60	40.00	4.10	24.48	1224.62	F-D-h-mf
91020	1730947	1730946	44.7691	-55.6185	1251					29.73	49.20	10.25	24.48	1236.77	F-D-h-mf
91020	1730948	1730947	44.7678	-55.6187	1252					41.00	58.44	8.20	17.85	1242.35	F-D-h-mf
91020	1730950	1730949	44.7652	-55.6185	1259					38.95	56.38	6.67	12.24	1253.43	F-D-h-mf
91020	1730952	1730951	44.7636	-55.6160	1261				23.58	36.90		11.28	14.79	1257.49	F-D-h-mf
91020	1730953	1730952	44.7631	-55.6143	1256				17.94	29.75	48.18	6.15	14.28	1247.87	G-D-h-sl
91020	1730954	1730953	44.7627	-55.6125	1244		0.00	10.25	21.53	35.88	56.38	7.69	17.34	1234.35	G-D-h-sl
91020	1730955	1730954	44.7622	-55.6106	1226	0.00	7.18	17.43	30.23	44.08	64.58				S-D-s-sp
91020	1730957	1730956	44.7612	-55.6068	1219	0.00	8.71	18.45	33.00	47.15					F-U-h
91020	1731000	1730959	44.7588	-55.6019	1240	0.00	10.76	21.53	35.88	50.23					G-U-h
91020	1731001	1731000	44.7588	-55.6019	1250	0.00	10.76	21.53	35.88	50.23		6.15	6.15	1250.00	G-D-s-mf

Cruise #	Day/time (Huntec)	Day/time (Ship)	Latitude of ship (dec deg)	Longitude of ship (dec deg)	DTS (ms)	Depth from seafloor to reflections (ms)						Thickness of surface MTDs (ms)	Estimated total thickness failed (ms)	Depth to pre- failure seafloor from sea-level (ms)	Seafloor Character
						Q100	Q99	Q97	Q95	Q93	Q91				
91020	1731005	1731004	44.7547	-55.5936	1286		7.18	16.91	30.75	45.10		3.08	7.65	1281.43	G-D-s-mf
91020	1731008	1731007	44.7522	-55.5885	1308		6.15	15.38	28.70	41.00	61.50	2.56	8.16	1302.40	G-D-s-mf
91020	1731010	1731009	44.7505	-55.5851	1320		4.61	12.81	27.68	40.00	59.45	1.50	6.63	1314.87	F-D-u-mf
91020	1731013	1731012	44.7480	-55.5799	1223		5.13	12.30	27.68			5.13	8.67	1219.46	F-D-u-mf
91020	1731015	1731014	44.7464	-55.5764	1350	0.00	12.30	23.06	39.00	52.28	70.73	0.00	0.00	1350.00	G-D-s-sc
91020	1731016	1731015	44.7455	-55.5745	1353	0.00	12.81	23.37	39.46	53.10	70.73				F-U-s
91020	1731018	1731017	44.7439	-55.5711	1352	0.00	13.33	23.06	40.49	52.79	71.75				F-U-s
91020	1731019	1731018	44.7430	-55.5693	1363		10.25	21.53	38.44	52.28	69.70	10.25	13.77	1359.48	G-D-s-sp
91020	1731020	1731019	44.7422	-55.5677	1380		5.64	15.38	33.80	46.13	65.60	5.64	14.28	1371.36	G-D-s-sc
91020	1731022	1731021	44.7408	-55.5649	1418		3.08	13.33		41.00		3.08	13.26	1407.82	G-D-s-sc
91020	1731023	1731022	44.7402	-55.5634	1428		5.13	16.40				5.13	11.73	1421.40	G-D-s-sc
91020	1731025	1731024	44.7389	-55.5607	1430		11.78	23.06				6.67	7.65	1429.02	F-D-s-mf
91020	1731030	1731029	44.7362	-55.5543	1470		9.23	19.48	36.90	51.76		4.10	6.12	1467.98	G-D-s-mf
91020	1731035	1731034	44.7333	-55.5485	1520		10.25	23.58		56.38		5.13	6.63	1518.50	G-D-s-mf
91020	1731040	1731039	44.7303	-55.5426	1545		6.67	14.35				0.00	3.57	1541.43	G-D-s-mf
91020	1740133	1740132	44.8569	-55.8347	750							5.10	Indeterminate	Indeterminate	G-D-s-mf
91020	1740136	1740135	44.8528	-55.8346	777							6.21	"	"	G-D-s-mf
91020	1740140	1740139	44.8472	-55.8335	859							3.06	"	"	G-D-s-mf
91020	1740142	1740141	44.8444	-55.8334	901							4.59	"	"	G-D-s-mf
91020	1740144	1740143	44.8416	-55.8332	945							5.61	"	"	G-D-s-mf
91020	1740147	1740146	44.8376	-55.8330	968							9.18	"	"	G-D-s-mf
91020	1740150	1740149	44.8334	-55.8328	984							12.75	"	"	G-D-s-mf
91020	1740152	1740151	44.8306	-55.8329	992							0.00	"	"	G-D-s-mf
91020	1740153	1740152	44.8292	-55.8330	996				30.60			0.00	"	"	F-D-s-mf
91020	1740155	1740154	44.8264	-55.8331	983				41.31			7.14	"	"	F-D-s-mf
91020	1740157	1740156	44.8236	-55.8331	997				44.37			8.98	"	"	G-D-s-mf
91020	1740158	1740157	44.8224	-55.8332	1005				33.15			0.00	"	"	G-D-s-mf
91020	1740201	1740200	44.8183	-55.8331	1062				33.15						G-D-s-sc
91020	1740205	1740204	44.8128	-55.8332	1117				32.13	43.86					G-D-s-sc
91020	1740210	1740209	44.8060	-55.8331	1159		0.00	14.21	23.97	37.23		0.00	"	"	G-D-s-mf
91020	1740212	1740211	44.8034	-55.8331	1174		10.71	21.31	29.07	42.84		8.16	"	"	G-D-s-mf
91020	1740215	1740214	44.7998	-55.8327	1200		10.20	21.82	28.00	40.80		9.18	"	"	G-D-s-mf

Cruise #	Day/time (Huntec)	Day/time (Ship)	Latitude of ship (dec deg)	Longitude of ship (dec deg)	DTS (ms)	Depth from seafloor to reflections (ms)						Thickness of surface MTDs (ms)	Estimated total thickness failed (ms)	Depth to pre- failure seafloor from sea-level (ms)	Seafloor Character
						Q100	Q99	Q97	Q95	Q93	Q91				
91020	1740220	1740219	44.7928	-55.8330	1232		10.20	20.54	27.54	38.25		7.65	"	"	G-D-s-mf
91020	1740225	1740224	44.7861	-55.8328	1282		6.12	13.77	20.91	30.60		6.12	"	"	G-D-s-mf
91020	1740227	1740226	44.7834	-55.8327	1305		6.63	15.30	20.91	30.60		3.15	"	"	G-D-s-mf
91020	1740230	1740229	44.7792	-55.8327	1335		7.14	13.77	21.00	30.00		0.00	"	"	G-D-s-mf
91020	1740235	1740234	44.7725	-55.8327	1382		4.08		19.38	29.07					G-D-s-sc
91020	1740236	1740235	44.7712	-55.8327	1394							51.00	"	"	G-D-s-sp
91020	1740240	1740239	44.7662	-55.8330	1450							40.80	"	"	G-D-h-mf
91020	1740245	1740244	44.7598	-55.8356	1482							41.82	"	"	G-D-h-mf
91020	1740250	1740249	44.7532	-55.8387	1525							40.22	"	"	G-D-h-mf
91020	1740255	1740254	44.7467	-55.8417	1552							38.04	"	"	G-D-h-mf
91020	1740257	1740256	44.7439	-55.8431	1565							30.42	"	"	G-D-h-mf
91020	1740258	1740257	44.7427	-55.8436	1564							0.00	"	"	G-D-h-mf
91020	1740301	1740300	44.7389	-55.8452	1569							5.44	"	"	G-D-h-mf
91020	1740305	1740304	44.7338	-55.8477	1590							7.60	"	"	G-D-h-mf
91020	1740310	1740309	44.7274	-55.8514	1601							4.89	"	"	G-D-h-mf
91020	1740315	1740314	44.7214	-55.8544	1630							5.44	"	"	G-D-h-mf
91020	1740320	1740319	44.7141	-55.8576	1645							8.69	"	"	G-D-h-mf
91020	1740324	1740323	44.7087	-55.8582	1658							0.00	"	"	G-D-h-mf
91020	1740325	1740324	44.7087	-55.8596	1660										G-D-h-sc
91020	1740330	1740329	44.7089	-55.8470	1790							0.00	"	"	G-D-h-mf
91020	1740331	1740330	44.7094	-55.8451	1822							13.26	"	"	G-D-h-mf
91020	1740333	1740332	44.7107	-55.8411	1880							13.26	"	"	G-D-h-mf
91020	1740334	1740333	44.7113	-55.8393	1882							17.34	"	"	G-D-h-mf
91020	1740336	1740335	44.7125	-55.8352	1925							0.00	"	"	S-D-h-mf
91020	1740339	1740338	44.7139	-55.8289	1976							0.00	"	"	S-D-s-sc
91020	1740341	1740340	44.7149	-55.8247	1940							21.42	"	"	S-D-s-mf
91020	1740342	1740341	44.7154	-55.8226	1912							24.48	"	"	S-D-s-mf
91020	1740344	1740343	44.7161	-55.8188	1855							5.10	"	"	S-D-s-mf
91020	1740346	1740345	44.7168	-55.8153	1822							7.14	"	"	S-D-s-mf
91020	1740401	1740400	44.7221	-55.7896	1433	0.00	6.63	16.83	26.00	37.74	47.94				F-U-s
91020	1740405	1740404	44.7235	-55.7829	1421	0.00	7.65	17.85	28.56	39.27	50.00				F-U-s
91020	1740410	1740409	44.7254	-55.7746	1400	0.00	8.98	19.38	30.60	42.64	54.06				F-U-s

Cruise #	Day/time (Huntec)	Day/time (Ship)	Latitude of ship (dec deg)	Longitude of ship (dec deg)	DTS (ms)	Depth from seafloor to reflections (ms)						Thickness of surface MTDs (ms)	Estimated total thickness failed (ms)	Depth to pre- failure seafloor from sea-level (ms)	Seafloor Character
						Q100	Q99	Q97	Q95	Q93	Q91				
91020	1740415	1740414	44.7273	-55.7664	1370	0.00	9.70	20.91	32.13	43.86	56.10				F-U-s
91020	1740417	1740416	44.7282	-55.7632	1363	0.00	8.98	20.40	31.62	43.35	56.10	0.00	0.00	1363.00	F-D-s-sp
91020	1740418	1740417	44.7287	-55.7616	1363		6.63	17.34	29.07	40.29	53.04	6.63	9.18	1360.45	F-D-s-mf
91020	1740420	1740419	44.7295	-55.7584	1362		7.14	18.36	29.58	41.31	54.06	7.14	10.20	1358.94	F-D-s-mf
91020	1740425	1740424	44.7316	-55.7503	1350		5.61	17.34	28.56	41.31	55.08	4.08	10.20	1343.88	G-D-s-mf
91020	1740428	1740427	44.7327	-55.7454	1328		5.10	17.34	28.56	40.80	55.08	4.08	10.20	1321.88	G-D-s-mf
91020	1740430	1740429	44.7335	-55.7421	1316		6.12	16.83	29.58	41.82	55.60	4.08	9.69	1310.39	G-D-s-mf
91020	1740435	1740434	44.7365	-55.7352	1285		6.94	17.34	30.60	42.33	56.10	3.57	11.73	1276.84	G-D-s-mf
91020	1740436	1740435	44.7374	-55.7349	1274	0.00	9.69	20.40	33.15	45.39	61.20	0.00	0.00	1274.00	S-D-s-sp
91020	1740437	1740436	44.7386	-55.7349	1261	0.00	10.71	21.93	34.68	46.41	62.73				G-U-s
91020	1740440	1740439	44.7404	-55.7307	1245	0.00	11.73	22.44	34.68	47.94	66.30				G-U-s
91020	1740442	1740441	44.7382	-55.7278	1248	0.00	11.22	21.93	34.68	47.94	69.36				G-U-s
91020	1740443	1740442	44.7367	-55.7281	1256	0.00	10.20	20.40	32.64	45.90	66.30	0.00	0.00	1256.00	G-D-s-sp
91020	1740445	1740444	44.7349	-55.7306	1280		7.55	17.95	30.60	43.35	64.77	4.08	8.16	1275.92	G-D-s-mf
91020	1740448	1740447	44.7324	-55.7356	1308		6.94	17.34	30.09	42.02	60.18	3.88	8.16	1303.72	G-D-s-mf
91020	1740450	1740449	44.7302	-55.7380	1334		5.10	15.30	28.56	39.78	55.08	3.06	8.16	1328.90	G-D-s-mf
91020	1740451	1740450	44.7288	-55.7388	1350		0.00	10.20	24.48	34.68	48.96	0.00	8.67	1341.33	S-D-s-sc
91020	1740453	1740452	44.7263	-55.7404	1402				21.93						S-D-s-sc
91020	1740454	1740453	44.7250	-55.7415	1430		3.06					0.00	7.14	1422.86	F-D-s-sp
91020	1740455	1740454	44.7237	-55.7427	1444		5.10	16.32	29.07	41.82	62.22	5.10	10.20	1438.90	G-D-s-mf
91020	1740458	1740457	44.7202	-55.7459	1460		6.12	17.34	30.09	41.82	62.73	6.12	10.20	1455.92	G-D-s-mf
91020	1740501	1740500	44.7168	-55.7488	1484		6.12	17.85	29.07	42.84	60.18	6.12	11.73	1478.39	G-D-s-mf
91020	1740505	1740504	44.7119	-55.7533	1520		6.12	17.34	29.07	40.29	55.08	6.12	9.69	1516.43	G-D-s-mf
91020	1740510	1740509	44.7063	-55.7586	1548		7.14	18.36	29.07	40.29	55.08	5.10	8.16	1544.94	G-D-s-mf
91020	1740520	1740519	44.6944	-55.7678	1656		5.61	16.32	28.56	42.84	64.26	5.61	8.16	1653.45	G-D-s-mf
91020	1740525	1740524	44.6884	-55.7732	1690		5.61	16.83	28.05	42.33	60.18	5.61	11.73	1683.88	G-D-s-mf
91020	1740528	1740527	44.6848	-55.7764	1705		8.16	18.87	30.60	44.37	61.20	8.16	12.24	1700.92	G-D-s-mf
91020	1740530	1740529	44.6825	-55.7784	1711	0.00	11.73	22.95	33.66	47.94	63.75	0.00	0.00	1711.00	G-D-s-sp
91020	1740535	1740534	44.6769	-55.7834	1750	0.00	11.73	22.95	33.66	47.94	63.75	0.00	0.00	1750.00	G-D-s-sp
91020	1740536	1740535	44.6758	-55.7844	1760		6.94	17.14	28.56	42.02	55.08	5.61	10.20	1755.41	G-D-s-mf
91020	1740538	1740537	44.6735	-55.7864	1785		5.10	15.81		38.76	55.08	2.55	10.20	1777.35	G-D-s-mf
91020	1740540	1740539	44.6712	-55.7886	1810		5.10	16.83				0.00	10.20	1799.80	G-D-s-mf

APPENDIX 2

Downcore plots for each of the eighteen piston cores (PC). All cores have a 'PC lithology' and 'PC sediment color' column. These two columns are the result of a) description sheets from when the cores were first split and b) visual descriptions completed by the author. Cores that sampled disturbed sediments have a 'PC interpretation' column showing the interpreted MTD facies sampled by the core.

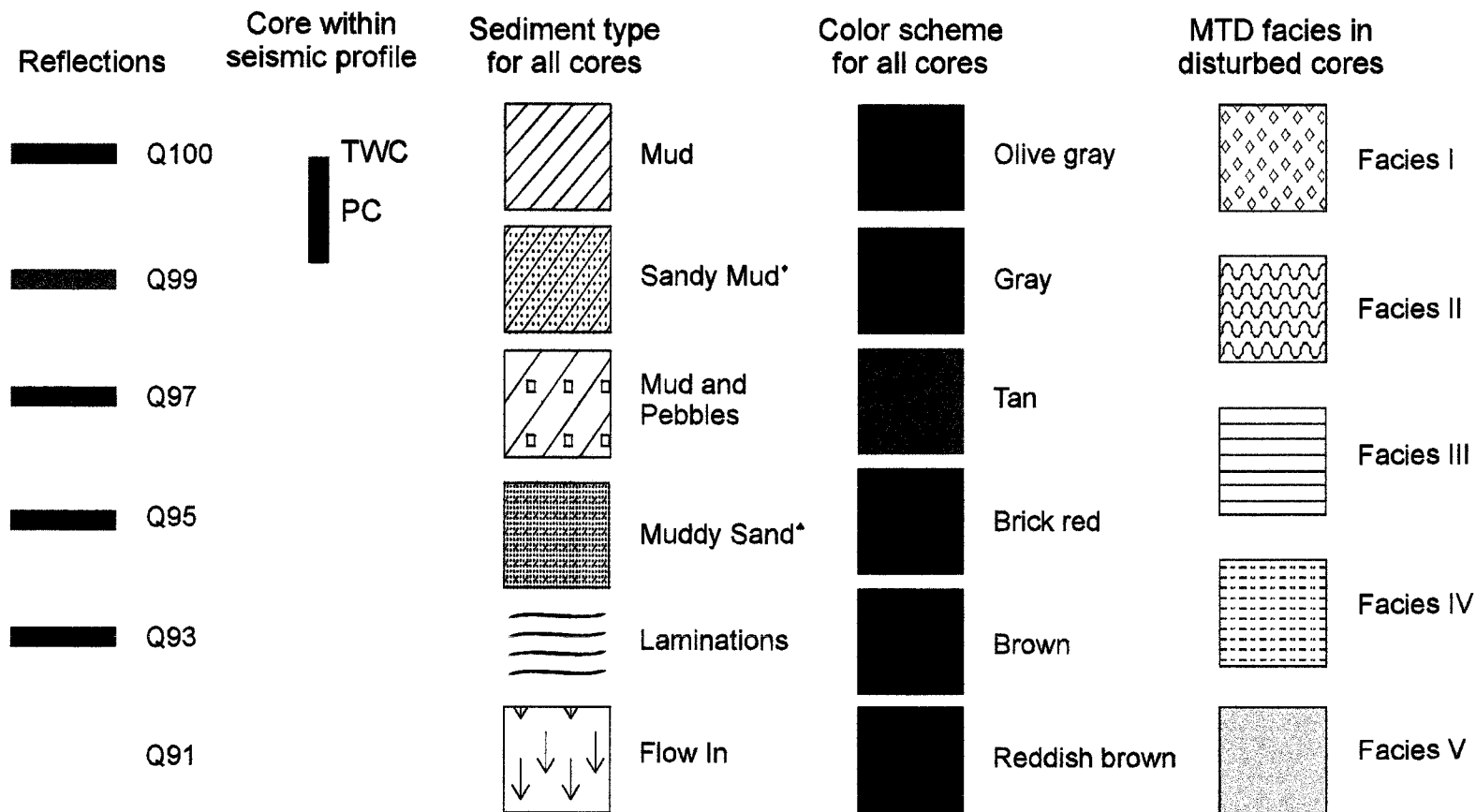
Depending on the year of acquisition, each core has columns for physical properties; older cores have minimal data and newer cores have a more complete analyses using MST and spectrophotometer equipment, i.e. magnetic susceptibility, bulk density, and L*, a*, and b* color measures.

Laminations within the 'PC lithology' column (seen as '~') signify grain size laminations. When placed in 'PC sediment color' columns, these symbols signify color laminations, e.g. laminated reddish-brown sediment- laminations apparent from subtle color variations.

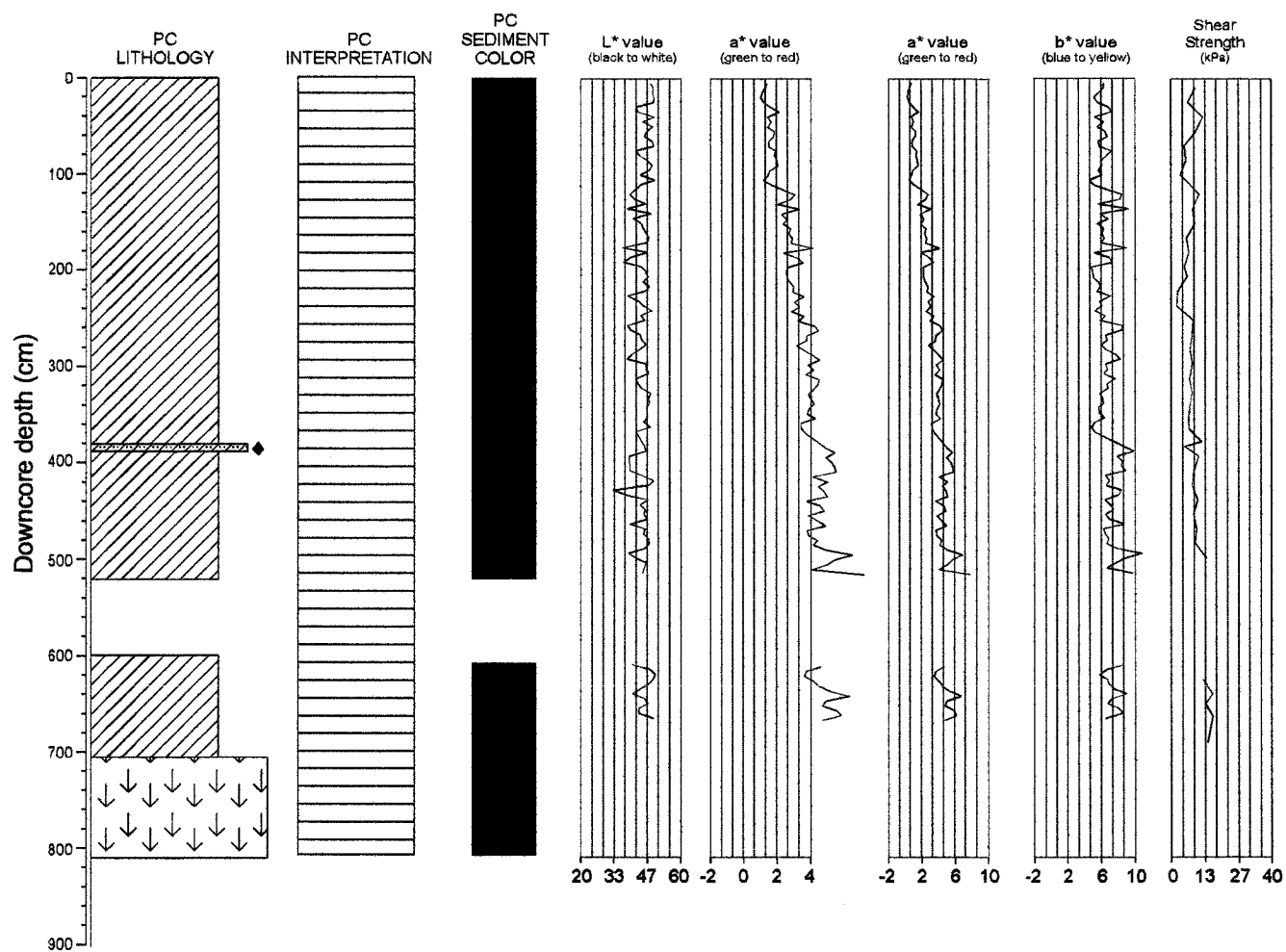
Following each downcore plot is a Hunttec DTS seismic reflection profile (supplementary 12 kHz or 3.5 kHz profile if Hunttec DTS was unavailable) showing the projected position of the piston core (PC), and for disturbed cores the associated trigger weight core (TWC), within the acoustic stratigraphy. MTD facies interpretations are included with the seismic reflection profile for cores sampling disturbed sediments. Reflections that could be traced onto the seismic profile are shown.

Only one core, 99036-05, does not have a complementary seismic reflection profile, because quality of the data over the core site is very poor.

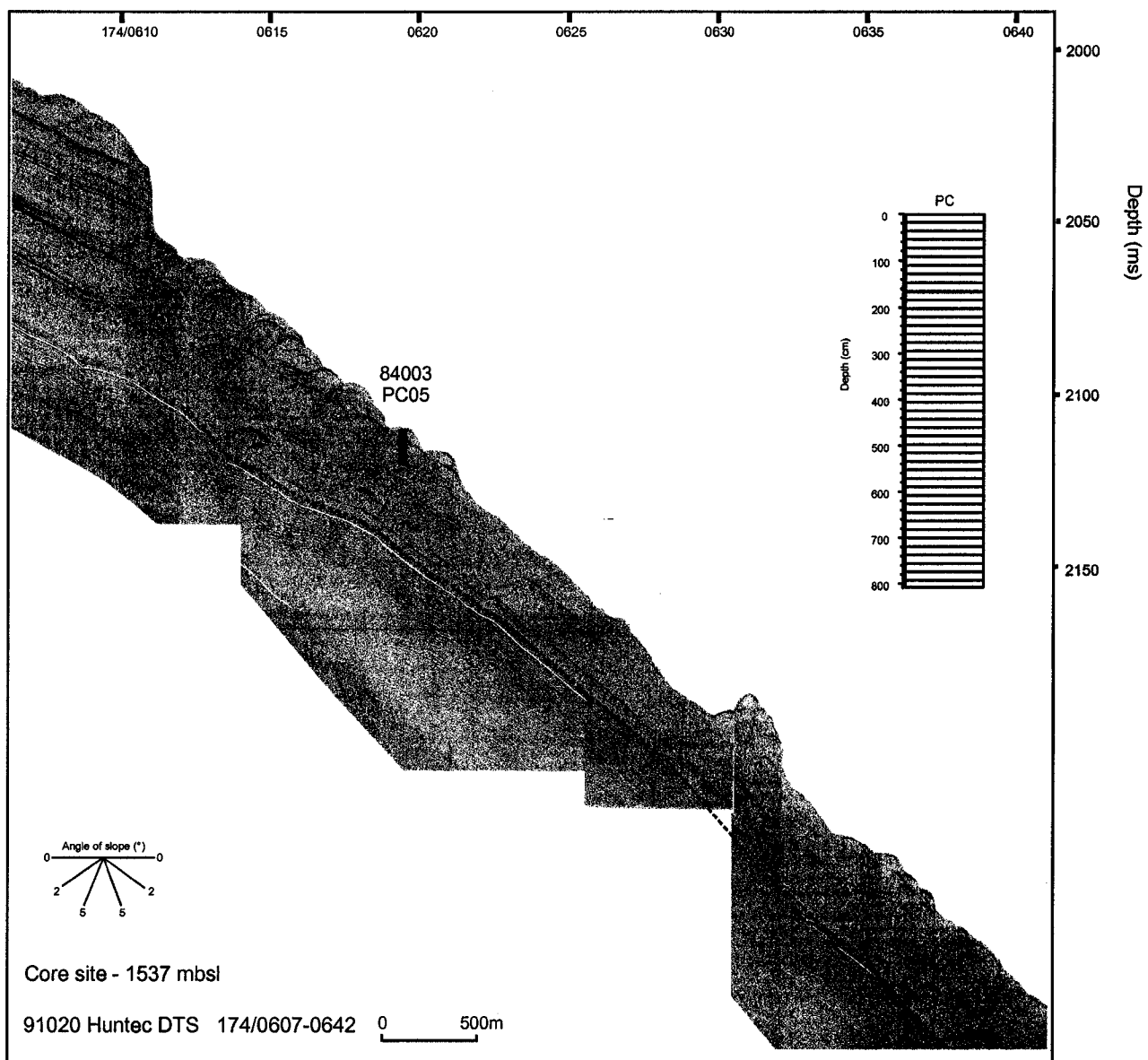
Downcore plots are in order of cruise, e.g. first plot in this Appendix is 84003-05, except for plot 90015-07 because it and 86034-03 are on the same page.



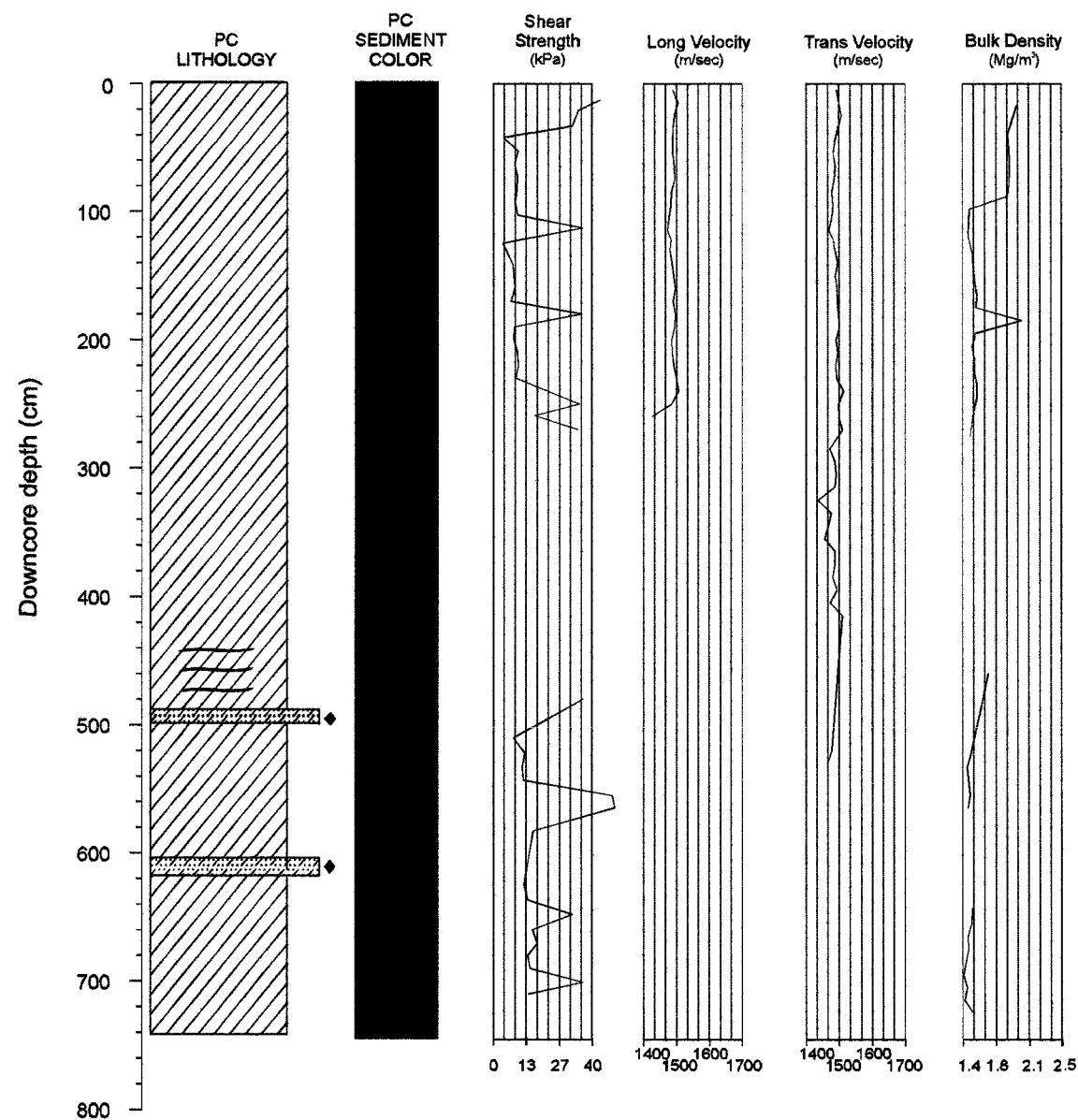
Legend for seismic reflection profiles and downcore description plots of the eighteen sediment cores from St. Pierre Slope. Some sediment type names have superscripts that aid in identifying thin layers in the downcore plots. 'Adjusted' values for the 'a' color trace are on a non-standard scale and are for comparison of reddish-brown to brownish-red sediments found in deeper water cores.



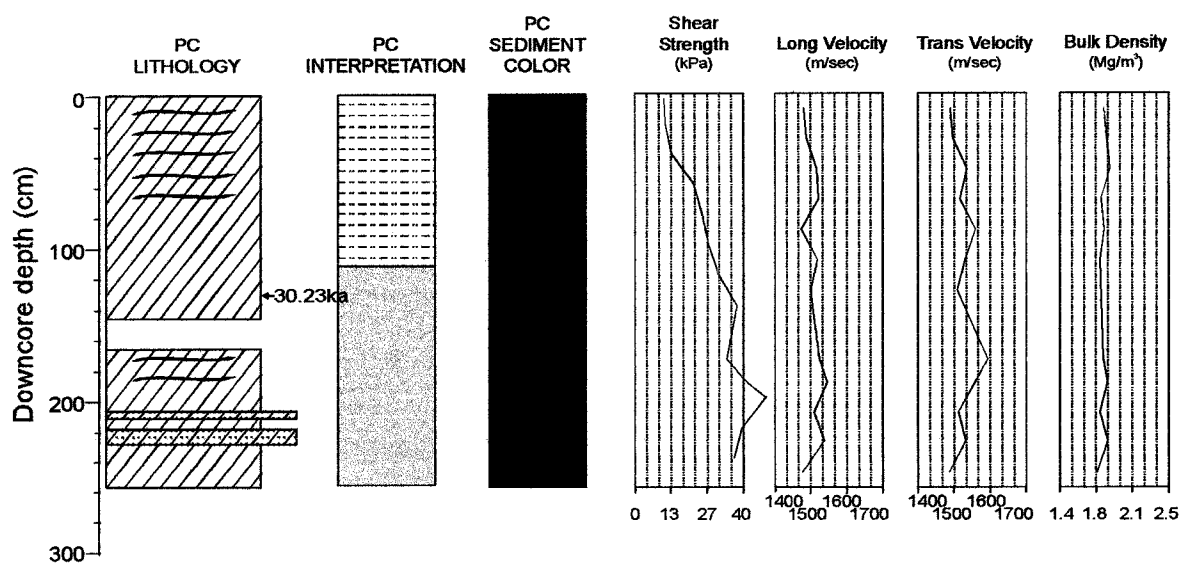
Downcore lithology, color, and physical property plots for piston core 05 obtained during cruise 84005. Downcore lithologies interpreted as MTD facies are shown.



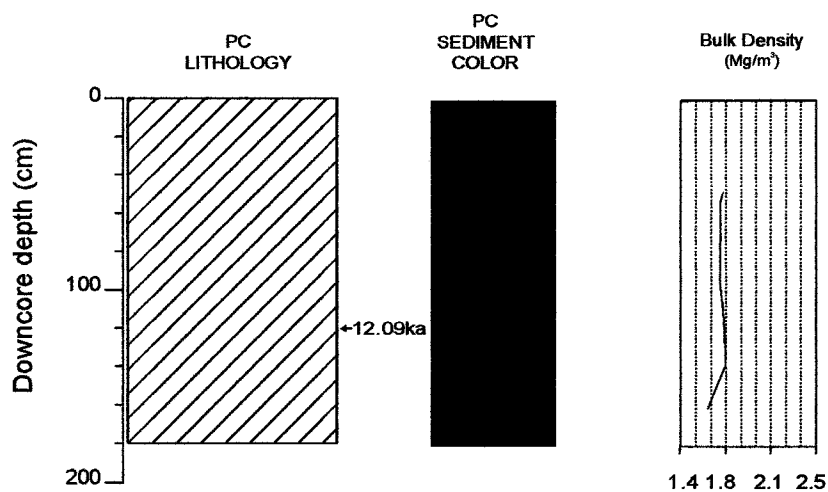
Relative position of piston (PC) core 05 from cruise 84003 within Hunttec DTS seismic reflection data.



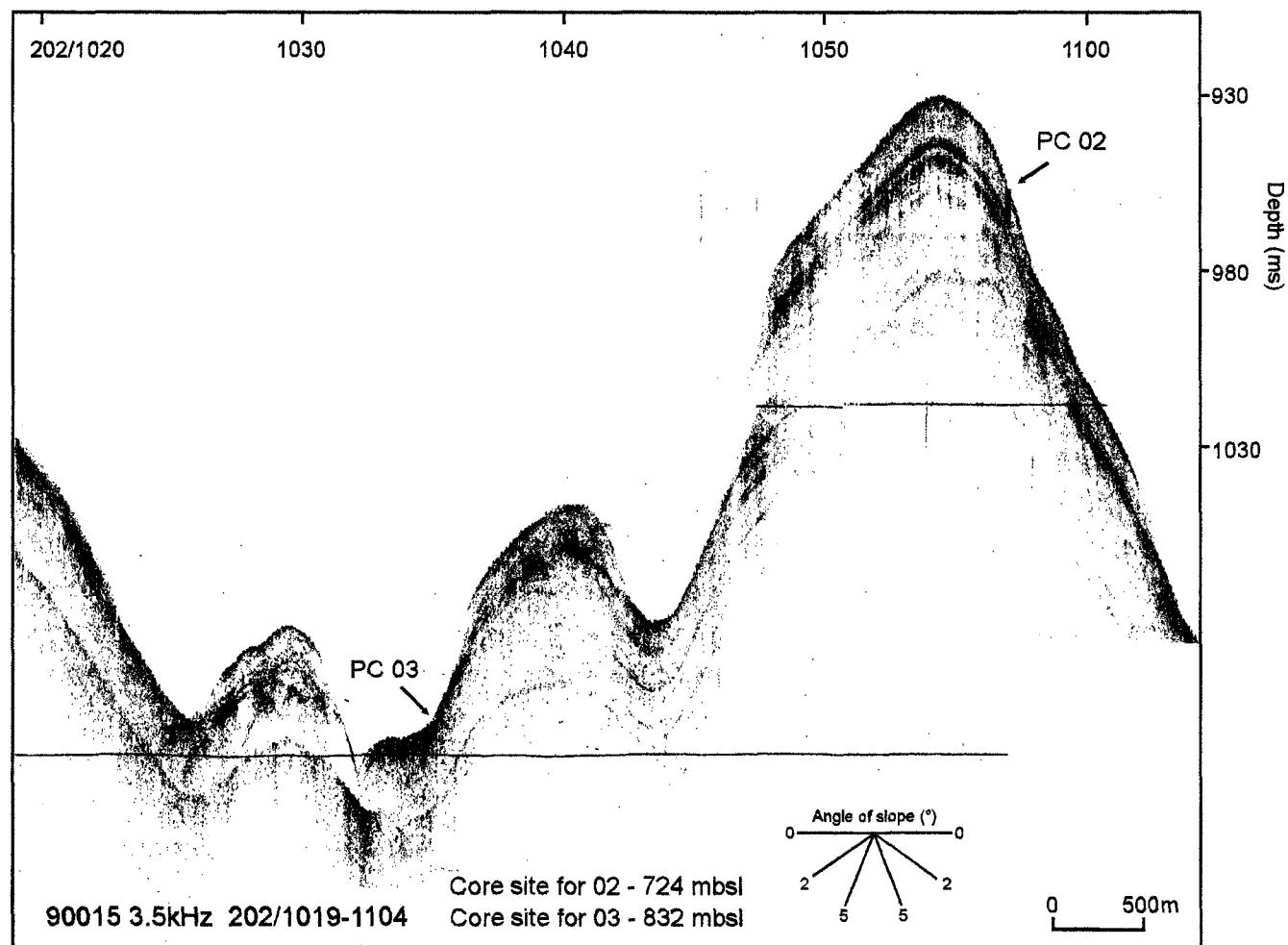
Downcore lithology, color, and physical property plots for piston core 02 obtained during cruise 86034. Cracking from 500-515 cm.



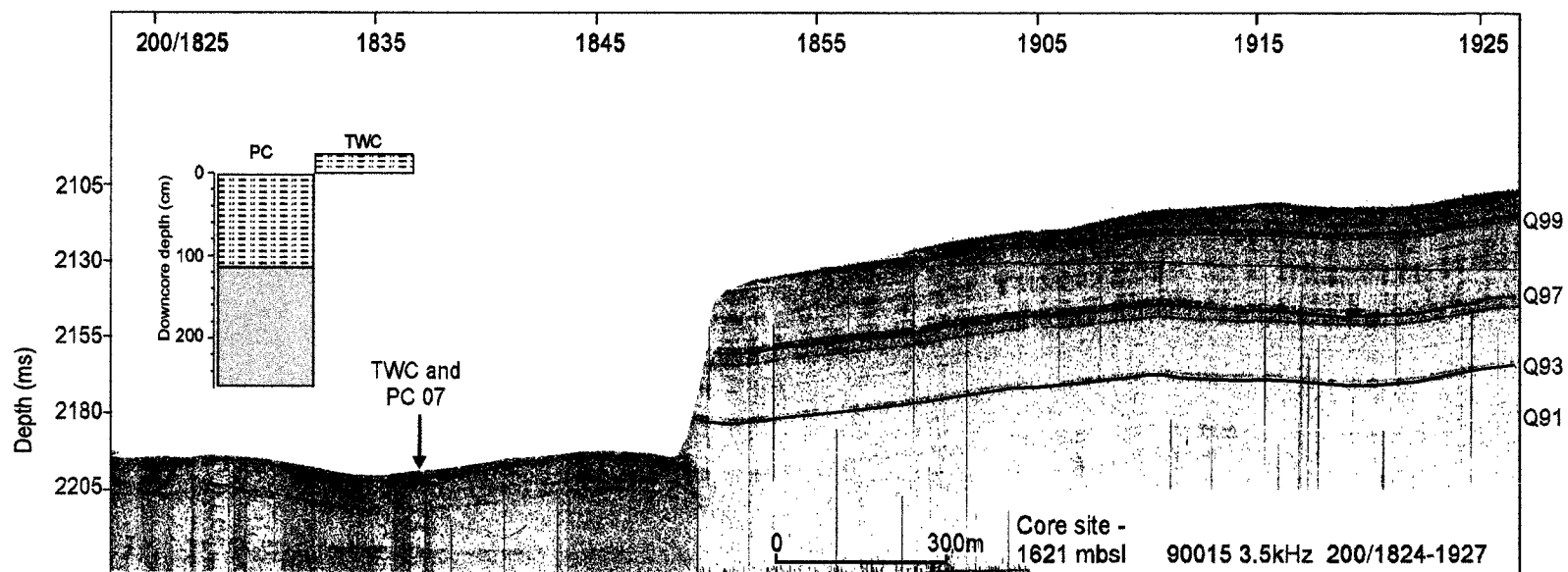
Downcore lithology, color, and physical property plots for piston core 07 obtained during cruise 90015. See text for detailed discussion concerning this core.



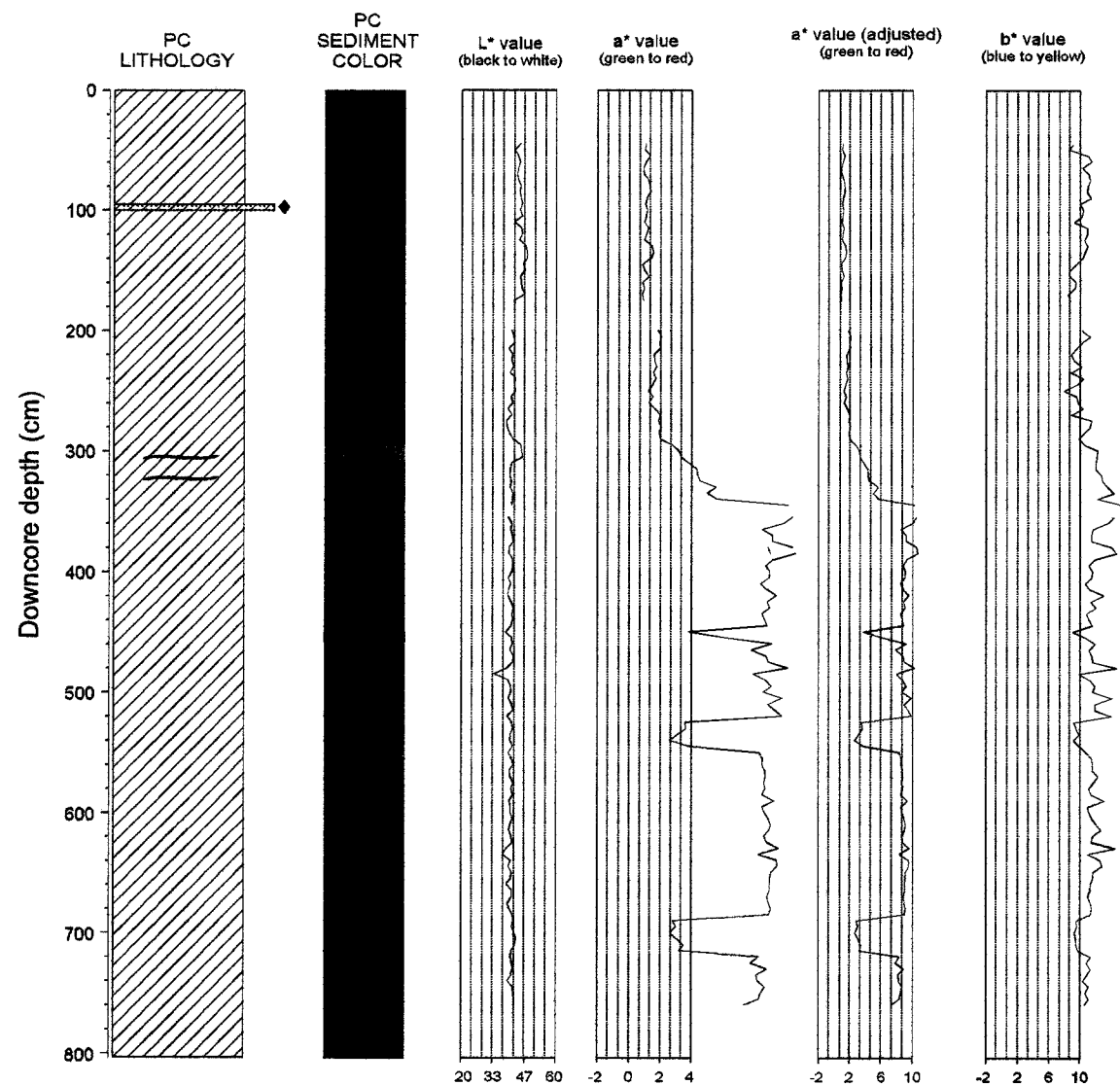
Downcore lithology, color, and physical property plots for piston core 03 obtained during cruise 86034.



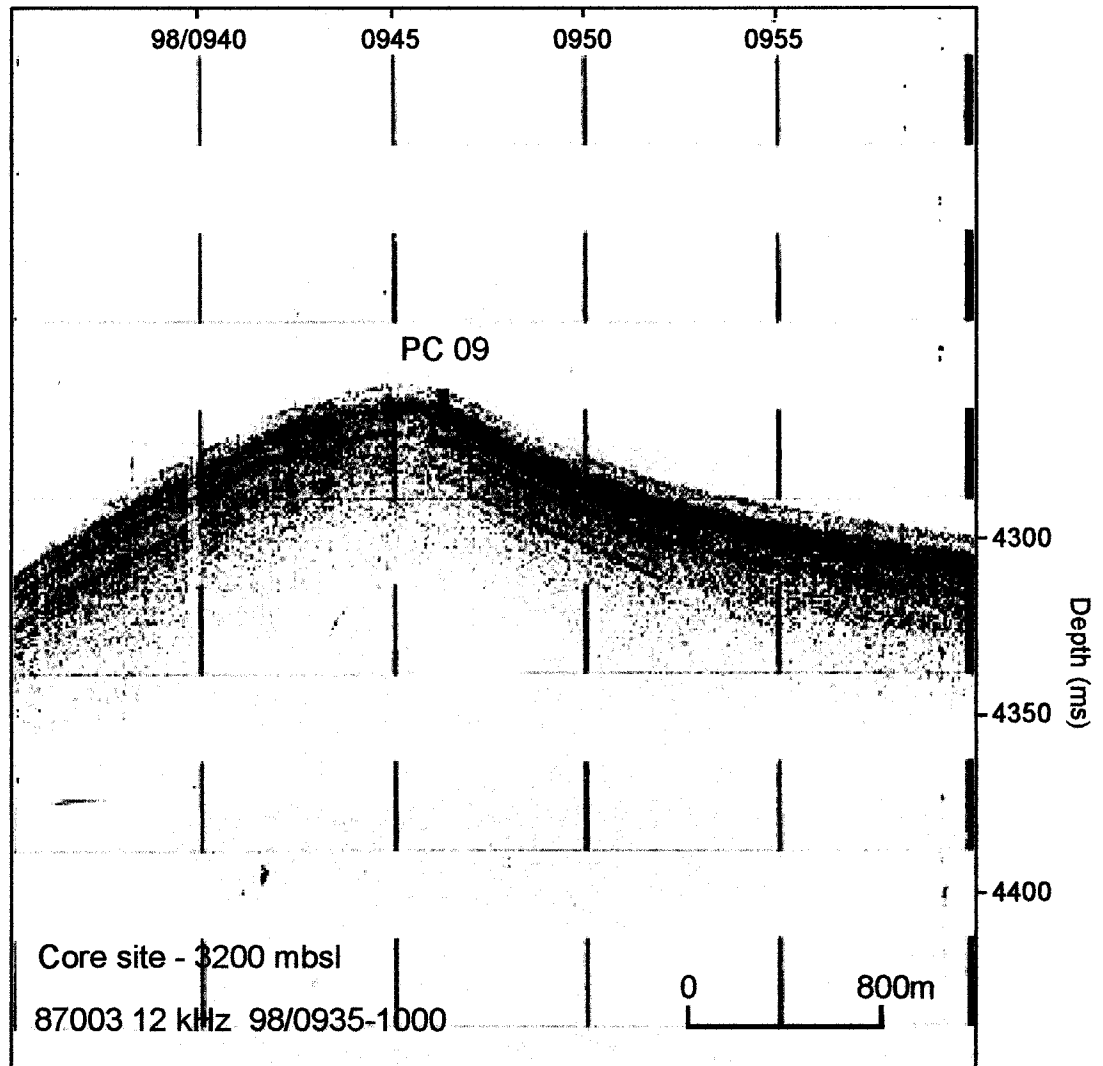
Relative position of piston cores (PC) 02 and 03 from cruise 86034 within 3.5 kHz seismic reflection data. Reflections could not be traced to profile due to poor acoustic character correlation.



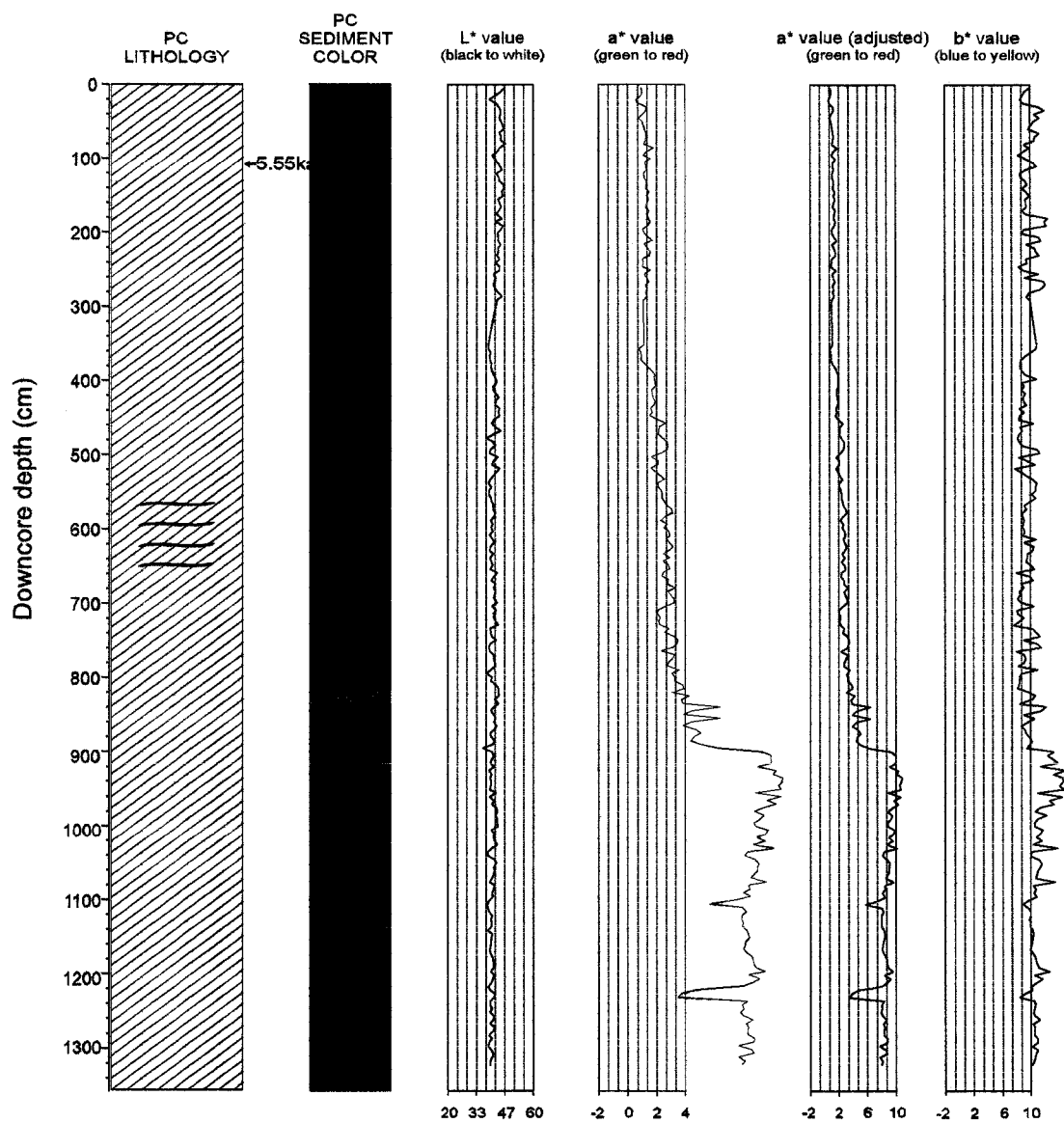
Relative position of trigger weight (TWC) and piston (PC) cores 07 from cruise 90015 within 3.5 kHz seismic reflection data. PC samples sediment just below Q91.



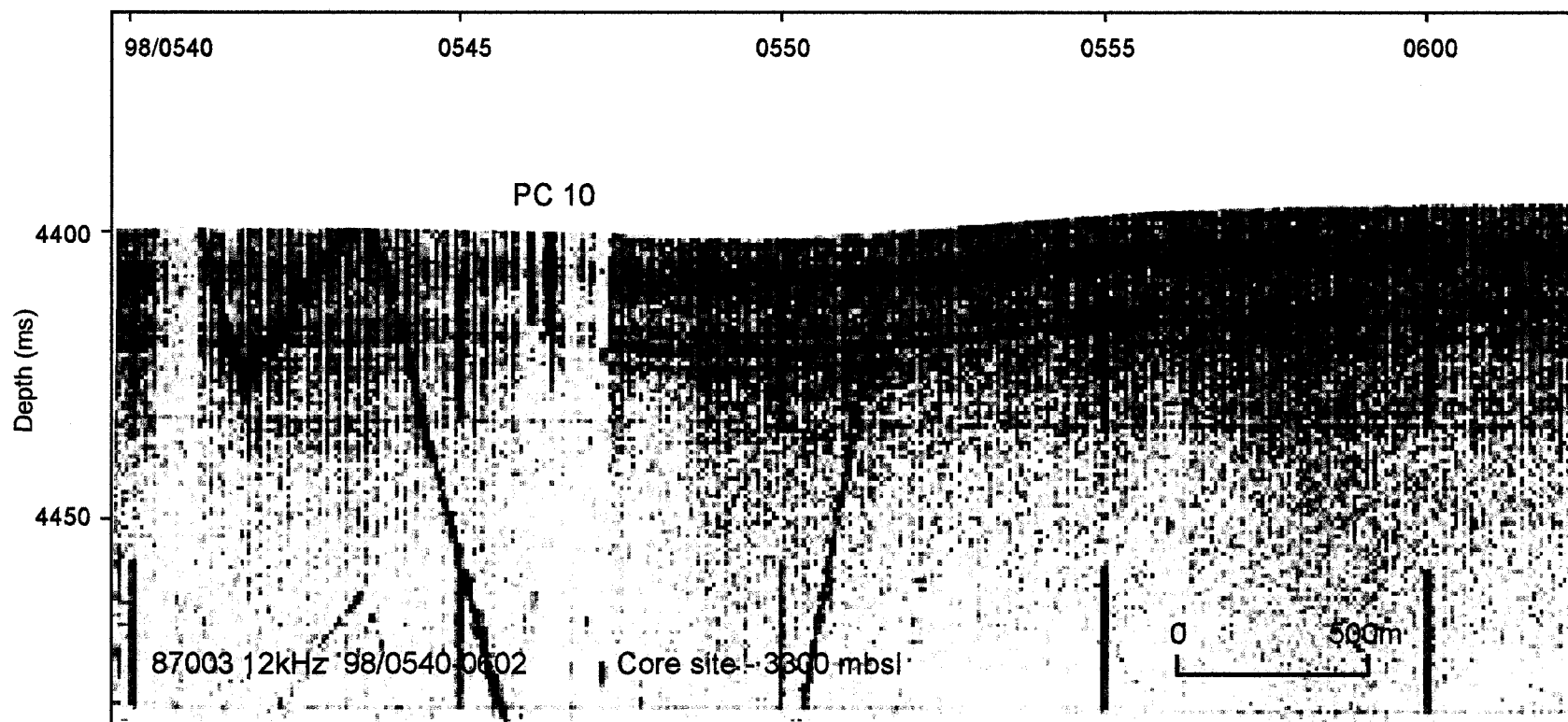
Downcore lithology, color, and physical property plots for piston core 09 obtain during cruise 87003. Laminae in the reddish brown facies below 500 cm are faint.



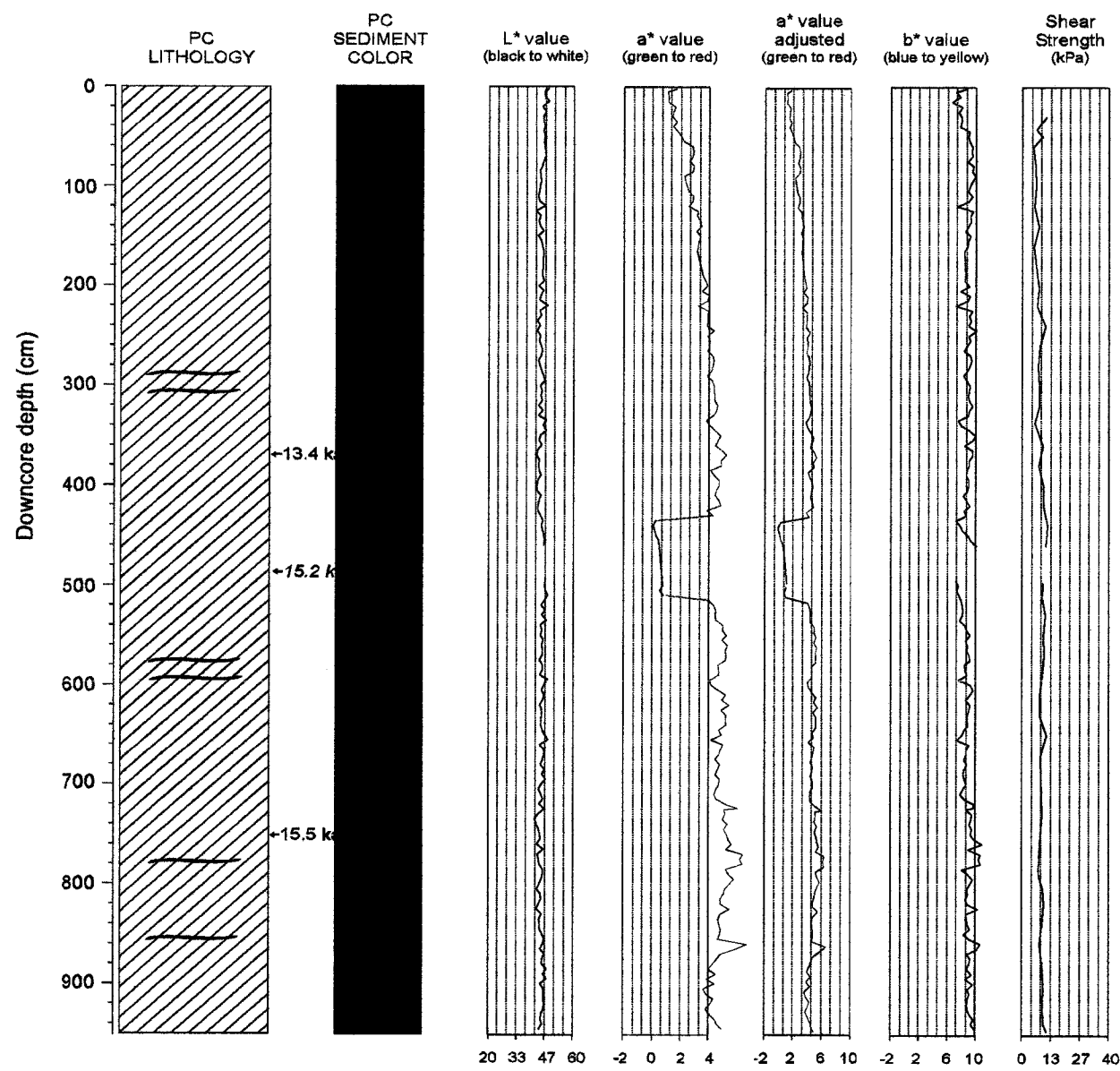
Relative position of piston core (PC) 09 from cruise 87003 within 12 kHz seismic reflection data. Reflections could not be traced to profile due to lack of tie-lines.



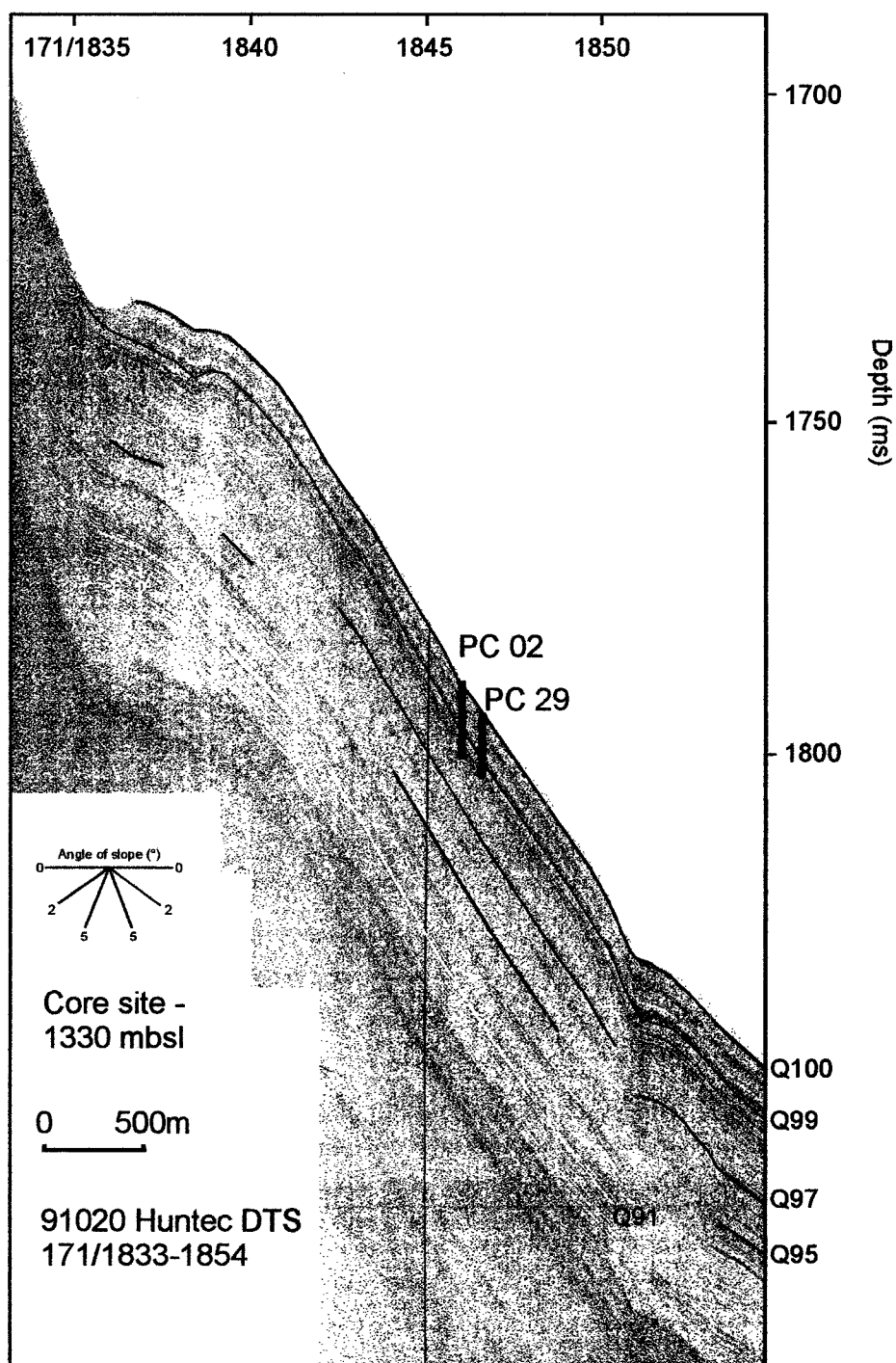
Downcore lithology, color, and physical property plots for piston core 10 obtained during cruise 87003. Laminae in the reddish brown facies below 900 cm are faint.



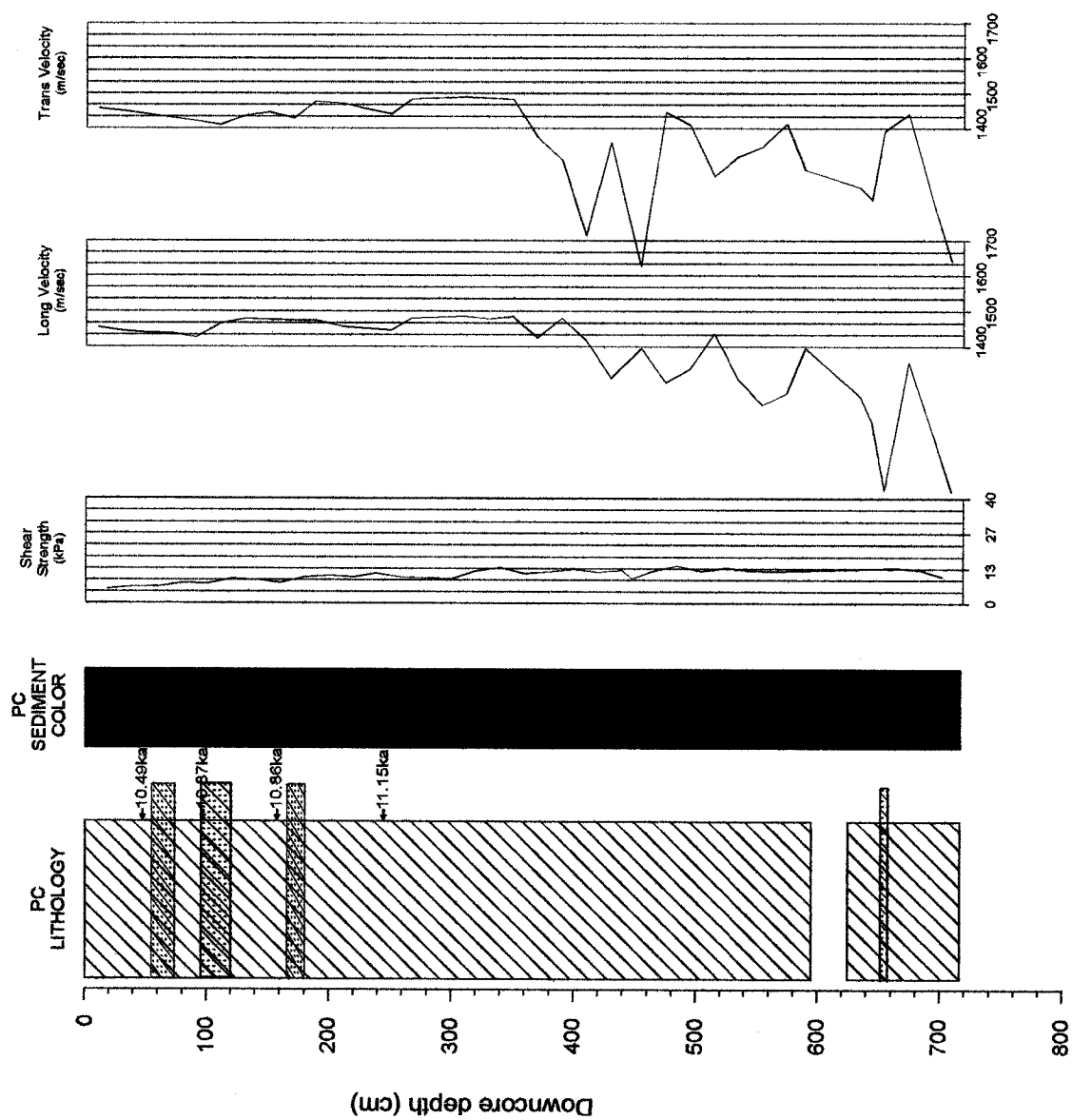
Relative position of piston core (PC) 10 from cruise 87003 within 12 kHz seismic reflection data. Reflections could not be traced to profile due to lack of tie-lines.



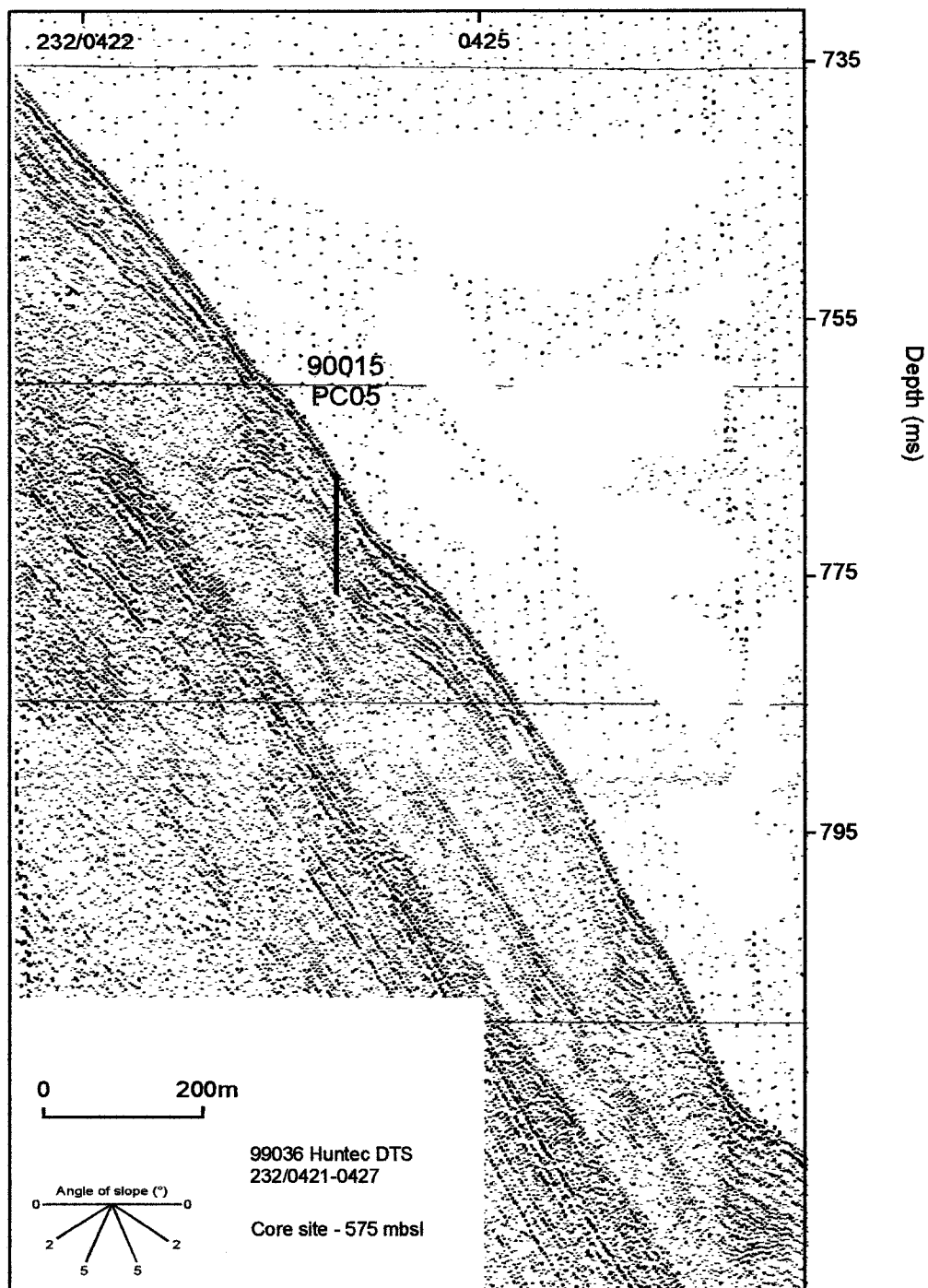
Downcore lithology, color, and physical property plots for piston core 02 obtained during cruise 90015. Cracking from 820 cm to bottom of the core. Radiocarbon age of 15.2 ka is from 86034-09.



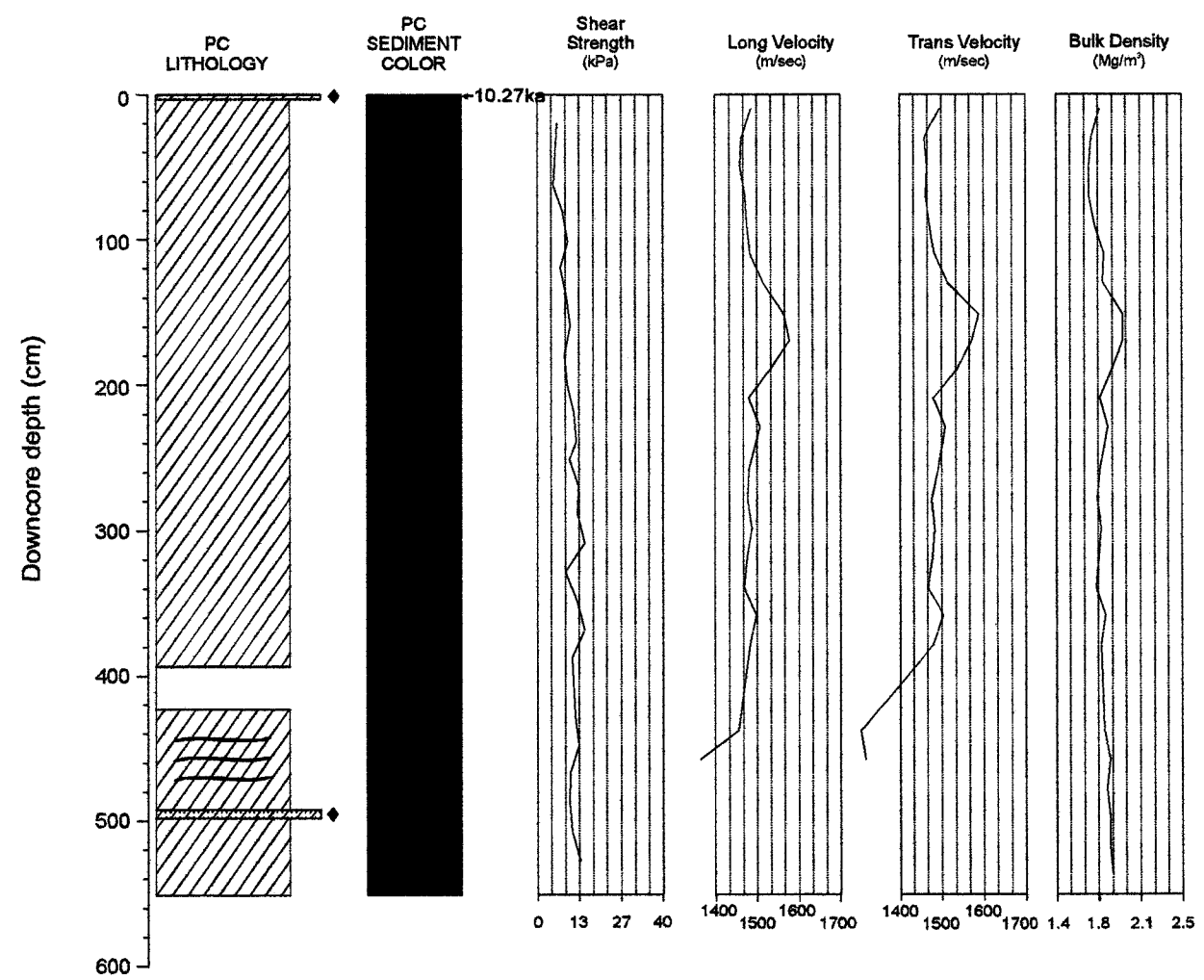
Relative position of piston core (PC) 02 from cruise 90015 within Hunttec DTS seismic reflection data. PC penetrates reflections Q100 and possibly Q99. PC 91020-29 is 250 W of this PC and has been projected into the profile.



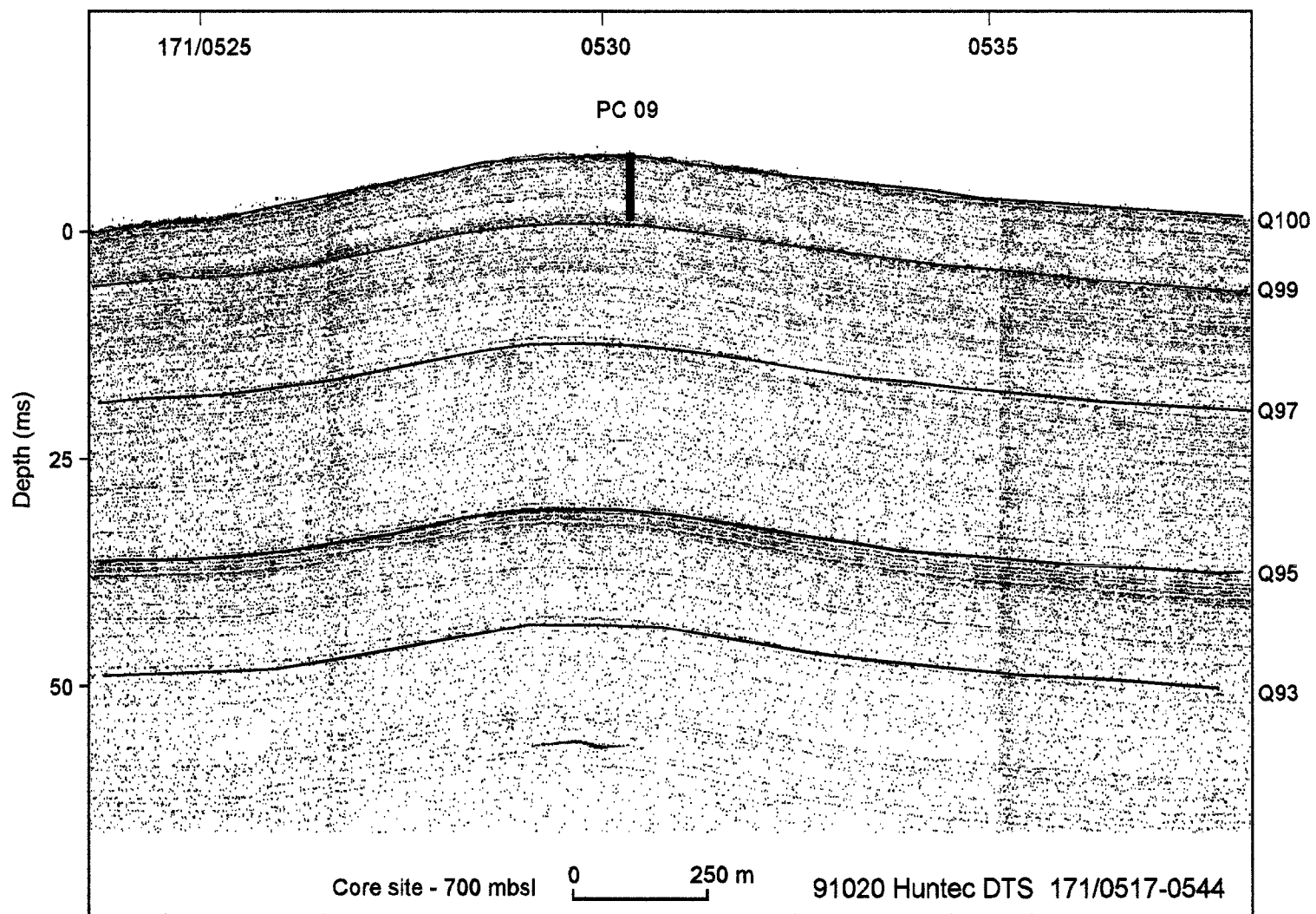
Downcore lithology, color, and physical property plots for piston core 05 obtained during cruise 90015.



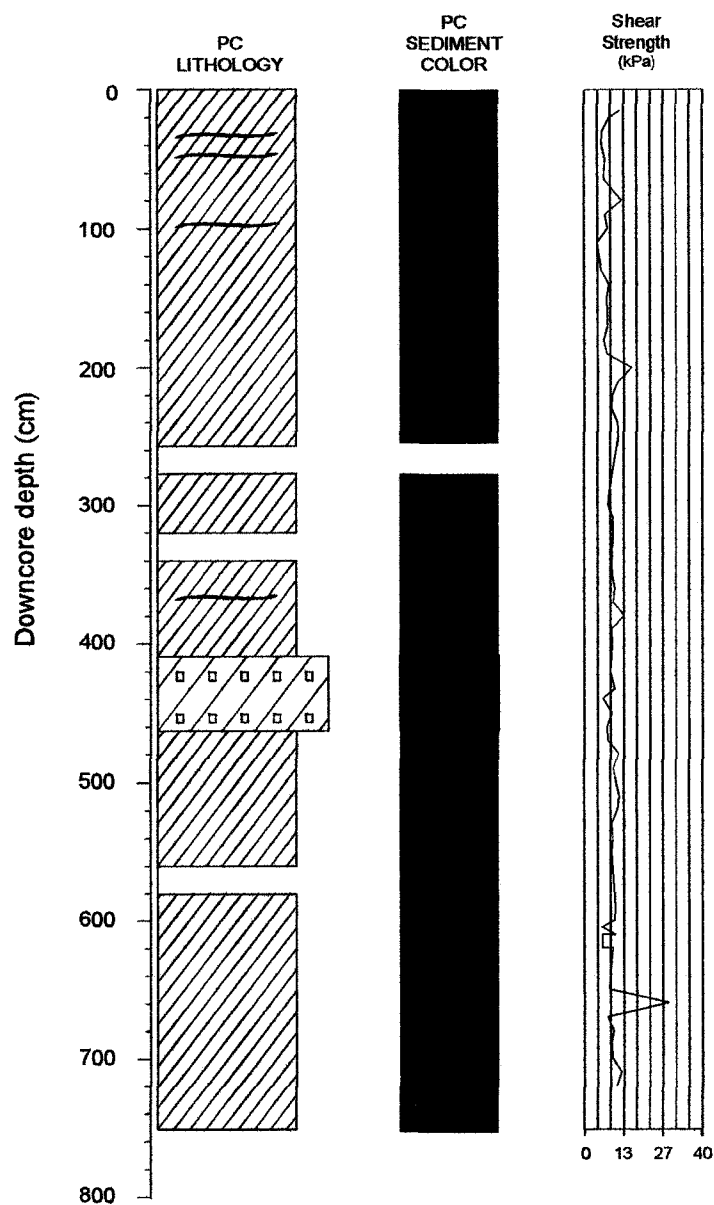
Relative position of piston (PC) core 05 from cruise 90015 within Hunttec DTS seismic reflection data. Core appears to sample undisturbed stratigraphy. Reflections could not be traced to profile due to poor acoustic character correlation.



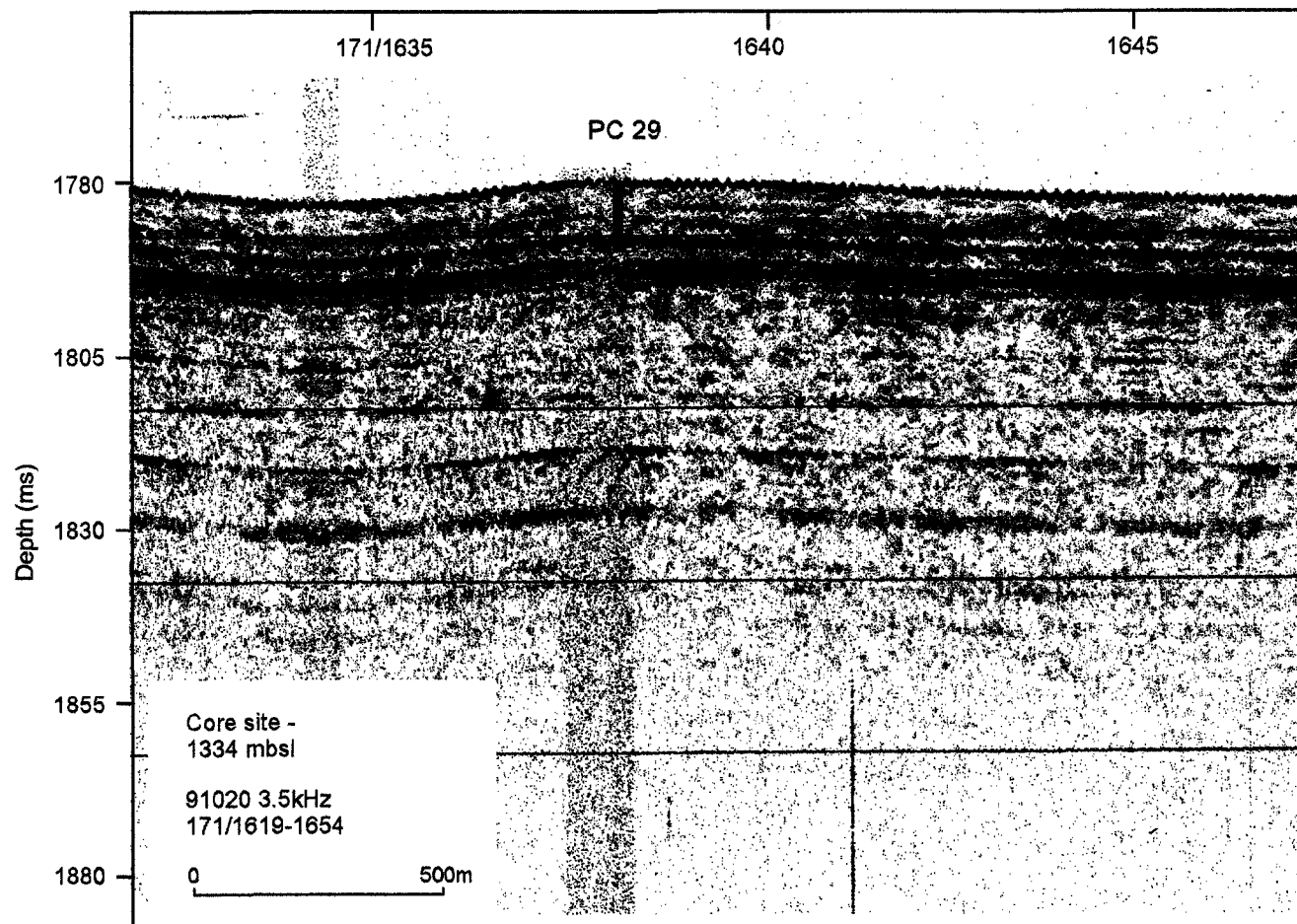
Downcore lithology, color, and physical property plots for piston core 09 obtained during cruise 90015.



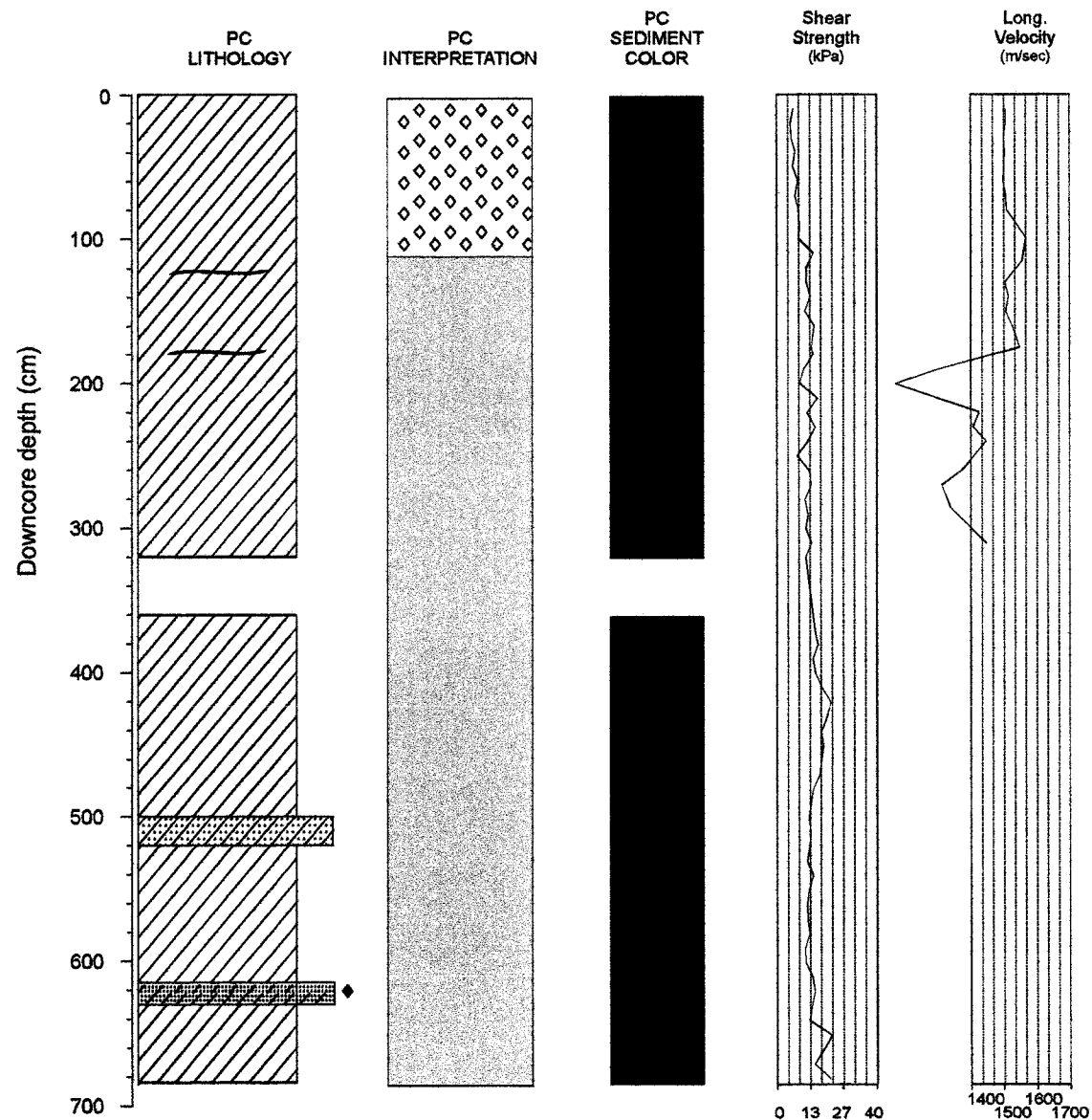
Relative position of piston core (PC) 09 from cruise 90015 within Huntect DTS seismic reflection data. Core penetrates reflection Q100.



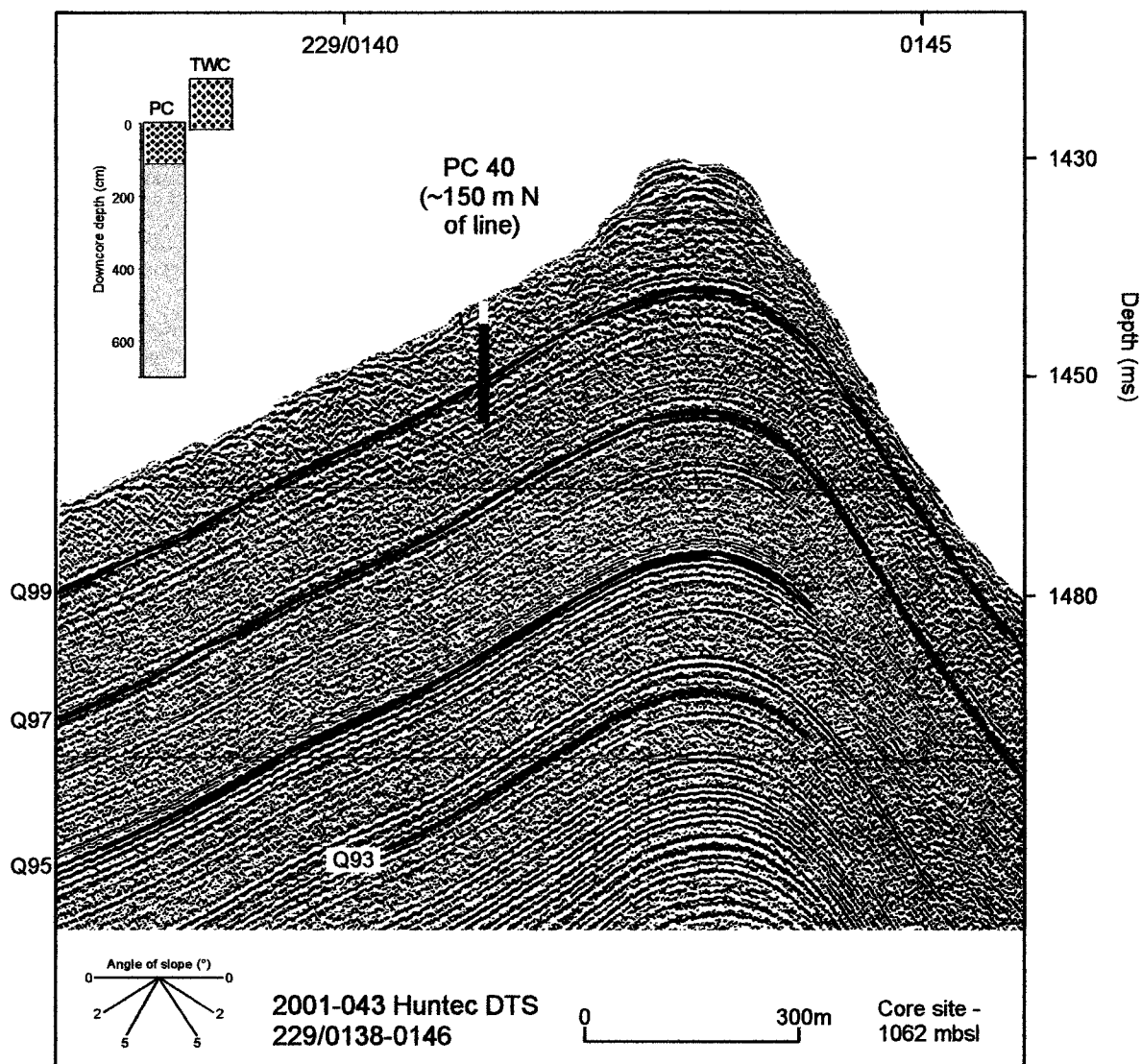
Downcore lithology, color, and physical property plots for piston core 29 obtained during cruise 91020. Cracking from 520-560 cm. At 410-460 cm is a buried MTD.



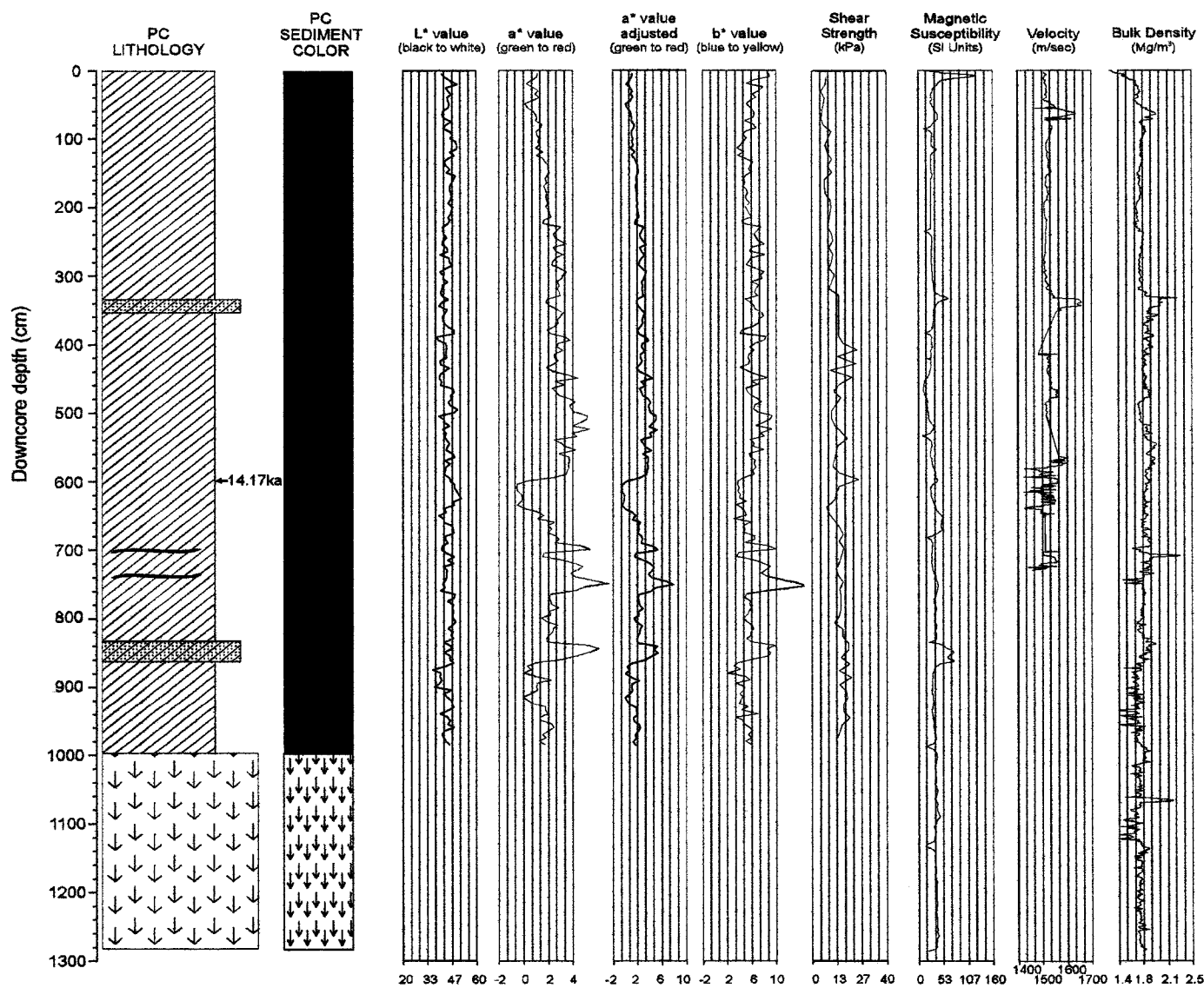
Relative position of piston (PC) core 29 from cruise 91020 within 3.5 kHz seismic reflection data. PC is 250 m W of piston core 90015-02 and projecting this core into Huntect DTS associated with 90015-02 suggests that this core penetrates reflections Q100 and Q99 (see 90015-02).



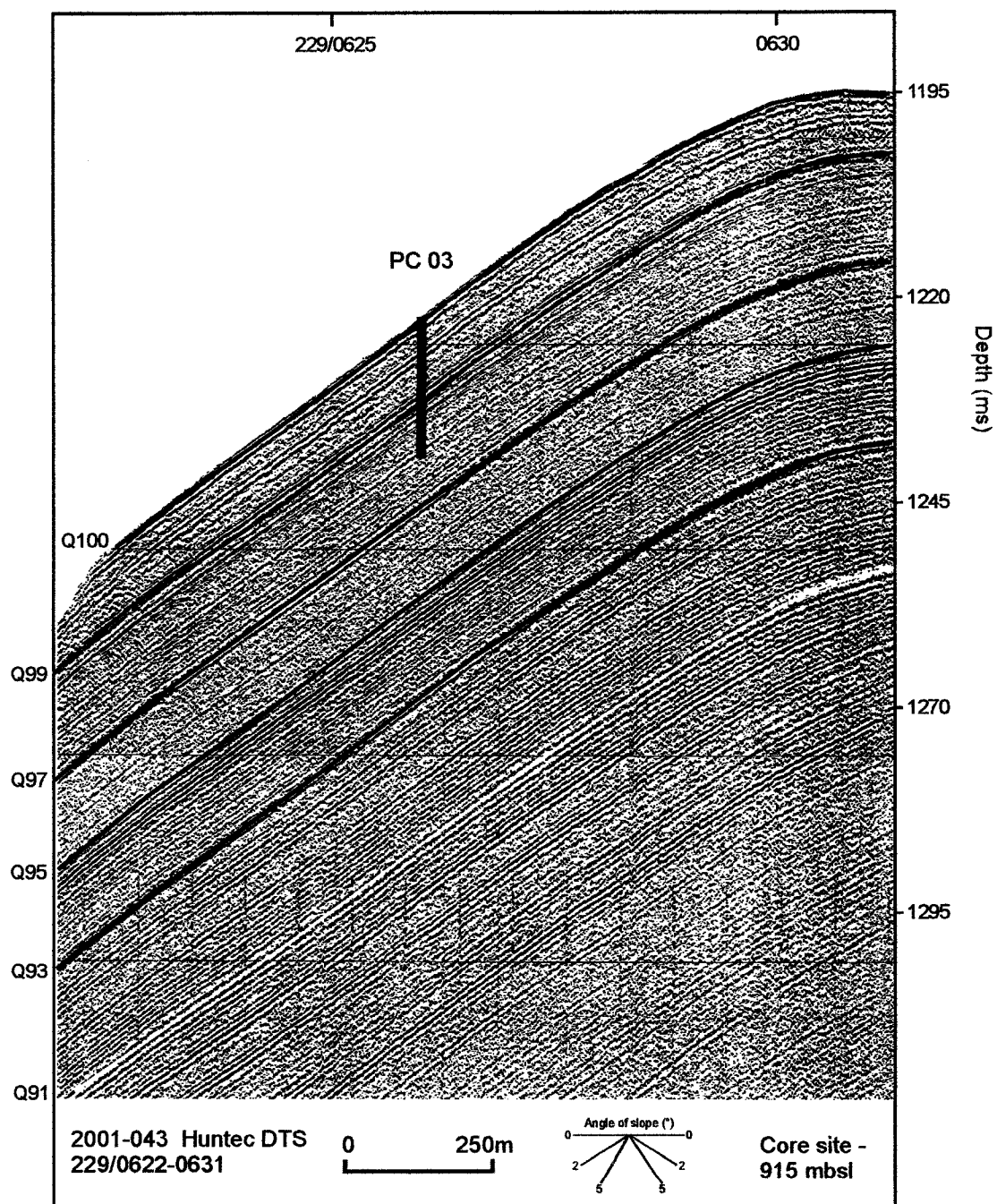
Downcore lithology, color, and physical property plots for piston core 40 obtained during cruise 91020. Downcore lithologies interpreted as MTD facies are shown. Cracking from 360-500 cm.



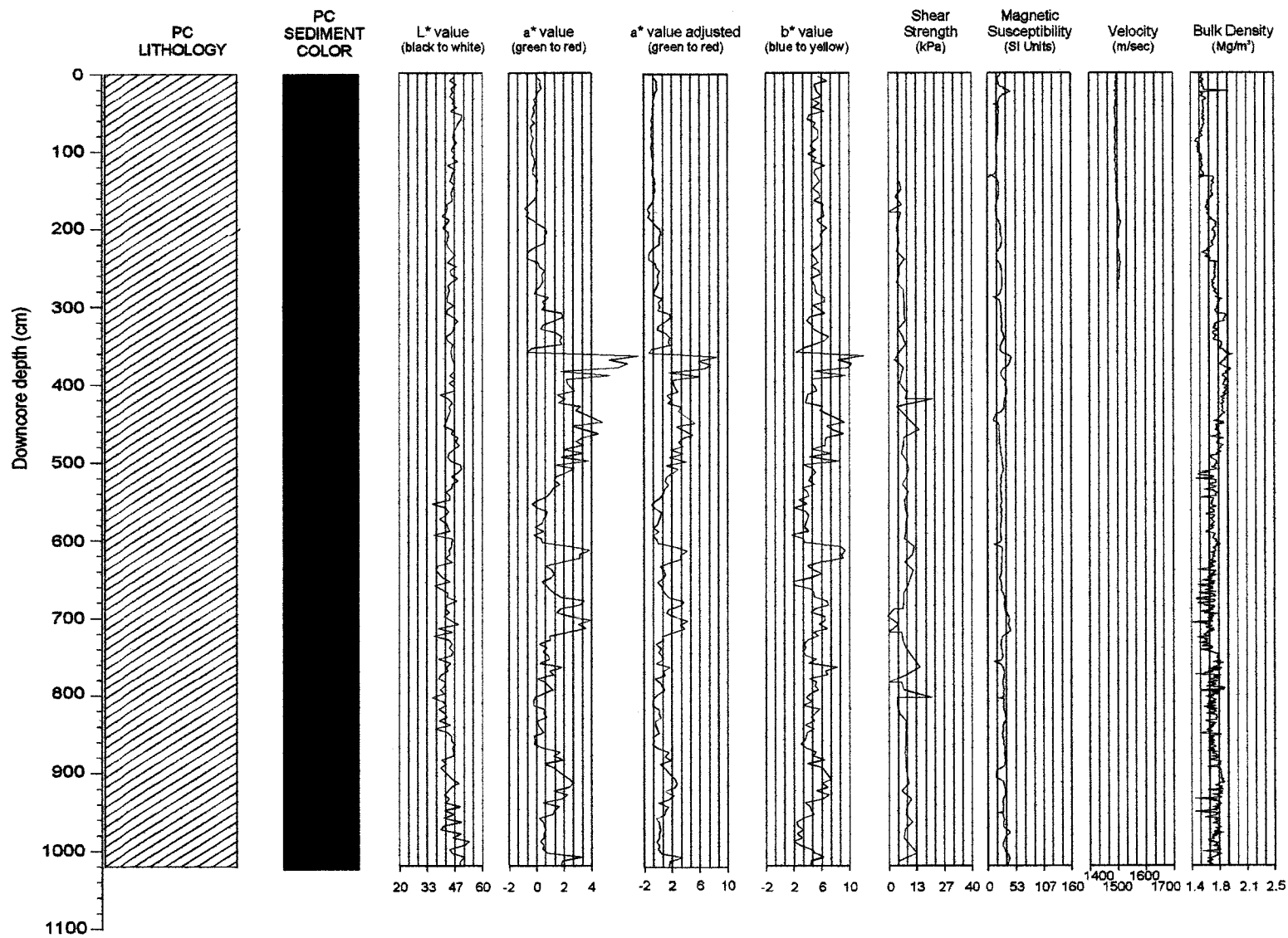
Relative position of trigger weight (TWC) and piston (PC) cores 40 from cruise 91020 within Huntect DTS seismic reflection data. PC penetrates reflection Q99.



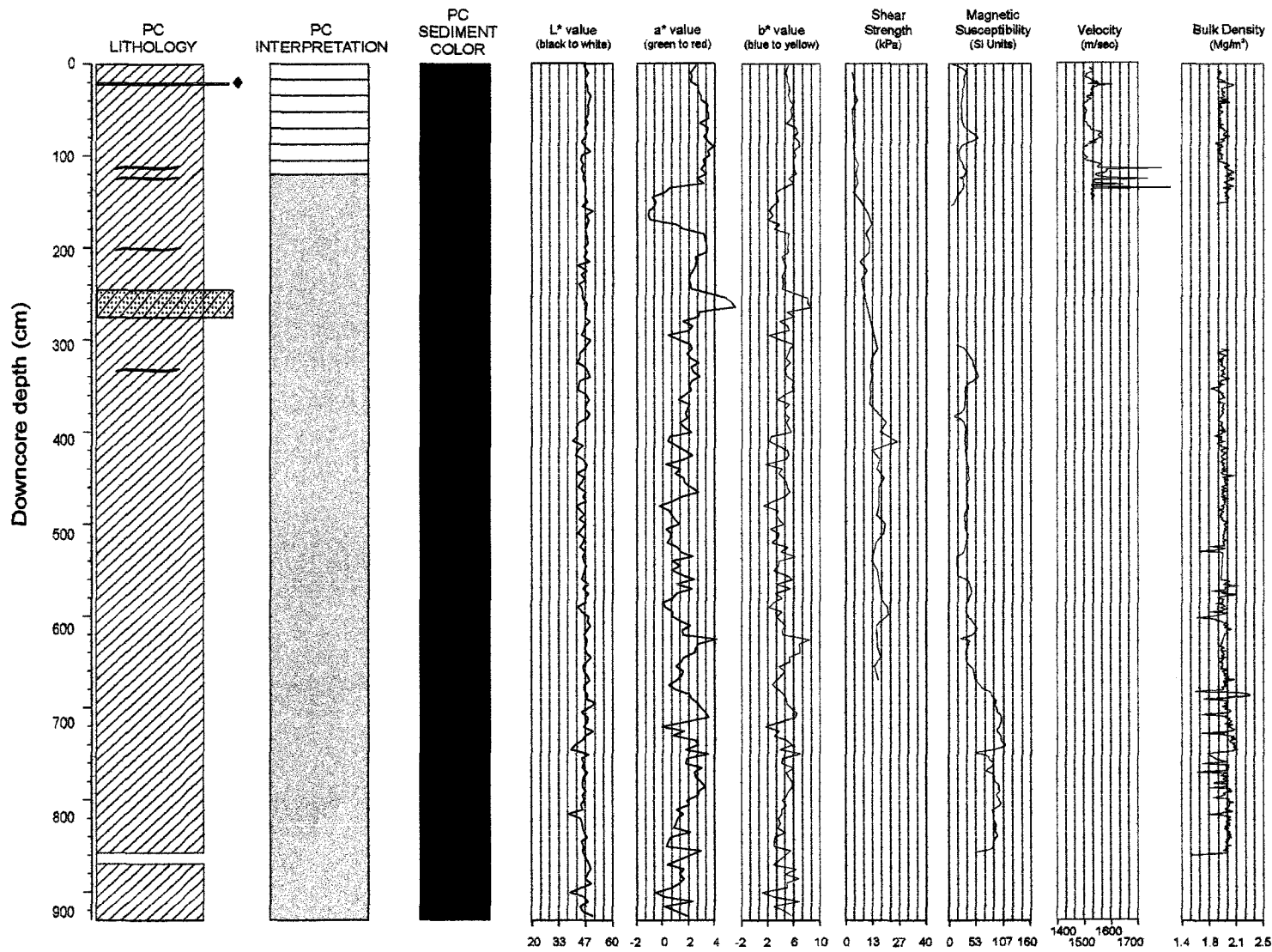
Downcore lithology, color, and physical property plots for piston core 03 obtained during cruise 99036. Gas sample from base recovered 0.37 % methane. Cracking from 740-1000 cm.



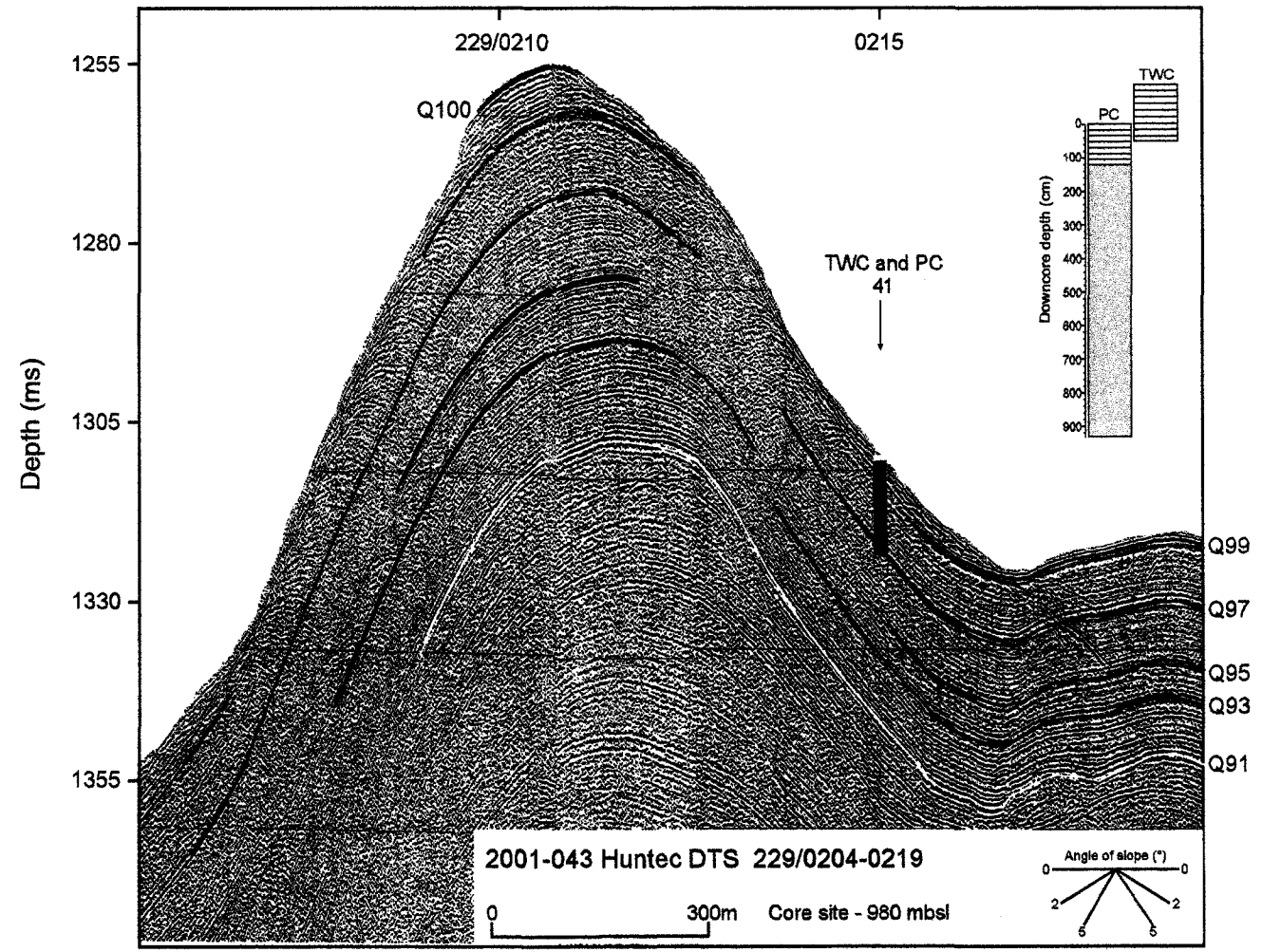
Relative position of piston core 03 from cruise 99036 within Hunttec DTS seismic reflection data. Core penetrates reflections Q100 and Q99.



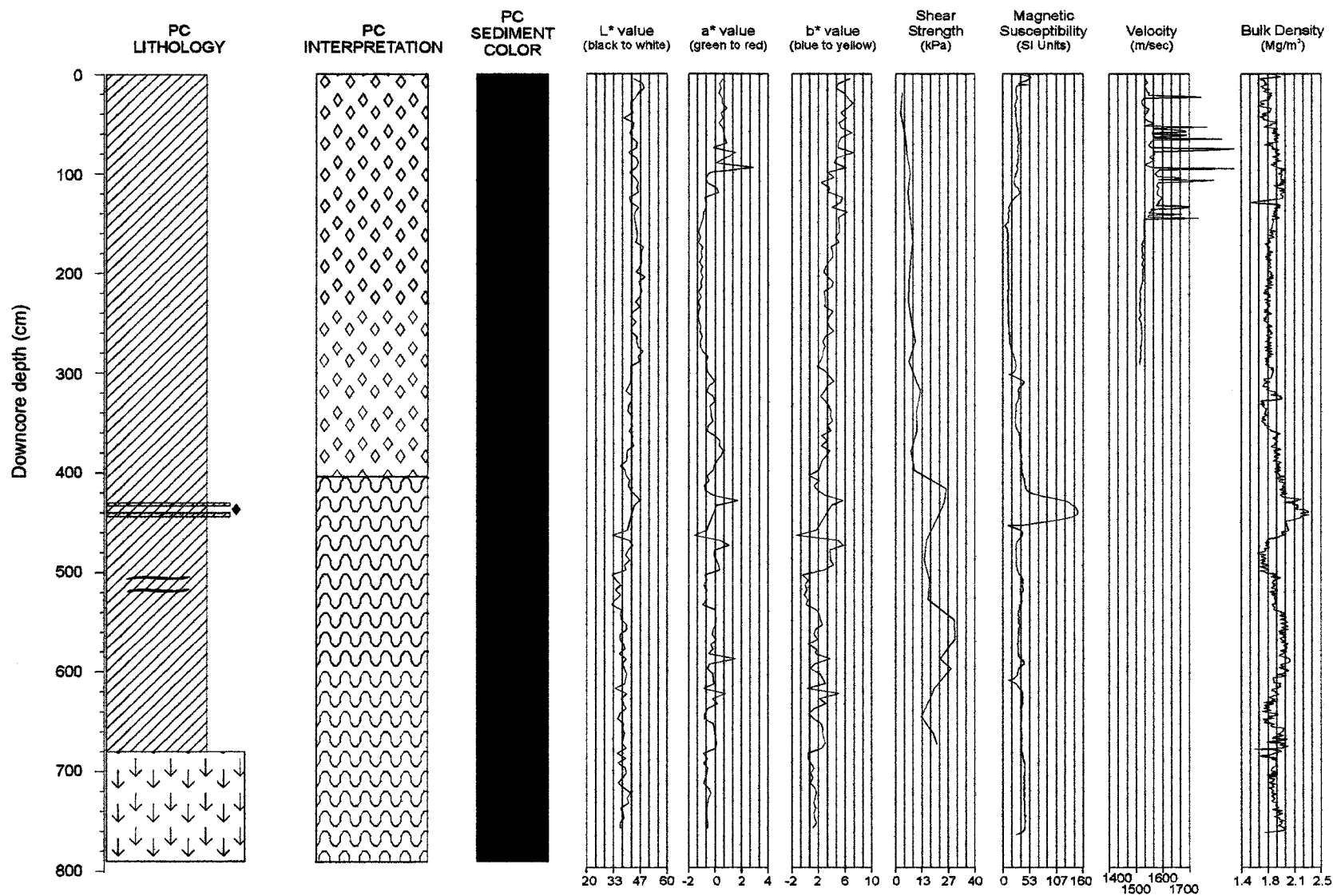
Downcore lithology, color, and physical property plots for piston core 05 obtained during cruise 99036. Minor cracking from 510 cm to bottom of the core. Gas sample yielded 0.3% of methane.



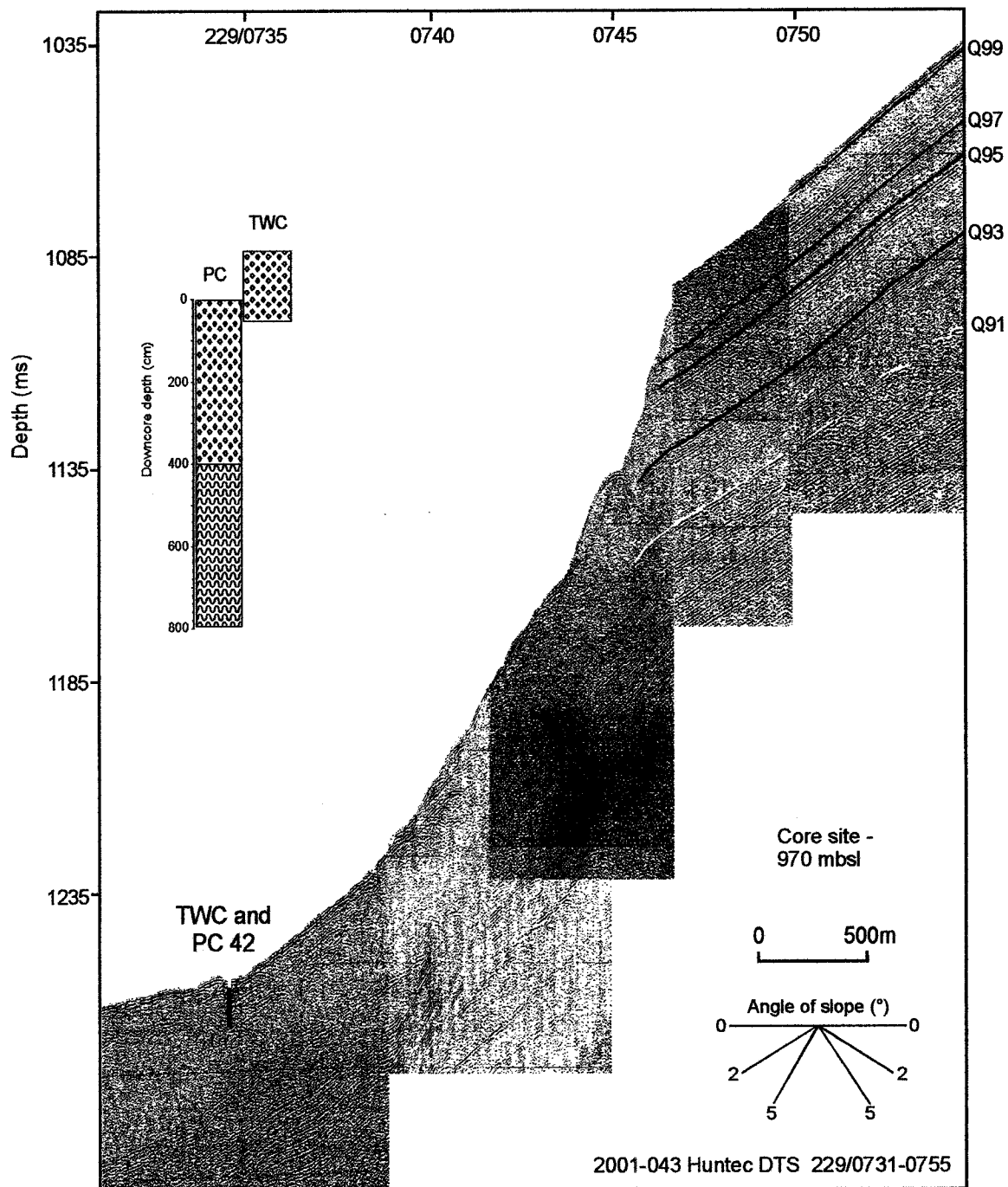
Downcore lithology, color, and physical property plots for piston core 41 obtained during cruise 2001043. Downcore lithologies interpreted as MTD facies are shown. Minor cracking from 220 cm to the end of the core.



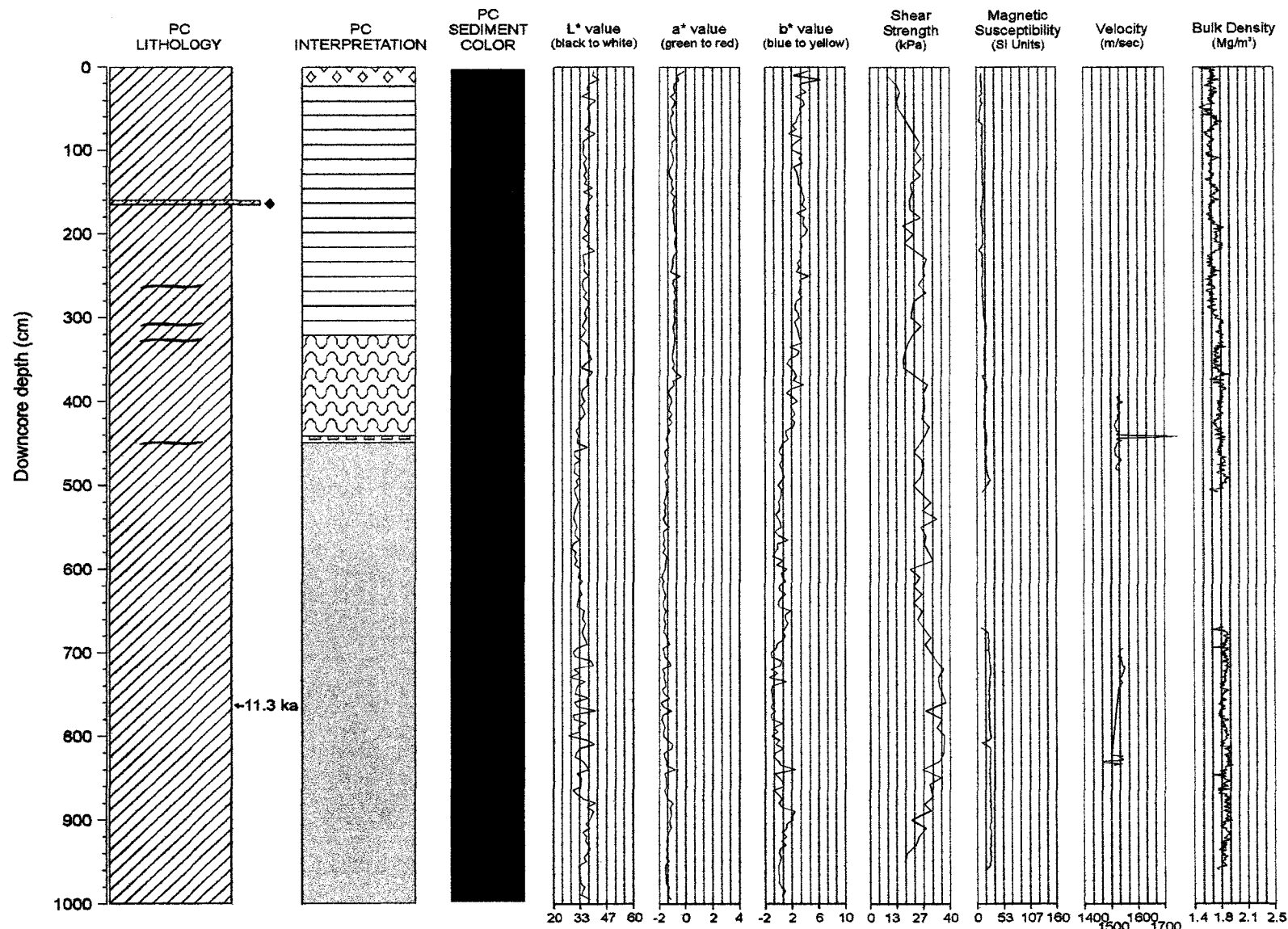
Relative position of trigger weight (TWC) and piston (PC) cores 41 from cruise 2001043 within Huntect DTS seismic reflection data. PC penetrates reflections Q99 and Q97.



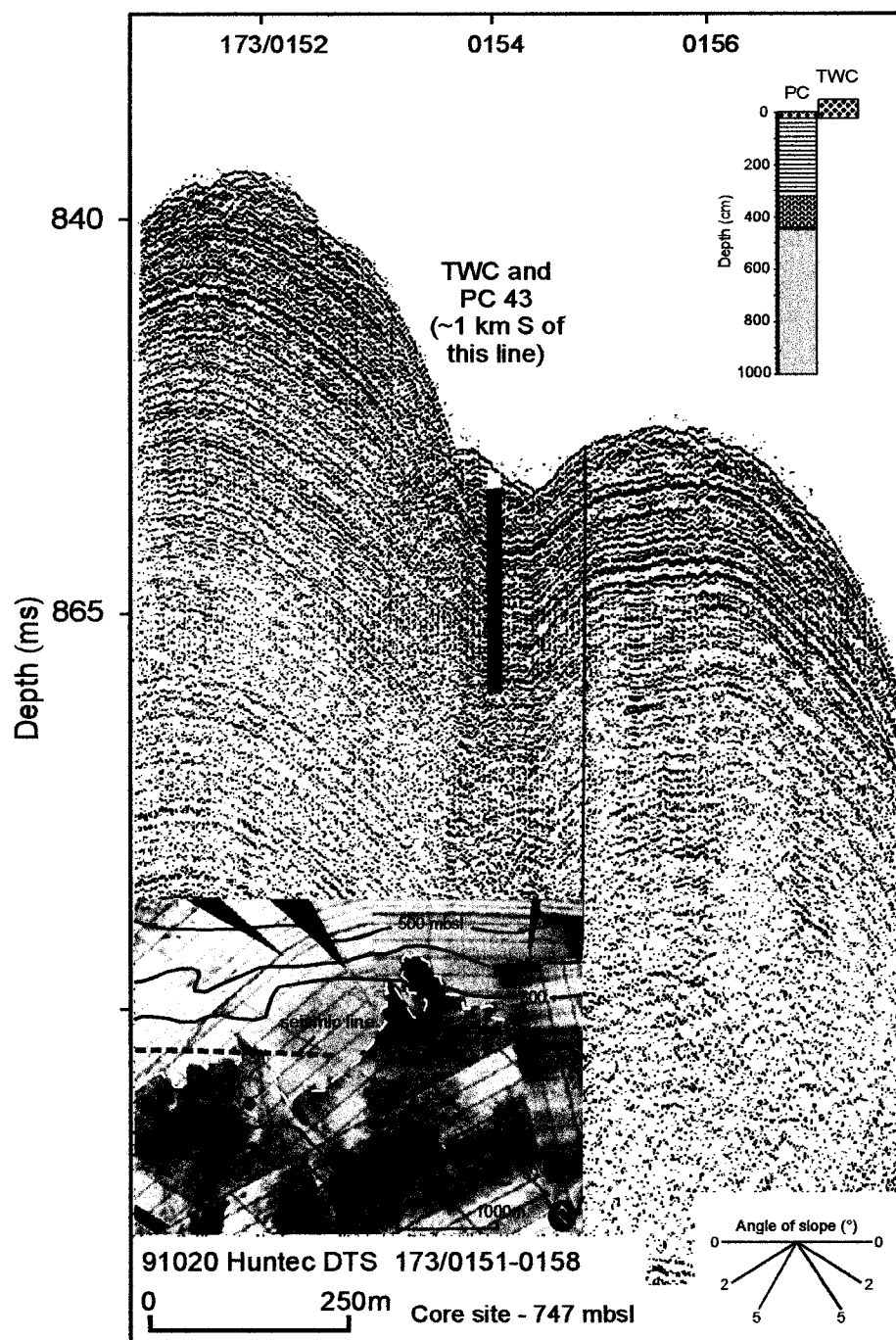
Downcore lithology, color, and physical property plots for piston core 42 obtained during cruise 2001043. Downcore lithologies interpreted as MTD facies are shown. Detectable gas within the core.



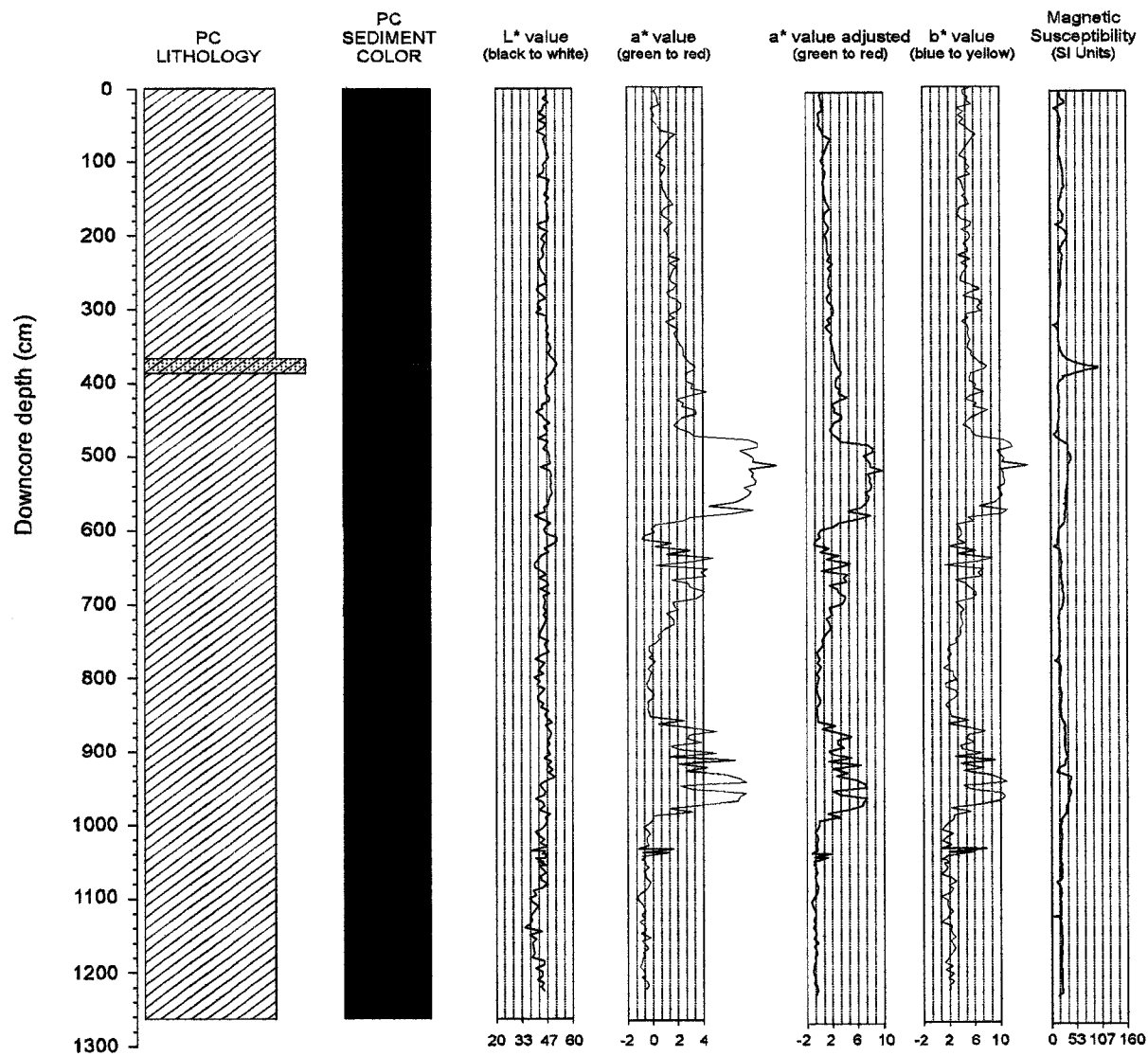
Relative position of trigger weight (TWC) and piston (PC) cores 42 from cruise 2001043 within Hunttec DTS seismic reflection data.



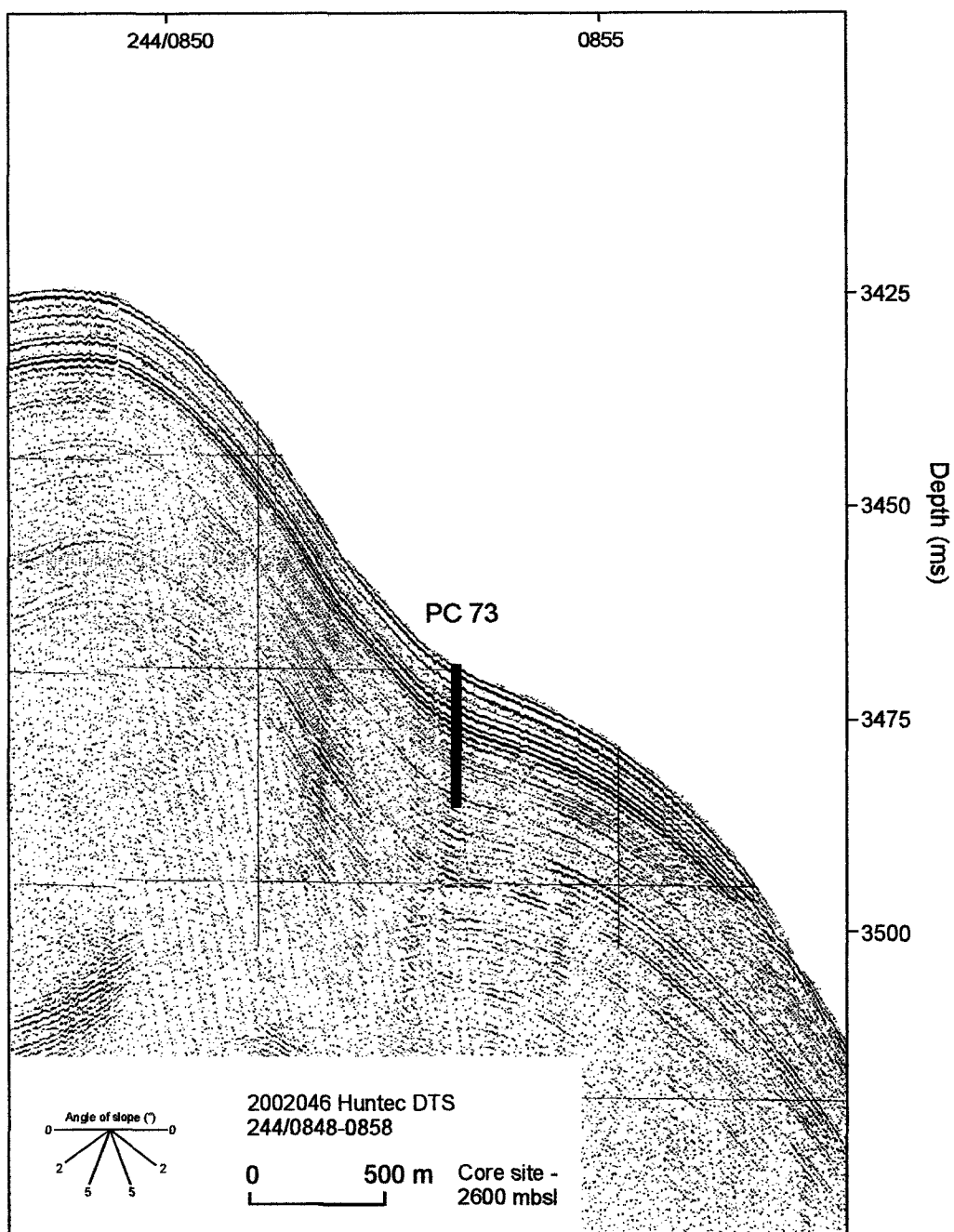
Downcore lithology, color, and physical property plots for piston core 43 obtained during cruise 2001043. Downcore lithologies interpreted as MTD facies are shown. Radiocarbon age from 84003-PC11, core is located ~20 m SW within the same MTD.



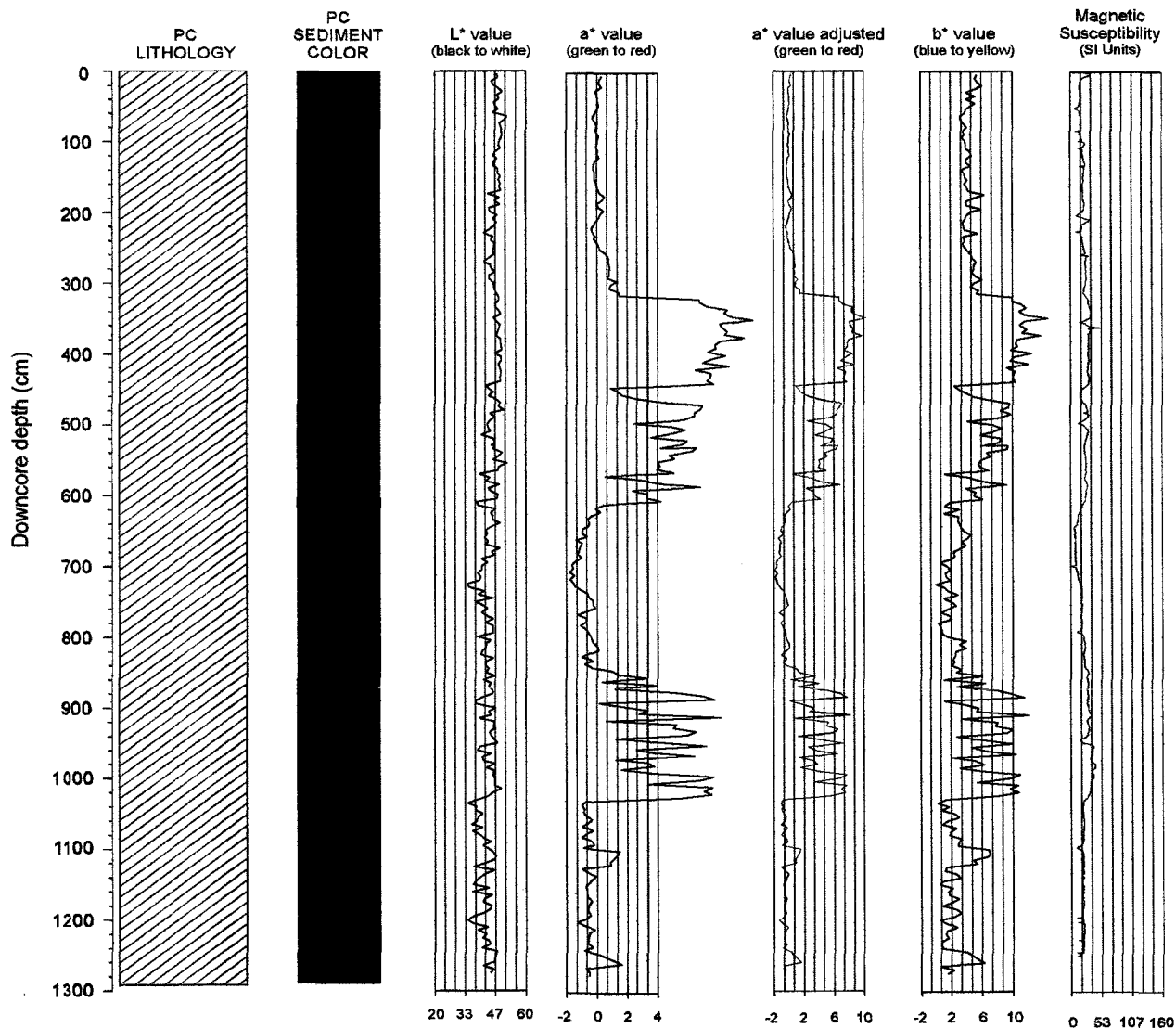
Relative position of trigger weight (TWC) and piston (PC) cores 43 from cruise 2001043 within Huntect DTS seismic reflection data. Although cores are located 1 km south of seismic line, complementary SeaMARC I sidescan data suggests that both the line and cores are located within the same MTD. Reflections could not be traced to profile due to lack of tie-lines and poor acoustic character correlation. In sidescan sonar, the core can be seen down-slope of a scarp (inset).



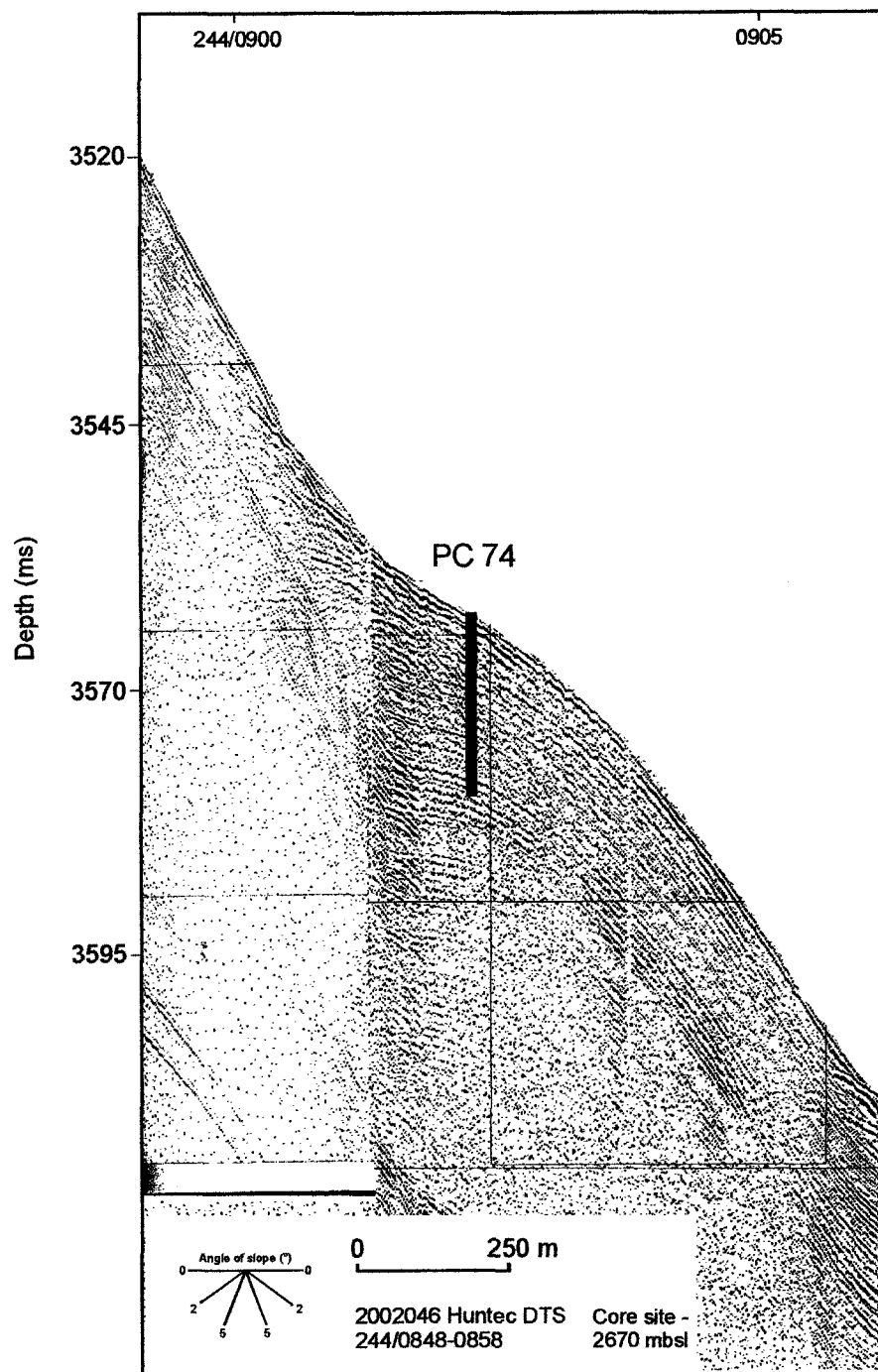
Downcore lithology, color, and physical property plots for piston core 73 obtained during cruise 2002046. Cracking from 775-830 cm and 900-985cm.



Relative position of piston (PC) core 73 from cruise 2002046 within Hunttec DTS seismic reflection data. Reflections could not be traced to profile due to lack of tie-lines. PC is located ~1.5 km east of piston core 200246-74.



Downcore lithology, color, and physical property plots for piston core 74 obtained during cruise 2002046. Cracking from 790-840cm and 950-1025cm.



Relative position of piston core (PC) 74 from cruise 2002046 within Hunttec DTS seismic reflection data. Reflections could not be traced to profile due to lack of tie-lines. PC is located ~1.5 km west of piston core 200246-73.